รายงานวิจัยฉบับสมบูรณ์

โครงการ : เทคโนโลยี RNA interference เพื่อประสิทธิผลของการเพาะเลี้ยงกุ้งในประเทศไทย

โดย

ศาสตราจารย์เกียรติคุณ ดร.สกล พันธุ์ยิ้ม และคณะ

20 มิถุนายน 2561

สัญญาเลขที่ DBG5980011

รายงานวิจัยฉบับสมบูรณ์

โครงการ : เทคโนโลยี RNA interference เพื่อประสิทธิผลของการเพาะเลี้ยงกุ้งในประเทศไทย

คณะผู้วิจัย	สังกัด
1. นายสกล พันธุ์ยิ้ม, Ph.D.	ภาควิชาชีวเคมี คณะวิทยาศาสตร์และสถาบันชีววิทยาศาสตร์โมเลกุล มหาวิทยาลัยมหิดล
2. นางสาวพงโสภี อัตศาสตร์, Ph.D.	สถาบันชีววิทยาศาสตร์โมเลกุล มหาวิทยาลัยมหิดล
3. นางสาวเฉลิมพร องศ์วรโสภณ, Ph.D.	สถาบันชีววิทยาศาสตร์โมเลกุล มหาวิทยาลัยมหิดล
4. นายอภินันท์ อุดมกิจ, Ph.D.	สถาบันชีววิทยาศาสตร์โมเลกุล มหาวิทยาลัยมหิดล
5. นายวันชัย อัศวลาภสกุล, Ph.D.	ภาควิชาจุลชีววิทยา คณะวิทยาศาสตร์ จุฬาลงกรณ์มหาวิทยาลัย
6. นางสาวสุพัตรา ตรีรัตน์ตระกูล, Ph.D.	สถาบันชีววิทยาศาสตร์โมเลกุล มหาวิทยาลัยมหิดล

สนับสนุนโดยสำนักงานกองทุนสนับสนุนการวิจัย

สารบัญ

Research Outputs
(ทุนวิจัยพื้นฐานเชิงยุทธศาสตร์)

Abstract

Increasing efficiency of shrimp culture in Thailand through RNAi technology was undertaking by two aspects; increasing egg production in the female without a cruel eye ablation, and the control of loss by major shrimp viruses. DsRNA-GIH (Gonad inhibiting hormone) of 400 bp was produced in *E.coli* and mixed with cathionic cholesterol-base liposome for injection. Shrimps injected with the dsRNA gave a comparable or better egg production than those receiving the eye ablation treatment. However, they showed no sign of weakness and mortality. It is evident that dsRNA injection increased an efficiency of egg-production.

Control of shrimp viruses by application of dsRNA was performed by the injection which knocked-down viral genes (protease or RNA polymerase) or shrimp genes required for viral replication (e.g. Rab proteins). To increase the efficiency, VLP (virus-like-particles) was prepared from the cloned coat protein of PstDNA in *E.coli*. By engineering VLP to entrap dsRNA-YHV in *E.coli*, the VLP gave inhibition of YHV replication in shrimp. This paves the way to increase efficiency of YHV protection in the shrimp culture.

This research yielded seven Q1/Q2 international publications and five manuscript-in-preparations. Five Ph.D. students and two M.Sc. students were enrolled to conduct research on RNA interference technology.

บทคัดย่อ

การใช้เทคโนโลยี RNAi มาเพิ่มประสิทธิภาพของการเลี้ยงกุ้งในประเทศไทย ควรใช้การเพิ่มประสิทธิภาพการผลิตไข่กุ้งเพศเมีย โดยไม่ต้องตัดตาซึ่งเป็นการทารุณและอาจมีการห้ามปฏิบัติในอนาคต และเนื่องจากการเลี้ยงกุ้งได้รับความเสียหายอยู่เสมอจากการติดเชื้อไวรัสที่สำคัญ เช่น ไวรัสหัวเหลือง จึงได้มีการผลิต dsRNA ที่มีประสิทธิภาพ ได้แก่ dsRNA-GIH (Gonad inhibiting hormone) ขนาด 400 bp ใน *E.coli* แล้วนำ dsRNA ดังกล่าวผสมกับ cathionic cholesterol-base liposome เพื่อฉีดกุ้งเพศเมียในการกระตุ้นการวางไข่ พบกุ้งซึ่งฉีด dsRNA-GIH สามารถกระตุ้นการวางไข่ได้ทัดเทียมหรือดีกว่าวิธีการตัดตาซึ่งใช้อยู่ในปัจจุบัน ซึ่งพบว่ากุ้งตัดตาจะอ่อนแอและตายในที่สุด จะเห็นว่าการใช้ฉีด dsRNA-GIH เพิ่มประสิทธิภาพการวางไข่ และปราศจากการทารุณสัตว์

การใช้ dsRNA ในการควบคุมไวรัสสำคัญในกุ้ง เช่น ไวรัสหัวเหลือง กระทำโดยการฉีด dsRNA-YHV เพื่อกำจัด mRNA ของไวรัสหัวเหลือง (protease gene หรือ RNA polymerase gene) หรือ mRNA ของยีนสำคัญของกุ้ง ซึ่งไวรัสใช้ในการเพิ่มจำนวน (e.g. Rab proteins) ส่งผลให้ไม่มีการเพิ่มจำนวนไวรัสในกุ้ง เราได้พัฒนา VLP (virus-like-particles) โดยสร้างใน *E.coli* ซึ่งเมื่อสร้างรวมกับ dsRNA ก็จะได้ VLP ซึ่งสามารถ knock-down ยีนของไวรัส ทำให้ไวรัสเพิ่มจำนวนไม่ได้ เป็นวิธีการที่จะเพิ่มประสิทธิภาพของการป้องกัน YHV ในกุ้ง ลดการตายของกุ้งจากการติดเชื้อไวรัส

งานวิจัยนี้มีผลงานตีพิมพ์ในวารสารวิชาการนานาชาติ (Q1 / Q2) จำนวน 7 ฉบับ และผลิตผลงานพร้อมตีพิมพ์ จำนวน 5 ฉบับ มีนักศึกษาปริญญาเอก จำนวน 5 คน ปริญญาโท 2 คน

เนื้อหางานวิจัย

In vitro assembly of *Penaeus monodon* densovirus (PmDNV)-like particles produced in a prokaryote expression system

Viral diseases are a significant problem in the shrimp aquaculture industry as outbreaks can cause significant mortality and economic loss. While it has been shown that triggering the shrimp RNA interference pathway through dsRNA is a potentially viable treatment pathway, this approach is hampered by the lack of a suitable delivery mechanism. Virus-like particles (VLPs), which are structurally similar to native viruses but lack the genetic material, could possibly be developed as a delivery vehicle. To generate a candidate VLP, the *Penaeus monodon* densovirus (*Pm*DNV) capsid protein was cloned with an added histidine tag and expressed in an *E. coli* expression system. While the protein was expressed in inclusion bodies, the recombinant *Pm*DNV capsid protein could be dissolved and subsequently purified by nickel affinity column chromatography. The formation of VLP from this purified r*Pm*DNV capsid protein was investigated by transmission electron microscopy, and *Pm*DNV-VLPs were observed that looked similar to the native *Pm*DNV virion. Our results suggest that the *Pm*DNV-like particle could be promisingly applied towards vaccination and that this *Pm*DNV-like particle can potentially serve as a system for delivery of nucleic acids to trigger innate immunity in shrimp.

Introduction

Penaeus monodon densovirus (*Pm*DNV; formerly hepatopancreatic parvovirus or HPV) is an icosahedral naked virus approximately 22–24 nm in diameter that contains a single-stranded linear DNA genome of approximately 6 kb (Safeena, Rai & Karunasagar 2012). A *Pm*DNV isolated and characterized in Thailand consisted of 6321 nucleotides with three long open reading frames (ORFs). Two of the ORFs encode the non-structural proteins (NS1 and NS2), while the third encodes the structural (VP) protein (Sukhumsirichart, Attasart, Boonsaeng & Panyim 2006). The virus is associated with a shrimp developmental disease that results in growth-stunted shrimp (Srisuk, Chaivisuthangkura, Sukhumsirichart, Sridulyakul, Longyant, Rukpratanporn & Sithigorngul 2011). *Pm*DNV specifically infects the hepatopancreas tubule epithelial cells only, while in contrast, infectious hypodermal and hepatopoietic necrosis virus (IHHNV), another type of shrimp parvovirus, infects ectodermal, mesodermal and connective tissues (Dhar, Robles-Sikisaka, Saksmerprome & Lakshman 2014). As such, IHHNV has a broad tissue specificity, while *Pm*DNV is remarkably specific, infecting only the hepatopancreas. The hepatopancreas is an important organ in the shrimp digestive system as this organ is involved with critical functions such as the synthesis and secretion of digestive enzymes and the adsorption of digested dietary products (Ceccaldi 1989).

The capsid proteins of a number of animal viruses have been shown to form virus-like particles (VLPs) by self-assembly *in vitro* and *in vivo*, and VLPs have a structure and characteristic similar to natural virus particles. They are specific to target cells (Buonaguro, Tagliamonte, Tornesello & Buonaguro 2011; Liew, Chuan & Middelberg 2012; Shao, Paul, Abbasi, Chahal, Mena, Montes, Kamen & Prakash 2012), and VLPs have the potential for delivery of therapeutic agents to target cells. For example, a Simian virus 40 (SV 40)-like particle that encapsulated nucleic acid has

been used for gene transfer (Enomoto, Kukimoto, Kawano, Yamaguchi, Berk & Handa 2011). Human John Cunningham viruslike particles have been used to transfer exogenous DNA into human kidney cells (Ou, Wang, Fung, Tsai, Chao, Hseu & Chang 1999), and parvovirus capsid proteins can be successfully expressed and can self-assemble to form virus-like particles for siRNA delivery (Shao et al. 2012). Moreover, VLPs from shrimp viruses such as *Macrobrachium rosenbergii* nodavirus (*Mr*NV) and IHHNV have been able to form virus-like particle and can enter into shrimp cells (Hou, Wu, Xu & Yang 2009; Goh, Tan, Bhassu & Tan 2011). Therefore, the objective of this study was to express the mature *Pm*DNV capsid protein to form VLPs *in vitro*

Materials and methods

Cloning the PmDNV capsid protein

The mature PmDNV capsid protein gene was amplified with specific primers: cpPmDNV-F (5' GCT AGC GCT GCT GCG GGC GGC GGC GG-3') and cpPmDNV-R (5'-CTC GAG TTA TAC ATT AAC TCT ATA TTT CTT C-3') containing *Nhe*I and *Xho*I restriction site (underlined), respectively. The PCR reaction consisted of 100 ng *Pm*DNV genome as a template, 1x ThermoPol reaction buffer, 0.2 mM dNTPs, 4 mM $MgSO_4$, 1 unit of *Vent* DNA polymerase (New England Biolabs, Massachusetts, USA) and 0.2 µM (each) of cp*Pm*DNVF and cp*Pm*DNV-R primers. The PCR amplification was carried out as follows: pre-heating at 94°C for 3 min followed by 30 cycles of 94°C for 45 s, 55°C for 30 s, 72°C for 2 min, then at 72°C for 10 min. The PCR product was digested with *Nhe*I and *Xho*I restriction enzyme and ligated into pET28a expression vector at the restriction sites.

The recombinant plasmids were transformed into *E. coli* DH5a and extracted using QIAGEN Plasmid Extraction Kit (QIAGEN, Hilden, Germany). The insert was verified by PCR with specific *Pm*DNV capsid protein primers and DNA sequencing.

Expression and solubility testing of rPmDNV capsid protein

To express a heterologous protein containing uncommon amino acids, the Rosetta-gami, an *E. coli* strain which has rare codon tRNA (Correa & Oppezzo, 2015), was used in this study. The recombinant plasmid (pET28a-cp*Pm*DNV) was transformed into *E. coli* Rosetta-gami (pLysS), and cells were grown in LB medium containing 50 µg mL^{-1} kanamycin and 34 µg mL^{-1} chloramphenicol at 30°C with shaking until OD_{600} = 0.4. Protein expression was induced with isopropyl-β-D-thiogalactopyranoside (IPTG) at a final concentration of 0.4 mM, and cells were further incubated at 30°C for 3 h after which cells were harvested by centrifugation at 18 890xg for 10 min at 4°C. The expected recombinant proteins were analysed by SDS-PAGE and Western blotting analysis using antihistidine (R&D System Inc., Minneapolis, MN, USA) and anti-*Pm*DNV (kindly provided by Dr. Parin Chaivisuthangkura, Faculty of Science, Srinakharinwirot University) antibodies. For protein solubility testing, the cell pellet of the recombinant bacteria was resuspended in lysis buffer (ENZhance Lysis Buffer, NSTDA) and the solubilized proteins were collected by centrifugation at 18 890xg for 10 min at 4°C and precipitated by trichloroacetic acid (TCA). The insoluble fraction was washed with double-distilled water. The soluble and insoluble fractions were analysed by SDS-PAGE and Western blotting analysis.

Purification of rPmDNV capsid protein

Induced *E. coli* cells expressing the *Pm*DNV capsid protein were lysed with lysis buffer, and proteins were pelleted by centrifugation. The *Pm*DNV capsid protein was purified using Ni+ - NTA affinity chromatography and anionic denaturing detergents according to a previously published method (Schlager, Straessle & Hafen 2012). The cell pellet was resuspended in PCL buffer (8 mM Na_2HPO_4, 286 mM NaCl, 1.4 mM KH_2PO_4, 2.6 mM KCl, 1% SDS (w/v), pH 7.4), and the suspension was sonicated at room temperature for 2 min and incubated on ice for 30 min. Soluble proteins were separated by centrifugation at 7150xg for 20 min at 4°C and then concentrated using an Amicon Ultra-4 MWCO 10 kDa (Merck Millipore, Merck KGaA, Darmstadt, Germany) spin column. The solution was subsequently increased to 5 mL with PCW binding buffer (8 mM Na_2HPO_4, 286 mM NaCl, 1.4 mM KH_2PO_4, 2.6 mM KCl and 0.1% sarkosyl (w/v), pH 7.4) and was then loaded onto a Ni^+-NTA affinity column (HisTrap HP; GE Healthcare, Sweden) which was then washed with PCW buffer. The recombinant *Pm*DNV capsid protein was purified by gradient elution of PCE buffer (8 mM KH_2PO_4, 286 mM NaCl, 1.4 mM KH_2PO_4, 2.6 mM KCl, 0.1% sarkosyl (w/v), pH 7.4) containing 40, 100, 200, 300 and 500 mM imidazole, respectively. The remaining protein was eluted by washing the column with stripping buffer (PCW buffer containing 50 mM EDTA). Fractions were subsequently analysed by SDS-PAGE and Western blotting analysis. Protein concentration was determined by the Bradford assay.

Electron microscopy

The purified r*Pm*DNV mature capsid protein was concentrated using an Amicon Ultra-4 MWCO 10 kDa (Merck Millipore, Merck KGaA) spin column, and the purified protein was dropped onto a carbon grid. After incubation for 5 min at room temperature, the purified protein was stained with 1% phosphotungstic acid (PTA) for 5 min at room temperature. The carbon grids were subsequently visualized with a JEOL JEM-1400 electron microscope operating at 120 kV.

Results and discussion

Cloning PmDNV capsid protein

Some viral capsid proteins have the ability to form into virus-like particles, with the potential encapsulation of heterologous DNA, RNA or other molecules. While the full-length capsid protein has been used to make virus-like particles for some shrimp viruses such as IHHNV (Hou et al. 2009) and *Mr*NV (Goh et al. 2011), the *Pm*DNV capsid protein has an N-terminal cleavage site (Sukhumsirichart et al. 2006). Therefore, this study sought to clone the mature capsid protein. To generate PmDNV virus-like particles, specific primers were used to amplify a portion of the PmDNV genome, with the insert generated being subsequently cloned into the pET28a expression vector. Finally, the identity of the clones was confirmed by DNA sequencing. Alignment of the deduced amino acid sequences with the *Pm*DNV capsid protein sequence data from GenBank (Accession No. AAY84085) showed some minor amino acid differences (Fig. 1), which may reflect natural variation in the genome sequence.

Expression and solubility testing of rPmDNV capsid protein

Expression of the recombinant protein was induced by the addition of 0.4 mM IPTG and culture at 30°C for 3 h, and Western blotting analysis of the expressed protein lysate showed a band of approximately 64 kDa that was immunoreactive to both anti-*Pm*DNV and antihistidine monoclonal antibodies (Fig. 2), respectively. In addition, a lower band was also detected that might be the result of incomplete disruption of disulphide bonds by the SDS sample buffer. To determine protein solubility, the soluble and insoluble fractions of induced cells expressing r*Pm*DNV capsid protein were analysed by SDS-PAGE and Western blotting analysis. The result showed that the mature *Pm*DNV capsid protein was mostly expressed in an insoluble form (Fig. 3).

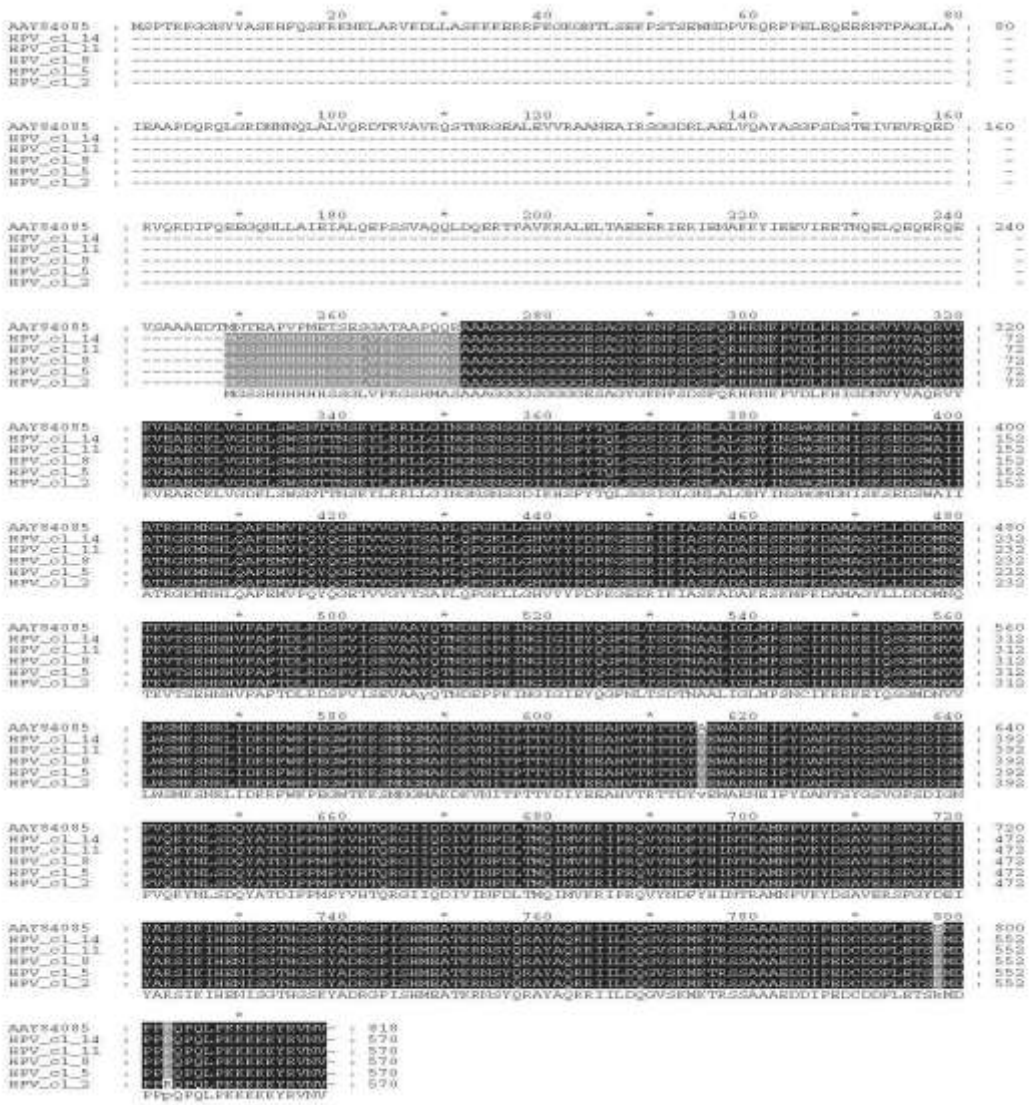

Figure 1 Alignment of the deduced amino acid sequence of recombinant mature *Pm*DNV capsid protein clones with the GenBank sequence (Accession No. AAY84085).

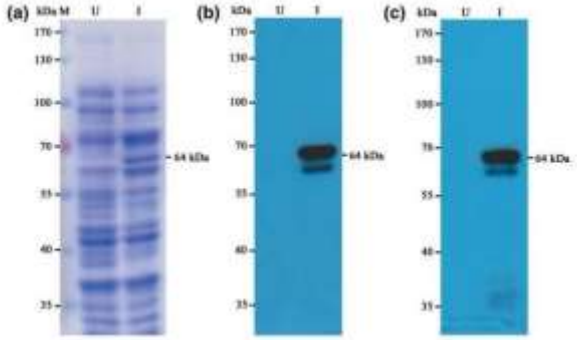

Figure 2 SDS-PAGE and Western blotting analysis of mature r*Pm*DNV capsid protein in *E. coli* Rosetta-gami (pLysS). (a) SDS-PAGE analysis, (b) Western blotting analysis with antihistidine and (c) anti-*Pm*DNV monoclonal antibodies. Lane M: prestained protein marker; Lane U: uninduced *E. coli* Rosetta-gami r*Pm*DNV; Lane I: induced *E. coli* Rosetta-gami r*Pm*DNV.

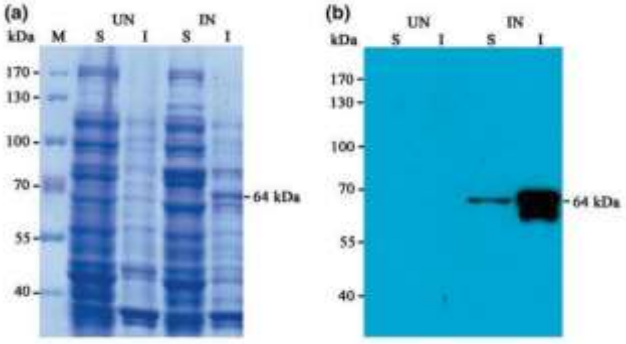

Figure 3 SDS-PAGE and Western blotting analysis of solubility of rPmDNV mature capsid protein. (a) SDS-PAGE and (b) Western blotting analysis using an antihistidine monoclonal antibody UN: uninduced and IN: induced. Lane M: prestained protein marker; Lane S: soluble fraction; Lane I: inclusion fraction in and E. coli Rosetta-gami (pLysS) using lysis buffer extraction.

Purification of rPmDNV capsid protein and PmDNV-VLPs assembly

To purify the r*Pm*DNV mature capsid protein, the soluble fraction of induced cell lysates were loaded onto nickel affinity columns and after washing, the proteins were eluted with imidazole concentrations ranging from 40 to 500 mM, and the fractions were subjected to analysis by SDSPAGE and Western blotting. The results showed that the r*Pm*DNV capsid protein was eluted with PCE Buffer containing 200 mM imidazole (Fig. 4). The eluted r*Pm*DNV mature capsid protein was concentrated and dropped onto carbon-coated grids and stained with 1% phosphotungstic acid. After staining, the grids were examined under a transmission electron microscope. The results (Fig. 5) showed that the purified r*Pm*DNV mature capsid protein was able to form VLPs by selfassembly, and the size and shape of *Pm*DNV-VLPs were similar to the native *Pm*DNV virions (Flegel 2006). The results of this study show that the mature *Pm*DNV

capsid protein can be assembled in vitro to form virus-like particles. This indicates that the folding of the expressed *Pm*DNV capsid protein was not affected by histidine fusion (Hou et al. 2009; Goh et al. 2011), and post-translational modification is not necessary for the protein to fold. Previous evidence has shown that virus-like particles are able to carry plasmid, single-stranded RNA or double-stranded RNA into host cells (Hou et al. 2009; Jariyapong, Chotwiwatthanakun, Somrit, Jitrapakdee, Xing, Cheng & Weerachatyanukul 2014; Jariyapong, Chotwiwatthanakun, Direkbusarakom, Hirono, Wuthisuthimethavee & Weerachatyanukul 2015). Thus, the PmDNV-like particles that were developed in this study can be further applied to deliver plasmid or dsRNA into shrimp for activation of innate immune responses to protect shrimp against viral infection.

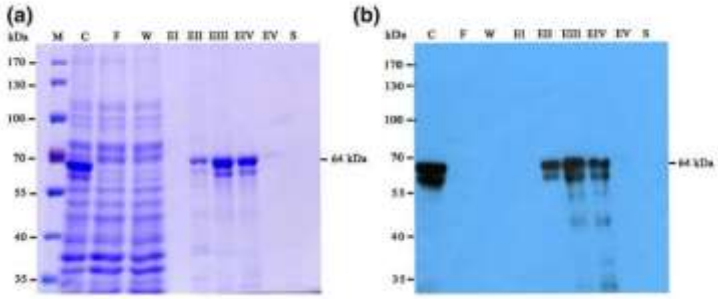

Figure 4 SDS-PAGE and Western blotting analysis of purified r*Pm*DNV protein using HisTrap column (a) SDSPAGE and (b) Western blotting analysis using antihistidine monoclonal antibody. Lane M: prestained protein marker; Lane C: induced recombinant cpPmDNV; Lane F: flow through; Lane W: wash; Lane EI-EV: elute recombinant cpPmDNV with PCW buffer containing 40, 100, 200, 300 and 500 mM Imidazole, respectively; Lane S: strip.

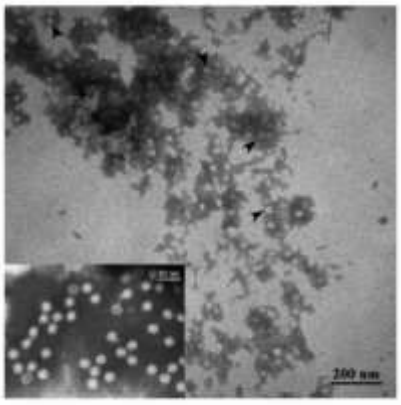

Figure 5 Electron micrographs of *Pm*DNV-VLPs (arrowed). Insert shows EM of native semipurified hepatopancreatic parvovirus from P. monodon (*Pm*DNV) and is reprinted from Aquaculture 258, Flegel, T.W.. Detection of major penaeid shrimp viruses in Asia, a historical perspective with emphasis on Thailand. Pages 1–33, Copyright (2006), with permission from Elsevier.

References

1. Buonaguro L., Tagliamonte M., Tornesello M.L. & Buonaguro F.B. (2011) Development in virus-like particle-based vaccines for infectious diseases and cancer. Vaccine 10, 1569–1583.
2. Ceccaldi H.J. (1989) Anatomy and physiology of digestive tract of crustaceans decapods reared in aquaculture. Advance Tropical Aquaculture 9, 243–259.
3. Correa A. & Oppezzo P. (2015) Overcoming the solubility problem in E.coli: available approaches for recombinant protein production. In: Insoluble Proteins: Methods and Protocols (ed. by E. Garcia-Fruitos), pp. 27–44. Springer Science+Business Media, New York, NY, USA.
4. Dhar A.K., Robles-Sikisaka R., Saksmerprome V. & Lakshman D.K. (2014) Biology, genome organization and evolution of Parvoviruses in marine shrimp. Advances in Virus Research 89, 85 –129.
5. Enomoto T., Kukimoto I., Kawano M., Yamaguchi Y., Berk A.J. & Handa H. (2011) In vitro reconstitution of SV40 particles that are composed of VP1/2/3 capsid protein and nucleosomal DNA and direct efficient gene transfer. Virology 420,1 –9.
6. Flegel T.W. (2006) Detection of major penaeid shrimp viruses in Asia, a historical perspective with emphasis on Thailand. Aquaculture 258,1 –33.
7. Goh Z.H., Tan S.G., Bhassu S. & Tan W.S. (2011) Viruslike particles of Macrobrachium rosenbergii nodavirus produced in bacteria. Journal of Virological Methods 175, 74 –79.
8. Hou L., Wu H., Xu L. & Yang F. (2009) Expression and self-assembly of virus-like particles of infectious hypodermal and hematopoietic necrosis virus in *Escherichia coli*. Archives of Virology 154, 547–553.
9. Jariyapong P., Chotwiwatthanakun C., Somrit M., Jitrapakdee S., Xing L., Cheng H.R. & Weerachatyanukul W. (2014) Encapsulation and delivery of plasmid DNA by virus-like nanoparticles engineered from Macrobrachium rosenbergii nodavirus. Virus Research 179, 140–146.
10. Jariyapong P., Chotwiwatthanakun C., Direkbusarakom S., Hirono I., Wuthisuthimethavee S. & Weerachatyanukul W. (2015) Delivery of double stranded RNA by Macrobrachium rosenbergii nodavirus-like particles to protect shrimp from white spot syndrome virus. Aquaculture 435, 86 –91.
11. Liew M.W.O., Chuan Y.P. & Middelberg A.P.J. (2012) High yield and scalable cell-free assembly of virus-like particles by dilution. Biochemical Engineering Journal 67, 88 –96.
12. Ou W.C., Wang M., Fung C.Y., Tsai R.T., Chao P.C., Hseu T.H. & Chang D. (1999) The major capsid protein, VP1, of human JC virus expressed in *Escherichia coli* is able to self-assemble into a capsid-like particle and deliver exogenous DNA into human kidney cells. Journal of General Virology 80, 39 – 46.
13. Safeena M.P., Rai P. & Karunasagar I. (2012) Molecular biology and epidemiology of Hepatopancreatic parvovirus of Penaeid shrimp. Indian Journal of Virology 23, 191–202.
14. Schlager B., Straessle A. & Hafen E. (2012) Use of anionic denaturing detergents to purify insoluble proteins after overexpression. BMC Biotechnology 12,1 –7.

15. Shao W., Paul A., Abbasi A., Chahal P.S., Mena J.A., Montes J., Kamen A. & Prakash S. (2012) A novel polyethyleneimine-coated adeno-associated virus-like particle formulation for efficient siRNA delivery in breast cancer therapy: preparation and in vitro analysis. International Journal of Nanomedicine 7, 1575–1586.
16. Srisuk C., Chaivisuthangkura P., Sukhumsirichart W., Sridulyakul P., Longyant S., Rukpratanporn S. & Sithigorngul P. (2011) Improved immunodetection of *Penaeus monodon* densovirus with monoclonal antibodies raised against recombinant capsid protein. Aquaculture 311, 19 –24.
17. Sukhumsirichart W., Attasart P., Boonsaeng V. & Panyim S. (2006) Complete nucleotide sequence and genomic organization of Hepatopancreatic parvovirus (HPV) of *Penaeus monodon*. Virology 346, 266–277.

Suppression of PmRab11 inhibits YHV infection in *Penaeus monodon*

Yellow head virus (YHV) is one of the most serious pathogens that causes worldwide shrimp production loss. It enters the cells via clathrin-mediated endocytosis and utilizes small GTPase Rab proteins such as PmRab5 and PmRab7 for intracellular trafficking. In this study, molecular cloning and functional analysis of Rab11 during YHV infection were investigated. PmRab11 cDNA was cloned by Rapid amplification of cDNA ends (RACEs). It contained two forms of sizes 1200 and 1050 bp distinct at the 5′ UTR. The coding region of PmRab11 was 645 bp, encoding 214 amino acids. It also demonstrated the characteristics of Rab11 proteins containing five GTP-binding domains, five Rab family domains, four Rab subfamily domains and a prenylation site at the C-terminus. Suppression of PmRab11 using dsRNA-PmRab11 either before or after YHV-challenge resulted in significant inhibition of YHV levels in the hemocytes and viral release in the supernatant in both mRNA and protein levels. In addition, the silencing effect of PmRab11 in YHV-infected shrimps resulted in a delay in shrimp mortality for at least 2 days. Immunofluorescence study showed co-localization between PmRab11 and YHV at 24e72 h post YHV-challenge. In contrast, the co-localization signals were absence in the PmRab11 knockdown hemocytes and the YHV signals accumulated at the perinuclear region at 24 h post YHV-challenge. Then, accumulation of YHV was hardly observed after 48e72 h. These results suggested that PmRab11 is required for YHV infection in shrimp.

Introduction

Thailand is the world's important exporter of shrimp products, especially the black tiger shrimp, *Penaeus monodon*. At present, losses of shrimp production are caused by various viral diseases. One of the major causative agents is the yellow head virus (YHV) which causes extensive and rapid mortality in black tiger shrimp [1,2]. YHV is a positive sense, single-stranded RNA virus that is classified as a member of Gill-associated virus, belonging to the genus Okavirus, family Roniviridae in the order Nidovirales [3]. YHV genome is approximately 26 kb, containing four long open reading frames (ORF1a, ORF1b, ORF2, and ORF3) [4e6]. The enveloped rod-shaped YHV particles are 150–200 nmin length and 40–50 nm in diameter [1,7]. The virion has prominent surface spikes and contains internal helical nucleocapsid [8,9]. It contains three structural proteins, the transmembrane glycoproteins gp116 and gp64 are found in the viral envelope, and the nucleoprotein p20 [6,10].

Recently, the mechanism of YHV transportation has been proposed. After YHV enters into the cell, it is transported via endosomal compartments [11,12] and released its genome into the cytoplasm for replication. Then, the nucleocapsid is synthesized and transported to the ER-Golgi compartment where the envelope is formed [2,13]. Finally, the enveloped viral particle is exocytosed at the plasma membrane. However, this exocytosis process of YHV out of the cells is not well understood. Normally, enveloped viruses are budded at the membrane in order to generate the envelope that surrounded the nucleocapsid [14]. In this process, the nucleocapsid is wrapped in a cellular membrane containing virus-specific envelope proteins. The viral envelope protein serves to target the host cell receptor [15]. Some viruses bud at the plasma

membrane (PM), whereas others are assembled and budded at intracellular membranes along the secretory pathway such as the nuclear envelope, rough and smooth endoplasmic reticulum (ER), endosomes, intermediate or pre-Golgi compartment, Golgi cisternae and the trans-Golgi-network (TGN) [16]. However, the cytoplasmic transportation of viral genome or viral particle to plasma membrane requires the host proteins

One of the cellular proteins that is involved in intracellular trafficking process is Rab11. Rab11 is a small GTPase protein belongs to the Ras superfamily, whose function is in transportation of the vesicles through the TGN [17], apical recycling of endosomes [18] and the perinuclear recycling of endosomal compartments before redirecting the vesicular cargo back to the apical plasma membrane. The Rab GTPase protein acts as molecular switches that shuffle between two conformational states, the GTP bound 'active' form and the GDP-bound 'inactive' form. In the active form, Rab protein is associated with membranes by hydrophobic geranylgeranyl groups at the C-terminal and recruited the specific effector molecules such as sorting adaptors, tethering factors, kinases, phosphatases and motor proteins in vesicle transport process [18]. Our previous studies found that several Rab proteins are hijacked by YHV [11,12]. Specifically, the transportation of YHV particles required PmRab5 which is a key protein in vesicles transport to early endosome; whereas, PmRab7 is involved in YHV transportation from early endosome to late endosome and lysosome. The silencing effects of PmRab5 or PmRab7 in YHV-infected *P. monodon* inhibited YHV expression, suggesting that PmRab5 and PmRab7 are involved in intracellular trafficking of YHV [11,12].

Recently, several evidence revealed that some RNA viruses such as vesicular stomatitis virus, sendai virus, influenza A, measles virus, mumps virus, and hantavirus use Rab11-dependent pathway to assemble and release out of the cells [19e25]. Whether YHV which is also a e RNA viruse requires Rab11 for its transport out of the cell remains to be elucidated. Furthermore, subtractive hybridization study found that RAB11 is one of the responsive genes that is upregulated after YHV infection [26]. Therefore, here, molecular cloning of the full-length cDNA in *P. monodon* Rab11 (PmRab11) and its probable function during YHV infection were performed.

Materials and methods

Black tiger shrimp culture

Juvenile viral-free pathogen black tiger shrimps (*P. monodon*) of about 10–30 g were obtained from commercial shrimp farms in Thailand. Before use, shrimps were tested for YHV and white spot syndrome virus infection by using diagnostic strip test (Pacific Biotech Co. Ltd., Thailand). Shrimps were grown in a plastic box containing oxygenated seawater at 10 ppt salinity and were acclimatized for 2 days before the experiment was carried out. They were fed with commercial shrimp feed every day. The salt water was changed every 2 days.

Yellow head virus (YHV) stock

The infectious YHV was propagated by injection of YHV to viral free shrimp. Then, hemolymph was collected from YHV-infected moribund shrimp and mixed with AC-1 solution (27 mM Sodium citrate, 34.33 mM NaCl, 104.5 mM Glucose, 198.17 mM EDTA, pH 7.0). Next, the hemolymph was centrifuged at 20,000xg for 20 min at 4°C to remove hemocyte debris. Free YHV particles were collected by ultracentrifugation

(100,000xg) for 1 h. Virus pellets were suspended with 150mMNaCl and stored at –80°C until used. The viral nucleic acid was purified from the YHV stock using high pure viral nucleic acid kit (Roache Diagnostics, Germany) and subjected to RT-PCR to determine viral titer using primers YHV_F: 5′-CAAGGACCACCTGGTACCGGTTAAGAC-3′ and YHV_R: 5′-GCGGAAACGACTGACGGCTACATTCAC-3′ [11].

Molecular cloning of the full length PmRab11cDNA

The partial sequence of PmRab11 served as template to design primers for 5′ and 3′ RACE. 5′ and 3′ RACE were performed as previously described [11]. Briefly, 5′ RACE method was performed by using 5Rab11_R1 specific primer (Table 1) to generate the first strand cDNAs by Superscript III® reverse transcriptase (Invitrogen). Then, 5Rab11_R1 and PRT primers (Table 1) were used to synthesize the first PCR product which was diluted to 1: 100 for used as template in the nested PCR with 5Rab11_R2 and PM1 primers (Table 1). To obtain the 3′ end of PmRab11 cDNA, 3′ RACE PCR was performed by PRT primer to generate the first-strand cDNAs. Then, the PCR reaction containing 3Rab11_F1 and PM-1 primers was performed. Next, two nested PCRs were performed using 3Rab11_F2 and PM-1 primers and 3Rab11_F3 and PM-1 primers (Table 1). Then, all expected bands of the 5′ and 3′ RACE PCR products were purified by Gel/PCR fragments extraction kit (Geneaid), cloned into pGEM-T-easy vector (Promega) and sequenced (First Base Co. Ltd, Malaysia).

The sequences of the 5′ and 3′ ends obtained from RACE-RCR were assembled together with the partial sequence of PmRab11 in order to obtain the full-length cDNA by using Contig Express tool from Vector NTI Advance 11.5.1 program. Finally, a PCR was performed to amplify the full-length PmRab11 cDNA using *Taq* DNA polymerase (New England Biolabs) with primers that were designed based on the 5′ and 3′ end sequences, fullRab11_F and fullRab11_R primers (Table 1). PCR condition was: 95°C for 5 min, followed by 30 cycles of 95°C for 30 s, 51°C for 30 s, 72°C for 1.30 min and 72°C for 7 min in the final step. Finally, the PCR product was purified, cloned and subjected to sequence following the protocol that was described earlier.

Table 1 List of synthetic oligonucleotide primers.

Name	Sequences (5′……3′)	Experiments
PRT	CCGGAATTCAAGCTTCTAGAGGATCCTTTTTTTTTTTTTTT	Reverse transcription
5Rab11_R1	GGCCGTCTCTACATTAGTGGAGCC	5′RACE
5Rab11_R2	ATTCTGATCTGCATGATCTCTGAGC	
3Rab11_F1	CACTTACACTAATGTAGAACGTTGGC	3′RACE
3Rab11_F2	GCTGATGTTAAGGCTATTCACGTGG	
3Rab11_F3	AAGGCATTTGCAGAAAAGGAGGGAC	
PM1	CCGGAATTCAAGCTTCTAGAGGATCC	
FullRab11_F	GGA GAG GCG TAA CGG TTC GC	Full-length
FullRab11_R	TTTTTTTTTAGAGAACAGGACAAACAGAG	
slRab11_F	GCTCTAGATCCACCATTGGTGTTGAG	Sense-loop of dsRNA
slRab11_R	GGGGTACCGCATTTACAGTTGGTTCCAC	
asRab11_F	GGAATTCCCCTCGAGTCCACCATTGGTGTTGAG	Antisense of dsRNA
asRab11_R	GGGGTACCACAATGCGGTAGATTTCTG	
PmRab11_F	ATGGGGAACAGGGACGACGAGTATG	Detection of PmRab11
PmRab11_R	GGCCTCTTCTGTGGGAACTGACCGC	
PmRab5_F	GGAGCTGCATTTCTGACACAGACAG	Detection of PmRab5
PmRab5_R	GGTCTGGGCCTCTTCATATTCAACC	
PmRab7_F	ATGGCATCTCGCAAGAAGATT	Detection of PmRab7
PmRab7_R	TTAGCAAGAGCATGCATCCTG	
PmActin_F	GACTCGTACGTCGGGCGACGA	Detection of PmActin
PmActin_R1	AGCAGCGGTGGTCATCACCTG	
PmActin_R2	CGTAGATGGGCACGGTGTGGG	
YHV_F	CAAGGACCACCTGGTACCGGTTAAGAC	Detection of YHV
YHV_R	GCGGAAACGACTGACGGCTACATTCAC	

Sequence analysis of PmRab11

The full-length cDNA sequence of PmRab11 was analyzed against the NCBI's blastn database (http://blast.ncbi.nlm.nih.gov/ Blast.cgi). The coding sequences were translated to amino acid sequence by using Expasy's tool (http://web.expasy.org/translate/). Amino acid sequence identity between PmRab11 and Rab11 proteins of other species was performed by using alignX of Vector NTI. In addition, the initiation codon and poly-A signal were identified by using ATGpr (http://atgpr.dbcls.jp/) and Poly (A) signal miner (http://dnafsminer.bic.nus.edu.sg/PolyA.html). Multiple sequence alignment of PmRab11 was performed to identify the conserved domains of Rab11 protein by using the conserved domain database of NCBI (http://www.ncbi.nlm.nih.gov/Structurecdd/wrpsb.cgi). Prenylation site was identified by using Prenylation Prediction Suite (http://mendel.imp.ac.at/PrePS/)., Phylogenetic tree analysis of PmRab11 was performed based on the neighbor-joining methods (http://www.phylogeny.fr/) [27]. The phylogeny was constructed by phylogeny frunder "One Click" mode. The pipeline is already set up to run and connect well recognized programs: MUSCLE for multiple alignment, Gblocks for automatic alignment curation, PhyML for tree building and TreeDyn for tree drawing.

Construction of recombinant plasmid expressing dsRNAPmRab11

A recombinant plasmid containing sense-loop and antisense fragment of PmRab11 was constructed using pGEM®-3zf(+) vector (Promega) as a plasmid backbone. A sense-loop fragment of size 494 bp was amplified from PmRab11 cDNA using slRab11_F and slRab11_R primers containing *Xba*I and *Kpn*I sites, respectively (Table 1). The amplification of the antisense fragment of size 404 bp was performed using asRab11_F and asRab11_R primers containing *Eco*RI/ *Xho*I and *Kpn*I, respectively (Table 1). Then, the sense and antisense fragments were cloned into pGEM®-3zf(+) vector to obtain a recombinant clone containing the stem-loop fragment of PmRab11. Then, the stem-loop fragment, size 898 bp, was digested by *Hin*dIII and *Xho*I and subcloned to an expression vector, pET-17b to produce dsRNA-PmRab11 by in vivo bacterial expression. The region of dsRNA-PmRab11 is located at the nucleotides 124–510 from the start codon. In addition, a recombinant plasmid containing a stem-loop fragment of GFP (kindly provided by Asst. Prof. Witoon Tirasophon) was used to express dsRNA-GFP which served as an unrelated dsRNA [28].

Expression and extraction of dsRNA-PmRab11

A recombinant plasmid pET-17b containing a stem-loop of PmRab11 was transformed into *E. coli* HT115 which is a ribonuclease III mutant strain to produce dsRNA-PmRab11 [28]. dsRNAPmRab11 expression was induced by 0.1 mM IPTG. dsRNA-PmRab11 was extracted and purified by ethanol method [29]. The quality of dsRNAwas characterized by ribonuclease digestion assay using RNase A and RNase III (New England Biolab, USA). Yield of dsRNA-PmRab11 was determined by agarose gel electrophoresis and compared to the intensity of 2-log DNA marker. The intensity was measured by an ImageJ program.

Suppression of PmRab11 expression by dsRNA-PmRab11

In order to determine specific inhibition of PmRab11 expression, injection of dsRNA-PmRab11 was performed. Shrimps were injected in the muscle with 1.25 or 2.5 µg/g shrimp of dsRNA-PmRab11. Injection of unrelated dsRNA-GFP and 150 mM

NaCl were used as controls. Then, hemolymph from individual shrimp was collected at 24, 48 and 72 h post-dsRNA or NaCl injection and mixed with anticoagulants I (27 mM sodium citrate, 34.33 mM NaCl, 104.5 mM glucose, 198.17 mM EDTA, pH 7.0) in a ratio 1:1. Total RNAs was extracted from hemolymph by TRI REAGENT® LS (Molecular Research Center). Semi-quantitative RT-PCR was performed to monitor the levels of PmRab11 expression using PmRab11 specific primers. In addition, to examine the specificity of the knockdown effect of PmRab11, these cDNAs were used as templates for detection of other Rab genes expression using PmRab5 and PmRab7 specific primers (Table 1) [11,12].

Suppression effect of PmRab11 during YHV infection

To investigate the function of PmRab11 on YHV infection, shrimps were intramuscularly injected with dsRNA-PmRab11 at 1.25 µg/g shrimp. Injection of 150 mM NaCl and unrelated dsRNAGFP were used as control groups. After 24 h, shrimps were challenged with 10^{-2} dilution of YHV (dose of YHV that leads to 100% mortality within 3 days). The hemolymph was collected at 24, 48, 72 and 96 h post-YHV challenge. Then, the hemocytes and supernatant were fractionated by centrifugation at 650xg for 15 min. Total RNAs in hemocytes and supernatant were extracted by TRI REAGENT® and TRI REAGENT® LS (Molecular Research Center), respectively. The levels of PmRab11 and YHV expression were monitored by semi-quantitative RT-PCR using PmRab11 and YHV specific primers (Table 1), respectively. PmActin was used as an internal control. Finally, the relative expressions of PmRab11 and YHV in hemocytes were normalized by PmActin. However, PmActin cannot be amplified from the supernatant fraction, thus the YHV levels was analyzed from equal amount of the total RNAs.

RNA isolation and RT-PCR

Total RNA from hemocytes or supernatant was isolated by Trizol® reagent (Molecular Research Center) following the manufacturer's procedure. The RNA concentration was measured by Nanodrop ND-1000 spectrophotometer (Nanodrop Technologies). Total RNAs (2 µg) was used as template to generate the first-strand cDNA by Improm-II™ reverse transcriptase (Promega) using PRT primer (Table 1). PmRab11 expression was monitored by multiplex PCR using PmRab11-F and PmRab11-R primers and PmActin-F and PmActin-R1 primers for PmActin detection which served as an internal control. The PCR was carried out according to this condition: 95°C for 5 min, followed by 30 cycles of 95°C for 30 s, 61°C for 30 s, 72°C for 45 s and 72°C for 7 min in the final step. Expressions of PmRab5, PmRab7 and YHV were determined according to the previous methods [11,12]. PCR products were analyzed on 1.5% agarose gel electrophoresis. The intensity of each band after subtracting the background was quantified by using ImageJ program (Version 1.50b). The relative expression level of the gene of interest was normalized against PmActin level and expressed as an arbitrary unit.

Investigation of protein levels of YHV in hemocytes and supernatant

In order to investigate YHV protein levels in hemocytes and supernatant of the complete PmRab11 knockdown shrimp, shrimps were injected with dsRNA-PmRab11 at 1.8 mg/g shrimp by intramuscular injection. Injection of NaCl and unrelated dsRNA-

GFP were used as control groups. After 24 h, shrimps were challenged with 10^{-2} dilution of YHV by intramuscular injection. The hemolymph was collected at 24, 48, 72 and 96 h post-YHV injection. The hemolymph from 3 shrimps in the same group at the same time was pooled. Then, total RNA from 200 µl of the pooled hemolymph was extracted by TRI REAGENT® LS method and RT-PCR was performed in order to detect PmRab11 and YHV expression at mRNA level. To extract total protein for Western blot analysis, 2 ml of the pooled hemolymph was fractionated to separate hemocytes and supernatant by centrifugation at 650xg. Total proteins from hemocytes were extracted by using 100 µl buffer T (8M urea, 2 M thiourea, 0.4% Triton X-100, 60 mM DTT, 1 mM PMSF, 1 x Protease inhibitor cocktail (Sigma)). Whereas, total proteins from 100 µl of supernatant were precipitated by 10% TCA at final concentration and dissolved in 100 µl of buffer T. Then, Western blot was performed to detect YHV level in both fractions.

Western blot analysis

Hemocyte and supernatant proteins were extracted by using buffer T. The protein lysate (50 µg) was electrophoresed in 12% SDS poly acrylamide gel (SDS-PAGE). Then, proteins were transferred from gel onto a nitrocellulose membrane (Bio-Rad) by electrophoresis with 1X transfer buffer [0.025 M Trise-HCl pH 8.3, 0.192 M glycine, and 20% (v/v) methanol]. Then the membrane was blocked with blocking solution [5% skimmed milk in 0.2% PBST (0.2% (v/v) Tween-20 in 1X PBS)] for 2 h. Next, the membrane was soaked with 0.05% PBST (0.2% (v/v) Tween-20 in 1X PBS) containing primary antibody for 2 h. To detect YHV levels, the mouse anti-gp64 antibody was used as primary antibody at the dilution 1: 1000 in 0.2% PBST. In addition, dilution 1: 1000 in 0.2% PBST of the rabbit anti-β-tubulin primary antibody was used to detect β-tubulin which is an internal control. Then, the primary antibody was removed. The membrane was washed with 0.2% PBST for 10 min, 3 times and incubated with blocking solution containing horseradish peroxidase- conjugated secondary antibody (Sigma) in dilution 1:5000. Then, the membrane was washed 1 time with 0.2% PBST and 3 times with 1X PBST. Finally, the signal was detected by adding the Luminata™ Forte Western HRP Substrate (Millipore Corporation) for 5 min and exposed to X-ray film. PmRab11 and b-tubulin have sizes of about 23 and 60 kDa, respectively.

Shrimp mortality assay

Suppression effects of PmRab11 with or without YHV challenge on shrimp mortality were investigated. Shrimps size about 1 g (n = 15 shrimps per group) were injected with 1.25 or 2.5 µg/g shrimp of dsRNA-PmRab11 24 h with or without YHV challenge. Injection of 150 mM NaCl and unrelated dsRNA-GFP were used as controls. The experiment was performed in triplicates and the number of dead shrimps were recorded every day for 10 days.

Immunofluorescence assay of YHV and PmRab11 in YHVinfected hemocytes

Shrimp was injected with 1.8 µg/g shrimp of dsRNA-PmRab11 24 h prior to YHV challenge. The injection of 150 mM NaCl and unrelated dsRNA-GFP were used as control groups. Then, 250 µl of hemolymph was collected at 24, 48 and 72 h after YHV challenge. The hemocytes were separated by centrifugation at 550xg for 10 min

at 4°C. Cell pellet was resuspended in 500 µl of L-15 medium. Then, hemocytes mixture was seeded in 24 wells plate containing a coverslip and incubated at room temperature. After for 2 h, culture media was discarded and 500 µl of ice cold 4% (w/v) paraformaldehyde was added into each wells. After incubation at room temperature for 20 min, the supernatant was removed and fixed hemocytes were washed with 1X PBS for 5 min, 3 times. Then, they were permeabilized by adding 350 µl of 0.1% (v/v) Triton X-100 in 1X PBS for 5 min. After the supernatant was discarded and the permeabilized hemocytes were proceeded to immunofluorescence staining according to the previous method [10]. Except that the rabbit polyclonal anti-Rab11 antibody (ab3612, Abcam, USA) and mouse monoclonal anti-gp64 of YHV antibody (kindly provided by Professor Paisarn Sithigorngul, Department of Biology, Faculty of Science, Srinakharinwirot University) were used. After washing, the secondary antibodies which are goat anti-rabbit IgG, Alexa Fluor® 596 and goat anti-mouse IgG, Alexa Fluor® 488 (Invitrogen) were used for detection of PmRab11 and YHV. The nuclei were stained by TO-PRO®-3 iodide (Invitrogen). Finally, a cover slip was mounted with 8 µl of ProLong antifade (Invitrogen). The slide was kept at 4°C until visualized under confocal microscope (Fluoview FV10i - DOC, Olympus).

Statistical analysis

The relative mRNA levels of PmRab11 normalized with PmActin were presented as mean ± standard error of mean (SEM). The statistical analysis of the relative mRNA expression levels was tested by using analysis of variance (ANOVA). A probability (P) value at less than 0.05 was used to define significant difference. Cumulative percent mortality was plotted as mean ± SEM.

Results

Full-length cDNA cloning and sequences analysis of PmRab11

The full-length cDNAwas obtained from 5′ and 3′ RACE protocol. It has 2 forms of sizes 1217 and 1065 bp with the same coding sequences of 645 bp. The 5′ and 3′ untranslated region (UTR) have sizes 247 bp and 324 bp, respectively (Fig. 1). The sequence of PmRab11 cDNA of 2 variants were submitted into the GenBank database under the accession number KY241479 and KY241480, respectively. PmRab11 protein has size of 214 aa. The theoretical pI and molecular weight are 5.22 and 23.85 kDa, respectively. In addition, this protein shared the characteristics of Rab11 protein family when compared to others species such as five GTP biding domains (G1-G5), five Rab family domains (RabF1-5), four Rab subfamily domains (RabSF1-4) and a prenylation site that usually terminated in CC or CXC motif at the C-terminus (Fig. 2). The amino acid sequence identity showed that PmRab11 protein shared 100% amino sequence identity with Rab11 of Pacific white shrimp (*Litopenaeus vannamei*) and shared approximately 80% with Rab11 of vertebrates such as zebrafish (*Danio rerio*). In addition, the phylogenetic tree revealed that PmRab11 protein was closely related to Rab11 of vertebrate and arthropods (Fig. 3). It was not clustered with other Rab proteins including Rab5, Rab6 and Rab7. These results indicate that PmRab11 is a highly conserved protein.

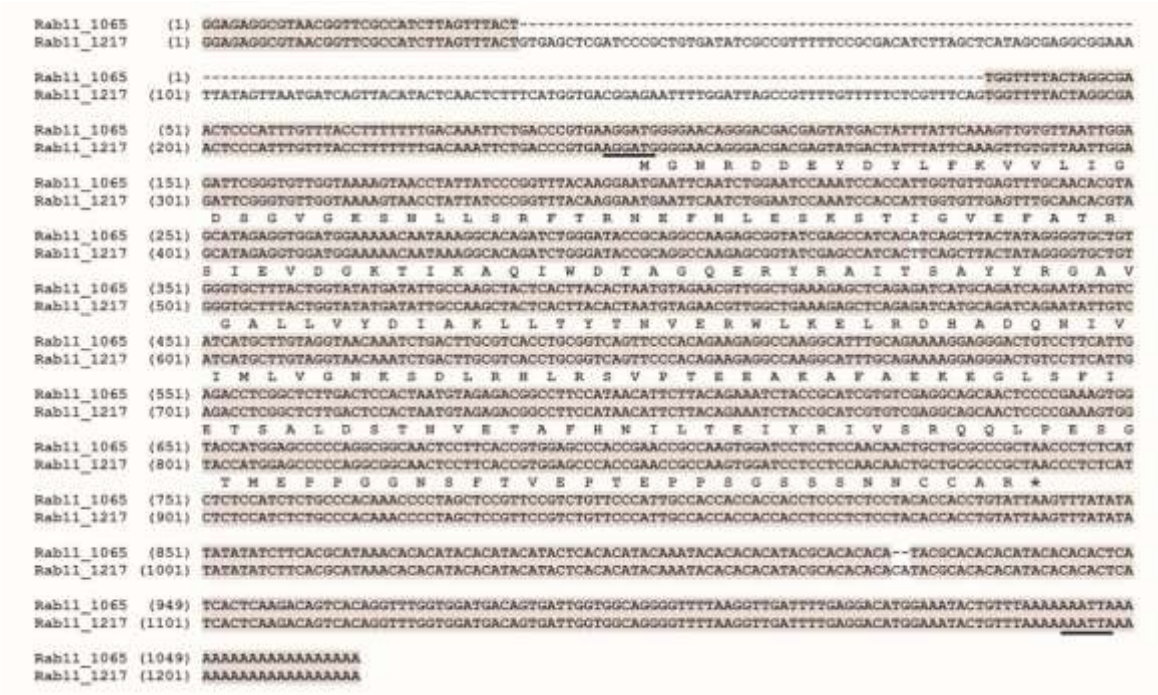

Fig. 1. Two forms of the full-length cDNAs and their deduced amino acid sequences of PmRab11. The full-length cDNA of PmRab11 has 2 forms of sizes 1217 and 1065 bp containing the open reading frame of size 645 bp. The deduced amino acid sequences of PmRab11 is represented in the capital letter under the respective codon. Kozak consensus sequences (AGGATG) and poly A signal (AAATTA) are indicated in underline.

Suppression of PmRab11 expression by dsRNA-PmRab11

To investigate whether the PmRab11 expression can be suppressed by using RNAi approach. Double-strands RNA targeting PmRab11 was produced and injected into shrimp muscle. The expression levels of PmRab11 in dsRNA-PmRab11 injected shrimp were signifi cantly reduced at more than 90%, 24 h post-dsRNAPmRab11 injection at both dosages (1.25 and 2.5 mg/g shrimp) when compared to 0 h. The suppression effect of PmRab11 was maintained for at least 72 h post-dsRNA injection ($P < 0.001$, n ¼ 4/time point) (Fig. 4A). As the nucleotide sequences of dsRNAPmRab11 contained many conserved domains such as Rab family domains, Rab subfamily domains and GTP binding domains, it is possible that some of the regions of dsRNA-PmRab11 are similar to other Rab genes. Therefore, a specific inhibition to PmRab11 expression was investigated. The results showed that suppression of PmRab11 by injection of dsRNA-PmRab11 has no effect on the levels of PmRab5 and PmRab7 expression from 24 to 72 h postdsRNA injection (Fig. 4B). Large standard deviation of PmRab7 after 24 h dsRNA injection may be due to varying expression of PmRab7 among shrimp samples.

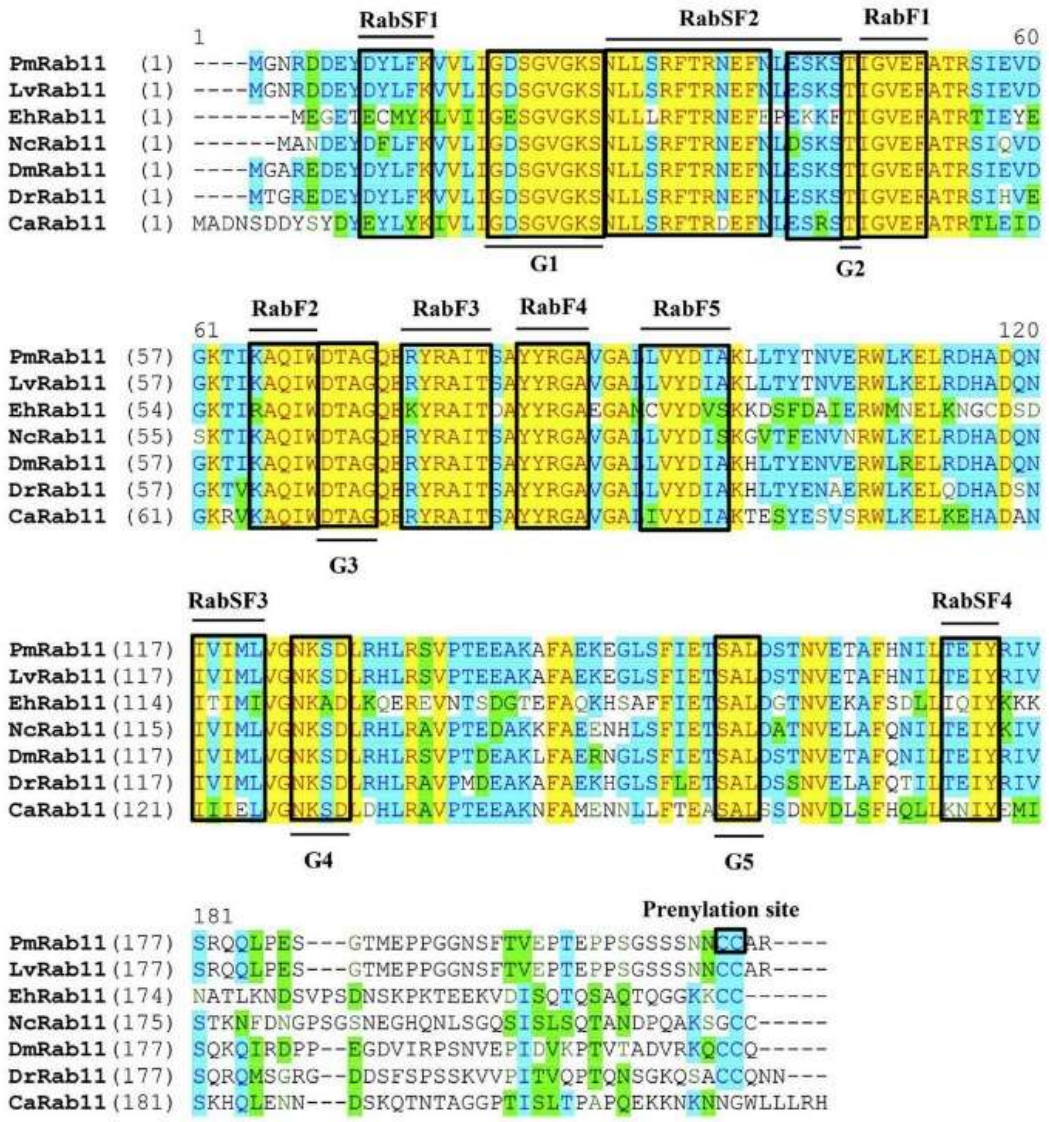

Fig. 2. Multiple sequence alignment showing conserved domains of PmRab11 compared to Rab11 proteins from other species. The conserved domains of PmRab11 shared characteristics of Rab11 among other species such as five GTP binding domains (G1-G5), five Rab family (RabF1-5) domains, four Rab subfamily (RabSF1-4) domains and a prenylation site (CCXX motif) at the C-terminus.

Suppression effect of PmRab11 during YHV infection

To investigate whether PmRab11 protein is essential for YHV transport out of the cell, suppression of PmRab11 was performed 24 h prior to YHV challenge. PmRab11 expression level in hemocytes was significantly decreased approximately 50% in shrimp injected with dsRNA-PmRab11 within 48 h post-dsRNA-PmRab11 injection. The knockdown effect of PmRab11 was increased to 75% at 72 and 96 h post-dsRNA injection ($P < 0.001$, $n = 4$/time point) (Fig. 5A). In addition, YHV levels

in hemocytes and supernatant of PmRab11 knockdown group were significantly decreased from 48 to 72 h post-YHV infection when compared to NaCl injected group ($P < 0.01$ for hemocytes and $P < 0.001$ for supernatant, $n = 4$/time point) (Fig. 5B and C). Notably, shrimps in 2 control groups died at 96 h while shrimp in PmRab11 knockdown group still alive at this time point.

Protein analysis revealed that an envelope glycoprotein gp64 of YHV cannot be detected in the hemocytes and supernatant of the PmRab11 knockdown group from 24 to 72 h post-YHV challenge. At 96 h post-YHV challenge, low levels of YHV can be detected in both hemocytes and supernatant while shrimp in both control groups died at this time point. On the other hand, high YHV level can be detected in hemocytes and supernatant of NaCl-injected groups at 48 and 72 h. However, low level of YHV expression can still be observed in dsRNA-GFP injected group at 48 h and even increased at 72 h post-YHV infection (Fig. 6A and B, Supplementary Fig. 1).

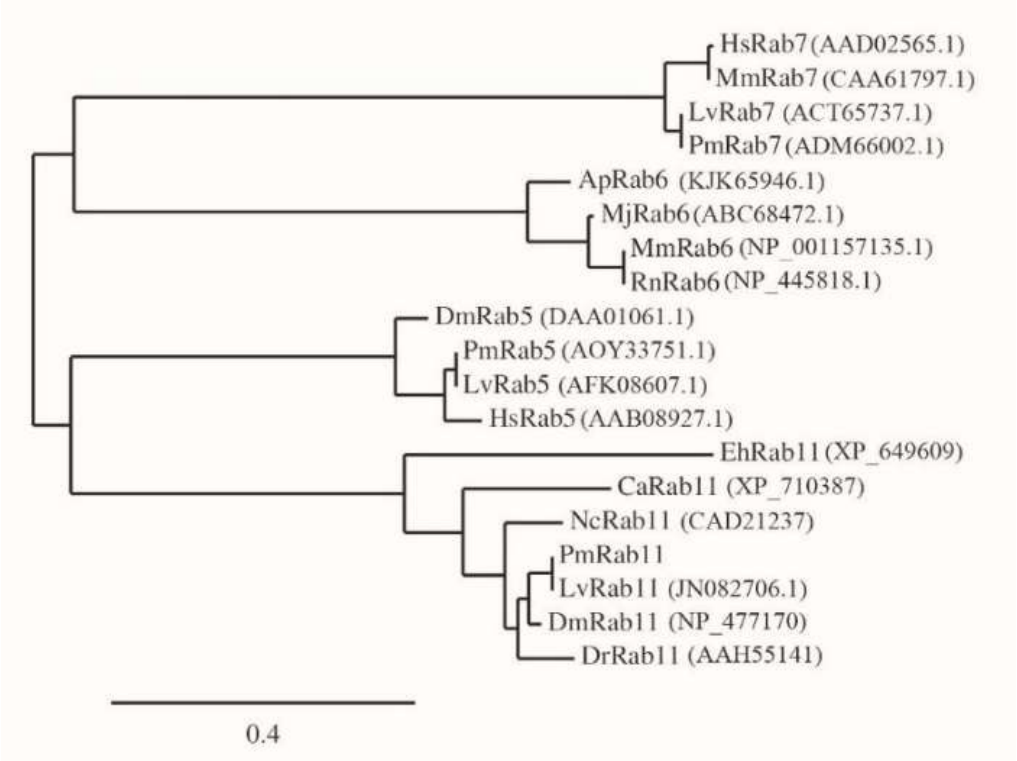

Fig. 3. Phylogenetic analysis of Rab11 of P. monodon compared with Rab11, Rab5, Rab6 and Rab7 of other species. The amino acid sequences of the coding region of Rab proteins of *P. monodon* and of other species were used to perform phylogenetic tree analysis based on the neighbor- joining methods by using the program from (http://www.phylogeny.fr/). The abbreviation of species is as follows: Homo sapiens (Hs), *Mus musculus* (*Mm*), *Litopenaeus vannamei* (*Lv*), *Penaeus monodon* (*Pm*), *Aspergillus parasiticus* (*Ap*), *Marsupeneus japonicus* (*Mj*), *Rattus norvegicus* (*Rn*), *Drosophila melanogaster* (*Dm*), *Entamoeba histolytica* (*Eh*), *Candida albicans* (*Ca*), *Neurospora crassa* (*Nc*), and *Danio rerio* (*Dr*). The accession number is in the parenthesis. PmRab11 cDNA of 2 variants were submitted into the GenBank database under the accession number KY241479 and KY241480, respectively.

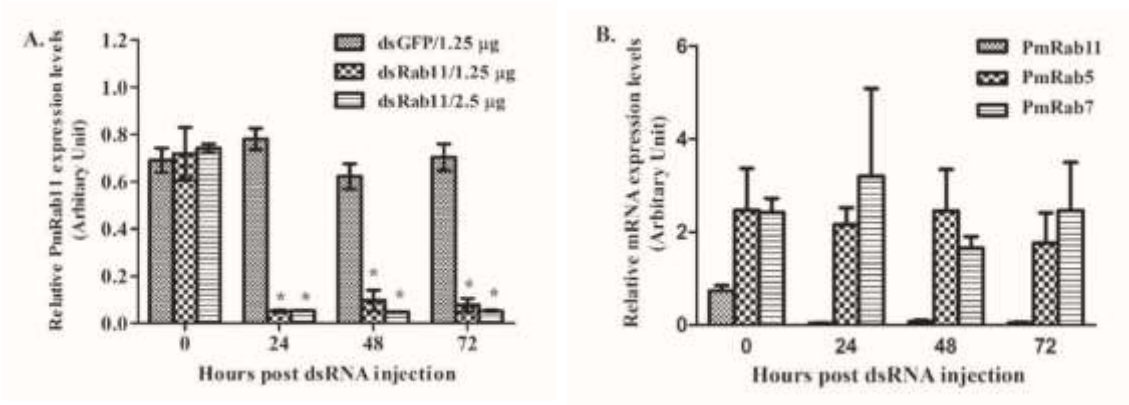

Fig. 4. Suppression of PmRab11 gene by dsRNA-PmRab11. (A) Relative mRNA expression levels of PmRab11 in shrimps injected with dsRNA-PmRab11 at 1.25 and 2.5 µg/g shrimp compared with 1.25 µg/g shrimp of dsRNA-GFP injection are presented as mean ± SEM, n = 4/time point. (B) Relative mRNA expression levels of PmRab11, PmRab5 and PmRab7 are presented as mean ± SEM, n = 3e4/time point. The relative mRNA expression levels of these genes were normalized with PmActin. (*) statistically significant difference between dsRNA-PmRab11 and dsRNA-GFP injected groups at each time point.

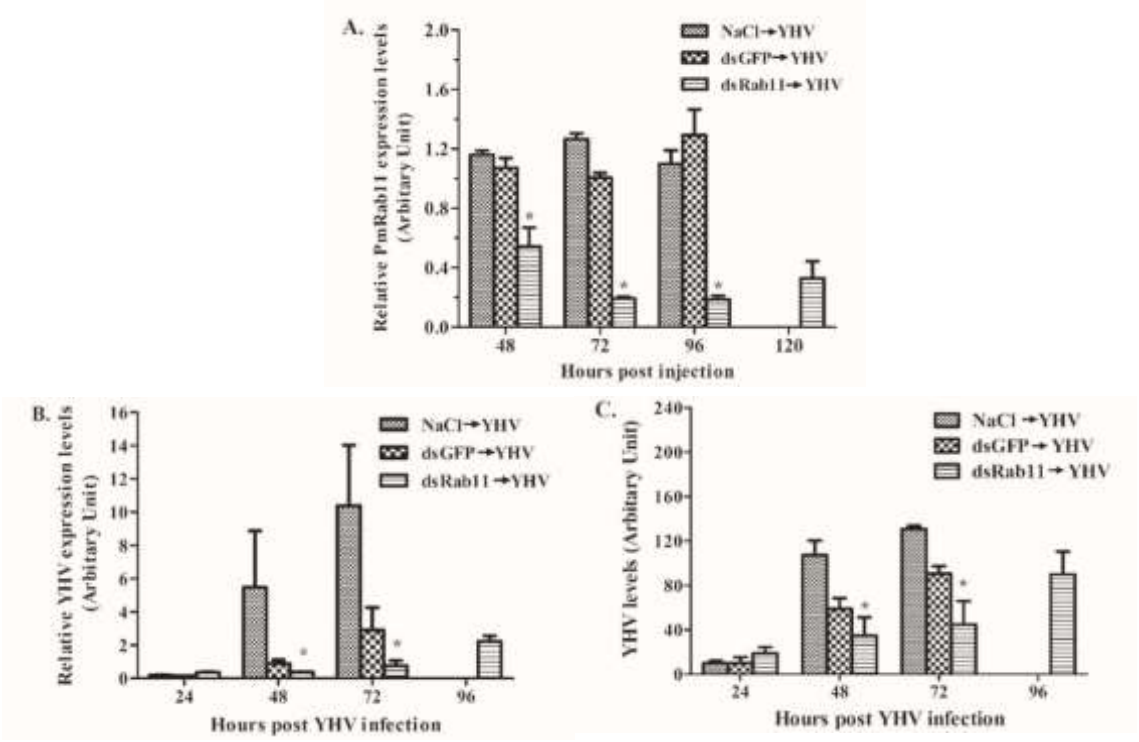

Fig. 5. Suppression of PmRab11 during YHV infection. (A) Relative expression of PmRab11 was detected from hemocytes of shrimps injected with 1.25 µg/g shrimp of dsRNA-PmRab11 followed by YHV, compared with dsRNA-GFP and NaCl injected shrimps at various time courses. Relative mRNA expression levels of YHV in hemocytes (B) and YHV levels in supernatant (C) was monitored. The data are presented as mean ± SEM, n = 4/time point. (*) statistically significant difference between dsRNA-PmRab11 and NaCl injected groups at each time point.

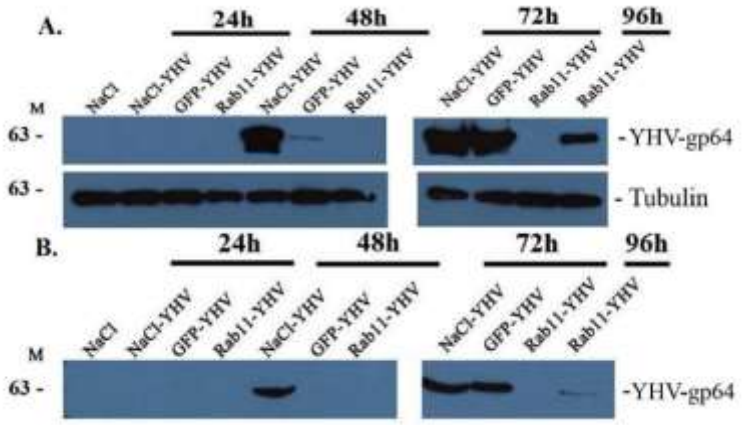

Fig. 6. Suppression effect of PmRab11 on YHV protein levels. Western blot analysis showed protein levels of YHV in hemocytes (A) and supernatant (B) of shrimps injected with 1.8 mg/g shrimp of dsRNA-PmRab11 followed by YHV, compared with dsRNA-GFP and NaCl injected shrimps at various times. Monoclonal antibody to YHV-gp64 was used to detect YHV while tubulin was used as a control.

Shrimp mortality assay

To investigate the suppression effect of PmRab11 on shrimp mortality, shrimp was injected with 1.25 µg/g shrimp of dsRNA-PmRab11. Then, shrimp mortality was recorded for 10 days. The results showed that injection of dsRNA-PmRab11 caused 100% shrimp death at day 7. In contrast, injection of 1.25 µg/g shrimp dsRNA-GFP and NaCl resulted in less than 10% shrimp mortality within 10 days (Fig. 7A). In addition, the cumulative mortalities of shrimp that injected with dsRNA-PmRab11 at 1.25 µg/g shrimp followed by YHV challenge was delayed at least 2 days when compared to the control groups (Fig. 7B).

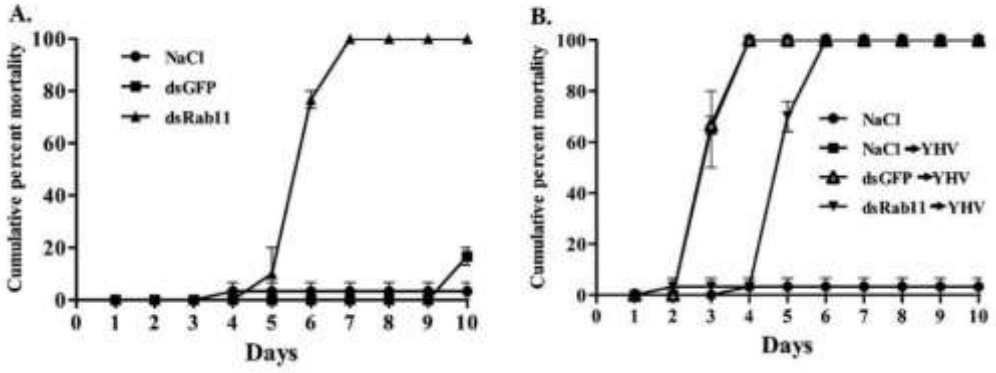

Fig. 7. Cumulative percent mortality of PmRab11-knockdown shrimp with or without YHV challenge. The cumulative percent mortality of shrimps injected with 1.25 µg/g shrimp of dsRNA-PmRab11 compared to injections of dsRNA-GFP or NaCl followed by absence (A) or presence (B) of YHV challenge were investigated. The data are presented as mean ± SEM, n = 45/experiment.

Co-localization of YHV and PmRab11 in YHV infected hemocytes

The PmRab11 protein level in individual hemocytes was observed using immunofluorescence assay. Shrimp was injected with dsRNA-PmRab11 at 1.8 μg/g shrimp, then PmRab11 protein levels was detected at various time points. The result demonstrated that the PmRab11 protein was gradually decreased from 24 to 96 h post-dsRNA-PmRab11 injection (Fig. 8A). Second, the localization of PmRab11 and YHV was investigated by injection with dsRNAPmRab11 at 1.8 μg/g shrimp and followed by YHV. The low signals of PmRab11 protein and YHV glycoprotein 64 (gp64) can be observed inside the hemocytes of PmRab11 knockdown shrimp at 24 h post-infection (Fig. 8B). In contrast, high signals of PmRab11 and gp64 can be detected in shrimp that was injected with dsRNAGFP and NaCl followed by YHV challenge at this time point. In addition, co-localization of PmRab11 and YHV can be clearly observed at 24–72 h post-infection in hemocytes of both control groups. In contrast, the PmRab11 knockdown group showed low level of YHV and PmRab11 at these time points (Fig. 8C and D).

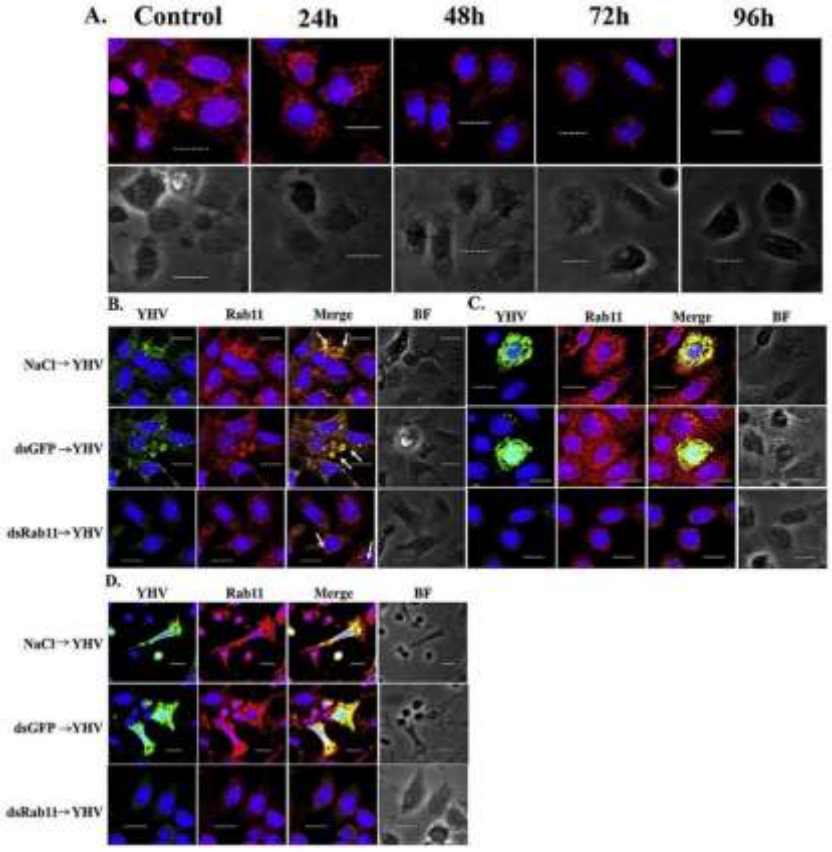

Fig. 8. Co-localization of PmRab11 and YHV in YHV-infected hemocytes. The pictures show hemocytes during PmRab1-knockdown at various times (A). Co-localization of PmRab11 and YHV was investigated at 24 h (B), 48 h (C) and 72 h (D) post-YHV challenge. Red, green and blue colours represented PmRab11, YHV-gp64 and nucleus, respectively. Arrow indicated the co-localization signal of PmRab11 and YHV. Scale is 10 mm. (For interpretation of the references to colour in this figure legend, the reader is referred to the web version of this article.)

Discussion

At present, the mechanisms of YHV internalization and transportation inside the cell have been proposed. The viral glycoprotein gp116 on YHV envelope binds to the YHV binding protein, PmYRP65 on the cell membrane [30,31] then internalizes into the cell via clathrin-dependent endocytosis [32,33]. After that, the vesicle containing YHV particle is transported to the early and late endosome by Rab5 and Rab7, respectively [11,12] before the viral genome is released to the cytoplasm for replication and translation. Electron microscopy revealed that enveloped YHV virion is formed at TGN [2,13]. However, the mechanism of the transport of YHV from TGN to PM is not well understood. The earlier studies of other (±) ssRNA viruses such as flaviviruses and coronaviruses found that viral budding from TGN to PM is dependent on Rab11-mediated pathway through cytoskeleton network [34,35]. Interestingly, Rab11 of YHV-infected shrimp was shown to be upregulated after 24 h of infection [26]. A comparative proteomic analysis showed that the protein disulfide isomerase (PDI) was increased during YHV infection [36]. PDI is normally localized in the lumen of ER catalyzing the formation and isomerization of disulfide bonds [37]. It has also been reported to be involved in the folding and assembly of viral proteins in the ER [38]. The YHV structural proteins, gp116 and gp64, contain 26 and 24 cysteine residues, respectively, suggesting a possible role for PDI to form inter- and intra-molecular disulfide bonds during the folding of these viral proteins [13]. Therefore, it is possible that PmRab11 also play a role in the transport of YHV out of the cell.

Two forms of PmRab11 cDNAs of sizes 1200 and 1050 bp were found to be different at the 5′ UTR. This may be because the gene was transcribed from different alleles. The existence of the two variants of PmRab11 was confirmed by amplification of the fulllength cDNA and by 5′ RACE (Supplementary Fig. 2). The nucleotide deletion at the 5′ end of the two forms has not been observed for other Rab11. However, at least three isoforms of Rab11 proteins such as Rab11A, Rab11B and Rab11C (occasionally called Rab25) have been reported and shown to localize differently at specific organelles. Rab11A and B localize at the Golgi, RE and early endosomes and may be involved in membrane trafficking pathway by transportation of the target protein from TGN/RE to plasma membrane [39]. While Rab11C is expressed only in certain epithelial cells and may be involved in vesicular trafficking from recycling endosome to plasma membrane [39,40]. The deduced PmRab11 protein shared a characteristic signature of Rab11 with other species and closely related to Rab11 in invertebrate, especially in shrimp species (100% amino acid sequence identity with Rab11 of Pacific white shrimp, *Litopenaeus vannamei*). The PmRab11 function was characterized by using RNAi approach. Knockdown of PmRab11 by dsRNA-PmRab11 specifically inhibited PmRab11 expression within 24 h but not PmRab5 and PmRab7 expression. Suppression of PmRab11 led to 100% shrimp death at day 7. Similar results were demonstrated in the knockdown effect of endogenous genes that are involved in the trafficking process in shrimp including PmRab5, PmRab7 and clathrin heavy chain [11,12,33]. In addition, Rab11 is an essential gene in the regulation of transportation of the endocytosed proteins [18,41,42].

The role of Rab11 during YHV infection was investigated by suppression of PmRab11. The PmRab11 expression was suppressed approximately 50% at 48 h post-dsRNA injection (or 24 h post-YHV infection) (Fig. 5A). This is in contrast to the result of PmRab11 knockdown alone (without YHV infection) that PmRab11 expression was

inhibited more than 90% at this time point (Fig. 4A). Interestingly, subtractive hybridization found that Rab11 was upregulated at 24 h post-YHV infection [26]. Therefore, it is possible that an incomplete PmRab11 knockdown is caused by upregulation of PmRab11 expression in response to YHV infection. In addition, viral titre inside and outside the cell was determined by semiquantitative RT-PCR. The results showed that YHV levels in hemocytes and supernatant of PmRab11 knockdown group were significantly decreased from 48 to 72 h post-YHV infection when compared to the NaCl-injected group. Notably, not only PmRab11 expression was recovered at 120 h post-dsRNA injection, but also the YHV released was increase at this time point. This relationship demonstrated that PmRab11 is required for YHV infection. Similar results were observed in the plaque assay of virus infected cells that were treated with siRNA targeting Rab11 such as hantavirus [25], Influenza A [43], and hepatitis C virus [44].

To estimate the YHV's protein level in hemocytes and supernatant, Western blot was performed using antibody against YHVgp64 which is one of the viral glycoproteins on YHV envelope. Unfortunately, our Rab11 antibody cannot be used to detect Rab11 protein byWestern blot under the denaturing condition, suggesting that it required the native structure of epitopes. The results revealed that YHV protein level cannot be observed in both fractions of all experimental groups at 24 h post-dsRNA injection (Fig. 6). Previous study in PmRab5 knockdown during YHV infection found that YHV is internalized and transported via PmRab5 from PM to early endosome around 10 mine6 h post-infection [10]. After that, viral replication occurred and nucleocapsid was found in cytoplasm at 24 h post-YHV infection [13]. Thus, the, low level of YHV-gp64 protein at the early phase of infection and the failure to detect the protein in Western blot at this time point. At 48 h postdsRNA injection, high YHV protein level in the NaCl-injected group can be observed. Whereas, the dsRNA-GFP injected group showed low YHV protein level at this time point. Many studies found that the innate antiviral immunity in invertebrates including shrimp was induced by any dsRNA in a sequence-independent manner [45,46]. High levels YHV protein in hemocytes and supernatant of the NaCl injected group and dsRNA-GFP injected group could be observed at 72 h. In contrast, YHV levels could not be detected in both fractions of PmRab11 knockdown group at 24–72 h postdsRNA injection. For the (±) ssRNA virus including YHV, the replication process occurs in the cytoplasm [47] and the viral envelop glycoproteins are co-translationally inserted into ER membranes. Then, modification of the glycoproteins occurs during their passage through the secretory pathway. For example, all structural proteins of members of the Flaviviridae family such as hepatitis C and dengue virus are co-translated as a single polyprotein and are inserted into the ER membrane [48]. An individual glycoprotein is generated by proteolytic cleavage and the RNA-binding core protein that is known as the nucleocapsid is assembled within the ER, and transported to Golgi apparatus. It is possible that these events may also occur for YHV which is one of the (±) ssRNA. The single polyprotein containing gp116 and gp64 is co-translated and inserted into the ER membrane. The proteolytic cleavage resulted in individual gp116 and gp 64 that exposed the N-terminal domain to the cytosolic side [7]. Then, the viral nucleocapsid and glycoproteins are transported to the Golgi apparatus for maturation. At TGN, the budding of YHV envelope virion can be observed under electron microscope [2,13]. Normally, Rab11 is involved in the vesicle transport from TGN to the PM [49]. After

PmRab11 knockdown, YHV cannot bud and has no target organelle to transport to. Therefore, the YHV protein in Golgi network might be transported to lysosome for degradation. However, the mechanism in this process remains to be elucidated. Similar results can be observed in the dengue virus [50]. In addition, the mortality assay revealed that injection of dsRNA-PmRab11 can delay shrimp mortality when compared to both control groups. Similar results of the delay in shrimp mortalities can be demonstrated for the knockdown effects of other Rab proteins including PmRab7 and PmRab5 during YHV infection [11,12].

Co-localization between YHV and PmRab11 was observed by immunofluorescence assay. The results showed co-localization between YHV-gp64 and PmRab11 was seen from 24 to 72 h post-YHV injection in both control groups (Fig. 8). Accumulation of YHV can be found at the PM of hemocytes. Similar results were also seen from other viruses that used Rab11-dependent pathway in the [21,22,43], measles virus [23], mumps virus [24], hantavirus [25], hepatitis C virus [44] and dengue virus [50]. In contrast, low level of co-localization signals between PmRab11 and YHV can be observed in the perinuclear region at 24–72 h in the PmRab11 knockdown group. This is supported by an overexpression of Rab11 dominant negative mutant in hepatitis C, hantavirus or dengue infected cell. The virus was accumulated at the perinuclear region that was identified as TGN [25,44,50]. In addition, overexpression of Rab11 constitutively active mutant in influenza A virus infection showed that Rab11 is aggregated with vRNP at the perinuclear region and cannot be transported out of the cell [21e23]. These evidence suggested a possible role of Rab11 in transportation of YHV.

Other Rab such as Rab6 has been shown to play important roles in virus infection of shrimp. Rab6 is involved in the regulation of phagocytosis against white spot syndrome virus (WSSV) infection through the interaction with the WSSV envelope protein VP466, bactin, and tropomyosin which could activate the GTPase activity of Rab6 and subsequently induce the rearrangement of actin fibers in invertebrates [51,52]. An increase in Rab6 activity was demonstrated in WSSV resistant shrimp. Silencing of Rab6 by a specific siRNA significantly increasedWSSV replication in shrimp [53,54]. In addition, Rab6 plays an important role in the regulation of phagocytosis against bacterial infection in *Marsupenaeus japonicus* [55].

In summary, the virus budding process and its cellular trafficking inside the cell are core study in virology, Therefore, the identification of the routes for viral infection and release including the discovery of the cellular and viral components involved in various processes are essential. These are an important knowledge that will provide insights into host-pathogen interaction in order to improve a potential approach for therapeutic intervention against viral diseases.

References

1. S. Boonyaratpalin, K. Supamataya, J. Kasornchandra, S. Direkbusarakom, U. Aekpanithanpong, C. Chantanachookhin, Non-occluded baculo-like virus the causative agent of yellow-head disease in the black tiger shrimp *Penaeus monodon*, Fish. Pathol. 28 (1993) 103-109.
2. C. Chantanachookin, S. Boonyaratpalin, J. Kasornchandra, S. Direkbusarakom, U. Ekpanithanpong, K. Supamataya, S. Siurairatana, T.W. Flegel, Histology and ultrastructure reveal a new granulosis-like virus in *Penaeus monodon* affected by yellow-head disease, Dis. Aquat. Organ 17 (1993) 145-157.

3. P.J. Walker, J.R. Bonami, V. Boonsaeng, P.S. Chang, J.A. Cowley, L. Enjuanes, T.W. Flegel, D.V. Lightner, P.C. Loh, E.J. Snijder, K. Tang, Virus Taxonomy: Classification and Nomenclature of Viruses: Eighth Report of the International Committee on the Taxonomy of Viruses, Elsevier, 2005, pp. 975-979.
4. N. Sittidilokratna, R.A.J. Hodgson, J.A. Cowley, S. Jitrapakdee, V. Boonsaeng, S. Panyim, P.J. Walker, Complete ORF1b gene sequence indicates yellow head virus is an invertebrate nidovirus, Dis. Aquat. Organ 50 (2002) 87-93.
5. N. Sittidilokratna, N. Phetchampai, V. Boonsaeng, P.J. Walker, Structural and antigenic analysis of the yellow head virus nucleocapsid protein p20, Virus Res. 116 (2006) 21-29.
6. S. Jitrapakdee, S. Unajak, N. Sittidilokratna, R.A. Hodgson, J.A. Cowley, P.J. Walker, et al., Identification and analysis of gp116 and gp64 structural glycoproteins of yellow head nidovirus of *Penaeus monodon* shrimp, J. Gen. Virol. 84 (2003) 863-873.
7. A.K. Dhar, J.A. Cowley, K.W. Hasson, P.J. Walker, Genomic organization, biology, and diagnosis of taura syndrome virus and yellow head virus of penaeid shrimp, Adv. Virus Res. 63 (2004) 353-421.
8. C. Wongteerasupaya, J. Vickers, S. Sriurairatana, et al., A non-occluded, systemic baculovirus that occurs in cells of ectodermal and mesodermal origin and causes high mortality in the black tiger prawn *Penaeus monodon*, Dis. Aquat. Organ 21 (1995) 66-77.
9. E.C.B. Nadala, L.M. Tapay, P.C. Loh, Yellow head virus: a rhabdovirus-like pathogen of penaeid shrimp, Dis. Aquat. Organ 31 (1997) 141-146.
10. C. Soowannayan, T.W. Flegel, P. Sithigorngul, et al., Detection and differentiation of yellow head complex viruses using monoclonal antibodies, Dis. Aquat. Organ 57 (2003) 193-200.
11. P. Posiri, S. Panyim, C. Ongvarrasopone, Rab5, an early endosomal protein required for yellow head virus infection of Penaeus monodon, Aquaculture 459 (2016) 43-53.
12. C. Ongvarrasopone, M. Chanasakulniyom, K. Sritunyalucksana, S. Panyim, Suppression of PmRab7 by dsRNA inhibits WSSV or YHV infection in shrimp, Mar. Biotechnol. 10 (2008) 374-381.
13. P. Duangsuwan, Y. Tinikul, B. Withyachumnarnkul, C. Chotwiwatthanakun, P. Sobhon, Cellular targets and pathways of yellow head virus infection in lymphoid organ of *Penaeus monodon* as studied by transmission electron microscopy, Songklanakarin J. Sci. Technol. 33 (2011) 121-127.
14. M. Dubois-Dalcq, K.V. Holmes, B. Rentier, D.W. Kingsbury, Assembly of Enveloped RNA Viruses, Springer-Verlag KG, Vienna, Austria, 2013.
15. E. Wimmer, Cellular Receptors for Animal Viruses, vol. 28, Cold Spring Harbor Laboratory Press, Plainview, New York, USA, 1994.
16. S. Welsch, B. Müller, H.G. Kr€ausslich, More than one door - budding of enveloped viruses through cellular membranes, FEBS Lett. 581 (2007) 2089-2097.
17. W. Chen, Y. Feng, D. Chen, A. Wandinger-Ness, Rab11 is required for transgolgi network-to-plasma membrane transport and a preferential target for GDP dissociation inhibitor, Mol. Biol. Cell 9 (1998) 3241-3257.
18. H. Stenmark, Rab GTPases as coordinators of vesicle traffic, Nat. Rev. Mol. Cell Biol. 10 (2009) 513-525.

19. S.C. Das, D. Nayak, Y. Zhou, A.K. Pattnaik, Visualization of intracellular transport of vesicular stomatitis virus nucleocapsids in living cells, J. Virol. 80 (2006) 6368-6377.
20. R. Chambers, T. Takimoto, Trafficking of Sendai virus nucleocapsids is mediated by intracellular vesicles, PLoS One 5 (2010) e10994.
21. A.J. Eisfeld, E. Kawakami, T. Watanabe, G. Neumann, Y. Kawaoka, Rab11A is essential for transport of the influenza virus genome to the plasma membrane, J. Virol. 85 (2011) 6117-6126.
22. M.J. Amorim, E.A. Bruce, E.K. Read, A. Foeglein, R. Mahen, A.D. Stuart, P. Digard, A Rab11- and microtubule- dependent mechanism for cytoplasmic transport of influenza A virus viral RNA, J. Virol. 85 (2011) 4143-4156.
23. Y. Nakatsu, X. Ma, F. Seki, T. Suzuki, M. Iwasaki, Y. Yanagi, K. Komase, M. Takeda, Intracellular transport of the measles virus ribonucleoprotein complex is mediated by Rab11A- positive recycling endosomes and drives virus release from the apical membrane of polarized epithelial cells, J. Virol. 87 (2013) 4683-4693.
24. H. Katoh, Y. Nakatsu, T. Kubota, M. Sakata, M. Takeda, M. Kidokoro, Mumps virus is released from the apical surface of polarized epithelial cells, and the release is facilitated by a Rab11-mediated transport system, J. Virol. 89 (2015) 12026-12034.
25. R.K. Rowe, J.W. Suszko, A. Pekosz, Roles for the recycling endosome, Rab8, and Rab11 in hantavirus release from epithelial cells, Virology 382 (2008) 239-249.
26. A. Prapavorarat, S. Pongsomboon, A. Tassanakajon, Identification of genes expressed in response to yellow head virus infection in the black tiger shrimp, *Penaeus monodon*, by suppression subtractive hybridization, Dev. Comp. Immunol. 34 (2010) 611-617.
27. A. Dereeper, V. Guignon, G. Blanc, S. Audic, S. Buffet, F. Chevenet, et al., Phylogeny. fr: robust phylogenetic analysis for the non- specialist, Nucleic Acids Res. 36 (2008) W465-W469.
28. C. Ongvarrasopone, Y. Roshorm, S. Panyim, A simple and cost effective method to generate dsRNA for RNAi studies in invertebrates, ScienceAsia 33 (2007) 035-039.
29. P. Posiri, C. Ongvarrasopone, S. Panyim, A simple one-step method for producing dsRNA from E. coli to inhibit shrimp virus replication, J. Virol. Methods 188 (2013) 64-69.
30. W. Assavalapsakul, D.R. Smith, S. Panyim, Identification and characterization of a *Penaeus monodon* lymphoid cell- expressed receptor for the yellow head virus, J Gen. Virol. 80 (2006) 262-269.
31. W. Assavalapsakul, H.K.T. Kiem, D.R. Smith, S. Panyim, Silencing of PmYPR65 receptor prevents yellow head virus infection in *Penaeus monodon*, Virus Res. 189 (2014) 133-135.
32. T. Jatuyosporn, P. Supungul, A. Tassanakajon, K. Krusong, The essential role of clathrin- mediated endocytosis in yellow head virus propagation in the black tiger shrimp *Penaeus monodon*, Dev. Comp. Immunol. 44 (2014) 100-110.
33. P. Posiri, H. Kondo, I. Hirono, S. Panyim, C. Ongvarrasopone, Successful yellow head virus infection of *Penaeus monodon* requires clathrin heavy chain, Aquaculture 435 (2015) 480-487.

34. S. Welsch, B. Müller, H.G. Kr€ausslich, More than one door - budding of enveloped viruses through cellular membranes, FEBS Lett. 581 (2007) 2089-2097.
35. W. Weissenhorn, E. Poudevigne, G. Effantin, P. Bassereau, How to get out: ssRNA enveloped viruses and membrane fission, Curr. Opin. Virol. 3 (2013) 159-167.
36. A. Bourchookarn, P.-O. Havanapan, V. Thongboonkerd, C. Krittanai, Proteomic a nalysis of altered proteins in lymphoid organ of yellow head virus infected *Penaeus monodon*, BBA-Proteins Proteom 1784 (2008) 504-511.
37. R. Noiva, W.J. Lennarz, Protein disulfide isomerase. A multifunctional protein resident in the lumen of the endoplasmic reticulum, J. Biol. Chem. 267 (1992) 3553-3566.
38. A. Guichard, V. Nizet, E. Bier, R.W. Doms, R.A. Lamb, J.K. Rose, A. Helenius, Folding and assembly of viral membrane proteins, Virology 193 (1993) 545-562.
39. A.H. Hutagalung, P.J. Novick, Role of Rab GTPases in membrane traffic and cell physiology, Physiol. Rev. 91 (1) (2011) 119-149.
40. J.R. Goldenring, K.R. Shen, H.D. Vaughan, I.M. Modlin, Identification of a small GTP-binding protein, Rab25, expressed in the gastrointestinal mucosa, kidney and lung, J. Biol. Chem. 268 (25) (1993) 18419-18422.
41. B.D. Grant, J.G. Donaldson, Athways and mechanisms of endocytic recycling, Nat. Rev. Mol. Cell Biol. 10 (2009) 597-608.
42. S.C.D. van Ijzendoorn, Recycling endosomes, J. Cell Sci. 119 (2006) 1679-1681.
43. E.A. Bruce, P. Digard, A.D. Stuart, The Rab11 pathway is required for influenza A virus budding and filament formation, J. Virol. 84 (2010) 5848-5859.
44. K. Coller, N. Heaton, K. Berger, J. Cooper, J. Saunders, G. Randall, Molecular determinants and dynamics of hepatitis C virus secretion, PLoS Pathog. 8 (2012) e1002466.
45. J. Robalino, T. Bartlett, E. Shepard, S. Prior, G. Jaramillo, E. Scura, R.W. Chapman, P.S. Gross, C.L. Browdy, G.W. Warr, Double-stranded RNA induces sequence-specific antiviral silencing in addition to nonspecific immunity in a marine shrimp: convergence of RNA interference and innate immunity in the invertebrate antiviral response? J. Virol. 79 (2005) 13561-13571.
46. J. Robalino, C.L. Browdy, S. Prior, A. Metz, P. Parnell, P. Gross, G. Warr, Induction of antiviral immunity by double-stranded RNA in a marine invertebrate, J. Virol. 78 (2004) 10442-10448.
47. C. Harak, V. Lohmann, Ultrastructure of the replication sites of positive-strand RNA viruses, Virology 497 (2015) 418-433.
48. S. Mukhopadhyay, R.J. Kuhn, M.G. Rossmann, A structural perspective of the flavivirus life cycle, Nat. Rev. Microbiol. 3 (2005) 13-22.
49. W. Chen, Y. Feng, D. Chen, A. Wandinger-Ness, Rab11 is required for transgolgi network-to-plasma membrane transport and a preferential target for GDP dissociation inhibitor, Mol. Biol. Cell 9 (1998) 3241-3257.
50. E.G. Acosta, V. Castilla, E.B. Damonte, Differential requirements in endocytic trafficking for penetration of dengue virus, PLoS One 7 (2012) e44835.
51. T. Ye, W. Tang, X. Zhang, Involvement of Rab6 in the regulation of phagocytosis against virus infection in invertebrates, J. Proteome Res. 11 (2012a) 4834-4846.
52. T. Ye, R. Zong, X. Zhang, The role of white spot syndrome virus (WSSV) VP466 protein in shrimp antiviral phagocytosis, Fish. Shellfish Immunol. 33 (2012b) 350-358.

53. W. Wu, X. Zhang, Characterization of a Rab GTPase up-regulated in the shrimp *Peneaus japonicus* by virus infection, Fish Shellfish Immunol 23 (2007) 438-445.
54. W. Wu, R. Zong, J. Xu, X. Zhang, Antiviral phagocytosis is regulated by a novel Rab- dependent complex in shrimp *Penaeus japonicus*, J. Proteome Res. 7 (2008) 424-431.
55. R. Zong, W. Wu, J. Xu, X. Zhang, Regulation of phagocytosis against bacterium by Rab GTPase in shrimp *Marsupenaeus japonicus*, Fish. Shellfish Immunol. 25 (2008) 258-263.

In vitro study of a putative role of gonad-inhibiting hormone in oocyte growth stimulation in *Penaeus monodon*

Ovarian development in crustacean is controlled by several factors, among which a neuropeptide gonad-inhibiting hormone (GIH) is known to inhibit vitellogenin (Vg) synthesis in the ovary. It has been postulated that GIH may control Vg synthesis by inhibiting the release of gonad-stimulating factor (GSF) from brain and thoracic ganglia. To prove this hypothesis, this study was primarily aimed to investigate the influence of GIH on the release of GSF from thoracic ganglia of *Penaeus monodon*. Our result showed that GIH did not suppress the release of putative GSF from thoracic ganglia by calcium ionophore A23187 as the induction of oocyte growth in the ovary explants that were cocultured with thoracic ganglia in the presence of A23187 was not affected by the addition of recombinant GIH protein. In addition and interestingly, when the ovary explants were incubated with the recombinant GIH alone, the oocyte growth was increased at the rate comparable to that induced by A23187 in the presence of thoracic ganglia. Hence, our in vitro study demonstrated that the stimulation of GSF released from thoracic ganglia is independent of GIH, and that the GIH has a dual function in oocyte growth stimulation and inhibition of Vg synthesis in the early stage of ovarian development. This expands our knowledge on the regulation of ovarian development in shrimp by GIH. Further in vivo studies in this novel aspect of GIH function will be useful for the improvement of shrimp ovarian maturation in the future.

Introduction

Ovarian development is an important process in female reproduction. In general, primary oocytes that are mitotically divided from oogonia are arrested at prophase I to prepare for oocyte maturation (Von Stetina & Orr-Weaver, 2011). In crustaceans, there are two major phases in ovarian development; primary vitellogenesis that involves oocyte growth and follicular development and secondary vitellogenesis comprising vitellogenin (Vg) synthesis and accumulation, and cortical rod formation in later phase (Charniaux-Cotton, 1985). In penaeid shrimps, the ovary at previtellogenic stage of development contained small oocyte cells, particularly chromatin nucleolar oocytes (CNOs) and perinucleolar oocytes (POs). The PO is larger than CNO in size, and their nucleoli are located at nuclear membrane. Some PO cells are surrounded by follicle cells. In vitellogenic ovary, Vg is initially synthesized in ovarian follicle cells and accumulated in the oocyte cells leading to an increase in their size. Cortical rods are formed in fully grown oocytes (Ayub & Ahmed, 2002). Moreover, Vg is also expressed and secreted from hepatopancreas and accumulated in the ovary (Tseng, Chen, Kou, Lo & Kuo, 2001).

Hormonal control of ovarian development in shrimp is mediated by several factors such as peptide hormones, steroid hormones and neurotransmitters (Subramoniam, 2011). There were several reports about the existence of gonad-stimulating factor (GSF) in the brain and thoracic ganglia of crustaceans during the past two decades. For

example, injection of thoracic ganglia extract in kuruma prawn, *Penaeus japonicus* caused an increase of Vg in haemolymph (Yano, 1992). Vitellogenesis in *Paratya compressa* was also stimulated by both brain and thoracic ganglia extract (Takayanagi, Yamamoto & Takeda, 1986). In addition, the release of putative GSF from brain and thoracic ganglia could be stimulated by calcium ionophore (A23187) as demonstrated either in ovarian explants or by in vivo injection in the crayfish Procambarus clarkii (Sarojini, Nagabhushanam & Fingerman, 1995). However, the actual molecule responsible for this gonad-stimulating activity has not been identified and characterized so far.

On the other hand, vitellogenesis is inhibited by gonad-inhibiting hormone (GIH), a neuropeptide belonging to the crustacean hyperglycemic hormone (CHH) family (Chang, 2001). GIH is mainly expressed in the X-organ sinus gland complex of eyestalk ganglia and was shown to function in inhibition of *Vg* expression in several decapod crustaceans including *Homarus americanus*, *Nephrops norvegicus*, *Penaeus monodon* and *Litopenaeus vannamei* (Chen et al., 2014; De Kleijn, Sleutels, Martens & Van Herp, 1994; Edomi et al., 2002; Treerattrakool, Panyim, Chan, Withyachumnarnkul & Udomkit, 2008). Moreover, neutralization of rGIH by monoclonal antibody against *P. monodon*'s GIH also stimulated *Vg* expression in primary ovarian cells (Treerattrakool, Boonchoy, Urtgam, Panyim & Udomkit, 2014). GIH level in the haemolymph of *H. americanus* was highest in previtellogenic stage and declined in vitellogenic stages of ovarian development (De Kleijn et al., 1998), which was in agreement with that in *P. monodon* (Urtgam et al., 2015). These supported the function of GIH in suppression of *Vg* synthesis in previtellogenic ovary. In addition, previtellogenic stage is the phase at which oocyte growth occurs; therefore, this brings into question whether or not GIH inhibits the release or synthesis of GSF (Nagaraju, 2011), and may it play any role in oocyte growth during previtellogenic stage.

Therefore, this study aimed to investigate a role of GIH in suppressing the release of putative GSF from thoracic ganglia. In addition, the function of GIH in oocyte growth in previtellogenic ovary will also be studied.

Materials and methods

Expression and purification of recombinant GIH (rGIH) in yeast expression system

Recombinant yeast, Pichia pastoris KM71, containing the nucleotide sequence encoding for a mature GIH peptide in its genome was kindly provided by Dr. Supattra Treerattrakool. The expression and purification of the recombinant GIH (rGIH) were carried out as described by Treerattrakool et al. (2014). Briefly, *P. pastoris* KM71 carrying the expression cassette for rGIH was cultured in YPD (1% yeast extract, 2% peptone and 2% D-glucose) containing 100 µg/ml zeocin at 30°C for 2 days. The starter culture was inoculated at 0.1 OD_{600}/ml in BMGY medium (1% w/v yeast extract, 2% w/v peptone, 100 mM phosphate buffer pH 6.0, 1% v/v glycerol, 0.67% w/v YNB and 0.4 µg/ml biotin) and incubated at 30°C for 12–13 hr until an OD600 of 6–8 was obtained. Then, the expression of rGIH was induced in BMMY medium (1% w/v yeast extract, 2% w/v peptone, 100 mM phosphate buffer 6.0, 3% v/v methanol, 0.67% w/v YNB and 0.4

µg/ml biotin) at 30°C for 2 days. The culture medium was collected and precipitated with 40%–50% saturated ammonium sulphate to obtain rGIH. The precipitated rGIH was dissolved with 20% acetonitrile and subjected to solid-phase extraction using a Sep-Pak C-18 column (Waters). The purified rGIH was eluted in a fraction of 40% acetonitrile in 0.1% TFA. The purified rGIH was then evaporated and dissolved in PBS before use.

Validation of rGIH activity to inhibit vitellogenin (Vg) mRNA expression in primary ovariancells

The ovary was freshly isolated from previtellogenic female shrimp *P. monodon* (~100 g body weight) and immediately rinsed in culture medium (Leibovitz's L-15 medium (Gibco), 1% w/v D-glucose, 0.5% w/v NaCl, 3.33% w/v lactalbumin, 10% v/v FBS, 10% v/v shrimp meat extract) containing 100 U penicillin/streptomycin. The ovary was cut into small pieces and washed several times in the culture medium containing 1000 U and 2000 U of penicillin and streptomycin, respectively. After washing, pieces of ovary were minced until homogenous in the culture medium. Approximately 7.5 9 10^5 oocyte cells in 1 ml culture medium were seeded in each well of a 24-well plate and incubated overnight at 28°C. The culture medium was then replaced with fresh culture medium containing 200 ng of rGIH; the amount that was about twofold higher than that previously used to demonstrate the dose-dependent inhibition of rGIH on *Vg* expression by Treerattrakool et al. (2014) to ensure substantial *Vg* suppression in this study. After 24 hr, 500 ll of culture medium was discarded, and 500 ll of fresh culture medium containing the same concentration of rGIH was added and further incubated for 24 hr. The cells that were cultured with the addition of PBS instead of rGIH were used as a control. The primary ovarian cells were collected at 24 hr and 48 hr after treatment, and total RNA was extracted using RiboZol™ reagent (AMERESCO) according to the manufacturer's protocol. The expression of vitellogenin (*Vg*) in each sample was determined by reverse transcription real-time PCR as described below.

Quantification of Vg mRNA expression by reverse transcription real-time PCR (RT-qPCR

Relative RT-qPCR was performed to determine *Vg* mRNA level. Total RNA samples were first treated with DNase I to eliminate the contaminated genomic DNA. One microgram of the RNA was incubated with 19 DNase I buffer and 1 U DNase I (Thermo Scientific) at 37°C for 15 min, followed by 65°C for 5 min. Then, the DNase I-treated RNA was used to synthesize first-stranded cDNA with an oligo-dT primer. The sample was preheated at 70°C for 5 min, and then the reverse transcription mixture containing 1x ImProm-II™ buffer, 3 mM $MgCl_2$, 0.4 mM dNTP and 1 µg ImPromII™ reverse transcriptase (Promega) was added. The reaction was carried out in the following temperature profile; 25°C for 5 min, 42°C for 60 min and 70°C for 10 min. The cDNA was next used as a template in 1x SYB^R FAST Master Mix (KAPA Biosystems) and 0.25 µM Vg-specific primers (Vg-F; 5'-TCCATCTGCAGCAC CAATCTTCGC-3' and Vg-R; 5'-GCAACAGCCTTCATTCTGATGCCA 3'). The reaction was carried out in a

real-time PCR machine (RealPlex^4, Eppendorf) by incubating at 95°C for 3 min, then 40 cycles of 95°C for 5 s and 60°C for 30 s. The melting curve was performed at 95°C for 3 min, then 60°C for 30 s and 95°C for 3 min. Reference genes including elongation factor 1 alpha (EF1α), elongation factor 2, tubulin and calreticulin were analysed for appropriate reference gene by using Normfinder software (data not shown). EF1a was selected as a reference gene to normalize Vg expression using EF1a-specific primers (EF1α- F; 5'- GAACTGCT GACCAAGATCGACAGG- 3' and EF1α- R; 5' - GAGCATACTGTTG GAAGGTCTCCA-3'). The PCR products of both *Vg* and EF1α were purified by gel extraction kit (QIAGEN), and serial dilutions of the known amount of *Vg* and EF1α PCR product (10^2–10^8 copies) were used as a template to construct a standard curve. The copy number of *Vg* and EF1α in each sample was calculated by comparing its C_t value with that of the standard curve. The relative expression of *Vg* to EF1α was calculated from *Vg* copies normalized with EF1α copies. Each sample was amplified in duplicate.

Effect of rGIH on calcium ionophore (A23187) induced release of putative gonad-stimulating factor (GSF) from thoracic ganglia

Ovary explant culture was used as a system to determine the effect of rGIH on GSF-induced oocyte growth stimulation. To prepare the ovary explants, the ovary freshly isolated from previtellogenic female shrimp was excised into small pieces (approximately 3 x 3 x 3 mm^3), washed in M199 medium (Gibco) containing 1000 U and 2000 U penicillin and streptomycin and modified salts (232 mM NaCl, 15 mM $MgSO_4$, 10 mM KCl, 16 mM $CaCl_2$, 1 mM $NaHCO_3$ and 50 mM Hepes pH 7.4). The previtellogenic ovary explants were divided into two groups; the ovary explants that were cultured alone and the ovary explants that were cultured with thoracic ganglia from vitellogenic shrimp. Both groups were subjected to four treatments by the addition of different substances as follows: the first treatment was added with PBS, the second and third treatments with 200 ng of rGIH and 5 µM calcium ionophore A23187 (Sigma), respectively, and the last treatment with the combination of 200 ng of rGIH and 5 µm A23187 in 1 ml of culture medium containing 100 U penicillin/streptomycin in a 24-well plate (three pieces of the explants per well). The explants in all treatments were incubated at 28°C for 2 days. The oocyte growth in the ovary explants was determined by measuring the diameter of oocytes after haematoxylin and eosin staining. Briefly, the ovary pieces were fixed in 20 volumes of Davidson's fixative (33% v/v ethanol, 22% v/v formaldehyde, 11% v/v acetic acids) for 48 hr before processed by paraffin embedding and sectioning into tissue section of 5 µm thickness. The tissue sections were subsequently stained by haematoxylin and eosin, and the image was visualized and photographed under a light microscope. The oocyte growth was determined by two parameters, oocyte diameter and percentage of perinucleolar oocytes (%PO). The diameter of oocytes was measured as previously described (Ayub & Ahmed, 2002; Yano, 1988) using AXIOVISION REL 4.8 program (Carl Zeiss). The PO was identified

as the oocyte with diameter of approximately 30–70 µm, and having nucleolus located at the nuclear envelop. The %PO was calculated by the number of perinucleolar oocytes x 100 divided by total number of oocyte cells in the ovary section.

Effect of rGIH on oocyte growth in ovary explant culture

Ovary explant culture was prepared as described above, and then three pieces of the explant were cultured in 1 ml of well-mixed 200 ng of rGIH in the culture medium supplemented with 100 U penicillin/streptomycin in each well of a 24-well plate. The ovary explant culture was then incubated at 28°C for 2 days. The ovary pieces were proceeded to oocyte growth determination as described above.

Statistical analysis

The data were statistically analysed by ANOVA using SPSS program (IBM, SPSS statistics 20). The time course of *Vg* expression in rGIH-treated primary ovarian cells was analysed by two-way ANOVA with Bonferroni's test for pairwise comparison. Oocyte growth was analysed by randomized complete block design (RCBD) one-way ANOVA or two-way ANOVA due to variation of individual shrimp used for ovarian explant preparation.

Results

Verification of inhibitory effect of recombinant GIH on Vg expression

The 97 amino acid residues of the mature GIH used for rGIH expression were showed in Figure 1a. The rGIH was expressed from the yeast, *P. pastoris*, and subsequently purified following the purification procedure of Treerattrakool et al., 2014) (Figure 1b). In addition, the rGIH was also proven by Western blot analysis with anti-GIH mAb (Treerattrakool et al., 2014). The purified rGIH was validated for its activity to suppress *Vg* synthesis in vitro. The *Vg* mRNA level was significantly reduced by approximately 50% in rGIH-treated ovarian cells at 24 hr after the treatment compared with that in PBS-treated cells. Furthermore, the decrease of *Vg* expression in the rGIH-treated cells was prolonged to 48 hr after treatment (Figure 2).

Calcium ionophore induces the release of putative gonad-stimulating factor (GSF) from thoracic ganglia

To study whether the release of putative GSF from thoracic ganglia is under the influence of GIH or not, the ex vivo induction of GSF release was confirmed by a pharmaceutical agent, calcium ionophore (A23187). The ovary explants were incubated, either alone or together with thoracic ganglia explants, in the culture medium containing 5 µM A23187 for 2 days. The result showed that the percentage of PO (%PO) was significantly increased from 48.4 ± 2.8% in the PBS-treated ovary explants that were culture with thoracic ganglia to 64.7 ± 5.8% in the A23187-treated cocultured explants. By contrast, no significant difference of % PO was observed between the PBS and A23187 treatment in the ovary explants that were cultured alone in the absence of

thoracic ganglia (Figure 3a). Similarly, oocyte diameter was significantly increased in A23187-treated ovary explants that were cultured with thoracic ganglia (37.7 ± 1.7 µm) compared with that of the PBS-treated explants (31.1 ± 0.8 µm), whereas no significant change in oocyte diameter was observed between the two treatments when the ovary explants were cultured alone (Figure 3b). The result suggested that A23187 can stimulate the release of GSF from thoracic ganglia and therefore can be used as the assay system to study the effect of GIH on GSF release from thoracic ganglia.

Effect of rGIH on the release of putative GSF from thoracic ganglia

The influence of GIH on stimulation of GSF release was investigated in the ovary explant culture using A23187 to induce the release of putative GSF from thoracic ganglia. Similar to the result of previous experiment, the addition of A23187 did not affect oocyte growth when the ovary explants were cultured alone, but significantly increased %PO and oocyte diameter of the ovary explants that were incubated with thoracic ganglia (Figure 4, light grey bar). However, when 200 ng of rGIH was added to the A23187-treated culture of ovary explants with thoracic ganglia, similar level of oocyte growth stimulation (Figure 4, black bar) to that without rGIH was still obtained implying that the release of GSF from thoracic ganglia by A23187 was independent of GIH activity. Interestingly, incubation of the ovarian explants alone with rGIH or rGIH mixed with A23187 (Figure 4, dark grey and black bars, respectively) could stimulate oocyte growth regardless of the vitellogenin-inhibiting function of rGIH. For example, %PO was increased from 12.4 ± 1.8% in the PBS-treated ovary explants to 16.7 ± 1.5% and 16.2 ± 1.6% in ovary explants that were incubated with rGIH only and with both rGIH and A23187 respectively (Figure 4a). Similarly, a significant increase in oocyte diameter was also induced by the incubation with rGIH, either alone or in the presence of A23187 (Figure 4b).

Confirmation of oocyte growth stimulation activity of rGIH

To verify the effect of rGIH on oocyte growth, the ovary explant culture was incubated either with rGIH or with PBS for 48 h, and oocyte growth as determined by %PO and oocyte diameter of both groups were compared. The result in Figure 5 showed that the %PO (26.3 ± 2.3%) and oocyte diameter (26.0 ± 0.7 lm) of the ovary explants were significantly increased after 48 hr incubation with rGIH when compared with those in the PBS-treated explants (17.7 ± 2.2%PO and 23.2 ± 0.7 µm oocyte diameter respectively). The representative of ovary sections from rGIH and PBS-treated ovarian explants indicating PO and CNO was shown in Figure 5c. This result affirms the activity of rGIH to stimulate oocyte growth that was observed in the previous experiment.

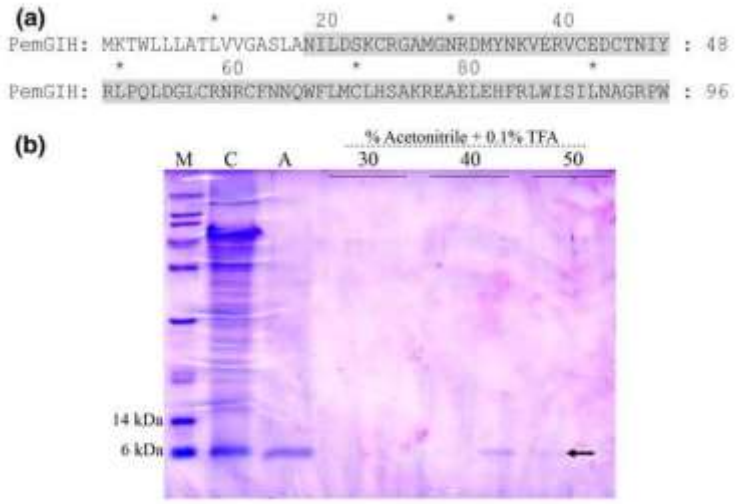

Fig. 1 rGIH amino acid sequence and its purification. (a) The amino acid sequences corresponding to *Penaeus monodon*'s mature GIH (GenBank Accession No. ABG33898) used for the expression of rGIH in *Pichia pastoris* are shaded in grey. (b) The SDS-PAGE was used to determine a purification pattern of rGIH peptide. The "C" and "A" represent culture medium containing rGIH and 40%–50% w/v saturated ammonium sulphate precipitated rGIH respectively. The precipitated rGIH was purified via Sep-Pak C-18 column, and it was eluted with different concentrations (30%–50% v/v) of acetonitrile containing 0.1% TFA. An arrow indicated the purified rGIH eluted in the fraction of 40%–50% acetonitrile. The "*" indicates the position of amino acid at 10 residues interval.

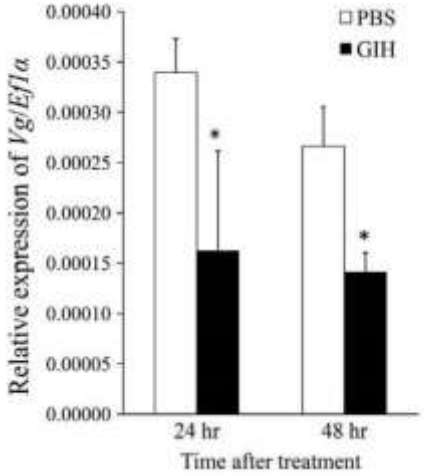

Fig. 2 Validation of rGIH activity on *Vg* inhibition in *Penaeus monodon*'s primary ovarian cells. The primary ovarian cells prepared from previtellogenic ovary of *P. monodon* were treated with 200 ng of rGIH or buffer for 24 hr and 48 hr ($n = 6$). *Vg* expression was determined by relative quantification real-time PCR. Bars and error bars represent mean and SEM respectively. Asterisk is significant difference between group at $p < .05$ by Bonferroni's test

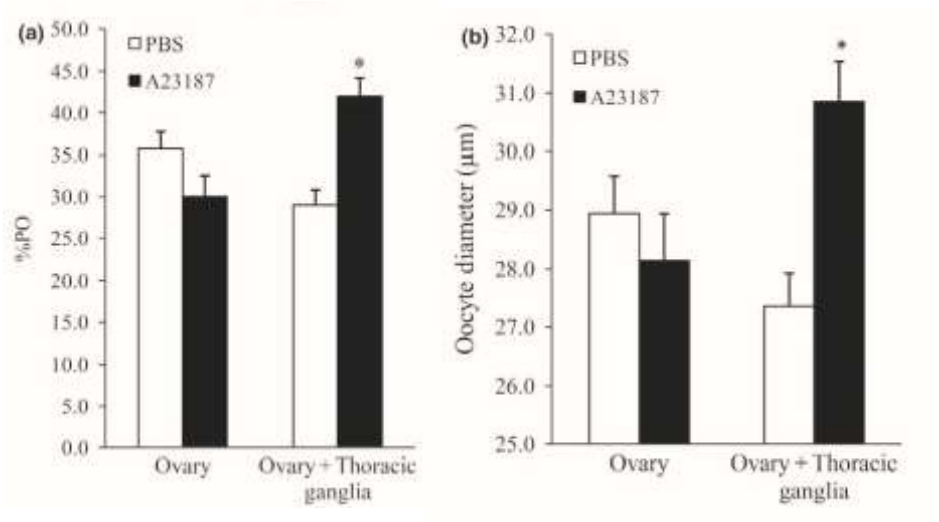

Fig 3 Effect of A23187-induced putative GSF release from thoracic ganglia on oocyte growth. The ovary explants of previtellogenic shrimp that were cultured alone or with thoracic ganglia were treated with 5 μm A23187 or PBS for 48 hr. The oocyte growth in the ovary explants of each treatment was determined by % PO (a) and oocyte diameter measurement (b). Bars and error bars represent mean and SEM of two independent experiments respectively. Asterisk is significant difference within a group at $p < .05$ by Bonferroni's test

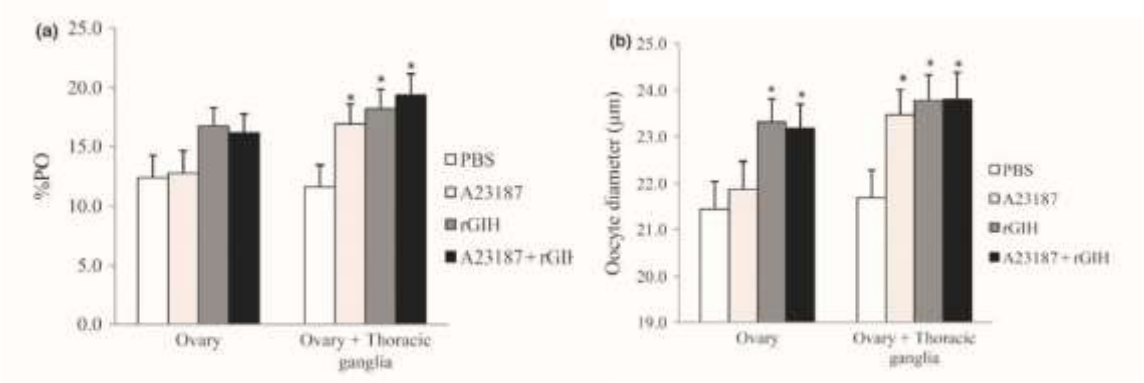

Fig. 4 Effect of rGIH on A23187-induced putative GSF from thoracic ganglia. The ovary explants of previtellogenic shrimp cultured either in the presence or the absence of thoracic ganglia were treated with PBS, A23187, rGIH and rGIH mixed with A23187 for 48 hr. Oocyte growth activity, % PO (a) and oocyte diameter (b), was used to determine the effect of putative GSF secretion. Bars and error bars represent mean and SEM ($n = 5$) respectively. Asterisks represent significant difference between groups compared to PBS treatment at $p < .05$ by RCBD one-way ANOVA, and pairwise comparison by least significant difference test

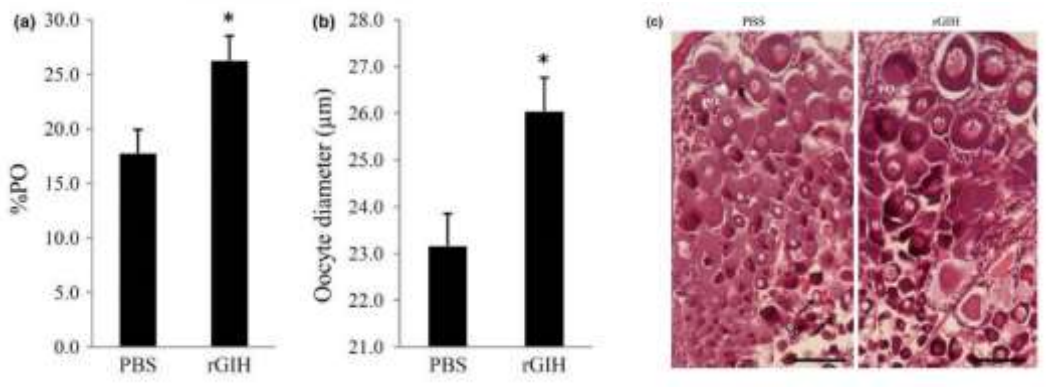

Fig. 5 Effect of rGIH on oocyte growth in *Penaeus monodon*'s ovary explants. The ovary explants of previtellogenic shrimp treated with 200 ng of rGIH or PBS for 48 hr were determined for their oocyte growth by % PO (a) and oocyte diameter measurement (b). Bars and error bars represent mean and SEM (n = 5) respectively. Asterisks depict significant difference between group as analysed by at $p < .05$ by RCBD one-way ANOVA. (c) Haematoxylin and eosin staining of ovarian section after treatment with rGIH. The ovary explants culture treated with rGIH or PBS was fixed, processed, sectioned and stained by H&E. Chromatin nucleolar oocyte (CNO) and perinucleolar oocyte (PO) are depicted by black and white arrows respectively. The rGIH-treated ovary explants contained higher proportion of PO with longer diameter than those treated with PBS. Bars indicate scale of 50 lM

Discussion

Several factors are known to mediate hormonal control of ovarian development in shrimp such as peptide hormones, steroid hormones and neurotransmitters (Subramoniam, 2011). Gonad-inhibiting hormone (GIH), a neuropeptide belonging to the crustacean hyperglycemic hormone (CHH) family, that was mainly expressed at X-organ sinus gland complex in crustacean eyestalk is well-studied in its function to inhibit vitellogenin (Vg) synthesis (Chen et al., 2014; Edomi et al., 2002; Treerattrakool et al., 2008). Recently, a recombinant GIH of *P. monodon* (rGIH) was successfully expressed as a secreted protein in the yeast *P. pastoris* and exhibited a dose-dependent *Vg* inhibition activity where about 50% inhibition of *Vg* expression in primary ovarian cells was achieved within 24 hr when supplied with 11.5 nM (approximately 100 ng/ml) rGIH. In addition, a monoclonal antibody against rGIH could markedly compromise the inhibitory function of rGIH on *Vg* expression (Treerattrakool et al., 2014). Our result here consistently confirmed the suppression of *Vg* expression in primary ovarian cells after treated with 200 ng/ml rGIH; this suppression could be prolonged to 48 hr (Figure 1). One mechanism of action of GIH on *Vg* inhibition has been hypothesized to occur through the inhibition of putative gonadstimulating factor (GSF) synthesis and/or

secretion (Nagaraju, 2011). In vertebrates, induction of vertebrate gonadotrophin secretion including follicle-stimulating hormone (FSH) and luteinizing hormone (LH) from pituitary gland was demonstrated in vitro by a pharmaceutical agent, a calcium ionophore (A23187) (Chuknyiska, Blackman & Roth, 1987; Kile & Nett, 1994; Simpson, Vernom, Jones & Rush, 1989). Similarly, A23187 was also able to induce the release of putative GSF from brain and thoracic ganglia in the crayfish, P. clarkii (Sarojini et al., 1995). Our study showed that A23187 treatment could stimulate oocyte growth in the ovary explant of *P. monodon* only when it was cultured with thoracic ganglia, but not when the ovary explant was cultured alone (Figure 3a,b). This suggested that A23187, by itself, did not affect oocyte growth, but was able to induce the release of putative GSF from thoracic ganglia, which subsequently stimulated oocyte growth in ovary explants. Thus, we further investigated whether GIH regulates putative GSF release from thoracic ganglia by A23187 induction.

The recombinant GIH (rGIH) protein was produced as a secreted protein from *P. pastoris* and exhibited in vitro activity in inhibition of *Vg* expression in primary ovarian cells (Figure 2) similar to that reported previously by Treerattrakool et al. (2014). Therefore, the rGIH in this study was functionally active. To ensure that the effect of rGIH on the inhibition of GSFs release, if there is any, would be clearly detected, the doubled concentration of the rGIH compared to the previous study (Treerattrakool et al., 2014) was used. The addition of rGIH to the A23187-treated ovary explants cultured with thoracic ganglia gave comparable level of oocyte growth to that without rGIH (Figure 4a,b) suggesting that rGIH may not suppress *Vg* expression through interfering with the release of GSF from thoracic ganglia as previously hypothesized. In addition, incubation with only rGIH in the absence of A23187 was sufficient to induce oocyte growth in the ovary explants that were cultured with thoracic ganglia and, more interestingly, even in the ovary explants alone (Figure 4a,b). Our result here suggested that GIH itself may also contain an unconventional oocyte growth stimulating activity.

We further confirmed the stimulatory activity of rGIH on oocyte growth by culturing ovary explants from previtellogenic *P. monodon* in the presence of rGIH for 48 hr. The result consistently showed that rGIH could induce oocyte growth in the treated ovary explants (Figure 5a,b). A number of studies have suggested the existence of substances with gonad-stimulating activity in brain and thoracic ganglia of crustaceans. For instances, an increase of *Vg* level in the haemolymph of kuruma prawn, *P. japonicas* was induced by injection of thoracic ganglia extract (Yano, 1992). Vitellogenesis in the shrimp *Paratya compressa* was also stimulated by the extract from brain and thoracic ganglia (Takayanagi et al., 1986). Because GIH expression was not limited only to the eyestalk, but it was also expressed in brain and thoracic ganglia in several crustaceans such as *P. monodon*, *L. vannamei* and *N. norvegicus* (Chen et al., 2014; Edomi et al., 2002; Treerattrakool et al., 2008), our result thereby suggested that GIH might be one of the factors in thoracic ganglia that is responsible for oocyte growth stimulation in previtellogenic ovary. At previtellogenic stage, high level of GIH (approximately 15 ng/ml in average) was detected in the haemolymph and significantly

declined in vitellogenic stage in *P. monodon* and the lobster, *H. americanus* (De Kleijn et al., 1998; Urtgam et al., 2015). This reflects the important function in vitellogenesis inhibition during previtellogenic phase of ovarian development in crustaceans. On the other hand, the abundance of GIH in previtellogenic stage suggests that the hormone may be involved in oocyte growth and follicular development that are primarily required before yolk synthesis in the early stage of ovarian development. Our result agreed well with this assumption and, thus, demonstrated an in vitro dual function of GIH that is required during previtellogenic stage; these should be further confirmed by in vivo study in the shrimp. The suppression of *Vg* synthesis at this stage may be necessary to allow oocyte growth and prepare for vitellogenin accumulation in higher vitellogenic stages.

The release of putative GSF from its synthesis and/or storage sites was known to be regulated by neurotransmitters such as dopamine and serotonin. Sarojini, Nagabhushanam and Fingerman (1996) demonstrated in *P. clarkii* that serotonin stimulated a release of putative GSF to induce oocyte growth whereas dopamine repressed it (Sarojini et al., 1996). Whether or not the stimulation of oocyte growth by GIH is under control of these neurotransmitters is not known. Therefore, the detailed mechanism of GIH regulation and its receptor at potential targets such as ovary and thoracic ganglia remains to be elucidated to unravel the control of ovarian development in shrimp.

References

1. Ayub, Z., & Ahmed, M. (2002). A description of the ovarian development stages of penaeid shrimps from the coast of Pakistan. Aquaculture Research, 33, 767–776.
2. Chang, E. S. (2001). Crustacean hyperglycemic hormone family: Old paradigms and new perspectives. American Zoologist, 41, 380–388.
3. Charniaux-Cotton, H. (1985). Vitellogenesis and its control in malacostracan crustacea. American Zoologist, 25, 197–206.
4. Chen, T., Zhang, L. P., Wong, N. K., Zhong, M., Ren, C. H., & Hu, C. Q. (2014). Pacific white shrimp (*Litopenaeus vannamei*) vitellogenesisinhibiting hormone (VIH) is predominantly expressed in the brain and negatively regulates hepatopancreatic vitellogenin (VTG) gene expression. Biology of Reproduction, 90(47), 1–10.
5. Chuknyiska, R. S., Blackman, M. R., & Roth, G. S. (1987). Ionophore A23187 partially reverses LH secretory defect of pituitary cells from old rats. American Journal of Physiology, 253, 233–237.
6. De Kleijn, D. P. V., Jansen, K., Waddy, S., Hegeman, R., Lai, W., Martens, G., & Van Herp, F. (1998). Expression of the crustacean hyperglycaemic hormones and the gonad-inhibiting hormone during the reproductive cycle of the female American lobster *Homarus americanus*. Journal of Endocrinology, 156, 291–298.

7. De Kleijn, D. P. V., Sleutels, F. J. G. T., Martens, G. J. M., & Van Herp, F. (1994). Cloning and expression of mRNA encoding prepro-gonadinhibiting hormone (GIH) in the lobster *Homarus americanus*. FEBS Letter, 353, 255–258.
8. Edomi, P., Azzoni, E., Mettulio, R., Pandolfelli, N., Ferrero, E. A., & Giulianini, P. G. (2002). Gonad-inhibiting hormone of the Norway lobster (*Nephrops norvegicus*): cDNA cloning, expression, recombinant protein production, and immunolocalization. Gene, 284, 93 –102.
9. Kile, J. P., & Nett, T. M. (1994). Differential secretion of follicle-stimulating hormone and luteinizing hormone from ovine pituitary cells following activation of protein kinase A, protein kinase C, or increased intracellular calcium. Biology of Reproduction, 50, 49 –54.
10. Nagaraju, G. P. C. (2011). Reproductive regulators in decapod crustaceans: An overview. Journal of Experimental Biology, 214,3 –16.
11. Sarojini, R., Nagabhushanam, R., & Fingerman, M. (1995). A neurotransmitter role for red-pigment-concentrating hormone in ovarian maturation in the red swamp crayfish *Procambarus clarkii*. Journal of Experimental Biology, 198, 1253–1257.
12. Sarojini, R., Nagabhushanam, R., & Fingerman, M. (1996). In vitro inhibition by dopamine of 5-hydroxytryptamine-stimulated ovarian maturation in the red swamp crayfish, *Procambarus clarkii*. Experientia, 52, 707–709.
13. Simpson, W. G., Vernom, M. E., Jones, H. M., & Rush, M. E. (1989). The role of calcium in gonadotropin-releasing hormone induction of follicle-stimulating hormone release by the pituitary gonadotrope. Endocrine Research, 15, 355–373.
14. Subramoniam, T. (2011). Mechanisms and control of vitellogenesis in crustaceans. Fisheries Science, 77,1 –21.
15. Takayanagi, H., Yamamoto, Y., & Takeda, N. (1986). An ovary-stimulating factor in the shrimp, *Paratya compressa*. Journal of Experimental Zoology, 240, 203–209.
16. Treerattrakool, S., Boonchoy, C., Urtgam, S., Panyim, S., & Udomkit, A. (2014). Functional characterization of recombinant gonad-inhibiting hormone (GIH) and implication of antibody neutralization on induction of ovarian maturation in marine shrimp. Aquaculture, 428–429, 166–173.
17. Treerattrakool, S., Panyim, S., Chan, S. M., Withyachumnarnkul, B., & Udomkit, A. (2008). Molecular characterization of gonad-inhibiting hormone of *Penaeus monodon* and elucidation of its inhibitory role in vitellogenin expression by RNA interference. FEBS Journal, 275, 970– 980.
18. Tseng, D. Y., Chen, Y. N., Kou, G. H., Lo, C. F., & Kuo, C. M. (2001). Hepatopancreas is the extraovarian site of vitellogenin synthesis in black tiger shrimp, *Penaeus monodon*. Comparative Biochemistry and Physiology Part A: Molecular & Integrative Physiology, 129, 909–917.

19. Urtgam, S., Treerattrakool, S., Roytrakul, S., Wongtripop, S., Prommoon, J., Panyim, S., & Udomkit, A. (2015). Correlation between gonad-inhibiting hormone and vitellogenin during ovarian maturation in the domesticated *Penaeus monodon*. Aquaculture, 437,1–9.
20. Von Stetina, J. R., & Orr-Weaver, T. L. (2011). Developmental control of oocyte maturation and egg activation in metazoan models. Cold Spring Harbor Perspectives in Biology. https://doi.org/101101/cshpe rspect.a005533.
21. Yano, I. (1988). Oocyte development in the kuruma prawn *Penaeus japonicus*. Marine Biology, 99, 547–553.
22. Yano, I. (1992). Effect of thoracic ganglion on vitellogenin secretion in kuruma prawn, *Penaeus japonicus*. Bulletin National Research Institute of Aquaculture, 21,9–14.

An essential role of Rieske domain oxy genase Neverland inthemolting cycle of black tiger shrimp, *Penaeus monodon*

Molting is an important process for development and growth in arthropods. In crustaceans, molt is regulated by ecdysteroids or molting hormones that are synthesized in Y-organs. However, ecdysteroid biosynthesis pathway in crustaceans and its participating enzymes have not been well studied so far. In this study, a Rieske domain oxygenase, the enzyme that acts as cholesterol 7,8-dehydrogenase by converting cholesterol to 7-dehydrocholesterol in the first step of the ecdysteroid biosynthesis was characterized in black tiger shrimp, *Penaeus monodon*. A full-length cDNA of *P. monodon*'s Rieske domain oxygenase Neverland (PmNvd) was successfully cloned. The expression of *PmNvd* was dominantly found in the Y-organ, and changed during molting period. The *PmNvd* mRNA level was low in intermolt and early premolt stages, then dramatically increased in the mid premolt stage suggesting its role in molt regulation. The function of *PmNvd* in the molting process was investigated by RNAi approach. Silencing of *PmNvd* transcript in shrimp by specific double-stranded RNA (dsNvd) led to prolonged molt duration with abnormal molting progression, i.e. the molting process got stuck at early premolt stage. In addition, 20-hydroxyecdysone titer in the hemolymph of dsNvd-injected shrimp was significantly reduced compared with that in NaCl-injected shrimp. These evidences suggested a crucial role of PmNvd in molt progression, particularly during the initiation of premolt phase via the regulation of ecdysteroid production.

Introduction

Molt or ecdysis is a physiological process that is critical for growth in arthropods. In penaeid shrimp, the molting stages can be classified based on morphological changes on epidermal tails (Promwikorn et al., 2004). Ecdysis or shading of old exoskeleton occurred with several physiological changes, including high rate of water uptake and absorption of many ions such as Mg^{2+} and Ca^{2+} (Phlippen et al., 2000). The molting cycle can be divided into postmolt (stages A, B), intermolt (stage C), premolt (stage D) and molting or ecdysis (E). Each stage can be divided into sub-stages according to physical changes of the cuticle as can be clearly observed at the tip of uropod under light microscope (Promwikorn et al., 2004).

In crustaceans, the molting process is controlled by several hormonal factors, particularly ecdysteroids or molting hormones and moltinhibiting hormone (MIH) (Nakatsuji and Sonobe, 2004; Nakatsuji et al., 2006). Ecdysteroids are important steroid hormones that play a crucial role in molting process in ecdysozoa animals. In insect, ecdysteroids are synthesized in prothoracic gland, whereas crustacean ecdysteroids are synthesized in Y-organs. In addition to their role in the molting process, ecdysteroids are also involved in other physiological processes including oogenesis, longevity and neuronal activity (Uryu et al., 2015). By contrast, crustacean neuropeptide hormone MIH plays a role in the inhibition of ecdysteroid production by suppressing the uptake of cholesterol, an ecdysteroid precursor in the Y-organ (Nakatsuji et al., 2009; Kang and Spaziani, 1995a, 1995b; Spaziani and Wang, 1993). Moreover, MIH was also shown to inhibit a secretion of ecdysteroids from Y-organs (Nakatsuji et al., 2006; Nakatsuji and Sonobe, 2004; Mattson and Spaziani, 1985).

Ecdysteroids are secreted into hemolymph as an inactive form. The inactive ecdysteroids are then catalyzed to an active form in periphery tissues such as epidermis (Mykles, 2011). There are several derivatives of ecdysteroids including ecdysone (E), 3-dehydroecdysone, ponasterone and 20-hydroxyecdysone (20-HE) depending on ecdysteroid biosynthetic process of each organism (Mykles, 2011). For example, 20-HE and E were mainly found in shrimp, *P. monodon* (Kuo and Lin, 1996), *Litopenaeus vannamei* (Blais et al., 1994) and *Macrobrachium rosenbergii* (Okumura and Aida, 2000), whereas ponasterone and 20-HE or 3-dehydro-20-HE were major ecdysteroids found in several crabs such as *Carcinus maenas* (Lachaise et al., 1981), *Callinectes sapidus* (Chung, 2010) and *Menippe mercenaria* (Rudolph et al., 1992).

Ecdysteroid biosynthesis involves several chemical reactions catalyzed by ecdysteroidogenic enzymes including Rieske domain oxygenase Neverland (Nvd) and the Halloween gene family of cytochrome P450s (Mykles, 2011). Nvd acts as a cholesterol 7,8-dehydrogenase (Yoshiyama-Yanagawa et al., 2011) or cholesterol 7-desaturase (Wollam et al., 2011) which converts cholesterol to 7-dehydrocholesterol (7dC) in an early ecdysteroid biosynthetic pathway. Subsequently, 7dC was catalyzed to 5β-ketodiol by a series of Halloween P450 enzymes; CYP307A1/Spook (Spo), CYP307A2/Spookier (Spok) and CYP6T3 (Mykles, 2011; Niwa and Niwa, 2014; Rewitz et al., 2007). These catalytic steps are collectively called the "Black Box" as the intermediates in between are unknown. The 5β-ketodiol is further converted to ecdysone by another set of Halloween genes family including CYP306A1/Phantom (Phm), CYP302A1/Disembodied (Dib), and CYP315A1/Shadow (Sad) (Niwa and Niwa, 2014). The ecdysone is secreted into the hemolymph of arthropods and moves to peripheral tissues where it is finally converted to an active ecdysteroids, 20-HE by a CYP314A1/Shade (Shd) enzyme (Petryk et al., 2003).

Nvd is found in several organisms such as roundworms and arthropods as well as vertebrates (Lang et al., 2012; Sumiya et al., 2014; Wollam et al., 2011; Yoshiyama-Yanagawa et al., 2011; Yoshiyama etal., 2006). It has been shown to be essential for larval development in *Drosophila* as the development of *Drosophila* larva was arrested upon *Nvd* silencing, and eventually led to larval death (Yoshiyama et al., 2006). Recent study showed that *Nvd* plays an important role in the molting process of the water flea, *Daphnia magna*. *Nvd*1 knockdown in *D. magna*'s embryo led to a defect in embryonic molting and development (Sumiya et al., 2016). Since the function of *Nvd* in decapod crustaceans has not been characterized so far, this study is aimed at characterization of an ecdysteroidogenic enzyme, Nvd and functional analysis in the molting process in *P. monodon.*

Materials and methods

RNA isolation and cDNA synthesis

P. monodon were kindly provided by Shrimp Genetics Improvement Center, Surat Thani, Thailand. All Shrimp were reared in 10 ppt seawater for one week before experiments began. Shrimp were anesthetized on ice prior to tissue collection. Total RNA was extracted from freshly collected shrimp tissues by RiboZol reagent (AMRESCO, USA) following the manufacturer's protocol. Two micrograms of RNA sample were treated with a mixture of 1× RQ1 buffer and 1 U of RQ1 RNase free DNase (Promega, USA) by incubating at 37°C for 10 min in order to eliminate contaminating genomic DNA. Subsequently, the RQ1treated RNA sample was mixed with oligo-dT

primer (PRT), heated at 70°C for 3 min, and then placed on ice prior to the addition of 1× Improm®-II buffer, 3.0 mM MgCl2, 0.5 mM dNTP and 1µl of Improm-II reverse transcriptase (Promega, USA). The reverse transcription reaction was performed at 25°C for 5 min, 42°C for 60 min and 70°C for 10 min. The cDNA was kept at -20°C until used.

Cloning of a full- length cDNA of Rieske- domain oxygenase Neverland of P. monodon (PmNvd)

In order to obtain a partial nucleotide sequence of *PmNvd*, deduced amino acid sequences of Nvd from several insects and a sequence from *L. vannamei* EST database that shows high similarity to insect Nvd (GenBank Accession No. FE178330) were used to design primers for RT-PCR amplification. Y-organs cDNA of *P. monodon* was used as a template to amplify a partial *PmNvd* cDNA with the degenerate primers dPmNvd-F1 and dPmNvd-R1 (Table 1). Then, nested PCR was performed by amplifying the 1st PCR product with PmNvd-F2 and dPmNvd-R1 primers. The PCR reactions composing of 1× standard *Taq* polymerase buffer (NEB Laboratory, USA), 0.2 mM dNTP, 0.2µM each primers and 1 U *Taq* polymerase (NEB Laboratory, USA). The PCR reactions were performed at 95°C for 3 min, then 35 cycles of 95°C for 30 s, 50°C for 30 s and 68°C for 30 s, and final extension at 68°C for 5 min. After obtaining the *PmNvd* partial nucleotide sequence, the 3′ and 5′ regions of *PmNvd* cDNA were amplified by rapid amplification of cDNA ends (RACE). For 3′ RACE, the oligo-dT-primed Y-organ cDNA was amplified with PmNvd-F3 and PRT primers, and the PCR product was further used to amplify with nested primers (PmNvd-F4 and PM1). For 5′ RACE, two microgram of Y-organ total RNA was used to synthesize the first-stranded cDNA with PmNvd-R1 primer designed from the partial cDNA sequence. The 3′ end of the first-stranded cDNA was tailed with dATP in a mixture of 1× TdT buffer (Promega) and 0.4 mM dATP. The sample was heated at 94°C for 3 min and placed on ice. Then, approximately 20 U TdT (Promega) was added to the mixture, and the reaction was performed at 37°C for 30 min, followed by 65°C for 10 min. The A-tailed cDNA was used as a template in the PCR reaction with PmNvd-R2 and PRT primers. The first PCR product was subsequently used as a template for nested PCR with PmNvd-R3 and PM1. The overlapping DNA sequences of the 3′ and 5′ RACE PCR products were verified by amplification of a full-length *PmNvd* cDNA with FullPmNvd-F and FullPmNvd-R primers by KAPA long Range DNA polymerase (KAPABiosystems). The nucleotide sequences of all primers were shown in Table 1.

Determination of PmNvd mRNA expression in shrimp by quantitative reverse transcription PCR (qRT-PCR)

In order to determine expression level of *PmNvd* in shrimp, several tissues including eyestalk, brain, thoracic ganglia, abdominal nerve cord, hepatopancreas, Y-organ, ovary and muscle were isolated from two previtellogenic female shrimp at premolt stage, and the expression of *PmNvd* in these tissues was determined by qRT-PCR. The Y-organ from juvenile shrimp (approximately 10 g) at different stages of molt ($n = 4 - 8$ each) which was classified by changing pattern of tail fan epidermis under light microscope (Promwikorn et al., 2004) were used to determine expression profile of *PmNvd* during the molting cycle. The first-stranded cDNA from each tissue was added with a mixture of 1× SYBR® FAST Master Mix (KAPA Biosystems) and

0.4 μM PmNvd-F4 and *PmNvd*-R2. The PCR reaction was performed at 95 °C for 3 min, then 40 cycles of 95 °C for 5 s and 60 °C for 30 s in a realtime PCR machine (Realplex4, Eppendorf). Subsequently, the PCR product was analyzed for a melting curve with a temperature profile of 95 °C for 30 s, 60 °C for 30 s, 95 °C for 30 s. Elongation factor 1 alpha (EF1α) was used as an internal control. The efficiency of *PmNvd* and *EF1α* specific primers were 101% and 100%, respectively. Relative quantification was performed using a standard curve constructed by amplifying serial dilution of known amount of purified PCR products (102–108 copies) of either *PmNvd* or *EF1α*.

Table 1 List of oligo-nucleotide used in this study.

Name	Propose	Sequence (5′ → 3′)
dPmNvd-F1	Partial sequence	TNGAYGCYTACTGCCCGCA
dPmNvd-R1	Partial sequence	GTCDGCNCCRTTYTCDGG
PmNvd-F2	Partial sequence	AGATGTCCATACCATGGTTGG
PmNvd-F3	3′RACE	GCTATTCAGAGGGTCTGATGGC
PmNvd-F4	3′RACE and qPCR	GCTCCTGTGCCCACATTC C
PmNvd-R2	5′RACE and qPCR	GGGAATCTCCTGAATATGTGCG
PmNvd-R3	5′RACE	CTT CAT GGT AGG TCC TTC CGC
FullPmNvd-F	PCR	ACTCCAGGATCATCATTTGTCG
FullPmNvd-R	PCR	GCATTATTTCCATGAGGCAGCG
XbaI-stNvd-F	dsNvd	GCTCTAGAAGGGACGACTTCCGCAATG
EcoRI-stNvd-R	dsNvd	CGGAATTCGGACGA TCTTCTGCCTGA GG
XhoI-stLNvd-F	dsNvd	CCGCTCGAGAGGGACGACTTCCGCAATG
EcoRI-stLNvd-R	dsNvd	CGGAATTCACTTGAGGATTTGGCGGTCC
PRT	cDNA synthesis	CCGGAATTCAAGCTTCTAGAGGATCCTTTTTTTTTTTTTTTT
PM1	RACE	CCGGAATTCAAGCTTCTAGAGGATCC
EF1α-F	qPCR	GAACTGCTGACCAAGATCGACAGG
EF1α-R	qPCR	GAGCATACTGTTGGAAGGTCTCCA
Actin-F	PCR	GACTCGTACGTGGGCGACGAGG
Actin-R	PCR	AGCAGCGGTGGTCATCTCCTGCTC

Construction and expression of double-stranded RNA specific to PmNvd (dsNvd)

The *PmNvd*-specific double-stranded RNA was produced as a stemloop (small hairpin) precursor in *Escherichia coli* using pET17b plasmid as an expression vector. The template of stem and stem-loop fragments were amplified with specific primers tagged with restriction enzyme sites: *Xba*I-stNvd-F and *Eco*RI-stNvd-R for amplification of the stem fragment and *Xho*I-stLNvd-F and *Eco*RI-stLNvd-R for the stem-loop fragment (Table 1). After amplification, the stem and stem-loop fragments were sequentially cloned into pET17b vector at the corresponding restriction sites, in a sense and antisense direction relative to the T7 promoter, respectively. The recombinant plasmid was then transformed into *E. coli* DH5α. After verification of the nucleotide sequence by automated DNA sequence (1st BASE Company, Malaysia), the correct recombinant plasmid was re-transformed into *E. coli* HT115 for dsRNA expression. The *E. coli* HT115 carrying the expression plasmid for dsNvd was cultured in LB medium containing 100 μg/ml ampicillin and 25 μg/ml tetracycline overnight at 37°C. The culture was inoculated at a dilution of 1:50 in the desired volume of LB medium, then the bacterial culture was incubated at 37°C, 250 rpm for 1.5–2 h until its OD_{600} reached 0.4–0.6. Subsequently, the culture was induced with 0.4 mM IPTG for 4 h prior to extraction of dsNvd by ethanol method (Posiri et al., 2013). Briefly, the bacteria cells were collected and re-suspended in PBS pH 7.4. Ethanol was added to a final concentration of 75% and incubated at room temperature for 5 min. Then the cells were centrifuged at 5000 g for 5 min, and the pellet was re-suspended with 150 mM NaCl

and incubated at room temperature for 1 h. The supernatant containing dsNvd was collected by centrifuged at 13,000 rpm for 10 min. The dsNvd was verified by RNase digestion assay with either 0.1 μg/ml RNase A or 1 U RNase III (Invitrogen) by incubation at 37°C for 5 min and analyzed on agarose gel electrophoresis.

Effect of PmNvd depletion on molt duration

Firstly, the effect of dsNvd on PmNvd silencing in *P. monodon* was determined. Approximately 10 g shrimp was injected with either NaCl or dsNvd at 2.5μg·g^{-1} shrimp. Then, the Y-organ was isolated on days 3 and 6 after dsRNA injection, and *PmNvd* expression was determined by semi-quantitative RT-PCR with PmNvd-F4 and PmNvd-R2 primers. Actin transcript was amplified with Actin-F and Actin-R primers as an internal control. To study the function of PmNvd during the molting cycle, shrimp at intermolt stage was injected with 2.5μg·g^{-1} shrimp of dsNvd twice, on day 0 and day 3, and the molting stage and molt duration of the shrimp were recorded compared to that of the control shrimp that were injected with NaCl.

Detection of 20-hydroxyecdysone (20-HE) titers in shrimp hemolymph by reverse phase high performance-liquid chromatography (RP-HPLC)

Shrimp at intermolt stage were injected with 2.5μg·g^{-1} shrimp of dsNvd or NaCl (n= 9 each), and the hemolymph ecdysteroid titers were measured by reverse-phase HPLC (RP-HPLC). Approximately 200–400 μl of hemolymph from individual shrimp was collected in 100 μl of anticoagulant (10 mM Tris pH 7.4, 250 mM sucrose and 100 mM sodium citrate). The hemolymph from shrimp in the same group was pooled, and then hemocytes were removed by centrifugation at 800 g for 10 min. The plasma was then extracted with 75% methanol followed by centrifugation at 13,000 rpm for 10 min. The supernatant was collected and dried by evaporation. The sample was dissolved in 35% methanol and subsequently subjected into Sep-Pak C-18 cartridge (Waters). The hemolymph ecdysteroids eluted with 100% methanol were dried by evaporation and re-dissolved in 10–15μl of 35% methanol. Five microliters of the sample were injected into the Acclaim® RLSC C-18 (2.2 μm, 2.1× 100 mm, Dionex) column connected with HPLC machine (Ultimate 3000 UHPLC, Dionex). The chromatography was performed by gradient elution with 35% to 60% methanol for 20 min at a flow rate of 0.3 ml/min. The signals were detected by UV absorbance at wavelength of 240 nm. The 20-HE (Abcam) at different concentrations (25–200 ng/μl) that was eluted at retention time of approximately 8.8 min was used to construct a standard curve. The peak area was calculated by Chameleon® software version 6.8.

Results

Cloning of a full-length cDNA of PmNvd

A 1727 bp full-length cDNA of Rieske domain oxygenase Neverland of *P. monodon* (*PmNvd*) was successfully cloned (GenBank Accession No. KU360639). It was composed of a 160 bp 5'UTR, a 1341 bp coding region for a putative 447 amino acids and a 226 bp 3' UTR (Fig. 1). The deduced PmNvd contains a signal peptide at the first 14 amino acid residues and a transmembrane motif^{33}WxxF^{59} as predicted by SOSUI (Gomi et al., 2004). In addition, the Rieske [2Fe-2S] domain motif^{107}AxxG^{209} with the highly conserved sequence C-X-H-$X_{16–17}$-C-X_2-H was predicted by pfam, and a non-heme iron-binding motif E-X_3-D-X_2H-X_4-H waspredicted by COACH server

(Yang et al., 2013a, 2013b). An amino acid sequence alignment, particularly the Rieske domain (Fig. 2A) and the non-heme iron binding domain, indicated that the deduced PmNvd was highly similar to Rieske domain oxygenase Neverland of other species such as *Bombyx mori*, *Drosophila melanogaster* and *Caenorhabditis elegans* (Fig.2B). Furthermore, phylogenetic analysis in Fig. 3 revealed that PmNvd was separated from Nvd of insects, nematodes and chordates. It was clustered in the same group as Nvd of the sea urchin, *Hemicentrotus pulcherrimus*, but on separate branch from Nvd1 and Nvd2 of the planktonic crustacean *D. magna*.

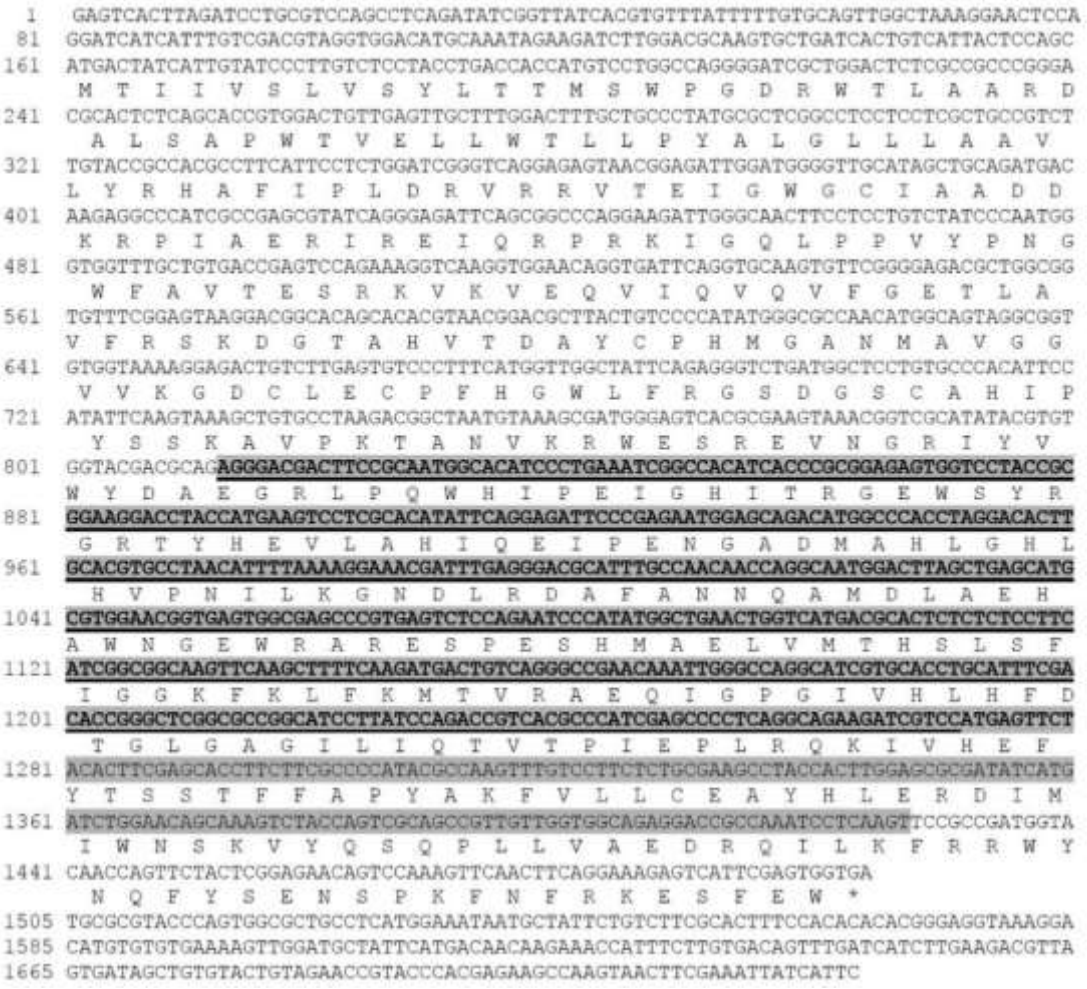

Fig. 1. Nucleotide and deduced amino acid sequences of PmNvd (GenBank Accession No. KU360639). The full-length *PmNvd* cDNA of 1727 nucleotides is shown with its deduced 447 amino acid residues as one-lettered symbols underneath the corresponding codons. The region used for dsRNA design is highlighted, where underlined nucleotides represent the stem region of the dsRNA. An asterisk indicates the stop codon.

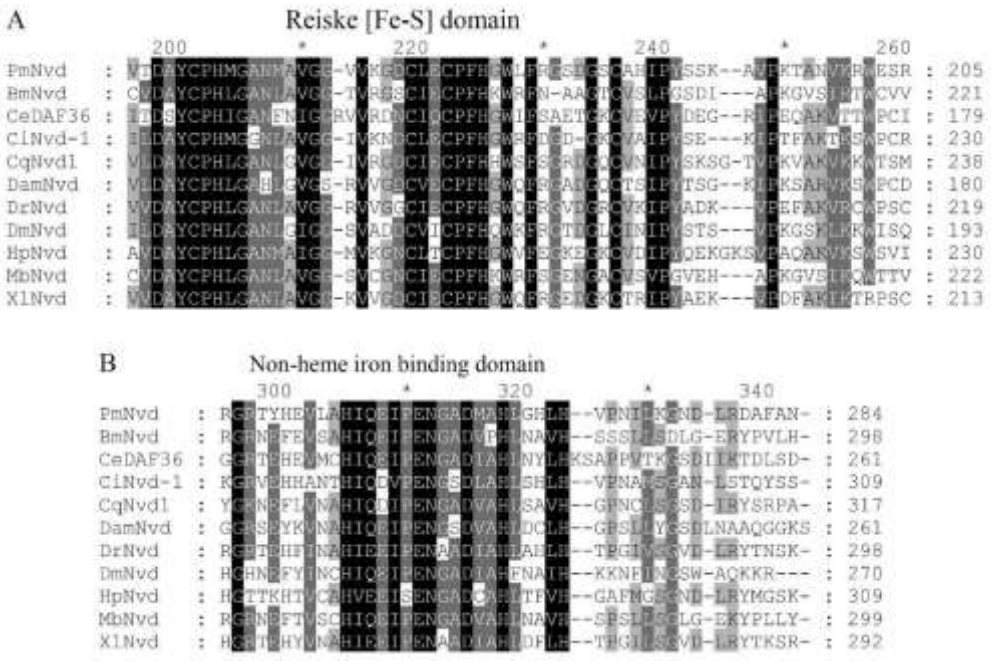

Fig. 2. Alignment of conserved domains of amino acid sequences of invertebrate Rieske domain oxygenase Neverland. The Rieske [Fe-S] domain (A) and non-heme iron binding domain (B) of the deduced amino acids of *P. monodon*'s Nvd (Accession No. KU360639) are compared with the same conserved domain of Nvd from other invertebrates including *B. mori* (Accession No. NM_001044161; BmNvd), *C. elegans* (Accession No. NM_073228; CeDAF36), *Ciona intestinalis* (Accession No. AB607952; CiNvd-1), *Culex quinquefasciatus* (Accession No. XM_001847974; CqNvd), *D. magna* (Accession No. AB839171; DamNvd), *Danio rerio* (Accession No. AB607951; DrNvd), *D. melanogaster* (Accession No. NM_001104200; DmNvd), *Mamestra brassicae* (Accession No. AB649116; MbNvd), *Hemicentrotus pulcherrimus* (Accession No. AB607954; HpNvd) and *Xenopus laevis* (Accession No. AB607950; XlNvd) using ClustalW software. The conserved amino acid residues were highlighted in black, and amino acids with lesser similarity levels are shaded in gray.

Determination of PmNvd mRNA expression in shrimp tissues

In order to determine the expression of *PmNvd* mRNA in the shrimp, *PmNvd* transcript levels in various tissues were detected by qRT-PCR. The result in Fig. 4 showed that *PmNvd* expression was mainly found in the Y-organ but not in other tissues i.e., eyestalk, brain, thoracic ganglia, hepatopancreas, gills, muscle and lymphoid. Furthermore, investigation of *PmNvd* expression in the Y-organ at different stages of the molting cycle showing that PmNvd was expressed at low level in the shrimp at intermolt (C) and early premolt (D0) stages (Fig. 5). A dramatic increase of *PmNvd* expression occurred at the premolt stage D1 prior to a slight decline at later premolt stages, D2 and D3. Subsequently, the expression level of *PmNvd* dropped to the basal level at late premolt stage (D4) and after ecdysis.

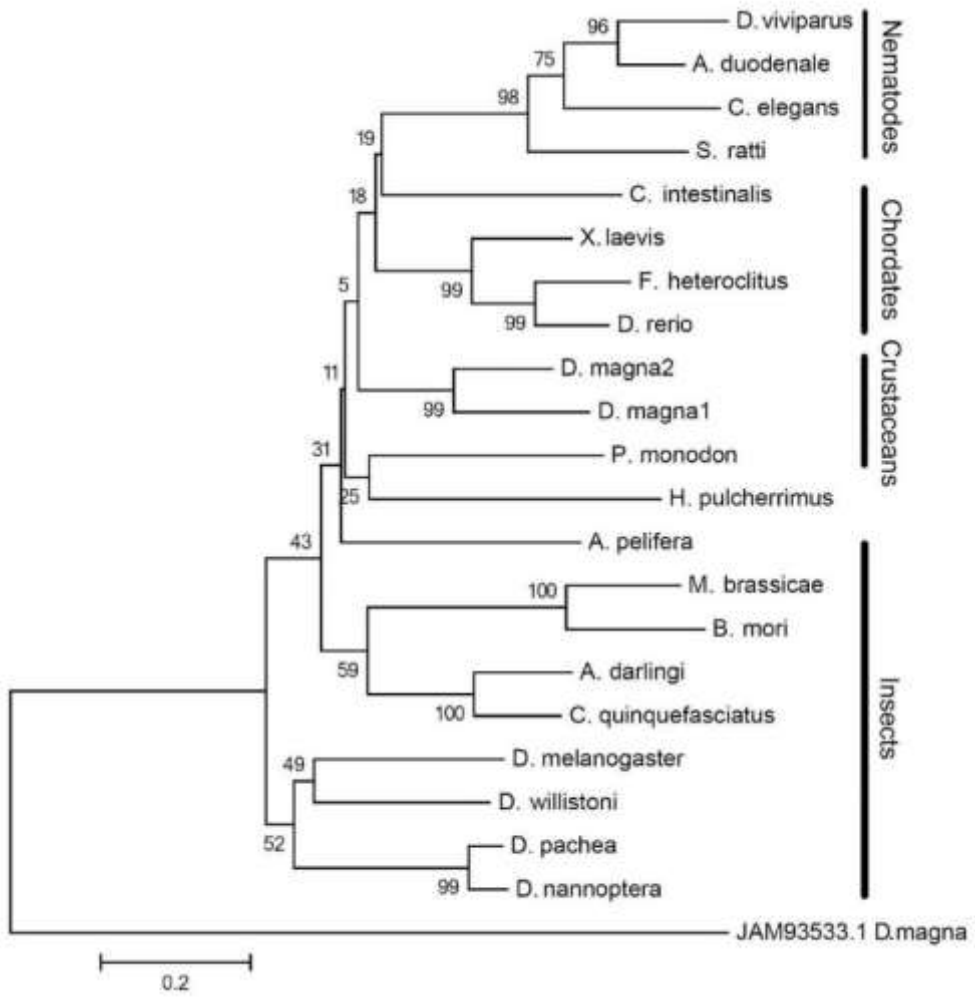

Fig. 3. Phylogenetic analysis of PmNvd. The full sequences of deduced amino acids of Nvd from several organisms were used to construct the phylogenetic tree. The sequences were aligned by MUSCLE multiple sequence alignment. The phylogenetic tree was generated by a Neighbor-Joining method based on the Poisson correction model using MEGA 6.06 software. The phylogeny test was performed by a bootstrap method at 1000 replicates. The tree is drawn to scale with branch length representing the number of substitutions per site. The amino acid sequences of Nvd include PmNvd, *Aedes darlingi* (Accession No. ETN63840), *Ancylostoma duodenale* (Accession No. KIH60101), *Apis melifera* (Accession No. BAJ54122), *B. mori* (Accession No. NP_001037626), *C. elegans* (Accession No. NM_073228), *C. intestinalis* (Accession No. BAK39961), *C. quinquefasciatus* (Accession No. EDS27493), *D. magna* Nvd1 and Nvd2 (Accession No. BAQ02388 and BAQ02389, respectively), *D. melanogaster* (Accession No. NP_001097670), *D. nannoptera* (Accession No. AFD97359), *D. pachea* (Accession No. AFU25035), *D. Rerio* (Accession No.BAK39960), *D.willistoni* (Accession No. XP_002070225), *Dictyocaulus viviparus* (Accession No. KJH52421), *Fundulus heteroclitus* (Accession No.JAQ79933), *H. pulcherrimus* (Accession No. BAK39963), *M. brassicae* (Accession No. BAN66310), *Strongyloides ratti* (Accession No. CEF66692) and *X. laevis* (Accession No. BAK39959) The iron-sulfur protein's *D. magna* (Accession No. JAM93533) was used as an outgroup.

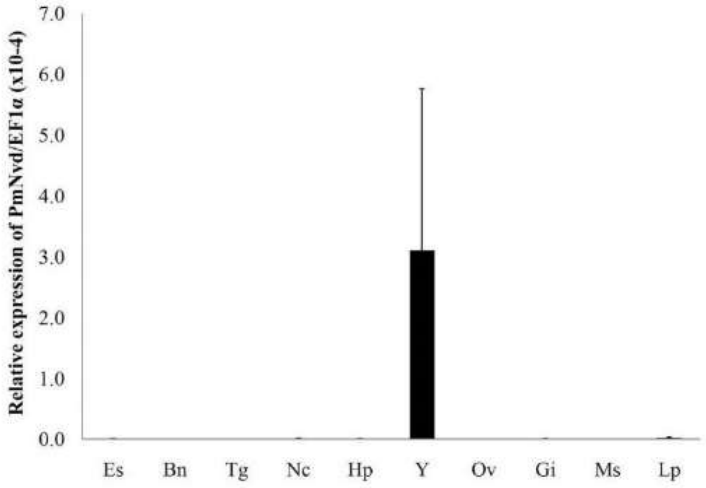

Fig. 4. Expression of *PmNvd* mRNA in *P. monodon* tissues. The mRNA expression level of *PmNvd* in various shrimp tissues including eyestalk (Es), brain (Bn), thoracic ganglia (Tg), nerve cord (Nc), hepatopancreas (Hp), Y-organ (Y), ovary (Ov), gills (Gi), muscle (Ms) and lymphoid organ (Lp) were determined by qRT-PCR, and presented as relative expression levels compared with that of EF1α of the same sample. The expression profiles from two adult female shrimp were shown. Bars and error bars represent mean and SEM, respectively.

Effect of PmNvd knockdown on molting duration

In order to study the function of PmNvd in shrimp, a double-stranded RNA targeting *PmNvd* coding sequence (dsNvd) was expressed in *E. coli* HT115 as a small hairpin precursor. An approximately 500 bp small-hairpin dsNvd was validated for dsRNA characteristic by RNase digestion. The result in Fig. 6A suggested that the single-stranded loop region of the small hairpin dsNvd was digested by RNase A resulting in a 459 bp of dsNvd, whereas the dsNvd was completely digested with RNase III, thus confirming its double-stranded structure. The knockdown efficiency of dsNvd was further determined by monitoring *PmNvd* expression in the Y-organ of the shrimp after injected with dsNvd. Fig. 6B–C revealed that *PmNvd* transcript in the dsNvd-injected shrimp was significantly suppressed to an undetectable level by RT-PCR on day 3 after dsNvd injection compared with that in NaCl-injected shrimp. Moreover, *PmNvd* expression in dsNvd-injected shrimp began to recover partially on day 6.

The effect of *PmNvd* depletion on molt duration was further investigated by following the progress of molting cycle of *PmNvd* knockdown shrimp. Since the *PmNvd* transcript level in dsNvd-injected shrimp seemed to recover after day 3, the shrimp in this experiment were injected with dsNvd twice on days 0 and 3 to assure effective *PmNvd* silencing. Approximately 80% of shrimp were arrested at early premolt stage (D0) on day 3 after the first injection with 2.5μg·g^{-1} shrimp dsNvd, while approximately

90% of NaCl-injected shrimp could proceed to later premolt stages (D1-D3) (Fig.7A). Moreover, about 80% of dsNvd-injected shrimp remained at early premolt stage(D0) on day 7 after injection while the majority of NaCl-injected shrimp continuously progressed to late premolt stage (D4). Interestingly, approximately 80% of dsNvd-injected shrimp were arrested at early premolt stage for approximately 12 days after the second injection whereas all NaCl-injected shrimp had completed the first round of the molting cycle (Fig. 7B). Nevertheless, molting of the dsNvd-injected shrimp started to progress gradually after 15 days post injection and could eventually molt in an average of 26.1 ± 3.8 days (Fig. 7B) while the control shrimp had already molted for three cycles with the average molting duration of 9.0 ± 1.1, 10.3 ± 1.4 and 9.8 ± 0.8 days, respectively (Fig. 7B).

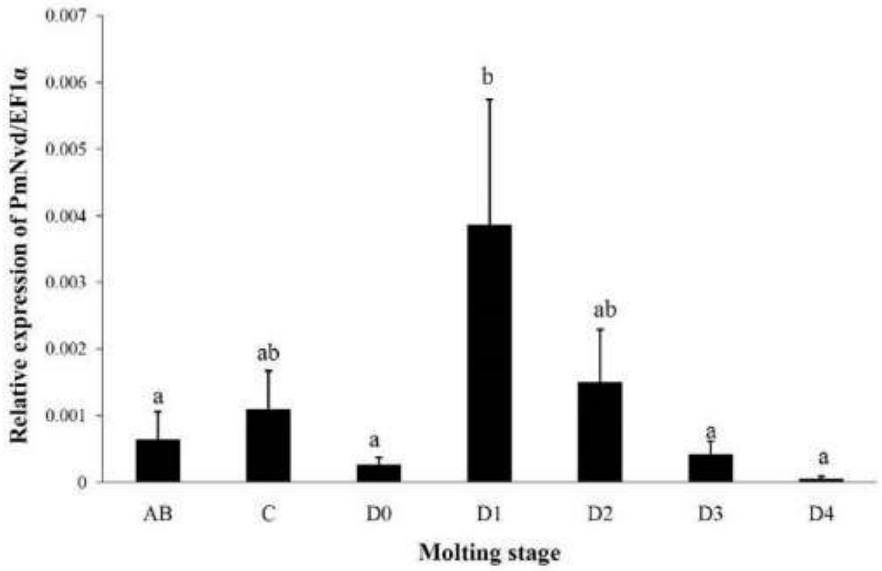

Fig. 5. Expression of *PmNvd* mRNA in the Y-organs at different molting stages. The Yorgans isolated from approximately 10 g *P. monodon* at different molting stages (n=4 –8 each) were used to determine the *PmNvd* expression level by qRT-PCR. Shrimp molting stages are characterized by physical changes of the cuticle at the tip of uropod as observed under light microscope (Promwikorn et al., 2004) as follows: postmolt (A, B) - the complete formation of setal cones; intermolt (C) – rigid integument and formation of the new cuticle is completed; early premolt (D0) - starting of the retraction of the epidermal tissue from the cuticle; premolt (D1–D3) - clear zone between the setal cones and the epidermis is clearly recognized at D1 and getting wider from D1 to D3, the edge of the epidermis becomes wavy at D2, and the white thin layer is clearly seen at the edge of the epidermis in D3; late premolt (D4) - serrated edge of the epidermis, light-reflecting at the edge of the white layer and epidermis present a paralleled-band pattern. Bars and error bars represent mean of relative expression levels compared with that of EF1αof the same sample and SEM, respectively. Different alphabets represent significant difference between groups ($p < 0.05$) as analyzed by ANOVA and pair-wise comparison by Tukey HSD.

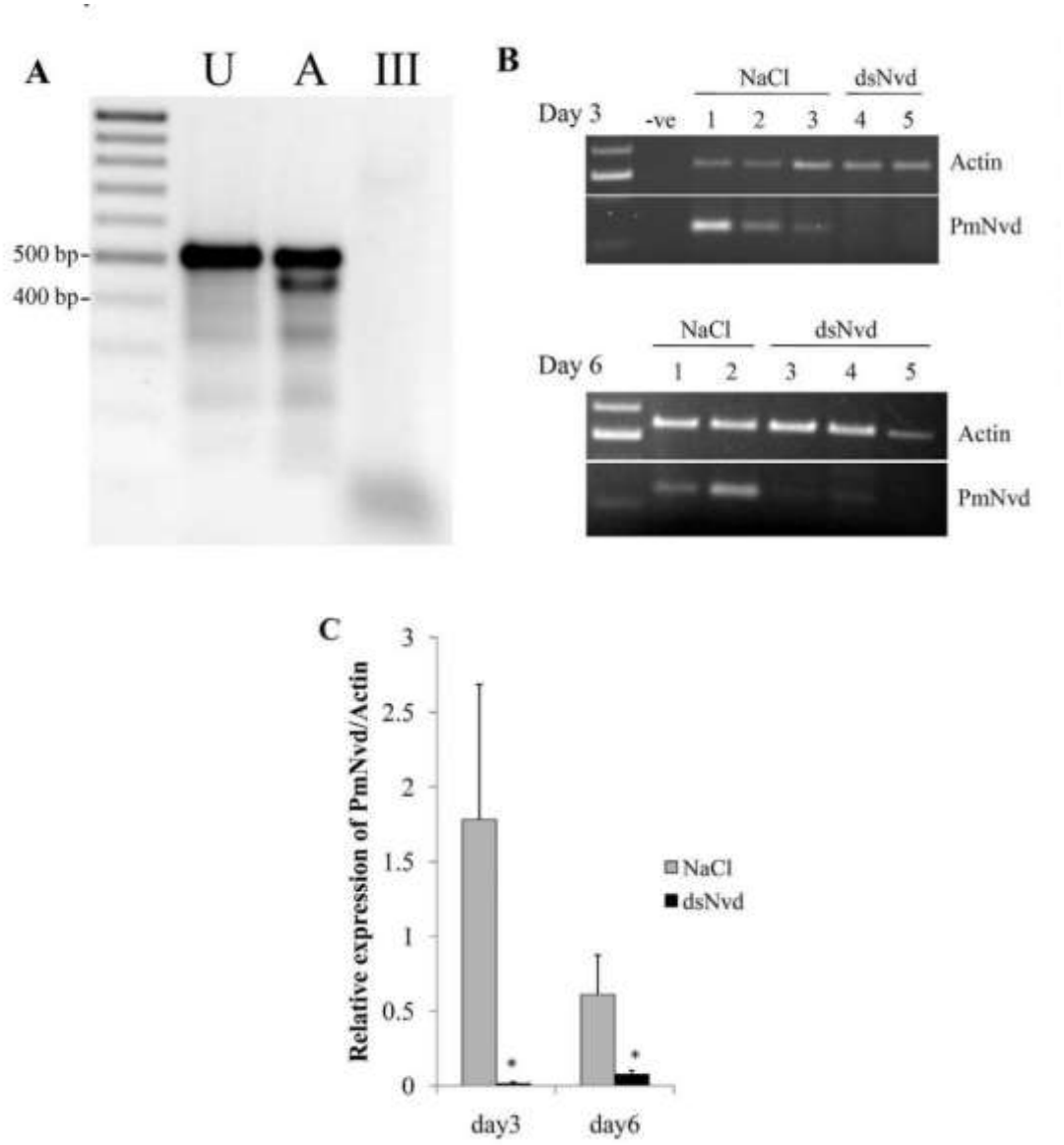

Fig. 6. Production and efficiency of *PmNvd*-specific dsRNA (A). The integrity of PmNvd-specific dsRNA (dsNvd) expressed in *E. coli* HT115 was verified by RNase digestion. The dsNvd digested with RNase A (A), RNase III (III) or water as a negative control (U) was separated in agarose gel compared with a DNA ladder marker. (B) The efficiency of *PmNvd* knockdown in shrimp was determined on days 3 and 6 after dsNvd injection.The *PmNvd* transcript in the Y-organ of shrimp injected with dsNvd or NaCl was determined by semi-quantitative RT-PCR. Actin was used as an internal control. Numbers represent individual shrimp, and –ve is a negative control of PCR reaction. (C) Relative expression of *PmNvd* to *actin* calculated from the intensity of RT-PCR products of both transcripts is shown in a bar graph. Bars and error bars represent means and SEM, respectively. Asterisks indicate a significant difference at $p < 0.05$ between groups analyzed by *t*-test.

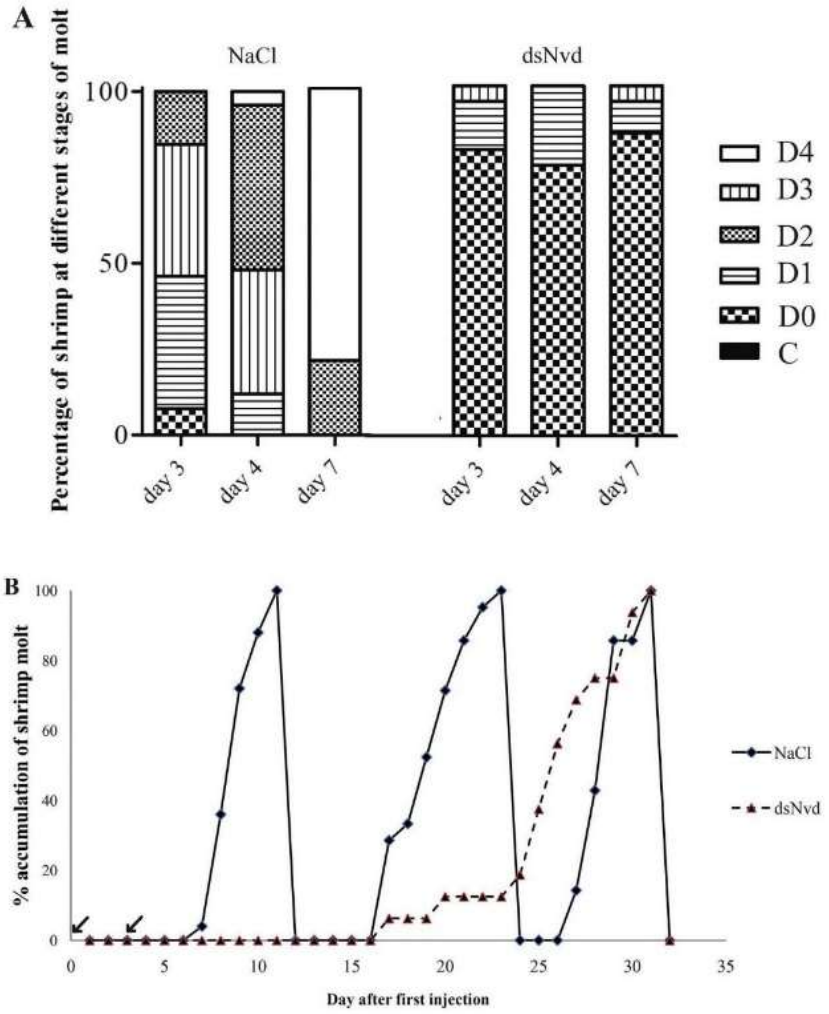

Fig. 7. Effect of *PmNvd* silencing on molt progression and molt duration. Approximately 10 g *P. monodon* was injected with dsNvd (n= 22) or NaCl (n= 25) twice on days 0 and day 3. (A) The numbers of shrimp in each group that were in different stages of molt (depicted by different filled patterns) were recorded on days 3, 4 and 7 and presented as the percentage compared to the total numbers of shrimp in that group. (B) The duration of molting cycle of shrimp is presented as the percentage of accumulated number of shrimp that molted in each day after dsNvd injection. Solid and dash lines represent NaCl and dsNvd-injected shrimp, respectively. Arrows indicate the day on which the shrimp were injected with dsNvd or NaCl.

Hemolymph ecdysteroid titer upon PmNvd knockd

In order to examine whether the interruption of the molting cycle by *PmNvd* depletion is related to ecdysteroid production or not, ecdysteroid (20-HE) titers in the hemolymph of *PmNvd* knockdown shrimp were determined by RP-HPLC. On day 3 after dsRNA injection, most of the shrimp in both dsNvd-injected group and the control group were at intermolt (C) and early premolt (D0) stages, and some (approximately

20%) of the control shrimp were in premolt stage D1 (Fig. 8A). Ecdysteroid titers of the shrimp in both groups were measured. The peak corresponding to the same retention time of 20-HE standard was calculated for 20-HE equivalent of ecdysteroid titers (Fig. 8B). The result showed that the hemolymph 20-HE in dsNvd-injected shrimp was retained in lower level at 9.9 ± 4.7 ng/ml compared with that in NaCl-injected shrimp (47.3 ± 7.5 ng/ml) as shown in Fig. 8C.

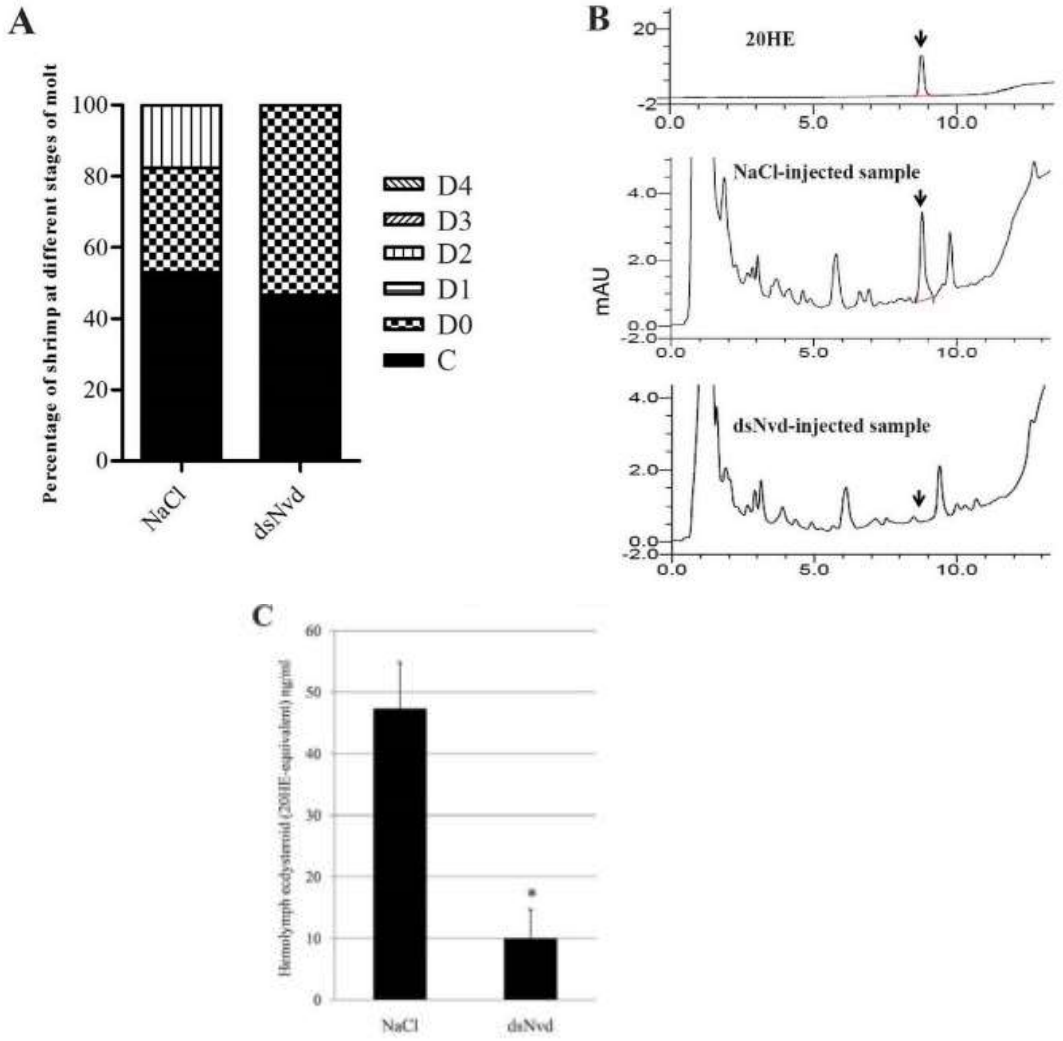

Fig. 8. Effect of *PmNvd* depletion on hemolymph ecdysteroid titer. P. monodon (~10g) at intermolt stage was injected with dsNvd (n= 12) or NaCl (n = 18). (A) After injection for 3 days, the molt stage of shrimp was recorded and presented as a percentage compared to total numbers of shrimp in that group. (B) The ecdysteroid titers in shrimp hemolymph were measured by RP-HPLC. The chromatogram of 20-HE in the standard, hemolymph from NaCl- or dsNvd injected shrimp was indicated as a peak eluted at 8.8 min retention time at the absorbance of 240 nm. (C) Pooled hemolymph from 3 shrimp in each group was used for the calculation of 20-HE levels from the peak area of RP-HPLC. Bars and error bars represent mean and SEM, respectively. Asterisk is significant difference at $p < 0.05$ analyzed by t-test.

Discussion

Rieske domain containing oxygenase Neverland (Nvd) functions in converting cholesterol to 7-dehydrocholesterol (7dC) in the early ecdysteroid biosynthetic pathway. Nvd were present in both vertebrates such as *Ciona intestinalis*, Danio rerio and *Xenopus laevis* (YoshiyamaYanagawa et al., 2011) and invertebrates such as *D. magna* (Sumiya et al., 2014), *Drosophila spp*. (Lang et al., 2012) and *B. mori* (Yoshiyama et al., 2006) including the DAF-36 of *C. elegans* (Wollam et al., 2011; Yoshiyama-Yanagawa et al., 2011). However, *Nvd* has not been identified in shrimp so far. In this study, the full-length Nvd cDNA was successfully obtained from a marine shrimp, P. monodon, and its deduced amino acid sequence revealed a high similarity to Nvd of other organisms (Fig. 2). Nvd was demonstrated to be located at microsomal membrane in CHO cells (Yoshiyama-Yanagawa et al., 2011) and S*f*9 cells (Wollam et al., 2011), and thus, is most likely localized to endoplasmic reticulum. The presence of a putative transmembrane motif in PmNvd structure may also indicate its localization at microsomal membrane. Furthermore, the Rieske domain (2Fe-2S motif) and nonheme Fe^{2+} binding domain of PmNvd were highly conserved among that in other species (Fig. 2). The phylogenetic analysis revealed that Nvd of *P.monodon* is more closely related to thatof seaurchin than that of *D. magna*, and distinguish from that of insects, chordates and nematodes, suggesting that *P. monodon*'s Nvd evolutionarily diverged from *D. magna* and other organisms.

Nvd is expressed in the prothoracic gland in insects such as *B. mori* and *D. melanogaster* as well as in the ring gland of *D. melanogaster* embryo (Yoshiyama et al., 2006) which is a source of ecdysteroid production, while *DAF*-36, a Nvd homolog of *C. elegans*, is expressed in the intestinal cytoplasm and head mesodermal cells (Rottiers et al., 2006). In *D. magna*, Nvd is mainly found in the gut, but less in ovary and other tissues (Sumiya et al., 2014). In *P. monodon*, *PmNvd* was dominantly expressed in the Y-organ, a source of ecdysteroid synthesis in crustaceans, but not found in ovaries (Fig. 4). This is similar to the expression of *Phantom* (*Phm*), one of the ecdysteroidogenic enzymes, that was specifically expressed in the Y-organ of kuruma prawn, *Marsupenaeus japonicus* (Nakatsuji et al., 2006). Furthermore, Nvd of a crayfish, *Pontastacus leptodactylus*, was also found in Y-organ's transcriptome data (Tom et al., 2013). These results suggest theexistence of ecdysteroidogenic pathway in the Y-organ of penaeid shrimp. According to phylogenetic analysis in Fig. 3, PmNvd is diverse from Nvd of *D. magna* and insects. This may explain different sources of ecdysteroid biosynthesis among insects, shrimp and *D. magna* that are from different evolutionary patterns. In addition, *PmNvd* in the Y-organ was expressed at the highest level in premolt stage of the molting cycle (Fig. 4). This is also similar to an increase of *M. japonicus*'s *Phm* expression during premolt stage (Nakatsuji et al., 2006). Moreover, *Nvd* expression in insects was increased before ecdysis in the 4th and 5th instar larvae of *B. mori* and *D. melanogaster* (Yoshiyama et al., 2006). The expression profile of Nvd is in accordance with the highest level of hemolymph ecdysteroids that was also found in the premolt stage in several crustaceans including *P. monodon* (Kuo and Lin, 1996), *P. vannamei* (Blais et al., 1994), *C. sapidus* (Chung, 2010), *C. maenas* (Styrishave et al., 2008), *Emerita asiatica* (Gunamalai et al., 2004), *Armadillidium vulgare* (Suzuki et al., 1996) and *Homarus americanus* (Snyder and Chang, 1991). The relationship between *Nvd* expression and ecdysteroid production at premolt stage suggested apossible role of PmNvd in ecdysteroid biosynthesis.

In this study, the role of PmNvd in the molting cycle was demonstrated by *PmNvd* knockdown in the shrimp. The *PmNvd*-specific dsRNA was successfully produced in the bacterial system, and it could completely suppress *PmNvd* transcript in the Y-organ within 3 days after injection into shrimp (Fig. 6B-C). Interestingly, molting progression in *PmNvd*-depleted shrimp was arrested at early premolt stage (D0) resulting in a delay of the molt duration (Fig. 7). Similarly, silencing of *Nvd* in *D. melanogaster* larvae also led to developmental arrest into pupae stage and eventually death (Yoshiyama et al., 2006). The development of the larvae could not be recovered by cholesterol administration (Lang et al., 2012; Yoshiyama et al., 2006). However, it was rescued by the treatment with 7dC in concurrence with an increased ecdysteroid titer (Yoshiyama et al., 2006) suggesting the function of Nvd in the conversion of cholesterol to 7dC at the early step of ecdysteroid production. Furthermore, a dramatic decrease of hemolymph 20-HE titer in dsNvd-injected shrimp (Fig. 8B) indicated that *PmNvd* is basically involved in ecdysteroid biosynthesis. The arrest of molting progression at the early premolt stage upon *PmNvd*-depletion conformed to *PmNvd* expression profile that increased in the premolt stage (Fig. 5). This result suggested that there was a checkpoint of the molting process between early premolt and premolt stages that is dependent of hemolymph ecdysteroids titer. In addition, several studies reported the important role of Nvd in embryonic development and metamorphosis. For example, depletion of *Nvd* in *D. magna* resulted in lethal embryo (Sumiya et al., 2016) similar to that in *D. melanogaster* larvae (Yoshiyama et al., 2006). Therefore, Nvd is required for the progression in the premolt stage of ecdysis during both metamorphosis and growth via the regulation of ecdysteroid production.

References

1. Blais, C., Sefiani, M., Toullec, J.-Y., Soyez, D., 1994. In vitro production of ecdysteroids by Y-organs of Penaeus vannamei (Crustacea, Decapoda). Correlation with hemolymph titers. Invertebr. Reprod. Dev. 26, 3–11.
2. Chung, J.S., 2010. Hemolymph ecdysteroids during the last three molt cycles of the blue crab, Callinectes sapidus: quantitative and qualitative analyses and regulation. Arch. Insect Biochem. Physiol. 73, 1–13.
3. Gomi, M., Sonoyama, M., Mitaku, S., 2004. High performance system for signal peptide prediction: SOSUIsignal. Chem-Bio. Inf. J. 4, 142–147.
4. Gunamalai, V., Kirubagaran, R., Subramoniam, T., 2004. Hormonal coordination of molting and female reproduction by ecdysteroids in the mole crab Emerita asiatica (Milne Edwards). Gen. Comp. Endocrinol. 138, 128–138.
5. Kang, B.K., Spaziani, E., 1995a. Uptake of high-density lipoprotein by Y-organs of the crab, Cancer antennarius. I. Characterization in vitro and effects of stimulators and inhibitors. Arch. Insect Biochem. Physiol. 30, 61–75.
6. Kang, B.K., Spaziani, E., 1995b. Uptake of high-density lipoprotein by Y-organs of the crab, Cancer antennarius. II. Formal characterization of receptor-mediation with isolated membranes. Arch. Insect Biochem. Physiol. 30, 77–91.
7. Kuo, C.M., Lin, W.W., 1996. Changes in morphological characteristics and ecdysteroids during the moulting cycle of tiger shrimp, Penaeus monodon Fabricus. Zool. Stud. 352, 118–127.

8. Lachaise, F., Goudeau, M., Hetru, C., Kappler, C., Hoffmann, J.A., 1981. Ecdysteroids and ovarian development in the shore crab, Carcinus maenas. H-S Z Physiol. Chem. 362, 521–529.
9. Lang, M., Murat, S., Clark, A.G., Gouppil, G., Blais, C., Matzkin, L.M., Guittard, É., Yoshiyama-Yanagawa, T., Kataoka, H., Niwa, R., Lafont, R., Dauphin-Villemant, C., Orgogozo, V., 2012. Mutations in the Neverland gene turned Drosophila pachea into an obligate specialist species. Science 337, 1658–1661.
10. Mattson, M., Spaziani, E., 1985. Characterization of molt-inhibiting hormone (MIH) action on crustacean Y-organ segments and dispersed cells in culture and a bioassay for MIH activity. J. Exp. Zool. 236, 93–101. Mykles, D.L., 2011. Ecdysteroid metabolism in crustaceans. J. Steroid Biochem. Mol. Biol. 127, 196–203.
11. Nakatsuji, T., Sonobe, H., 2004. Regulation of ecdysteroid secretion from the Y-organ by molt-inhibiting hormone in the American crayfish, Procambarus clarkii. Gen. Comp. Endocrinol. 135, 358–364.
12. Nakatsuji, T., Sonobe, H., Watson, R.D., 2006. Molt-inhibiting hormone-mediated regulation of ecdysteroid synthesis in Y-organs of the crayfish (Procambarus clarkii): involvement of cyclic GMP and cyclic nucleotide phosphodiesterase. Mol. Cell. Endocrinol. 253, 76–82.
13. Nakatsuji, T., Lee, C.Y., Watson, R.D., 2009. Crustacean molt-inhibiting hormone: structure, function, and cellular mode of action. Comp. Biochem. Physiol. A Physiol. 152, 139–148.
14. Niwa, R., Niwa, Y.S., 2014. Enzymes for ecdysteroid biosynthesis: their biological functions in insects and beyond. Biosci. Biotechnol. Biochem. 78, 1283–1292.
15. Okumura, T., Aida, K., 2000. Fluctuations in hemolymph ecdysteroid levels during the reproductive and non-reproductive molt cycles in the giant freshwater prawn Macrobrachium rosenbergii. Fish. Sci. 66, 876–883.
16. Petryk, A., Warren, J.T., Marques, G., Jarcho, M.P., Gilbert, L.I., Kahler, J., Parvy, J.P., Li, Y., Dauphin-Villemant, C., O'Connor, M.B., 2003. Shade is the Drosophila P450 enzyme that mediates the hydroxylation of ecdysone to the steroid insect molting hormone 20-hydroxyecdysone. Proc. Natl. Acad. Sci. U. S. A. 100, 13773–13778.
17. Phlippen, M.K., Webster, S.G., Chung, J.S., Dircksen, H., 2000. Ecdysis of decapod crustaceans is associated with a dramatic release of crustacean cardioactive peptide into the hemolymph. J. Exp. Biol. 203, 521–536.
18. Posiri, P., Ongvarrasopone, C., Panyim, S., 2013. A simple one-step method for producing dsRNA from E. coli to inhibit shrimp virus replication. J. Virol. Methods 188, 64–69.
19. Promwikorn, W., Kirirat, P., Thaweethamsewee, P., 2004. Index of molt staging in the black tiger shrimp (Penaeus monodon). Songklanakarin J. Sci. Technol. 26, 765–772.
20. Rewitz, K.F., O'Connor, M.B., Gilbert, L.I., 2007. Molecular evolution of the insect Halloween family of cytochrome P450s: phylogeny, gene organization and functional conservation. Insect Biochem. Mol. Biol. 37, 741–753.
21. Rottiers, V., Motola, D.L., Gerisch, B., Cummins, C.L., Nishiwaki, K., Mangelsdorf, D.J., Antebi, A., 2006. Hormonal control of C. elegans dauer formation and life span by a Rieske-like oxygenase. Dev. Cell 10, 473–482.

22. Rudolph, P.H., Spaziani, E., Wang, W.L., 1992. Formation of ecdysteroids by Y-organs of the crab, Menippe mercenaria. Gen. Comp. Endocrinol. 88, 224–234.
23. Snyder, M.J., Chang, E.S., 1991. Ecdysteroids in relation to the molt cycle of the American lobster, Homarus americanus: I. Hemolymph titers and metabolites. Gen. Comp. Endocrinol. 81, 133–145.
24. Spaziani, E., Wang, W.L., 1993. Biosynthesis of ecdysteroid hormones by crustacean Yorgans: conversion of cholesterol to 7-dehydrocholesterol is suppressed by a steroid 5α-reductase inhibitor. Mol. Cell. Endocrinol. 95, 111–114.
25. Styrishave, B., Lund, T., Andersen, O., 2008. Ecdysteroids in female shore crabs Carcinus maenas during the moulting cycle and oocyte development. J. Mar. Biol. Assoc. UK 88, 575–581.
26. Sumiya, E., Ogino, Y., Miyakawa, H., Hiruta, C., Toyota, K., Miyagawa, S., Iguchi, T., 2014. Roles of ecdysteroids for progression of reproductive cycle in the fresh water crustacean Daphnia magna. Front. Zool. 11, 1–12.
27. Sumiya, E., Ogino, Y., Toyota, K., Miyakawa, H., Miyagawa, S., Iguchi, T., 2016.
28. Neverland regulates embryonic moltings through the regulation of ecdysteroid synthesis in the water flea Daphnia magna, and may thus act as a target for chemical disruption of molting. J. Appl. Toxicol. 36 (11), 1476–1485.
29. Suzuki, S., Yamasaki, K., Fujita, T., Mamiya, Y., Sonobe, H., 1996. Ovarian and hemolymph ecdysteroids in the terrestrial isopod Armadillidium vulgare (Malacostracan Crustacea). Gen. Comp. Endocrinol. 104, 129–138.
30. Tom, M., Manfrin, C., Giulianini, P.G., Pallavicini, A., 2013. Crustacean oxi-reductases protein sequences derived from a functional genomic project potentially involved in ecdysteroid hormones metabolism - a starting point for function examination. Gen. Comp. Endocrinol. 194, 71–80.
31. Uryu, O., Ameku, T., Niwa, R., 2015. Recent progress in understanding the role of ecdysteroids in adult insects: germline development and circadian clock in the fruit fly Drosophila melanogaster. Zool. Lett. 1, 1–9.
32. Wollam, J., Magomedova, L., Magner, D.B., Shen, Y., Rottiers, V., Motola, D.L., Mangelsdorf, D.J., Cummins, C.L., Antebi, A., 2011. The Rieske oxygenase DAF-36 functions as a cholesterol 7-desaturase in steroidogenic pathways governing longevity. Aging Cell 10, 879–884.
33. Yang, J., Roy, A., Zhang, Y., 2013a. Protein-ligand binding site recognition using complementary binding-specific substructure comparison and sequence profile alignment. Bioinformatics 29, 2588–2595.
34. Yang, J., Roy, A., Zhang, Y., 2013b. A semi-manually curated database for biologically relevant ligand-protein interactions. Nucleic Acids Res. 41, 1096–1103.
35. Yoshiyama, T., Namiki, T., Mita, K., Kataoka, H., Niwa, R., 2006. Neverland is an evolutionally conserved Rieske-domain protein that is essential for ecdysone synthesis and insect growth. Development 133, 2565–2574.
36. Yoshiyama-Yanagawa, T., Enya, S., Shimada-Niwa, Y., Yaguchi, S., Haramoto, Y., Matsuya, T., Shiomi, K., Sasakura, Y., Takahashi, S., Asashima, M., Kataoka, H., Niwa, R., 2011. The conserved Rieske oxygenase DAF-36/Neverland is a novel cholesterol-metabolizing enzyme. J. Biol. Chem. 286, 25756–25762.

Piwi controls transposon expression and spermatogenesis in *Penaeus monodon*

Piwi proteins comprise a subfamily of Argonaute that plays a major role in germline development by association with a distinct class of small RNAs called Piwi interacting RNA (piRNA). Although the functions of Piwi in the development of germline cells as well as transposon regulation were reported in a number of mammalians and insects, developmental expression and function of Piwi subfamily in crustaceans is poorly known. This study is aimed at cloning and characterization of a *Piwi* cDNA in the black tiger shrimp, *Penaeus monodon*. The cDNA encoding a Piwi protein of *P. monodon* (PmPiwi) was obtained by rapid amplification of cDNA ends (RACE). The *PmPiwi1* coding cDNA contains 2,811 nt encoding a putative protein of 936 amino acids, and was specifically expressed in testis and ovary, suggesting its possible function in gametogenesis. RNAi experiment showed that suppression of *PmPiwi1* expression led to a significant up-regulation of retrotransposon *gypsy2* and DNA element transposon *mariner* in shrimp testis. Investigation of the function of *PmPiwi1* in spermatogenesis by sperm count showed significantly lower number of sperms in the spermatophore sac of *PmPiwi1*-knockdown shrimp compared with that in the control shrimp. Our study thus reported for the first time the cDNA encoding a Piwi protein in the shrimp *P. monodon*. Its roles in controlling transposons and spermatogenesis as implied by the results in this study will be important for understanding sperm development and could be useful for the improvement of reproduction in male shrimp in the future.

Introduction

Argonaute is a central protein component of an RNA-induced silencing complex (RISC) in a small RNA-mediated gene silencing pathway called RNA interference (RNAi). Argonaute protein family is characterized by the presence of two major conserved domains: the PAZ domain that binds specifically to small non-coding RNAs, and the PIWI domain that forms a catalytic triad Asp-Asp-His (DDH) required for the cleavage of a target mRNA that is complementarily bound to the small RNA [1, 2]. Phylogenetic analysis classifies proteins in the Argonaute family into Ago and Piwi subfamilies. The Ago subfamily is ubiquitously expressed and normally functions in association with small interfering RNAs (siRNAs) and/or micro RNAs (miRNAs). In contrast to the Ago subfamily, Piwi proteins exhibit a germline-specific expression pattern and bind to a distinct class of small RNA called PIWI-interacting RNAs or piRNAs in germline cells [1, 3, 4].

Piwi proteins and their small RNA partners, piRNAs are implicated in transcriptional gene expression, post-transcriptional gene regulation and transposon silencing [5-7] that are important during germline development, particularly in spermatogenesis and oogenesis. Loss of *piwi* causes defects in germ cell development in diverse organisms [8, 9]. Piwi is most studied in *Drosophila*, whose genome codes for three Piwi members; Piwi, Aubergine (Aub) and Argonaute 3 (Ago3). Both Aub and Ago3 are cytoplasmic proteins that are restrictedly expressed in the germline granules called a nuage [10-14]. *Aub*-deficient flies displayed male sterility and maternal effect lethality [15]. By contrast, *Drosophila*'s Piwi seems to be predominantly expressed in

the nucleus and is necessary for self-renewing division of germline stem cells in both males and females [16, 17]. The depletion of Piwi led to infertility and axis specification defects in the developing egg chambers [16]. In the mouse, *Mus musculus*, three members of Piwi have been identified namely Miwi, Mili and Miwi2. Both Miwi and Mili are specifically expressed in the germ cells of testis, and are involved in meiotic regulation of spermatogenesis [18, 19]. On the other hand, Miwi2 is expressed in both germ cells and somatic cells, and is essential for maintaining germ-line stem cells [21]. Similarly, the two Piwi proteins of zebrafish, Ziwi and Zili, are essential for germ line maintenance. Ziwi is abundantly expressed during both mitotic and early meiotic stages of germ cell differentiation, while Zili is involved in germ cell differentiation similar to the mouse Miwi2 [8, 9]. Like in other organisms, the expression of two Piwi proteins in the silkworm *Bombyx mori*, Siwi and BmAgo3, was found in germline cells. Both of them are abundantly expressed in testes and ovaries indicating that they might be involved in spermatogenesis and oogenesis in *B. mori* [22]. Similarly, the regulation of spermatogenesis and oogenesis in the honey bee, *Apis mellifera* is regulated by two *piwi*-like genes, Am-*aub* and Am-*ago3* [23]. Recently, genes encoding three crustacean Piwi proteins have been first identified in the crab *Portunus trituberculatus*. All of *P. trituberculatus*' *piwi* genes were expressed in adult testis, thus suggesting their functions during spermatogenesis [24].

Recent studies have shown that piRNAs are central players in transposon silencing, which is particularly important for germ cell differentiation and genome maintenance during germline developmental process [9, 25]. The piRNAs are primarily derived from transposons and other repeated elements by a proposed ping-pong model that involves the three Piwi proteins in *Drosophila* [13, 14, 26]. The Piwi proteins are important for controlling transposon mobilization in the male germ cells. For examples, loss-of-*mili* and -*miwi2* mice exhibited transposon activation in male germline that consequently resulted in germ cells deficiency [21, 27]. In *Drosophila*, Piwi controlled expression and mobilization of retrotransposons. Mutation of *piwi* deregulates retrotransposon expression in the germline that finally led to embryonic defects [14, 28].

Although Piwi proteins have been extensively studied in diverse organisms, but Piwi in crustacean is less known. To help fulfill our knowledge in the control of gonad development in this large subphylum of arthropods, we cloned and characterized a cDNA encoding a member of Piwi proteins from the black tiger shrimp, *Penaeus monodon*. The expression of *PmPiwi* during gonad developmental stage, its function in controlling transposon expression and regulating spermatogenesis in the male germline of *P. monodon* were also investigated.

Materials and methods

Penaeus monodon samples

P. monodon were kindly provided by Shrimp Genetic Improvement Center, Surat Thani, Thailand. Male shrimps at three different maturation stages were used in this study: adolescent or immature shrimp about 4 months old or approximately 20 g bodyweight (bw) were defined as those forming spermatophores without sperm inside; sub-adult male shrimp were about 6 months of age with approximately 40 g bw; and adult male shrimp were over 10 months old. Female shrimp were divided into five reproductive maturation stages based on histochemical staining with hematoxylin and eosin according to Tan-Fermin and Pudadera, 1989 [29].

Cloning of a full-length Piwi cDNA of P. monodon (PmPiwi1)

Total RNA was extracted from the testis of *P. monodon* by TriSolution Plus Reagent (GMbiolab) as described in the manufacturer's protocol. Approximately 2 µg of total RNA were used for cDNA synthesis by incubating with 0.5 µM of oligo dT primer in a volume of 5 µl followed by incubating at 70°C for 5 min and cooling on ice for 5 min. Then, the mixture containing 5X Improm pt II™ reaction buffer, 3 mM $MgCl_2$, 0.5 mM each dNTP, and 1 µl of Impromt II™ reverse transcriptase (Promega) was added, and the reaction was continued at 42°C for 60 min, then at 70°C for 15 min. One microliter of the cDNA was used as a template for amplification of the partial *Piwi* cDNA with specific primers PIWI-F4 and PIWI-R4 (Table 1) at 95°C for 5 min followed by 35 cycles of 95°C for 30 sec, 57°C for 30 sec, and 68°C for 30 sec.

The 3' end of *PmPiwi1* cDNA were obtained from the oligo-dT-primed first strand cDNA by 3' RACE. The first amplification was performed with 3RACE1 primer designed from the partial Piwi cDNA obtained above and oligo-dT reverse primer. Subsequently, the nested PCR was performed using 3' inner primer 3RACE2 and PM1 primer. The PCR profile for 3'RACE was as follows; initial denaturation at 95°C for 5 min, annealing at 55°C for 30 sec and extension at 68°C for 2 min 30 sec for 35 cycles using *Taq* DNA polymerase (NEB® Inc.).

For 5' RACE, the first strand cDNA was synthesized using specific reverse primer of PmPiwi1 (5RACE-R1), followed by tailing of poly A at its 3' end using terminal deoxynucleotidyl transferase (Promega). The 5' cDNA of *PmPiwi1* was obtained by three rounds of 5'RACE using the following temperature profile: initial denaturation at 95°C for 5 min, annealing at 55°C for 30 sec and extension at 68°C for 2 min 30 sec for 35 cycles using *Taq* DNA polymerase (NEB® Inc.). Schematic diagrams of 3' and 5' RACE amplification are shown in Fig. 1, and all primers together with their nucleotide sequences are shown in Table 1.

The entire coding region of *PmPiwi1* was obtained by amplification with coding-F and coding-R primers using Expand High Fidelity enzyme (Roche) in a 25 µl reaction containing 1X Expand High Fidelity buffer with $MgSO_4$, 0.352 mM dNTP and 0.3 µM each primer. The amplification was carried out using the following temperature profile; denaturation at 94°C for 10 sec, annealing at 50°C for 30 sec and extension at 68°C for 2 min for 10 cycles, followed by the second round of amplification with 25 cycles of denaturation at 94°C for 15 sec, annealing at 50°C for 30 sec and extension at 68°C for 2 min 20 sec. All the primers used and their nucleotide sequences are listed in Table 1. The amplified fragments were purified and cloned into pGEM®-T easy (Promega). The nucleotide sequences were determined by automated DNA sequencing (1st BASE DNA Sequencing Services, Singapore) and analyzed by Blast program (http://www.ncbi.nlm.nih.gov/blast).

Table 1 Primers used in this study and their nucleotide sequences

Primer name	Primer sequence (5' to 3')	Experiment
oligo dT	CCGGAATTCAAGCTTCTAGAGGATCCTTT TTTTTTTTTTTTT	Cloning, mRNA expression and detection of PmPiwi1 knockdown
PM1	CCGGAATTCAAGCTTCTAGAGGATCC	
Actin-F	GACTCGTACGTGGGCGACGAG	
Actin-R	AGCAGCGGTGGTCATCTCCTGCTC	
Piwi-F4	TACCGCGACGGCGTGAGCGAG	
Piwi-R4	CAAAAGCTAGTTTATGTGCAT	
5RACE1	TAACGAGCGTGATGCCGTCGTG	
5RACE2	CGAGTCGAAGTGCTGGAAGA	
5RACE3	AATACCGATCCTCACGCTGG	
5RACE4	ATGGAGCGTGTGACTTGTCG3	
5RACE5	GAGGATCCATTGACATTCCTGAC	
5RACE8	GCCAGATCTCTAGCTTGTGC	
Piwi1-3RACE1	GATCAGCACCAGGATCTT	
Piwi1-3RACE2	TGGCCTCAAGATCTCACTCC	
Piwi1-F5	GATCAGCACCAGGATCTTCG	
Piwi1-F6	TGGCCTCAAGATCTCACTCC	
Coding-F1	ATGAAGGTGATATTCAGGAAGCG	
Coding-F2	ATGGATGGGGACCCAACTCC	
Coding-R	TCAGAGGAAGAAGAGCTTGTCA	
Sense-XbaI-F	GCTCTAGACCACGTGATTAAGGCTCTGG	dsRNA-PmPiwi1 synthesis
Sense-HindIII-R	CCCAAGCTTGGATCCATTGACATTCCTGAC	
dsPAZ-anti-XhoI-F	CCGCTCGAGCCACGTGATTAAGGCTCTGG	
dsPAZ-anti-Hind-R	CCCAAGCTTTGTCATGTAGCATAGCTCTGG	
MarinerF	CGGTTGGGAGAATAGGCAAATCA	Transposable elements expression
MarinerR	CCTTACAAACTGACGTTGATGGC	
GyPemo1bF	CTACAGCACCAACAACGTCCAA	
GyPemo1bR	CGTTTCCTCAAGCTGTATGAGGTG	
GyPemo2F	GATGCCTCAAACCTCGGGCT	
GyPemo2R	AGTGACGGAGGGCCCATGTG	
EF1αF	GAACTGCTGACCAAGATCGACAGG	
EF1αR	GAGCATACTGTTGGAGGTCTCCA	

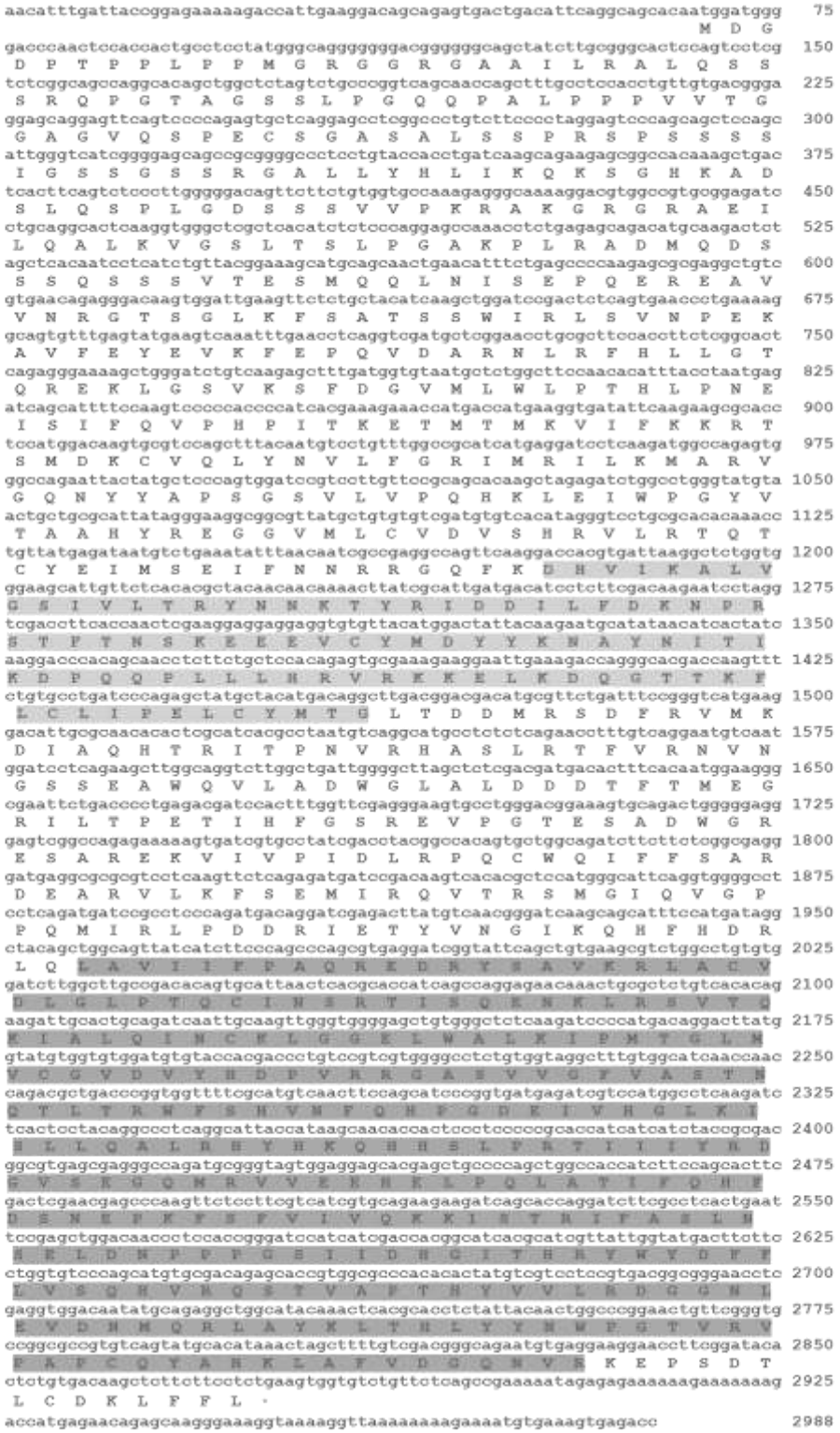

Fig. 1 Deduced amino acid sequence of PmPiwi1

The deduced amino acid sequence of PmPiwi1 is shown in one-letter symbol under corresponding codons. The PAZ and PIWI domains are highlighted in light gray and dark gray, respectively. The catalytic DDH residues are depicted by arrowheads.

Determination of PmPiwi1 expression in P. monodon

Adult male and female *P. monodon* (approximately 100 g bw) were used for tissue distribution determination. Several tissues such as brain, gill, hepatopancreas, heart lymphoid, abdominal nerve cord, throracic ganglia, testis, vas deferens, spermatophore and ovary were dissected and sliced into small pieces. About 100 mg of each tissue were homogenized in Trisolution Plus Reagent (GMbiolab), Approximately 2 μg of total RNA from each tissue were used for cDNA synthesis with oligo dT as described above. The *PmPiwi1* mRNA expression was determined by cDNA amplification with Coding-F1 and 5RACE-R5 primers by *Taq* DNA polymerase (NEB® Inc.) in a 25 μl PCR reaction using the PCR profile as previously described for the amplification of *PmPiwi1* coding cDNA. Actin was used as an internal control. All primers were shown in Table 1.

The mRNA expression levels of *PmPiwi1* in the ovary and testis at different developmental stages were determined by real-time PCR using KAPA SYBR® FAST qPCR kit (Kapa Biosystems) according to the manufacturer's protocol. The fluorescent signal was detected by Eppendorf Realplex (Eppendorf) machine. Relative expression level of *PmPiwi1* was compared with that of the reference gene (elongation factor 1 alpha: *Ef1*α), and the data was analyzed by $2^{-\Delta\Delta CT}$ method.

Double-stranded RNA preparation

The recombinant plasmid harboring the PAZ domain region of *PmPiwi1* cDNA was used as a template for *PmPiwi1* dsRNA production. The dsRNA was synthesized as a stem-loop precursor in *Escherichia coli* expression system. The template of the sense (stem) strand was amplified with sense-*Xba* I-F and sense-*Hind* III-R primers, whereas the anti-sense (stem-loop) strand template was amplified with anti-*Xho* I-F and anti-*Hind* -R primers. The reaction was performed by 30 cycles of denaturation at 95°C for 2 min, annealing at 55°C for 30 min and extension at 72°C for 1 min using *Pfu* DNA polymerase (Thermo scientific). The sense and anti-sense template fragment were sequentially cloned into pET17b vector at the restriction sites corresponding to their termini. The pET17b vector harboring *PmPiwi1* dsRNA template was expressed in *E. coli* strain HT115 with 0.4 mM IPTG induction at 37°C for 4 hr. The *PmPiwi1* dsRNA was extracted by TriSolution Plus Reagent with the addition of 5 ng RNaseA to digest host single strand RNA and the loop region of the stem-loop dsRNA precursor. The quality of dsRNA was determined by RNase digestion assay with RNaseA and RNaseIII.

In vivo silencing of PmPiwi1

In order to investigate the function of *PmPiwi1*, its expression was first suppressed by dsRNA-mediated silencing. To demonstrate the potency of dsRNA to knockdown *PmPiwi1* expression in the shrimp, male *P. monodon* approximately 50 g bw were injected with *PmPiwi1*-dsRNA (dsPiwi1) at 2.5 $\mu g.g^{-1}$ shrimp bw in a volume of 100 μl. Shrimp injected with 150 mM NaCl were used as a control group. The shrimp were injected twice on day 0 and day 7. Testes were collected on day14 after the first injection to determine silencing effect of dsRNA by detecting transcript levels of *PmPiwi1* in the testis by RT-PCR with specific primers as shown in Table 1.

Effect of PmPiwi1 silencing on transposon expression level

The consequence of *PmPiwi1* silencing on transposon expression was determined in the testis of *PmPiwi1*-silenced shrimp on day 14 after the first dsRNA injection.

Three types of transposon elements i.e. two LTR-retrotransposons; *gypsy1* (Accession no. HF548819), *gypsy2* (Accession no. HF548820.1) and DNA element transposon *mariner* (partially cloned in our laboratory, unpublished data) were examined. The expression level of each transposon was determined by real-time PCR with specific primers for each element as shown in Table 1 using KAPA SYBR® FAST qPCR kit (Kapa Biosystems) according to the manufacturer's protocol. The fluorescent signal was detected by Eppendorf Realplex (Eppendorf) machine. *Ef1*α was used as reference gene, and the data was analyzed by $2^{-\Delta\Delta CT}$ method.

Determination of sperm numbers in PmPiwi1-silenced shrimp

According to Jiang SG., et al 2009 [30], spermatophores and sperms in male *P. monodon* were first detected at 157 days of age or about 21.7 g bw. To ensure the formation of spermatophore, male shrimp approximately 40 g bw was used to determine the function *PmPiwi1* in spermatogenesis. The shrimp were divided into 2 groups; the first group was injected with *GFP*-dsRNA (dsGFP) as a control group, and the second group was injected with dsPiwi1 (n=4 each). The dsRNA was injected at a dose of 2.5 $\mu g.g^{-1}$ shrimp bw into the hemocoel at the base of the fifth pleopod. Previous study reported that spermatogenesis was related to molting cycle in *P. monodon*, and the newly formed spermatophores could be observed around day 3 after molt [31]. Therefore, to investigate the function of *PmPiwi1*, male shrimps were injected on day 3 after molting (molting stage C-D0), and tissues (testes and spermatophores) were collected on day 3 after the next molt. One of the two spermatophores (the left one) was collected and homogenized in 1 ml of Ca^{2+}-free seawater (370 mM NaCl, 15 mM KCl, 8.5 mM H_3BO_3, 4.75 mM NaOH, 20 mM $MgSO_4.7H_2O$, pH 7.4) at 4° C. Then, 25 µl of sperm suspension were mixed with 0.4% trypan blue and incubated at room temperature for 5 min. After that, 15 µl of the mixture were dropped on a hemacytometer, and the number of sperms were counted under light microscope. Data were analyzed using SPSS program. Differences between groups was analyzed by t-test at $P<0.05$ as statistical significance.

Results

Cloning and characterization of Piwi1 cDNA in P. monodon

The full-length nucleotide sequence of *PmPiwi1* cDNA was obtained by RACE strategy. The combined *PmPiwi1* cDNA fragment is 2,988 bp in length with a 66 bp 5' UTR, a putative 2,811 bp coding region and a 111 bp 3' UTR (Accession no. MH279567). The continuous reading frame of *PmPiwi1* was verified by RT-PCR. The deduced amino acid sequence of PmPiwi1 contains 936 residues with a predicted molecular weight of 105.31 kDa and a theoretical isoelectric point of 9.36. Identification of conserved domains by ScanProsite program (prosite.expazy.org/scanprosite) revealed that PmPiwi1 contains the signature PAZ and PIWI domains of the Argonaute family (Fig. 1). The predicted catalytic residues Asp-Asp-His (DDH) were also present at the C-terminal PIWI domain of PmPiwi1 similar to other members of the Argonaute family.

The percentage of similarity among PmPiwi1 and their homologues in other species are shown in table 2. Most of the similarities lay in the conserved PAZ and PIWI domains. Phylogenetic tree analysis revealed that PmPiwi1 was classified into the same group as insect Ago3, and closely clustered with Piwi1 of the crab *P. trituberculatus* (Fig. 2).

Table 2 Percentage of identity positions between *P. monodon* Piwis and other homologues

		***P. monodon*'s Piwi1**		
		ORF	**PAZ domain**	**PIWI domain**
P. trituberculatus	Piwi-1	59.6	65.2	74.7
	Piwi-2	33.2	45.7	46.6
	Piwi-3	29.7	41.3	44.9
B. mori	Siwi	29.4	42.4	40.6
	Ago3	40.1	33.9	54.3
A. mellifera	Aub	29.2	32.5	43.2
	Ago3	40.5	42.4	53.2
D. melanogaster	Piwi	29.1	36.3	38.7
	Aub	29.0	30.3	38.7
	Ago3	35.5	43.5	50.0
M. musculus	Miwi	34.4	37.4	44.7
	Mili	35.8	33.0	52.7
	Miwi2	29.0	47.8	38.7
D. rerio	Ziwi	36.3	42.4	51.2
	Zili	34.7	44.1	51.0

Expression of PmPiwi1 in P. monodon

The expression of *PmPiwi1* mRNA in *P. monodon* tissues was determined by RT-PCR. High levels of *PmPiwi1* transcript were detected in the testis and, at a lower level, in the ovary but was not detected in other tissues (Fig. 3A).

In order to investigate further whether or not the expression of *PmPiwi1* in the ovary changes upon ovarian development, the levels of *PmPiwi1 t*ranscript in the ovary at different developmental stages were determined by real-time PCR. The result in Fig. 3B showed that the expression levels of *PmPiwi1*were not significantly different throughout ovarian development from stage 0 to stage IV. In male shrimp, the expression levels of *PmPiwi1* in the testis was rather constant from immature to adult shrimp (Fig. 3C).

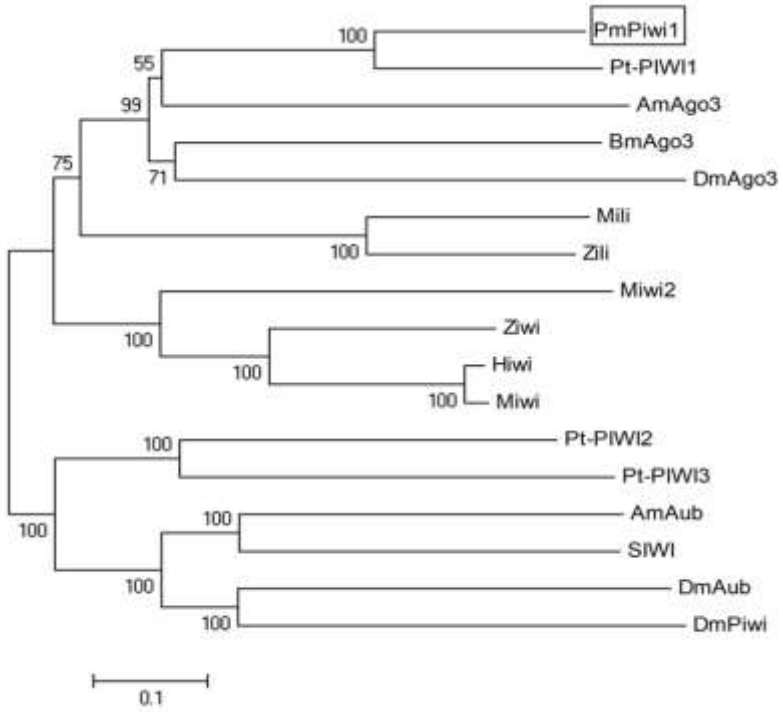

Fig. 2 Phylogenetic relationship among Piwi proteins.

Phylogenetic tree of Piwi proteins was constructed by Mega4 Program using the neighbor-joining distance analysis. The amino acid sequences analyzed include Piwi proteins of *B. mori*: SIWI (AB372006), BmAgo3 (AB372007).; *D. melanogaster*: DmPiwi (AAF53043.1), DmAub (AG18944.1), DmAgo3 (ABO27430.1); *A. mellifera*: AmAub (GQ444142), AmAgo3 (GQ444137); *P. trituberculatus*: Pt-PIW1 (KC203335), Pt-PIWI2 (KC203336), Pt-PIWI3 (KC203337); *D. rerio*: Ziwi (NP899181.1), Zili (NP001073668.2); *M. musculus*: Miwi (AAL3104.1), Mili (BAA93706.1), Miwi2 (AAN75583.1). Bootstrap values from 1000 replicates are indicated at the nodes.

Function of PmPiwi1 in transposon suppression

The efficiency of *PmPiwi1* silencing by specific dsRNA was investigated in the testis of *P. monodon*. The injection with double dosages of dsPiwi1 at 2.5 $\mu g.g^{-1}$ bw on day 0 and day 7 showed the highest suppression of *PmPiwi1*, approximately 96%, at 14 days post-injection (dpi.) (Fig. 4A). The expression of other *Agos* of *P. monodon* was not affected by dsPiwi1 (Fig. 4B), indicating the specificity of dsPiwi1 to knockdown its target transcript.

To determine the influence of *PmPiwi1* silencing on transposon expression in shrimp testis, the expression of *PmPiwi1* was suppressed by dsPiwi1 for 14 days as described above. The transcript levels of three types of transposons including two *gypsy*-like elements and a *mariner*-like element in *PmPiwi1*-knockdown shrimp were determined by real-time PCR. The results showed that the expression level of *gypsy1* was slightly increased, while *gypsy2* and *mariner*-like elements were significantly up-regulated in *PmPiwi1*-knockdown shrimp when compared with the control (Fig. 5).

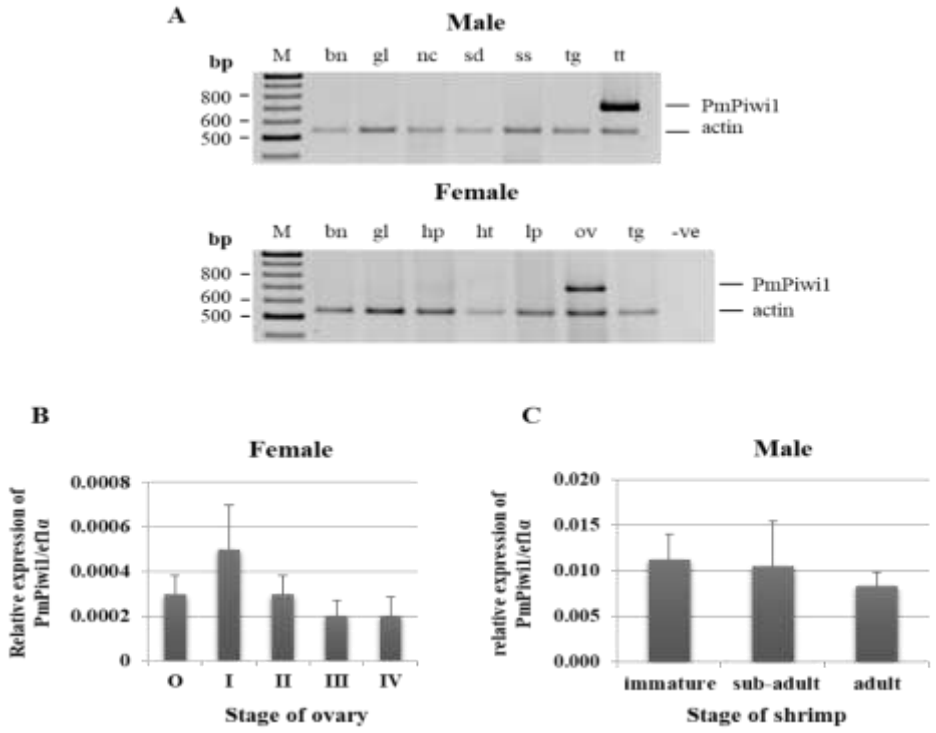

Fig. 3 Expression profile of *PmPiwi1* in *P. monodon*

A) Tissue distribution of PmPiwi1 expression in *P. monodon*. The mRNA transcript levels of *P. monodon* in eyestalk ganglia (Es), brain (Bn), gill (Gl), haemolymph (Hl), hepatopancreas (Hp), lymphoid organ (Lp), abdominal nerve cord (Nc), throracic ganglia (Tg), testis (Tt), sperm duct or vas deferens (Vd), spermatophore sac (Ss) and ovary (Ov) were detected by semi-quantitative RT-PCR. The level of actin transcript (550 bp) was also detected as an internal control. The pictures show the inverted images of ethidium bromide stained agarose gels. B) The expression levels of *PmPiw1* in shrimp ovaries at different stages of ovarian development i.e. undeveloped stage (stage O), pre-developed stage (stage I), early-developed stage (stage II), late developed stage (stage III) and mature stage (stage IV) were determined by real-time PCR (n = 4 each). Expression levels of *PmPiwi1* relative to that of *EF1α* were analyzed by $2^{-\Delta\Delta Ct}$ method and presented as mean ±SEM. C) The expression levels of *PmPiwi1* in the testis of adolescent or immature, sub-adult and adult *P. monodon* (n = 4 each) were determined by RT-PCR and analyzed as mentioned above.

Effect of PmPiwi1-knockdown on spermatogenesis in P. monodon

To investigate the function of *PmPiwi1* in sperm production, male shrimp were injected with dsPiwi1 at 2.5 $\mu g.\, g^{-1}$ bw on day 3 after molt, and the testes and spermatophores were collected on day 3 after the next molting. The efficiencies of *PmPiwi1* knockdown in this experiment (Fig. 6A) were comparable to the previous experiment. The numbers of sperm deposited in the spermatophores of *PmPiwi1*-knockdown shrimp were significantly reduced when compared with that in the dsGFP-injected and the control group (Fig. 6B). Moreover, the spermatophores of *PmPiwi1*-knockdown shrimp were apparently smaller than that of the control groups (Fig. 6C).

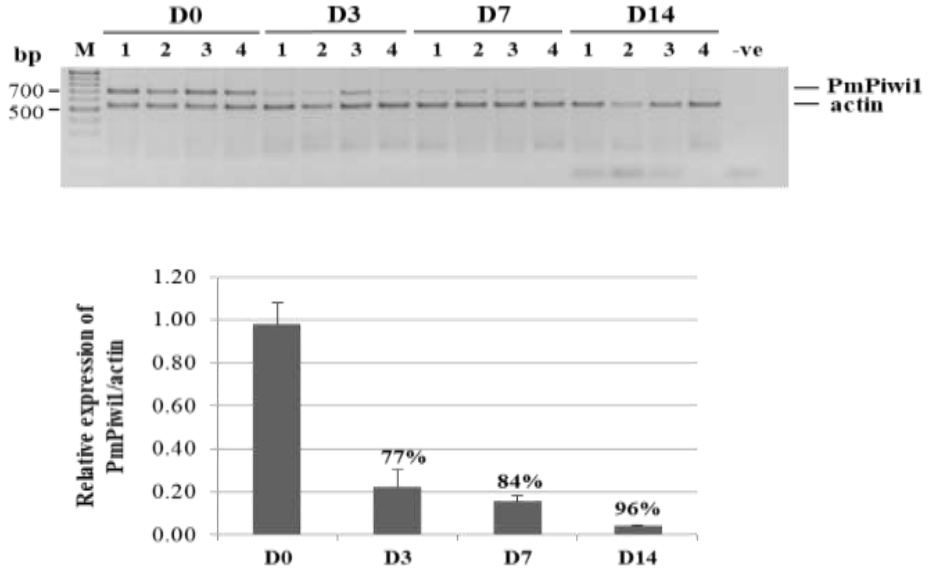

Fig.4. Efficiency of *PmPiwi1* suppression by dsPiwi1.

A) The *PmPiwi1* transcript levels in the testis of dsPiwi1-injected *P. monodon* at 14 dpi were determined by RT-PCR comparing to that of the control (NaCl injected shrimp). *Actin* transcript was amplified as an internal control. The intensity of each band of *PmPiwi1* and *actin* transcripts on the ethidium bromide-stained agarose gel (upper panel) was determined by Scion-Image program and used for the calculation of the relative expression levels of *PmPiwi1* and *actin* as shown in bar graph (lower panel). B) Specificity of *PmPiwi1* suppression by dsPiwi1 is demonstrated by determination of the expression levels of *PmAgo1, PmAgo3* and *PmAgo4* cDNAs in dsPiwi1-injected shrimp compared with the control. An asterisk indicates statistical difference between groups as determined by Turkey's test of independent sample t-test from SPSS program ($p<0.05$).

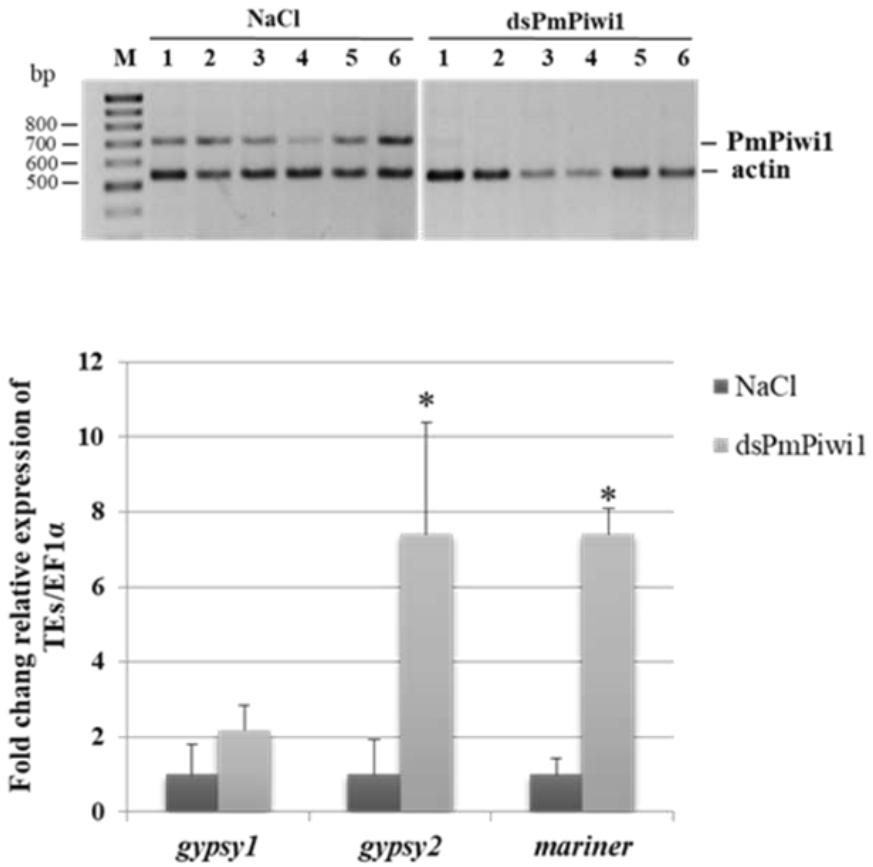

Fig.5. Transposon expression in the testis of *PmPiwi1*-knockdown *P. monodon*.

The expression of *PmPiwi1* in the testis of *P. monodon* was suppressed by the injection of dsPiwi1 as determined by RT-PCR compared to that of the control (NaCl injected shrimp). Actin transcript was amplified as an internal control (upper panel). The expression levels of three types of transposons (*gypsy1*, *gypsy2* and *mariner*-like elements) in the testis of *PmPiwi1*-knockdown shrimp and the control (NaCl-injected shrimp) were determined by real-time PCR (lower panel). Expression level of each transposon relative to that of *Ef1α* was analyzed by $2^{-\Delta\Delta Ct}$ method and shown as mean ±SEM (n = 6). Asterisk indicates statistical difference between the *PmPiwi1*-knockdown and NaCl-injected groups as analyzed by *t*-test from SPSS program ($\rho<0.05$).

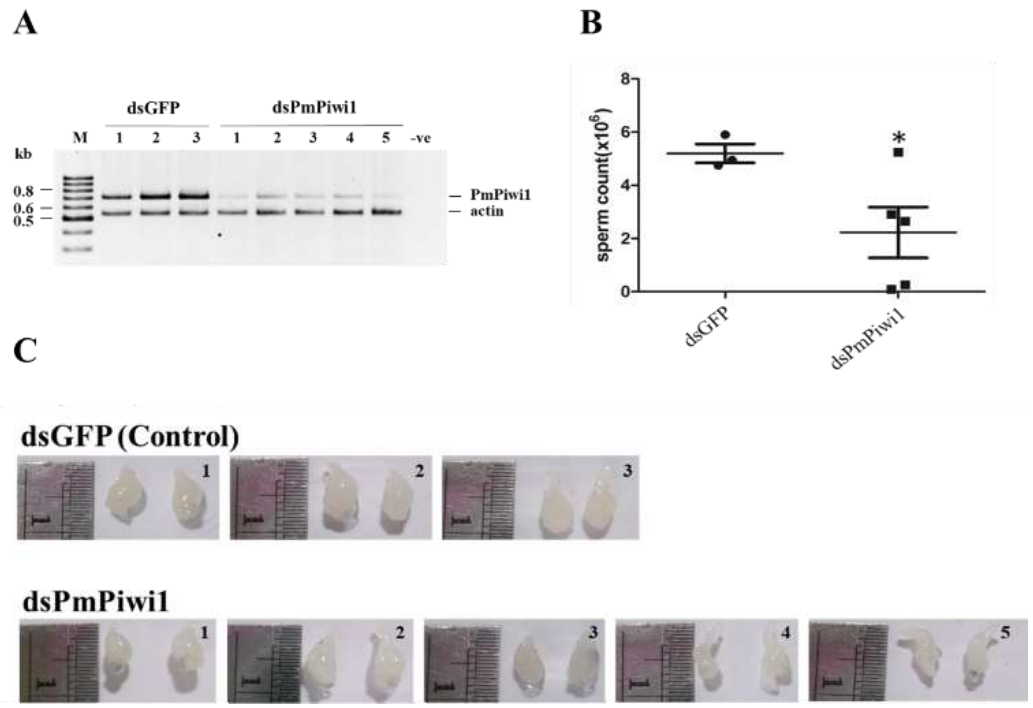

Fig. 6. Numbers of sperms in *PmPiwi1*-knockdown *P. monodon*

DsPiwi1 was injected into male *P. monodon* at 2.5 $\mu g.g^{-1}$ bw on day 3 after molt, and the testes and spermatophores were collected on day 3 after the next molt. Shrimp injected with dsGFP were used as a control group. A) The efficiency of dsPiwi1 to knockdown *PmPiwi1*expression in the testis was determined by RT-PCR compared to the control shrimp. B) The numbers of sperms in the spermatophore of *PmPiwi1*-knockdown and the control shrimp were counted using the hemacytometer under microscope. Asterisk indicates statistical difference of sperm numbers between both groups as determined by One-way ANOVA from SPSS program ($\rho<0.05$). C) Morphology of spermatophore of the *PmPiwi1*-knockdown shrimp (dsPmPiwi1) and dsGFP-injected shrimp (control) was compared.

Discussion

A cDNA encoding Piwi protein in the black tiger shrimp, *P. monodon* was identified and characterized. The alignment of the deduced amino acid sequences revealed that PmPiwi1 contained the conserved PAZ and PIWI domains, which are signature of the Argonaute family. Similarly to the PAZ domain of the Ago subfamily that forms a specific binding module for the 2-nt 3' overhang of small RNAs generated by RNase III-like enzyme such as Dicer, the PAZ domain of the PIWI subfamily forms a binding pocket that anchors the exonuclease-trimmed 3' end of piRNAs [32] The PIWI domain has similar fold to RNaseH with the catalytic triad DDH that is essential for slicing activity of the Ago subfamily [3]. In *Drosophila*, all three members of the PIWI subfamily (Ago3, Aub and Piwi) also possess the conserved DDH residues in their PIWI domain. Whereas the nuclease catalytic triad of Ago3 and Aub was essential for

the piRNA biogenesis pathway via the ping-pong cycle, it did not seem to be required for the function of *Drosophila*'s Piwi in repressing transcription of its targets [33]. The PIWI domain of PmPiwi1 also contained the conserved DDH residues, indicating that PmPiwi1 could form a nuclease catalytic triad, possibly for cleavage of the substrate RNA complementary to the bound piRNAs.

One feature that distinguishes Piwi proteins from the Ago subfamily proteins is the presence of putative asymmetric dimethylated arginine residues (arginine-glycine/RG, arginine-alanine/RA) or symmetrically dimethylated arginine (sDMA) composing of arginine flanked by glycine (GRG) or alanine (GRA or ARG) repeats at the N-terminal region. [34, 35]. Arginine methylation is an important post-transcriptional modification that mediates protein-protein interaction. Piwi proteins were reported to associate with multiple members of the Tudor protein family through sDMA methylation, which are necessary for piRNA function in transposon silencing and gametogenesis in both flies and mice [34-36]. The deduced PmPiwi1possesses multi-arginine methylation sites at the N-terminus, suggesting the potential to form heterodimeric complex with Tudor proteins and play role in the operation of piRNA pathway during germline development of the shrimp.

The restricted gonad expression of *PmPiwi1* conforms to the expression and the role in germline development, a conserved function of Piwi proteins across species. Different types of Piwi may display distinct expression profiles during sperm development suggesting that they have diverse functions in different phases of spermatogenesis. For example, in the murine *Mus musculus*, Miwi2 and Mili were restricted expressed only in the testis [20, 21, 37], whereas Miwi was detected in both testis and oocyte [20, 38]. Miwi is expressed from meiotic spermatocytes to elongating spermatids [20], whereas Mili is expressed from 3 dpp mitotically arrested prenatal germline stem cell to round spermatids [19, 37]. *Miwi*-deficient mice show spermatogenesis arrest at early spermiogenic stage while *Mili*-deficient mice are terminally blocked at zygotene or early pachytene stages of meiotic prophase I, [19, 20]. Miwi2 is detected from day 15.5 dpc to 3 dpp in mitotically arrested prenatal germline stem cells [39]. In addition, Miwi2 was also found in Sertoli cells, which are somatic supporting cells within seminiferous tubules [21]. *Miwi2* mutants not only displayed a meiotic progression defect in early prophase of meiosis I but also seemed to affect mitotic germ cell maintenance [21]. In addition, Miwi protein was detected in mouse oocyte, implicating that it may also function in folliculogenesis [38]. In *P. monodon*, the significant decrease in the number of sperms in spermatophore of *PmPiwi1*-knockdown shrimp compared with that in the control shrimp indicated the function of *PmPiwi1* during spermatogenesis. Since *PmPiwi1* transcript was detected in the testis but not in vas deferens and spermatophore, PmPiwi1 might be directly involved in meiotic regulation in spermatogenesis but not in sperm differentiation or sperm maturation. Although the gonad-specific expression of *PmPiwi1* suggests its function in both sperm and oocyte development, the detail at which steps PmPiwi1 play a role in gametogenesis control in the shrimp remains to be elucidated.

Piwi proteins have important function in the control of transposon in animal germline. *Piwi* knockout resulted in transposon activation, which led to germline defects. For example, derepression and up-regulation of endogenous retrotransposon *copia* was found in *loss-of-Piwi Drosophila* testes. Similarly, *Drosophila Piwi* mutant caused accumulation of *mdg1* transcripts at the apical tip of testes where Piwi protein was not detected [10, 28]. In the zebrafish, *Zili* mutant resulted in up-regulation of both retrotransposons

and DNA transposable element [9]. The increased expression levels of *gypsy* LTR-retrotransposons and DNA element *mariner* in the *PmPiwi1*-knockdown testis of *P. monodon* in this study suggested the function of *PmPiwi1* in the control of transposable elements in shrimp testis. Another member of Argonaute proteins, namely PmAgo4, that is highly expressed in *P. monodon*'s germline was also demonstrated to regulate transposable elements in shrimp testis [40]. Whether or not PmPiwi1 works in cooperation with PmAgo4 to protect shrimp germ cells from deleterious effects of excessive movement of transposable elements during gamete development needs further investigation. In addition, piRNA biogenesis and transposable elements activation in *Drosophila* and mice are known to be regulated by three members of Piwi proteins [10, 26, 33, 41]. Three types of Piwi transcripts were also identified in the crab, *P. trituberculatus* [24]. Therefore, identification of additional members of Piwi in *P. monodon* still awaits exploration.

In conclusion, a novel cDNA encoding *PmPiwi1* in *P. monodon* was identified. Its gonad-specific expression was correlated with potential roles in sperm production and regulation of transposable elements in shrimp testis. The possibility that PmPiwi1 functions together with PmAgo4 and other Piwi members to maintain integrity of shrimp germ cells from transposition effects as has been demonstrated in a number of organisms needs to be elucidated.

References

1. Carmell, M.A., et al., The Argonaute family: tentacles that reach into RNAi, developmental control, stem cell maintenance, and tumorigenesis. Genes Dev, 2002. 16(21): p. 2733-42.
2. Niraj, H.T. and J.-T. Leemor, Slicer and the Argonautes. Nature Chemical Biology, 2006. 3(1): p. 36-43.
3. Peters, L. and G. Meister, Argonaute proteins: mediators of RNA silencing. Mol Cell, 2007. 26(5): p. 611-23.
4. Seto, A.G., R.E. Kingston, and N.C. Lau, The coming of age for Piwi proteins. Mol Cell, 2007. 26(5): p. 603-9.
5. Vagin, V.V., et al., A distinct small RNA pathway silences selfish genetic elements in the germline. Science, 2006. 313(5785): p. 320-4.
6. Pal-Bhadra, M., et al., Heterochromatic silencing and HP1 localization in Drosophila are dependent on the RNAi machinery. Science, 2004. 303(5658): p. 669-72.
7. Grivna, S.T., B. Pyhtila, and H. Lin, MIWI associates with translational machinery and PIWI-interacting RNAs (piRNAs) in regulating spermatogenesis. Proc Natl Acad Sci U S A, 2006. 103(36): p. 13415-20.
8. Houwing, S., et al., A role for Piwi and piRNAs in germ cell maintenance and transposon silencing in Zebrafish. Cell, 2007. 129(1): p. 69-82.
9. Saskia Houwing, E.B.a.R.F.K., Zili is required for germ cell differentiation and meiosis in zebrafish. The EMBO JOURNAL, 2008. 27: p. 2702-2711.
10. Brennecke, J., et al., Discrete small RNA-generating loci as master regulators of transposon activity in Drosophila. Cell, 2007. 128(6): p. 1089-103.
11. Gunawardane, L.S., et al., A slicer-mediated mechanism for repeat-associated siRNA 5' end formation in Drosophila. Science, 2007. 315(5818): p. 1587-90.

12. Macdonald, A. N. H. a. P. M., aubergine encodes a Drosophila polar granule component required for pole cell formation and related to elF2C. Development, 2001. 128: p. 2823-2832.
13. Nagao, A., et al., Biogenesis pathways of piRNAs loaded onto AGO3 in the Drosophila testis. RNA, 2010. 16(12): p. 2503-15.
14. Nishida, K. M., et al., Gene silencing mechanisms mediated by Aubergine piRNA complexes in Drosophila male gonad. RNA, 2007. 13(11): p. 1911-22.
15. Schmidt, A., et al., Genetic and molecular characterization of sting, a gene involved in crystal formation and meiotic drive in the male germ line of Drosophila melanogaster. Genetics, 1999. 151: p. 749-760.
16. Cox, D.N., et al., A novel class of evolutionarily conserved genes defined by piwi are essential for stem cell self-renewal. Genes Dev, 1998. 12(23): p. 3715-3727.
17. Cox, D.N., Chao, A, and Lin H,, piwi encodes a nucleoplasmic factor whose activity modulates the number and division rate of germline stem cells. Development, 2000. 127: p. 503-514.
18. Kuramochi-Miyagawa, S., et al., Two mouse piwi-related genes; miwi and mili. Mechanisms of Development, 2001. 108: p. 121-133.
19. Kuramochi-Miyagawa, S., et al., Mili, a mammalian member of piwi family gene, is essential for spermatogenesis. Development, 2004. 131(4): p. 839-49.
20. Deng, W. a. L. H., miwi, a Murine homolog of piwi, encodes a cytoplasmic protein essential for spermatogenesis. Developmental Cell, 2002. 2: p. 819-830.
21. Carmell, M. A., et al., MIWI2 is essential for spermatogenesis and repression of transposons in the mouse male germline. Dev Cell, 2007. 12(4): p. 503-14.
22. Kawaoka, S., et al., Developmentally synchronized expression of two Bombyx mori Piwi subfamily genes, SIWI and BmAGO3 in germ-line cells. Biochem Biophys Res Commun, 2008. 367(4): p. 755-60.
23. Liao, Z., et al., Identification of two piwi genes and their expression profile in honeybee, Apis mellifera. Arch Insect Biochem Physiol, 2010. 74(2): p. 91-102.
24. Xiang, D.F., et al., Identification and expression pattern analysis of Piwi genes during the spermiogenesis of Portunus trituberculatus. Gene, 2014. 534(2): p. 240-8.
25. Chambeyron, S., et al., piRNA-mediated nuclear accumulation of retrotransposon transcripts in the Drosophila female germline. Proc Natl Acad Sci U S A, 2008. 105(39): p. 14964-9.
26. Saito, K., et al., Specific association of Piwi with rasiRNAs derived from retrotransposon and heterochromatic regions in the Drosophila genome. Genes Dev, 2006. 20(16): p. 2214-22.
27. Grivna, S.T., et al., A novel class of small RNAs in mouse spermatogenic cells. Genes Dev, 2006. 20(13): p. 1709-14.
28. Kalmykova, A.I., M.S. Klenov, and V.A. Gvozdev, Argonaute protein PIWI controls mobilization of retrotransposons in the Drosophila male germline. Nucleic Acids Res, 2005. 33(6): p. 2052-9.
29. Tan-Fermin, J.D. and R.A. Pudadera, Ovarian maturation stages of the wild giant tiger prawn, Penaeus monodon Fabricius. Aquaculture, 1989. 77(2–3): p. 229-242.
30. Jiang, S.-G., et al., Observations of reproductive development and maturation of male Penaeus monodon reared in tidal and earthen ponds. Aquaculture, 2009. 292(1-2): p. 121-128.

31. Prommoon, J., The relationship between molting cycle and sperm development of male domesticated broodstock Penaeus monodon. Dissertation in Aquatic Science. Faculty of Graduate Studied, Prince of Songkla University., 2010: p. 67.
32. Matsumoto, N., et al., Crystal Structure of Silkworm PIWI-Clade Argonaute Siwi Bound to piRNA. Cell, 2016. 167(2): p. 484-497.e9.
33. Rozhkov, N.V., M. Hammell, and G.J. Hannon, Multiple roles for Piwi in silencing Drosophila transposons. Genes Dev, 2013. 27(4): p. 400-12.
34. Vagin, V.V., et al., Proteomic analysis of murine Piwi proteins reveals a role for arginine methylation in specifying interaction with Tudor family members. Genes Dev, 2009. 23(15): p. 1749-62.
35. Kirino, Y., et al., Arginine methylation of Piwi proteins catalysed by dPRMT5 is required for Ago3 and Aub stability. Nat Cell Biol, 2009. 11(5): p. 652-8.
36. Nishida, K.M., et al., Functional involvement of Tudor and dPRMT5 in the piRNA processing pathway in Drosophila germlines. EMBO J, 2009. 28(24): p. 3820-31.
37. Unhavaithaya, Y., et al., MILI, a PIWI-interacting RNA-binding protein, is required for germ line stem cell self-renewal and appears to positively regulate translation. J Biol Chem, 2009. 284(10): p. 6507-19.
38. Ding, X., H. Guan, and H. Li, Characterization of a piRNA binding protein Miwi in mouse oocytes. Theriogenology. 79(4): p. 610-615.e1.
39. Aravin, A.A., et al., A piRNA Pathway Primed by Individual Transposons Is Linked to De Novo DNA Methylation in Mice. Mol Cell. 31(6): p. 785-799.
40. Leebonoi, W., et al., A novel gonad-specific Argonaute 4 serves as a defense against transposons in the black tiger shrimp Penaeus monodon. Vol. 42. 2014.
41. Manakov, Sergei A., et al., MIWI2 and MILI Have Differential Effects on piRNA Biogenesis and DNA Methylation. Cell Reports. 12(8): p. 1234-1243.

Involvement of *Lv*SID-1 in dsRNA uptake in *Litopenaeus vannamei*

In the past decade, RNA interference (RNAi) has emerged as a successful tool for functional genomics and antiviral applications in shrimp. However, the mechanism of extracellular dsRNA uptake into shrimp cells has not been determined. Systemic RNA interference defective-1 protein (SID-1) is a transmembrane protein which is required for dsRNA transport between cells in several organisms including *Caenorhabditis elegans* but not in Drosophila andsome insects. Recently, aSID-1homolog (*Lv*SID-1) was identified in whiteleg shrimp (*Litopenaeus vannamei*). Therefore, this study aimed to evaluate whether *Lv*SID-1 is involved in the uptake of dsRNA into shrimp cells. *Lv*SID-1 mRNA expression was up-regulated in gills and muscles but not in hepatopancreas of the shrimp that received long dsRNA introduced by injection. To elucidate the role of *Lv*SID-1 in dsRNA uptake, a strategy of sequential introduction of dsRNAs was employed. Shrimp were initially injected with a long dsRNA to induce *Lv*SID-1 mRNA expression. In a first experiment hemocytes of the *Lv*SID-1 induced shrimp were then collected and seeded in a chamber slide before incubation with Cy3-labeled dsRNA to monitor cellular uptake. Under a confocal microscope, the Cy3 signal in the *Lv*SID-1 induced hemocytes was significantly higher than the signal in naïve hemocytes. In a second experiment, *Lv*SID-1 induced shrimp were separately injected with a second dsRNAs specific to a shrimp endogenous gene (signal transduction and transcription protein (STAT) or clathrin heavy chain (CHC)). Levels of STAT or CHC suppression in the *Lv*SID-1 induced-shrimp compared with the control shrimp reflected the efficiency of uptake of the second dsRNA. Significantly, improved suppression of STAT and CHC was found in gills of the *Lv*SID-1 induced shrimp. These results suggest that *Lv*SID-1 participates in the uptake of injected dsRNA into shrimp cells. This study reports for the first time the involvement of the *Lv*SID-1 in dsRNA uptake in shrimp, which could help to improve the potency of RNAi mediated anti-viral approaches in shrimp in the future.

Introduction

RNA interference (RNAi) is a highly conserved post-transcriptional gene regulatory mechanism in eukaryotes (Campbell and Choy, 2005). Over the past decade, it has become a successful tool for functional genomics (Phetrungnapha et al., 2015; Sagi et al., 2013) with potential anti-viral applications (Assavalapsakul et al., 2014; Escobedo-Bonilla, 2011; Sagi et al., 2013; Shekhar and Lu, 2009) in shrimp. Moreover, much progress has been made in recent years with regard to diet-delivered RNAi due to its potential for practical usage in the farm, although its efficiency is currently highly variable (Chimwai et al., 2016; Sanitt et al., 2016; Sanitt et al., 2014; Sarathi et al., 2008; Sellars et al., 2011; Treerattrakool et al., 2013). Uptake of dsRNA by cells and its subsequent processing by the cellular core RNAi machinery prior to the target gene silencing are two main steps in the RNAi process. Although the core components and their roles are intensively studied nowadays (Agrawal et al., 2003; Chen et al., 2012; Dechklar et al., 2008), the mechanism of the cellular uptake of dsRNA by cells remains to be fully characterized.

In invertebrates, uptake of an extracellular dsRNA can occur through two different mechanisms. The first transmembrane channel-mediated mechanism, requires a multispan transmembrane protein called systemic RNA interference defective (SID), which was originally identified in Caenorhabditis elegans (C. elegans)(Winston et al., 2002; Winston et al., 2007). The SID is necessary for systemic RNAi in C. elegans (Rocheleau, 2012) and some insects (Aronstein et al., 2006; Cappelle et al., 2016; Miyata et al., 2014). A second, endocytosismediated mechanism, which requires receptor recognition and an endocytosis pathway, has been described in some insects particularly in Drosophila melanogaster (D. melanogaster)(Saleh et al., 2006; Ulvila et al., 2006).

Amongst the identified SID proteins (SID-1, SID-2, SID-3 and SID-5), the SID-1 protein is the best characterized in *C. elegans* and other animals including mammals (Winston et al., 2002; Duxbury et al., 2005; Feinberg and Hunter, 2003; Tsang et al., 2007). Although SID-1 orthologs sharing 11 transmembrane domains (like *C. elegans* SID-1) have been found in many organisms, participation of these SID-1s in dsRNA uptake remains obscure, particularly in insects. The SID-1 homologs (single or multiple) have been identified in most insects such as red flour beetle, *Tribolium castaneum* (Tomoyasu et al., 2008), locust, Locusta migratoria (Luo et al., 2012), and Schistocerca gregaria (Wynant et al., 2014). Knockdown of their SID-1 homologs did not impair RNAi indicating that their SID-1s are not required for cellular dsRNA uptake. However, SID-1 homologs seem to facilitate systemic RNAi in some insects such as the honey bee (*Apis mellifera*) (Aronstein et al., 2006), the western corn rootworm (*Diabrotica virgifera*) (Miyata et al., 2014), and the Colorado potato beetle (*Leptinotarsa decemlineata*) (Cappelle et al., 2016).

In shrimp, the sequence of a SID-1 homolog was first identified in *Litopenaeus vannamei* (*L. vannamei*) (Labreuche et al., 2010). It encodes a putative protein with an extracellular N-terminal domain and contains 11 predicted transmembrane domains similar to the SID-1 protein of *C. elegans* (CeSID-1). Moreover, up-regulated expression of the SID-1 upon dsRNA injection has been observed in the gills of *L. vannamei* (Labreuche et al., 2010) and in hemocytes of Kuruma shrimp, *Marsupenaeus japonicas* (Maralit et al., 2015). With these characteristics, the shrimp SID-1 (*Lv*SID-1) may function as a transmembrane channel and participate in extracellular dsRNA uptake in shrimp cell slike the *Ce*SID1. Therefore, this study aimed to evaluate whether *Lv*SID-1 is involved in the uptake of dsRNA into shrimp cells. Using sequential dsRNAs administration, shrimp were initially injected with a long dsRNA to induce *Lv*SID-1 mRNA expression. In a first experiment hemocytes of the *Lv*SID-1 induced shrimp were used to monitor cellular uptake of Cy3-labeled dsRNA. In a separated experiment, the *Lv*SID-1 induced shrimp were injected with a second dsRNAs specific to shrimp endogenous mRNAs. Levels of gene suppression in the *Lv*SID-1 induced shrimp as compared to control shrimp reflect the capability of cells to uptake the second dsRNA.

Materials and methods

Shrimp specimens

Post larval (Pl_{15}-Pl_{20}) white leg shrimp (*L. vannamei*) were purchased from Chuchai farm in Chonburi province, Thailand. They were maintained with aeration in a 500 L tank with seawater at 10 ppt salinity. They were fed daily with shrimp commercial diet (CP) until they reached a juvenile stage of roughly 300 mg or 1–2 g

(only for the Cy3-labeled dsRNA uptake experiment) of body weight. During experiments shrimp were kept in individual cages in the same tank to avoid cannibalism.

Production and verification of dsRNA

Each plasmid containing an appropriate dsRNA expression cassette was transformed into *E. coli* HT115 (a RNase III defective strain) (Ongvarrasopone et al., 2007). Six different dsRNAs namely dsSTAT (406 bp) (Attasart et al., 2013), dsGFP (380 bp) (Yodmuang et al., 2006), dsNS1 (425 bp) (Attasart et al., 2010), dsRab7 (393 bp) (Ongvarrasopone et al., 2008), dsCHC (402 bp) (Posiri et al., 2015) and dsRR2 (398 bp) (Attasart et al., 2009), targeting the shrimp signal transduction and transcription protein (STAT), jelly fish GFP, *Penaeus monodon* densovirus ns1, shrimp Rab7, shrimp chlathrin heavy chain and white spot syndrome virus rr2 mRNAs respectively, were used in this study. Bacterial cultures were grown over night from a single colony in LB medium containing 100 μg/ml ampicillin and 12.5 μg/ml tetracycline. The next day 0.5 OD of starter culture was inoculated in 15 ml of new medium and cells were grown until OD_{600} reached 0.4. Expression of dsRNA was induced with 0.4 mM of isopropyl-*β*-d thiogalactopyranoside (IPTG). The culture was grown for a further 4 h after induction. Cells were collected and dsRNA was extracted according to the protocol of Posiri et al. (2013), with some minor modifications. Briefly, one OD of bacterial cells, which was collected by centrifugation at 8,000×g at 4°C for 5 min, was resuspended in 100 μl 75% ethanol in phosphate buffer saline (PBS) and incubated at room temperature for 5 min. The treated cells were collected by centrifugation at 8000 ×gfor 5 minat4 °C. The cell pellet was resuspended in 100 μl of 150 mM NaCl and incubated at room temperature for 1 h. The cell suspension was centrifuged at 12000 ×g at 4 °C for 5 min to generate a cell-free supernatant. The dsRNA in the supernatant was diluted before loading into agarose gels to estimate the concentration by comparing with a standard marker. To assess dsRNA structure, 2 μg of dsRNA were digested with RNase A or RNase III enzymes. For the RNase A digestion reaction, 2 μg of dsRNA was incubated with 0.01 μg of RNase A in a final 1× RNase A buffer (500 mM sodium acetate, 10 mM Tris-Cl pH 7.5) in a total volume of 10 μl. For the RNase III digestion, 2 μg of dsRNA was incubated with 1× $MnCl_2$ (20 mM), 0.5 U of RNase III in a final 1× RNase III buffer (50 mM Tris-Cl, 1 mM DTT, 50 mM NaCl, pH 7.5 at 25°C). The reactions were incubated at 37°C for 5 min after which they were immediately loaded onto gels.

Evaluation of the LvSID-1 involvement in cellular dsRNA uptake in shrimp

Using sequential dsRNAs administration, shrimp were firstly injected with an unrelated dsRNA specific to the ns1 gene of *Penaeus monodon* densovirus (dsNS1) to induce *Lv*SID-1 mRNA expression, and then hemocytes of the *Lv*SID-1 induced shrimp were collected and seeded in a chamber slide before incubating with second Cy3-labeled dsRNA to monitor cellular uptake of dsRNA compared with naïve cells (2.4). In a separated experiment, the LvSID-1 induced shrimp were injected with a second dsRNA specific to shrimp STAT (dsSTAT) or shrimp clathrin heavy chain (CHC) (dsCHC) mRNAs (2.5). Levels of STAT or CHC suppression in the *Lv*SID-1 induced shrimp as compared to control shrimp reflect the capability of cells to uptake the second dsRNA.

Examination of cellular uptake of Cy3-labeled dsRNA in shrimp hemocytes

A dsRNA (393 bp) targeted to the shrimp Rab7 transcript (dsRab7) was labeled with Cy3 using the Silencer® siRNA labeling kit (Ambion). The Cy3-labeled dsRab7 wasverified byobservation ofits mobility shift in gel electrophoresis. The Cy3 dye solution, diluted to the same absorbance as the Cy3-labeled dsRab7 was used as a negative (background) control.

Hemolymph of the *Lv*SID-1 induced shrimp (in parallel with the control shrimp) were withdrawn and mixed with AC-1 solution (27 mM Sodium citrate, 34.33 mM NaCl, 104.5 mM Glucose, 198.17 mM EDTA, pH 7.0) at a 1:1 ratio before seeding in a chamber slide (Lab-Tek® Chamber Slide™). After 20–30 min, the supernatant was replaced with sterile 1× PBS. The attached hemocytes were incubated at 4°C for 15 min to inactivate endocytosis activity. Then PBS was replaced with cold Cy3-dsRab7 (1.5 µg/200 µl/well) or Cy3 Dye solution and hemocytes were incubated at 4°C for 10 min before synchronization of endocytosis by incubating at 28 °C for 1 h. Cells were washed with PBS twice before fixing with 4% paraformaldehyde for 20 min. Then the fixed cells were washed twice with PBS (3 min each) followed by incubation in 0.1% Triton X-100 in PBS for 15 min before washing with PBS. After washing three times, cell nuclei were stained with DAPI (Invitrogen) for 10 min and cells were washed three times with PBS (3 min each). Thereafter, the chamber and gasket were removed, cells were coated with Prolong® Gold antifade reagent (Molecular Probes®) and covered with a coverslip. The fluorescence signal was observed under a Zeiss LSM800 confocal microscope using laser wavelength at 548 nm (Cy3) and 561 nm (DAPI) for excitation and 561 nm (Cy3) and 465 nm (DAPI) for emission.

Injection of dsRNA into shrimp

The dsRNA solution was diluted in 150 mM NaCl with an appropriate concentration before injection. For *Lv*SID-1 induction, 5µg of dsRNA (dsNS1, dsRR2, dsSTAT, dsGFP) per 1 g of shrimp body weight ratio was used in all experiments. To reach approximately 50% mRNA suppression, 1 µg/g and 0.6 µg/g of dsSTAT and dsCHC respectively were injected into shrimp. Approximately 20 µl of dsRNA solution was injected into shrimp haemocoel using a 0.5 ml syringe with 29G needle.

Shrimp RNA extraction and cDNA synthesis

Shrimp tissues (hepatopancreas, gill and muscle) were dissected from *L. vannamei* (300–500 mg) using scissors and forceps. Total RNA of each tissue (approximately 10 mg) was extracted using RiboZol™ (amresco) following the manufacturer's instruction. The extracted RNA was kept at -30°C until used. The RNA (1–2 µg) was heated in a reaction tube containing 2 µM of random primers and RNase-free sterile distilled water. After heating at 70°C for 5 min and quickly cooling on ice, the primers were allowed to anneal with RNA at 25°C for 5 min. The following components, 1× ImProm-II™ reaction buffer, 0.5 mM dNTPs, 30 mM $MaCl_2$, 1µl of ImProm-II™ reverse transcriptase and RNase-free sterile distilled water were then added into the reaction. The cDNA synthesis reaction was undertaken at 42°C for 60 min and stopped by incubation at 70°C for 15 min.

Semi-quantitative RT-PCR

Two microliters of synthesized cDNA were used as template in a 25µl PCR reaction. The reaction mixture composed of 1× PCR buffer (75 mM Tris-HCl (pH 8.8 at

25°C), 20 mM $(NH_4)_2 SO_4$ and 0.01% Tween 20), 0.2 mM dNTPs, 0.2 μM of each primer, 2 mM of $MgCl_2$, 200 μM of dNTPs mix, 1 unit (0.5 μl) of *Taq* DNA polymerase (homemade) and sterile distilled water. For optimal condition, which did not give saturated amplified products, ratio of actin per specific gene primers were 1:6 (for LvSID-1), 1:4 (for STAT) and 1:4 (for CHC). The PCR conditions were holding at 94°C for 2 min, denaturation at 94°C for 10 s, annealing at 55°C for 30 s, and extension at 72°C for 1 min. The annealing temperature was varied depending on the melting temperature of each primer pair, as listed in Table 1. Amplification was undertaken for 25–30 cycles and subsequently held at 72°C for 5 min. The PCR products were analyzed by agarose gel electrophoresis. Levels of PCR products were then relatively quantified using the Scion Image program.

Table 1 List of primers and their purposes.

Name	Sequences (5′ ➔ 3′)	Purposes
stSID1-R2	AAAAAGAATTCACAGTACAGTCCAGAAGGCT	RT-PCR of SID-1
stSID1-F3	ATAGATAATGGATCAAGAGACC	RT-PCR of SID-1
Actin-F	GACTCGTACGTCGGGCGACGAGG	RT-PCR of Actin
Actin-R	AGCAGCGGTGGTCATCACCTGCTC	RT-PCR of Actin
STAT-F	ATGTCGTTGTGGAACAGAGC	RT-PCR of STAT
STAT-R	GTTTGTTGCATGTGAAACACCTCC	RT-PCR of STAT
CHC-F	CTTCTCCCAAGAACCAGAGGTGCAC	RT-PCR of CHC
CHC-R	ATTCCTCTTCTCCACCTCTTCCACC	RT-PCR of CHC
qSID1-F	CCTGTTTGGTTGCTTAGCTG	qRT-PCR of SID-1
qSID1-R	TGCTGTGGAAGAAGAATGCC	qRT-PCR of SID-1
EF1a-F	GAACTGCTGACCAAGATCGACAGG	qRT-PCR of EF1α
EF1a-R	GAGCATACTGTTGGAAGGTCTCCA	qRT-PCR of EF1α
qSTAT-F	AGCCTTCGCCATCCGTCCTC	qRT-PCR of STAT
qSTAT-R	TACATAGTTTGTGGTGTGTTGGG	qRT-PCR of STAT
Random primer	5′-NNNNNNN-3′	First strand cDNA synthesis

Quantitative real-time RT-PCR (qRT-PCR)

qRT-PCR was performed in a Mastercycler® ep realplex (Eppendorf) using the KAPA SYBR® FAST qPCR kit (KAPA Biosystems). Shrimp SID1, STAT and elongation factor alpha 1 (EF1α) were amplified using the primers for qRT-PCR listed in Table 1. The qRT-PCR reaction (20 μl) contained 10μl of 2× SYBR® FAST qPCR master mix, 4 μl of 1:20 diluted cDNA, 0.5 μl of 10 mM of each primer and 5 μl of sterile distilled water. The reaction was performed under the following condition: denaturation at 95°C for 3 min, followed by 40 cycles of 95°C for 5 s and 60°C for 30 s. A melting curved analysis was performed after PCR amplification in order to determine the specificity of primers and the cycle threshold (Ct) of each gene. Relative expression normalized against EF1α was calculated by comparative Ct method (Schmittgen and Livak, 2008).

Statistical analysis

Graphs are presented as mean ± standard error of mean (SEM). The statistical analysis was performed by using an appropriate statistic profile of GraphPad Prism 5 program. A *p*-value below 0.05 ($p < 0.05$) was considered as statistically significant.

Results

Expression of LvSID-1 mRNA and the response to long dsRNA

The level of *Lv*SID-1 mRNA in three tissues (hepatopancreas, gill and muscle) of normal shrimp was measured by quantitative real-time RT-PCR using primers listed in Table 1. The highest level of *Lv*SID-1 mRNA was in hepatopancreas, which was approximately 3 and 45 times higher than that found in gill and muscle, respectively (Fig. 1). To determine the response of *Lv*SID-1 expression to long dsRNA with various sequences, four different dsRNAs (dsSTAT, dsGFP, dsNS1 and dsRR2) were injected into shrimp hemolymph. Up-regulated mRNA expression of *Lv*SID-1 in gills was observed in shrimp treated with each of these dsRNAs indicating that this response was not sequence specific (Fig. 2). To determine the *Lv*SID-1 response in different tissues, dsGFP was injected into shrimp prior to tissue collection for analysis. The induction effect of dsGFP on *Lv*SID-1 was observed in gills and muscle of the treated shrimp. The response in gills was prolonged to the 4th day after challenge and then gradually decreased thereafter (Fig. 3a). In muscle, the effect was high to the 2nd day post injection and then reduced sharply (Fig. 3b). Unlike gills and muscle, the injected long dsRNA did not cause any significant variation in the *Lv*SID-1 mRNA expression level in hepatopancreas (Fig. 3c). This may be related to the high basal expression level of *Lv*SID-1 mRNA in this tissue.

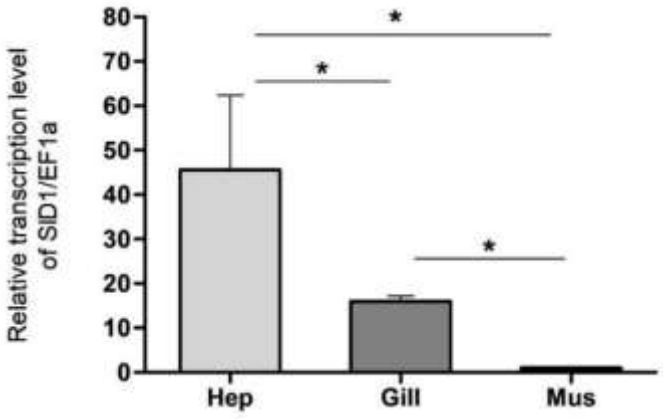

Fig. 1. Relative expression of *Lv*SID-1 mRNA in normal shrimp. Hepatopancreas (Hep), gill (Gill) and muscle (Mus) tissues were separately collected from individual shrimp (N = 4).The extracted RNA from each tissue was used to determine the expression of *Lv*SID-1 mRNA by quantitative real-time RT-PCR. The relative level of LvSID-1 mRNA normalized against the Ef1α mRNA level was plotted using GraphPad Prism 5 program. The statistical analysis was performed by Mann Whitney test at p-value less than 0.05 (*).

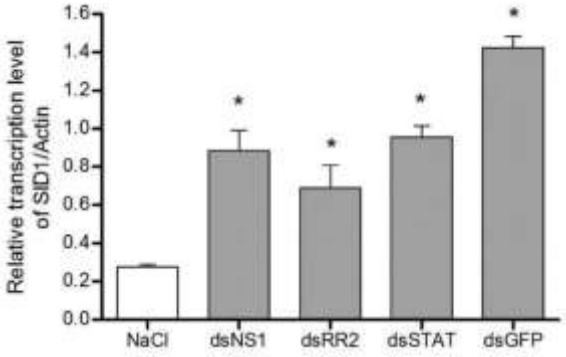

Fig. 2. Response of *Lv*SID-1 mRNA expression to injected long dsRNAs. Shrimp *(L. vannamei*) weighing approximately 300 mg were injected with 1.5 µg long dsRNAs (dsNS1, dsRR2, dsSTAT and dsGFP, N= 8, 8, 4, 3 and 5, respectively). At 48 h post injection, level of *Lv*SID-1 mRNA in gill tissue of the treated shrimp was determined by semi-quantitative RT-PCR. Relative level of the *Lv*SID-1 mRNA normalized by actin mRNA was plotted. Data is presented as mean ± SEM, the statistical analysis was performed by Mann Whitney test, *indicates significant difference from NaCl control at pvalue < 0.05.

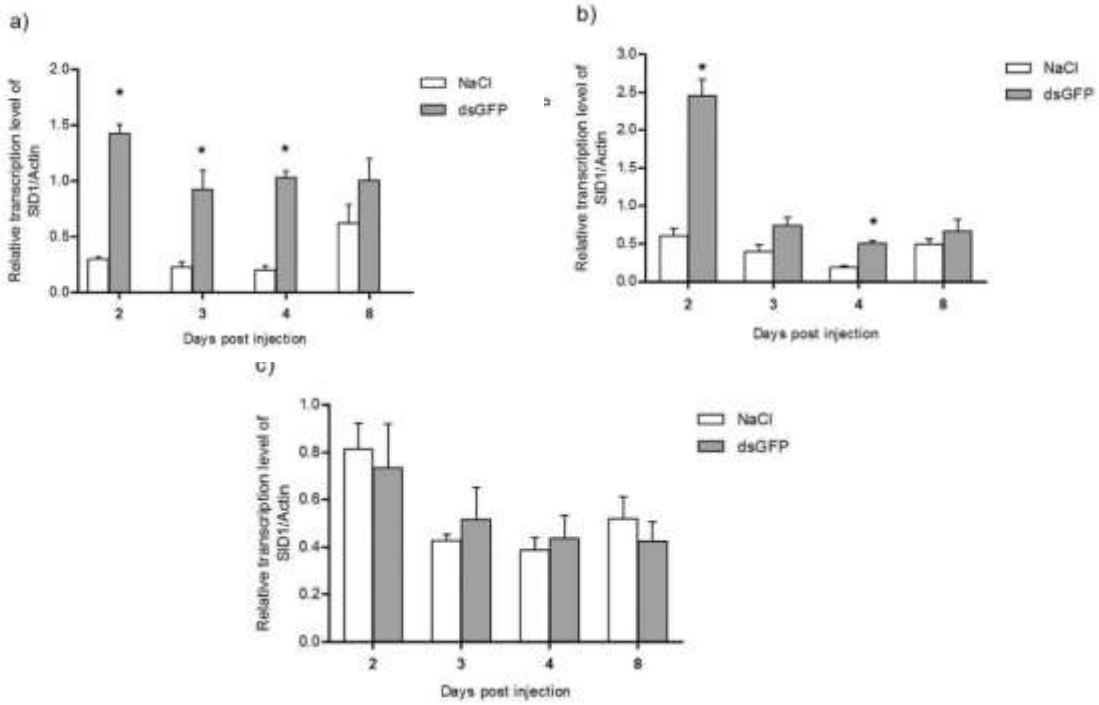

Fig. 3. Response of *Lv*SID-1 mRNA expression to injected dsGFP in different tissues. Shrimp (*L. vannamei*) weighing approximately 300 mg were injected with 1.5 µg dsGFP. The gills (a), muscle (b) and hepatopancreas (c) of the treated shrimp (N= 4) were isolated at different time points (2, 3, 4 and 8dpi). The extracted RNA from each tissue was used to determine the level of *Lv*SID-1 mRNA by semi-quantitative RT-PCR. Relative level of the *Lv*SID-1 transcript normalized by actin transcript was quantified by Scion Image and statistically analyzed by the Mann Whitney test (t-test). Data is presented as mean ± SEM with significant difference of the *Lv*SID-1 level between dsRNA injected group and NaCl control at p-value< 0.05 (*).

Effect of the LvSID-1 on uptake of dsRNA

As injection of dsRNA leads to an increase of *Lv*SID-1 mRNA expression in a sequence independent manner, there is difficulty in using dsRNAs to directly target the *Lv*SID-1 mRNA message for suppression to investigate its role in RNA imediated gene silencing. It may be the result from two effects of dsRNA specific to *Lv*SID-1 (dsSID-1) on its corresponding mRNA. The dsSID-1 can induce as well as silence the *Lv*SID-1 mRNA expression resulting in inefficient knockdown of *Lv*SID-1 (only 40% suppression of *Lv*SID-1 when compared to the control (dsGFP treated shrimp)) (Supplement data). Therefore, the role of *Lv*SID-1 was evaluated by monitoring the uptake efficiency of Cy3-labeled dsRNA as well as the silencing efficiency of target messages after increased expression of *Lv*SID-1 mRNA in a strategy utilizing sequential introduction of long dsRNAs. The first dsRNA was injected into shrimp to induce the *Lv*SID-1 expression. Thereafter, hemocytes from the *Lv*SID-1 induced shrimp (in parallel with hemocytes from control injected shrimp) were seeded in a chamber slide and incubated with a second dsRNA (Cy3-labeled dsRab7). Levels of the Cy3 (red) signal of the *Lv*SID-1 induced hemocytes was counted and compared with control injection cells (Fig. 4a). In a subsequent experiment *Lv*SID-1 induced shrimp were challenged with a second dsRNA by injection to silence the target gene mRNA (Fig. 5a). To provide robust evidence, two different second dsRNAs (dsSTAT and dsCHC) were used. The change in Cy3 signal and gene silencing efficiency amongst shrimp that have different levels of *Lv*SID-1 reflected capacity of the second dsRNA to be taken up.

Shrimp were pre-injected with the unrelated dsNS1 to induce the *Lv*SID-1 expression. At six days after injection, the dsNS1 up-regulated expression of *Lv*SID-1 mRNA as shown in Figs. 4b and 5b. The uptake efficiency of a second dsRNA was evaluated. After incubating the hemocytes with Cy3-labeled dsRab7, fluorescence signals (red) of the Cy3-labeled dsRab7 and blue signals of the DAPI nucleus staining were visualized under confocal microscope (Fig. 4c, d and e). The Cy3 signals were then counted and divided by the DAPI signals to evaluate the uptake efficiency of dsRNA. Level of Cy3 signals in the *Lv*SID-1 induced hemocytes (43.7%) was significantly higher than the signals of the control (non-induced hemocytes) (32.1%) (Fig. 4f), indicating that more dsRNA was taken up by the hemocytes that have higher *Lv*SID-1 expression.

Furthermore, the uptake efficiency of a second dsRNA was evaluated indirectly. The *Lv*SID-1 induced shrimp were challenged with a second dsRNA by injection to silence the target gene mRNA. The relative transcript of STAT, which was not affected by dsNS1 pre-injection (Fig. 5c), was clearly reduced in all shrimp receiving dsSTAT at 12 h post injection (hpi) compared to the control (Na-Na) (Fig. 5d). Interestingly at 24 hpi, the *Lv*SID-1 induced shrimp (Ns-St) showed levels of STAT suppression (71%) higher than that of the non-*Lv*SID-1 induced shrimp (Na-St) which showed an approximately 45% reduction (pvalue = 0.0207) (Fig. 5e). A similar result was observed when shrimp were injected with a different second dsRNA (dsCHC). The relative transcript of CHC was not affected by dsNS1 pre-injection (Fig. 6a). Higher CHC silencing level (66–78%) was detected in the *Lv*SID-1 induced shrimp at both 12 and 48 hpi when compared with the control non-induced shrimp who showed around 52–66% reduction (Fig. 6b and c), a result that was statistically significant for both time points (pvalue =0.0159 and 0.0317 respectively). These results indicated that the *Lv*SID-1 may be involved in the uptake of the second dsRNA in shrimp.

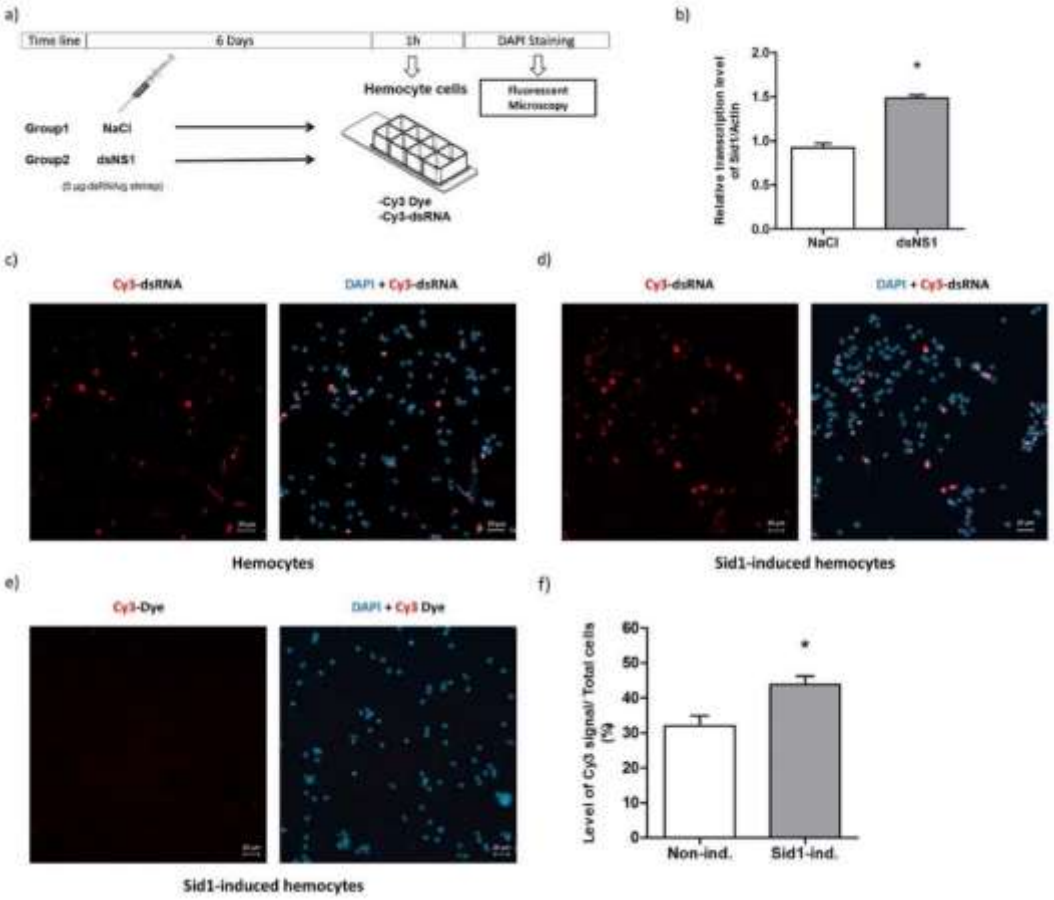

Fig. 4. Effect of the *Lv*SID-1 on uptake of Cy3-labeled dsRNA into hemocytes. Shrimp (300 mg) were initially injected with NaCl (Na) or dsNS1 (Ns) (1.5 μg) followed 6days later by hemolymph collection and hemocytes seeding in a chamber slide. Cellular uptake of Cy3-labeled dsRNA was observed under confocal fluorescent microscope (a). *Lv*SID-1 mRNA level after dsNS1 injection (N =4) was quantified and plotted (b). Increased *Lv*SID-1 level were used to determine the effect on cellular uptake of Cy3-labeled dsRab7. Red signals of Cy3-labeled dsRab7 and blue signals of DAPI staining nuclei of non-induced (hemocytes) (c) and SID-1-induced hemocytes (d) were counted (2–3 different areas for each shrimp (with triplicate shrimp examined)) and plotted (f). Cy3 dye alone as a negative (background) control (e). The statistical analysis was performed using Mann Whitney test at p-value less than 0.05 (*).

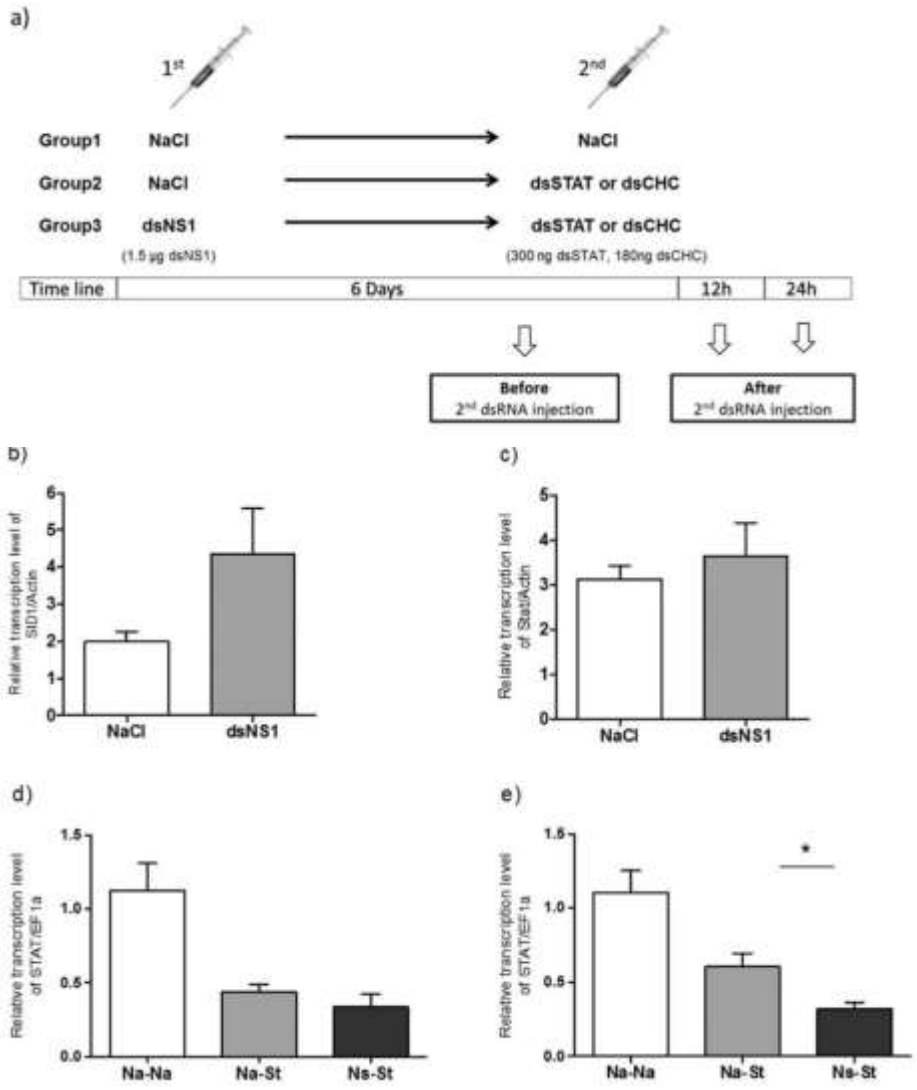

Fig. 5. Effect of the *Lv*SID-1 on uptake of injected dsSTAT. Shrimp (300 mg) were initially injected with NaCl (Na) or dsNS1 (Ns) (1.5 µg) followed 6days later by a second injection with dsSTAT (St) (300 ng). Level of the STAT mRNA was measured before and after injection of the dsSTAT as indicated in the diagram (a). *Lv*SID-1 (b) and STAT (c) mRNA levels before dsSTAT injection (N = 4) were quantified and plotted. Relative level of the STAT transcript of individual shrimp was measured at 12 (d) and 24 (e) hours post dsSTAT injection by RT-PCR,(N =7–8/group). The result was plotted in the graph as mean ± SEM. The statistical analysis was performed Mann Whitney test at *p*-value less than 0.05 (*).

Discussion

Direct injections of dsRNA into haemocoel or muscle are the most common methods for delivering dsRNA into shrimp (Labreuche et al., 2010; Sutthangkul et al., 2015). The dsRNA can circulate systemically in the hemolymph through the open circulatory system, in which the dsRNA may be taken up by cells in different tissues. In invertebrates,

at least two pathways for exogenous dsRNA uptake have been described so far, namely the systemic RNA interference defective (SID) transmembrane channel protein-mediated and the endocytosis-mediated mechanisms (Huvenne and Smagghe, 2010). Although SID-1 homologs have been found in *C. elegans* (Winston et al., 2002), shrimp (Labreuche et al., 2010) and many insects including *beetles Tribolium castaneum* (Tomoyasu et al., 2008), *Diabrotica virgifera* (Miyata et al., 2014), *Leptinotarsa decemlineata* (Cappelle et al., 2016), brown planthoppers (*Nilaparvatalu gens*) (Xuetal., 2013), honeybees (*Apis mellifera*) (Aronstein et al., 2006), silkworms (*Bombyx mori*) (Tomoyasu et al., 2008), desert locust (*Schistocera gregaria*) (Wynant et al., 2014) and migratory locust (*Locusta migratoria*) (Luo et al., 2012) except those of Diptera (Li et al., 2015; Tomoyasu et al., 2008; Winston et al., 2002), the participation of these SID-1indsRNA uptake have been demonstrated onlyin *C.elegans*, *D. virgifera*, *L. decemlineata*, *N. lugens* and *A. mellifera* (Cappelle et al., 2016). Even though the *T. castaneum* has three SID-1 homologs, they do not participate in dsRNA uptake indicating that some insect SID-1 have different functions and are not involved in dsRNA uptake (Tomoyasu et al., 2008; Xu and Han, 2008). Therefore, the presence of a SID-1 homolog does not mean that dsRNA uptake is through the SID-1 protein channel. In shrimp, SID-1 like has been found in several species such as *L. vannamei* (Labreuche et al., 2010), *M. japonicus* (Maralit et al., 2015) and *Crangon crangon* (Christiaens et al., 2014). Phylogenetic tree analysis showed that the shrimp SID-1 (*Lv*SID-1 and CcSID-1) are more similar to *Ce*SID-1 and different from insect SID-1 (Christiaens et al., 2014; Labreuche et al., 2010). In this study, the highest expression of the *Lv*SID-1 was observed in hepatopancreas compared to gills and muscle. As the hepatopancreas is the tissue that directly contacts with the environment in the case of feeding, this expression profile is similar to *C. elegans*, which showed the highest expression of the *Ce*SID-1 in tissues directly contact with the environment (Winston et al., 2002). This might relate to its function of dsRNA uptake from the environment. In response to dsRNA, up-regulation of *Lv*SID-1 mRNA expression was found in gills and muscle when shrimp were injected with long dsRNA. This response is consistent with the previous study by Labreuche et al. (2010) who reported that the *Lv*SID-1 mRNA expression in gill tissue was induced by long dsRNA (50–200 bp) but not by siRNA (Labreuche et al., 2010). In addition, the SID-1 mRNA in hemocytes of Kuruma shrimp was also up-regulated by non-specific dsRNA (Maralit et al., 2015). Unlike gills and muscle, the injected dsRNA did not cause any significant variation in the *Lv*SID-1 mRNA expression level in hepatopancreas. This may be related to the high basal expression level of the *Lv*SID-1 mRNA in this tissue. Taken together this information suggests that shrimp SID-1 may function as a transmembrane channel and participate in extracellular dsRNA uptake in shrimp cells as with CeSID-1. Nevertheless, the role of *Lv*SID-1 in dsRNA uptake requires further investigation.

Silencing of the SID-1 via RNAi is normally used to study its function in dsRNA uptake in insects. Suppression of the SID-1 mRNA reduced the RNAi efficiency in *D. virgifera* (Miyata et al., 2014) and *L. decemlineata* (Cappelle et al., 2016) indicating that they use SID-1 in dsRNA uptake. In contrast, in *T.castaneum* (Tomoyasu etal., 2008; Xiao et al., 2015; Xu and Han, 2008), *L. migratoria* (Luo et al., 2012) and S. gregaria (Wynant et al., 2014), silencing of the SID-1 homologs did not impair RNAi whereas silencing of clathrin and vacuolar ATPase or pharmacological inhibition reduced RNAi efficiency indicating that these insects do not use SID-1 but utilize clathrin-mediated endocytosis in the process of dsRNA uptake. Unfortunately, using RNAi mediated gene

suppression to study the *Lv*SID-1 function in this study was shown to be ineffective because of the induction effect of its cognate dsRNA (Supplement data). An alternative strategy to address the involvement of the SID-1 in dsRNA or siRNA uptake has been utilized in fish and mammalian cells, respectively (Duxbury et al., 2005; Ren et al., 2011). Uptake of siRNA into mammalian pancreatic ductal adenocarcinoma cells is generally limited. Over-expression of mammalian SID-1 enhances siRNA uptake and subsequent gene silencing is comparable to the transfection method (Duxbury et al., 2005). Improvements in dsRNA uptake efficiency and target gene suppression were obtained with over-expression of the mandarin fish SidT2 in fathead minnow (FHM) cells (Ren et al., 2011). Therefore in this study shrimp were injected with dsRNAs to induce *Lv*SID-1 mRNA expression, which was monitored at the RNA level by RT-PCR because of the lack of a specific antibody against *Lv*SID-1 protein. To ensure maximal translation of induced *Lv*SID-1 mRNA in shrimp a period of 6 days was allowed before administration of a second dsRNA. The efficiency of dsRNA uptake was evaluated directly by observation of the fluorescent signal of Cy3-labeled dsRNA in hemocytes, which have different levels of *Lv*SID-1, after exposing to the Cy3-labeled dsRNA. Significantly improved Cy3-labeled dsRNA uptake was obtained when hemocytes had higher *Lv*SID-1 expression levels, indicating that the *Lv*SID-1 facilitated uptake of dsRNA into shrimp hemocytes. Furthermore, efficiency of dsRNA uptake was also evaluated indirectly by determination of the potency of gene silencing amongst shrimp that have different levels of *Lv*SID-1 reflected capacity of the second dsRNA to be taken up. In the control experiment (no dsRNA, Na-Na), both STAT and CHC gene expression were unaltered, and these values were used as the normal level of STAT or CHC. In the second control group (non-induced *Lv*SID-1, Na-St or Na-Ch), the STAT or CHC mRNA level, which decreased from the normal levels, was used as the normal suppression level. However, the suppression was significantly more potent when *Lv*SID-1 was up-regulated in the induced *Lv*SID-1 groups (Ns-St or Ns-Ch). At this stage, the possibility of injection of the dsNS1 having some effects on the STAT or CHC transcriptional level can be ruled out because the STAT and CHC expression levels were indistinguishable from the control upon injection of dsNS1. In light of the increased uptake of Cy3-labeled dsRNA into hemocytes and increased suppression of STAT and CHC mRNA levels in gills when *Lv*SID-1 was up-regulated, SID-1 of *L. vannamei* may participate in the uptake of injected extracellular dsRNA into the shrimp cells. This study reports for the first time the involvement of the *Lv*SID-1 in dsRNA uptake in shrimp, which could help to improve the potency of RNAi mediated anti-viral approaches in shrimp in the future.

However, it has been shown that the Colorado potato beetle (*L. decemlineata*) required both the SID-1 and endocytosis pathways for dsRNA uptake into midgut cells (Cappelleetal.,2016). Hence, it cannot be concluded that the dsRNA uptake mechanism in shrimp is through the *Lv*SID-1 only. Any possible role of the endocytosis pathway on dsRNA uptake into shrimp cells needs to be investigated in the future. Supplementary data to this article can be found online at http://dx. doi.org/10.1016/ j.aquaculture.2017.09.027.

References

1. Agrawal, N., Dasaradhi, P.V.N., Mohmmed, A., Malhotra, P., Bhatnagar, R.K., Mukherjee, S.K., 2003. RNA interference: biology, mechanism, and applications. Microbiol. Mol. Biol. Rev. 67, 657–685.

2. Aronstein, K., Pankiw, T., Saldivar, E., 2006. SID-I is implicated in systemic gene silencing in the honey bee. J. Apic. Res. 45, 20–24.
3. Assavalapsakul, W., Kiem, H.K.T., Smith, D.R., Panyim, S., 2014. Silencing of PmYPR65 receptor prevents yellow head virus infection in *Penaeus monodon*. Virus Res. 189, 133–135.
4. Attasart, P., Kaewkhaw, R., Chimwai, C., Kongphom, U., Namramoon, O., Panyim, S., 2009. Inhibition of white spot syndrome virus replication in *Penaeus monodon* by combined silencing of viral rr2 and shrimp PmRab7. Virus Res. 145, 127–133.
5. Attasart, P., Kaewkhaw, R., Chimwai, C., Kongphom, U., Namramoon, O., Panyim, S., 2010. Inhibition of *Penaeus monodon* densovirus replication in shrimp by doublestranded RNA. Arch. Virol. 155, 825–832.
6. Attasart, P., Namramoon, O., Kongphom, U., Chimwai, C., Panyim, S., 2013. Ingestion of bacteria expressing dsRNA triggers specific RNA silencing in shrimp. Virus Res. 171 (1), 252–256.
7. Campbell, T.N., Choy, F.Y., 2005. RNA interference: past, present and future. Curr. Issues Mol. Biol. 7, 1–6.
8. Cappelle, K., de Oliveira, C.F., Van Eynde, B., Christiaens, O., Smagghe, G., 2016. The involvement of clathrin-mediated endocytosis and two Sid-1-like transmembrane proteins in double-stranded RNA uptake in the Colorado potato beetle midgut. Insect Mol. Biol. 25, 315–323.
9. Chen, Y.-H., Zhao, L., Jia, X.-T., Li, X.-Y., Li, C.Z., Yan, H., Weng, S.-P., He, J.-G., 2012.
10. Isolation and characterization of cDNAs encoding Ars2 and pasha homologues, two components of the RNA interference pathway in Litopenaeus vannamei. Fish Shellfish Immunol. 32, 373–380.
11. Chimwai, C., Tongboonsong, P., Namramoon, O., Panyim, S., Attasart, P., 2016. A formulated double-stranded RNA diet for reducing *Penaeus monodon* densovirus infection in black tiger shrimp. J. Invertebr. Pathol. 134, 23–26.
12. Christiaens, O., Delbare, D., Van Neste, C., Cappelle, K., Yu, N., De Wilde, R., Van Nieuwerburgh, F., Deforce, D., Cooreman, K., Smagghe, G., 2014. Differential transcriptome analysis of the common shrimp Crangon crangon: special focus on the nuclear receptors and RNAi-related genes. Gen. Comp. Endocrinol. 212, 163–177.
13. Dechklar, M., Udomkit, A., Panyim, S., 2008. Characterization of Argonaute cDNA from *Penaeus monodon* and implication of its role in RNA interference. Biochem. Biophys. Res. Commun. 367, 768–774.
14. Duxbury, M.S., Ashley, S.W., Whang, E.E., 2005. RNA interference: a mammalian SID-1 homologue enhances siRNA uptake and gene silencing efficacy in human cells. Biochem. Biophys. Res. Commun. 331, 459–463.
15. Escobedo-Bonilla, C.M., 2011. Application of RNA interference (RNAi) against viral infections in shrimp: a review. J. Antivir. Antiretrovir. S9. http://dx.doi.org/10.4172/jaa.S9-001.
16. Feinberg, E.H., Hunter, C.P., 2003. Transport of dsRNA into cells by the transmembrane protein SID-1. Science 301, 1545–1547.
17. Huvenne, H., Smagghe, G., 2010. Mechanisms of dsRNA uptake in insects and potential of RNAi for pest control: a review. J. Insect Physiol. 56, 227–235.

18. Labreuche, Y., Veloso, A., de la Vega, E., Gross, P. S., Chapman, R. W., Browdy, C.L., Warr, G.W., 2010. Non-specific activation of antiviral immunity and induction of RNA interference may engage the same pathway in the Pacific white leg shrimp *Litopenaeus vannamei*. Dev. Comp. Immunol. 34, 1209–1218.
19. Li, X., Dong, X., Zou, C., Zhang, H., 2015. Endocytic pathway mediates refractoriness of insect Bactrocera dorsalis to RNA interference. Sci Rep 5, 8700.
20. Luo, Y., Wang, X., Yu, D., Kang, L., 2012. The SID-1 double-stranded RNA transporter is not required for systemic RNAi in the migratory locust. RNA Biol. 9, 663–671.
21. Maralit, B., Komatsu, M., Hipolito, S., Hirono, I., Kondo, H., 2015. Microarray analysis of immunity against WSSV in response to injection of non-specific long dsRNA in kuruma shrimp, *Marsupenaeus japonicus*. Mar. Biotechnol. 17, 493–501.
22. Miyata, K., Ramaseshadri, P., Zhang, Y., Segers, G., Bolognesi, R., Tomoyasu, Y., 2014. Establishing an in vivo assay system to identify components involved in environmental RNA interference in the western corn rootworm. PLoS One 9 (7), e101661.
23. Ongvarrasopone, C., Roshorm, Y., Panyim, S., 2007. A simple and cost effective method to generate dsRNA for RNAi studies in invertebrates. Sci. Asia 33, 35–39.
24. Ongvarrasopone, C., Chanasakulniyom, M., Sritunyalucksana, K., Panyim, S., 2008. Suppression of PmRab7 by dsRNA inhibits WSSV or YHV infection in shrimp. Mar. Biotechnol. 10, 374–381.
25. Phetrungnapha, A., Kondo, H., Hirono, I., Panyim, S., Ongvarrasopone, C., 2015. Molecular cloning and characterization of Mj-mov-10, a putative RNA helicase involved in RNAi of kuruma shrimp. Fish Shellfish Immunol. 44, 241–247.
26. Posiri, P., Ongvarrasopone, C., Panyim, S., 2013. A simple one-step method for producing dsRNA from *E. coli* to inhibit shrimp virus replication. J. Virol. Methods 188, 64–69.
27. Posiri, P., Kondo, H., Hirono, I., Panyim, S., Ongvarrasopone, C., 2015. Successful yellow head virus infection of *Penaeus monodon* requires clathrin heavy chain. Aquaculture 435, 480–487.
28. Ren, R., Xu, X., Lin, T., Weng, S., Liang, H., Huang, M., Dong, C., Luo, Y., He, J., 2011. Cloning, characterization, and biological function analysis of the SidT2 gene from Siniperca chuatsi. Dev. Comp. Immunol. 35, 692–701.
29. Rocheleau, Christian E., 2012. RNA interference: systemic RNAi SIDes with endosomes. Curr. Biol. 22, R873–R875.
30. Sagi, A., Manor, R., Ventura, T., 2013. Gene silencing in crustaceans: from basic research to biotechnologies. Genes 4, 620–645.
31. Saleh, M. C., van Rij, R. P., Hekele, A., Gillis, A., Foley, E., O'Farrell, P. H., Andino, R., 2006. The endocytic pathway mediates cell entry of dsRNA to induce RNAi silencing. Nat. Cell Biol. 8, 793–802.
32. Sanitt, P., Attasart, P., Panyim, S., 2014. Protection of yellow head virus infection in shrimp by feeding of bacteria expressing dsRNAs. J. Biotechnol. 179, 26–31.
33. Sanitt, P., Apiratikul, N., Niyomtham, N., Yingyongnarongkul, B. - e., Assavalapsakul, W., Panyim, S., Udomkit, A., 2016. Cholesterol-based cationic liposome increases dsRNA protection of yellow head virus infection in *Penaeus vannamei*. J. Biotechnol. 228, 95–102.

34. Sarathi, M., Simon, M.C., Venkatesan, C., Hameed, A.S.S., 2008. Oral administration of bacterially expressed VP28dsRNA to protect *Penaeus monodon* from white spot syndrome virus. Mar. Biotechnol. 10, 242–249.
35. Schmittgen, T.D., Livak, K.J., 2008. Analyzing real-time PCR data by the comparative CT method. Nat. Protoc. 3, 1101–1108.
36. Sellars, M.J., Rao, M., Arnold, S.J., Wade, N.M., Cowley, J.A., 2011. *Penaeus monodon* is protected against gill-associated virus by muscle injection but not oral delivery of bacterially expressed dsRNAs. Dis. Aquat. Org. 95, 19–30.
37. Shekhar, M.S., Lu, Y., 2009. Application of nucleic-acid-based therapeutics for viral infections in shrimp aquaculture. Mar. Biotechnol. 11, 1–9.
38. Sutthangkul, J., Amparyup, P., Charoensapsri, W., Sepapin, S., Phiwsaiya, K., Tassanakajon, T., 2015. Suppression of shrimp melanization during white spot syndrome virus infection. J. Biol. Chem. 290 (10), 6470–6481.
39. Tomoyasu, Y., Miller, S.C., Tomita, S., Schoppmeier, M., Grossmann, D., Bucher, G., 2008. Exploring systemic RNA interference in insects: a genome-wide survey for RNAi genes in Tribolium. Genome Biol. 9, R10.
40. Treerattrakool, S., Chartthai, C., Phromma-in, N., Panyim, S., Udomkit, A., 2013. Silencing of gonad-inhibiting hormone gene expression in *Penaeus monodon* by feeding with GIH dsRNA-enriched Artemia. Aquaculture 404–405, 116–121.
41. Tsang, S.Y., Moore, J.C., Van Huizen, R., Chan, C.W.Y., Li, R.A., 2007. Ectopic expression of systemic RNA interference defective protein in embryonic stem cells. Biochem. Biophys. Res. Commun. 357, 480–486.
42. Ulvila, J., Parikka, M., Kleino, A., Sormunen, R., Ezekowitz, R.A., Kocks, C., Ramet, M., 2006. Double-stranded RNA is internalized by scavenger receptor-mediated endocytosis in Drosophila S2 cells. J. Biol. Chem. 281, 14370–14375.
43. Winston, W.M., Molodowitch, C., Hunter, C.P., 2002. Systemic RNAi in C. elegans requires the putative transmembrane protein SID-1. Science 295, 2456–2459.
44. Winston, W.M., Sutherlin, M., Wright, A.J., Feinberg, E.H., Hunter, C.P., 2007. Caenorhabditis elegans SID-2 is required for environmental RNA interference. Proc. Natl. Acad. Sci. U. S. A. 104, 10565–10570.
45. Wynant, N., Santos, D., Van Wielendaele, P., Vanden Broeck, J., 2014. Scavenger receptor-mediated endocytosis facilitates RNA interference in the desert locust, Schistocerca gregaria. Insect Mol. Biol. 23, 320–329.
46. Xiao, D., Gao, X., Xu, J., Liang, X., Li, Q., Yao, J., Zhu, K.Y., 2015. Clathrin-dependent endocytosis plays a predominant role in cellular uptake of double-stranded RNA in the red flour beetle. Insect Biochem. Mol. Biol. 60, 68–77.
47. Xu, W., Han, Z., 2008. Cloning and phylogenetic analysis of sid-1-like genes from aphids. J. Insect Sci. 8, 30.
48. Xu, H.J., Chen, T., Ma, X.F., Xue, J., Pan, P.L., Zhang, X.C., Cheng, J.A., Zhang, C.X., 2013. Genome-wide screening for components of small interfering RNA (siRNA) and micro-RNA (miRNA) pathways in the brown planthopper, Nilaparvata lugens (Hemiptera: Delphacidae). Insect Mol. Biol. 22, 635–647.
49. Yodmuang, S., Tirasophon, W., Roshorm, Y., Chinnirunvong, W., Panyim, S., 2006. YHVprotease dsRNA inhibits YHV replication in *Penaeus monodon* and prevents mortality. Biochem. Biophys. Res. Commun. 341, 351–356.

In vitro neutralization of yellow head virus infection in shrimp using recombinant PmYRP65 protein

Yellow head virus (YHV) is a major pathogen in the Southeast Asia shrimp aquaculture industry especially in Thailand, and YHV associated mortality results in significant economic loss. Although appropriate farm management strategies can decrease the YHV infection rate in shrimp, an epidemic of the virus remains, with no specific anti-YHV therapy. Previous reports have identified PmYRP65 as a protein that mediates YHV entry into susceptible cells, and studies using RNA interference have shown that systemic administration of double-stranded RNAs (dsRNAs) directed to PmYRP65 are able to provide protection against infection. This study sought to determine whether recombinant PmYRP65 protein (rPmYRP65) would be able to act as a competitive binding protein to neutralize YHV infection. To undertake this a cDNA encoding PmYRP65 was cloned, and rPmYRP65 was expressed, purified and characterized for its ability to neutralize YHV infection before injection into shrimp. The results showed that rPmYRP65 protein could significantly inhibit YHV infection by its receptor characteristic, through acting as a competitor to bind YHV. This study showed that rPmYRP65 has potential applications for neutralizing YHV infection of shrimp.

Introduction

In recent years the aquatic animal farming industries have dramatically expanded partly due to the increasing demand from the growing human population. This massive expansion of aquaculture together with an emphasis on high population-density farming has led to outbreaks of a number of diseases (Crane and Hyatt, 2011). In the shrimp farming industry in the Americas and Asia, viral diseases have had a significant impact on aquaculture (Walker and Mohan, 2009) and since it first emerged in Thailand in 1990, Yellow head virus (YHV) has been considered a devastating pathogen (Boonyaratpalin et al., 1993). YHV is a rod shaped-enveloped virus which contains a positive sense single stranded RNA and is classified as a member of the genus Okavirus, Family Roniviridae, and Order Nidovirales (Jitrapakdee et al., 2003; Sittidilokratna et al., 2002). The virus rapidly spreads in shrimp ponds inducing high mortality in a number of penaeid shrimp species (Boonyaratpalin et al., 1993; Flegel et al., 1997; Lightner et al., 1998; Lu et al., 1994; De la Rosa-Velez et al., 2006).

To enter host cells, viruses often utilize a protein expressed on the surface of the cell to mediate entry of the virus into the cell. These viral binding proteins (VBPs) are normally referred to as receptors, and a number of shrimp virus receptors have been identified including fibronectin for viral hemorrhagic septicemia virus (Bearzotti et al., 1999), integrin for white spot syndrome virus (WSSV) (Li et al., 2007) and laminin receptor (Lamr) for WSSV (Liu et al., 2016), Taura syndrome virus (TSV) and YHV (Busayarat et al., 2011). However, a number of other VBPs have been identified that do not function as receptors including actin for TSV (Senapin and Phongdara, 2006) and PmRab7 protein for Laem-Singh virus and YHV (Ongvarrasopone et al., 2010; Posiri et al., 2016). Several previous studies have shown that recombinant VBPs proteins can bind to the virus and inhibit infection. Examples include recombinant *Penaeus monodon* (Pm) Rab7 inhibiting WSSV (Sritunyalucksana etal., 2006; Thagun et al., 2012) as well as Pm Chitin-Binding Protein (PmCBP), *Marsupenaeus japonicus*

(Mj)-β-integrin, MjLectin-A, and MjLectin-B preventing WSSV infection (Chen etal., 2009; Lietal., 2007; Songetal., 2010). Importantly, recombinant PmLamr protein could decrease shrimp mortality in a YHV challenge experiment (Busayarat et al., 2011) as well as delay WSSV infection (Liu et al., 2016).

The yellow head virus receptor protein (PmYRP65) was first identified as a *Penaeus monodon* lymphoid cell-expressed receptor for YHV implicated in YHV entry into susceptible cells (Assavalapsakul et al., 2006). A subsequent study that knocked down PmYRP65 in shrimp using an RNA interference strategy showed that suppression of PmYRP65 transcription resulted in protection against infection (Assavalapsakul et al., 2014). However, it has not yet been established as to whether recombinant PmYRP65 protein would be able to neutralize YHV infection in shrimp. This study therefore sought to produce purified recombinant PmYRP65 and determine whether this was able to neutralize YHV infection of shrimp, and the results support this approach as a viable strategy to reduce YHV infection and to lessen mortality.

Materials and methods

Construction of a recombinant PmYRP65 expression plasmid

Total RNA was extracted from the dissected gills of a black-tiger shrimp using RiboZol™ RNA extraction reagent (AMRESCO, LCC., USA). Briefly, the gills were ground in Ribozol reagent and then incubated at room temperature for 5 min. Then chloroform was added, and the solution was mixed by vortex for 15 s. After incubation for 15 min at RT, the solution was centrifuged at 12,000 ×g for15 minat4°C. The upper phase was transfer red to a new tube, and the total RNA was precipitated by adding an equal volume of isopropanol followed by washing with 75% ethanol. The RNA pellet was re-suspended in RNase-free water. One microgram of total RNA was used as a template to produce cDNA using RevertAid™ reverse-transcriptase (Thermo Fisher Scientific Inc., USA) used according to the manufactures protocol. Briefly, total RNA and oligo (dT) primer were denatured at 70°C for 10 min and then immediately placed on ice, following which reverse transcription was performed at 37°C for 5 min, 42°C for 90 min, then 70°C for 5 min. One microlitre of cDNA was used for PCR amplification using 1× buffer, 4 mM of $MgSO_4$, 0.2 μM dNTPs, 0.2 μM of PmYRP65_XhoI_F (GGGGCTCGAGAAAAGACCGGAGGATAAGCCGGCGCAGAAGAAAGCC AAAGGTGCCAAGTCTGCCGAGGCAAAGG), 0.2 μM of PmYRP 65_X baI_R (GGGGTCTAGATCATCAGCATCTTCATCATCATCG), and 1 U of Vent DNA polymerase (Thermo Fisher Scientific Inc., USA) at 94°C for 1 min, 67°C for 30 s, 72°C for 2 min for 35 cycles and followed by a final incubation at 72°C for 10 min. The expected PCR product was purified and doubled digested with *Xho*I and *Xba*I (Thermo Fisher Scientific Inc., USA) at 37°C for 16 h. The digested DNA fragment was ligated into pCold™I DNA (Takara Bio Inc., Shiga, Japan) that has been digested with the same restriction enzymes and the ligation mix was subsequently transformed into *E. coli* DH5α. The recombinant plasmids were verified by selective medium, rapid size screening, restriction enzyme digestion analysis and further confirmed by DNA sequencing (1st Base DNA, Malaysia). The correct plasmid was then transformed into *E. coli* Rosetta-gami for PmYRP65 protein expression.

Expression and purification of rPmYRP65 protein

A single colony of a recombinant clone was cultured in LB medium containing 100 μg/μl of ampicillin and 34 μg/μl of chloramphenicol at 30°C until the optical density (OD) at 600 nm reach 0.4 after which culture was induced with is opropyl-β-D-thiogalactopyranoside (IPTG) at a final concentration of 0.3 mM followed by culture for 3 h.

The induced bacteria were collected by centrifugation and re-suspended in PCL buffer [PBS (286 mM NaCl, 8 mM Na_2HPO_4, 2.6 mM KCl, 1.4 mM KH_2PO_4), 1 mM DTT and 1% (w/v) SDS, pH 7.4] at 10 ml per 100 OD_{600} cell. The cell suspension was lysed by sonication until clear and then centrifuged at 8000 ×g at 4 °C for 10 min, after which the supernatant was passed through a 0.45 μM syringe filter, and the recombinant protein was immediately purified by a HisTrap column (GE Healthcare Life Sciences, USA) equilibrated with PCW binding buffer (PBS and 0.1% Sarkosyl (w/v), pH 7.4). After loading the filtrate on the column, the column was washed twice with 4 column volumes of PCW. The bound proteins were eluted by gradient elution with PCE (PCW buffer containing 60, 80, 100, 200, 300 and 400 mM imidazole). The remaining proteins were eluted by stripping buffer (PCW buffer containing 50 mM EDTA). All fractions were collected and analyzed by 10% SDS-PAGE and western blot analysis. The elution buffer in the selected fraction (300 mM imidazole) was replaced with PBS using an Amicon® Ultra-4 (Merck Millipore Ltd., Ireland) centrifugal filter and the amount of protein was determined by the Bradford assay (BIO-RAD Laboratories Inc., CA) at 595 nm with a BSA standard.

The samples were separated by 10% SDS–polyacrylamide gel electrophoresis on parallel gels, following which one gel was stained with Coomassie brilliant blue solution while the proteins in the second gel were transferred to apolyvinylidene difluoride (PVDF) membrane using a Mini Trans-Blot electrophoresis transfer cell (Bio-Rad Laboratories, Richmond, CA) at 120 A for 120 min. After transfer, the membrane was blocked to prevent nonspecific binding by immersion in blocking solution (PBS, 5% skim milk, 0.5% Tween-20) at room temperature for 5 min twice with gentle agitation. Then the membrane was incubated with 1:5000 dilution of a mouse anti-hexahistidine monoclonal antibody (R&D Systems Inc., Japan) in blocking solution at room temperature for 2 h, followed by a 1:5000 dilution of horseradish peroxidase-conjugated goat anti-mouse IgG1 antibody (Thermo Fisher Scientific Inc., USA). Signals were detected by autoradiography. The expected band of approximately 65 kDa was extracted from a 10% SDS-PAGE gel and after in-gel tryptic digestion peptides were analyzed by LC-MS/MS. The MS/MS spectra were searched against the MSDB nonredundant protein database (Imperial College, London UK) using the MASCOT search engine (Matrix Science, London, United Kingdom).

YHV neutralization assay using rPmYRP65 protein

L. vannamei shrimp (approximately 300–400 mg) were acclimated at 28 °C for 1–2 days prior to being divided into four groups for hemocoel injection with 1) PBS only, 2) rPmYRP65 alone (1.5 μg), 3) 5×10^{-8} LD50YHV (kindly provided by Chaimongkon D., Mahidol University, Nakorn Pathom, Thailand) and 4) rPmYRP65 (1.5μg) with 5×10^{-8} YHV. For the last group, rPmYRP65 was pre-incubated with YHV on ice for 1 h before injection. On day 3 post injection, the shrimp gills were collected, and RNA extracted to monitor YHV genome levels by semi-quantitative RT-PCR (n = 8) as described

below. The remaining shrimp (n = 10) were kept under standard conditions, with mortality recorded daily for 10 days. Moreover, to verify that rPmYRP65 was specifically neutralizing YHV, bovine-serum albumin (BSA) was used as an irrelevant protein to mix with YHV before injection in a similar procedure as previously described.

In a further experiment, 5 $\times 10^{-7}$ LD90 of YHV was mixed with 24μg of rPmYRP65. After pre-incubation on ice for 1 h, the mixture was injected into shrimp, in parallel with shrimp injected with 5 × 10^{-7} LD90 of YHV alone. All shrimp samples were collected to assess YHV genome levels on day two post injection (n =12).

Semi-quantitative RT-PCR

One microgram of total RNA was preheated with random primers (N_6) at 70°C for 5 min then placed immediately on ice for 2 min before reverse transcription using ReverseAid RT (Thermo Fisher Sciences, USA) at 25°C for 5 min, 42°C for 90 min and 65°C for 5 min. One microliter of cDNA reaction was used as a template for PCR comprising of 0.2 μM of Actin_F (GACTCGTACGTGGGCGACGAGG), 0.2 μM of Actin_R (AGCAGCGGTGGTCATCTCCTGCT), 0.067 μM of YHV_hel_F (CAAGGACCACCTGGTACCGGTAAGAC), 0.067 μM of YHV_hel_R (GCGGAAACGACTGACGGCTACATTCAC), 1× *Taq* buffer, 2 mM of $MgCl_2$, 0.2 μM dNTPs and 1 U of *Taq* DNA polymerase (Thermo Fisher Scientific Inc., USA) with 25 cycles of 94°C for 10 s, 55°C for 30 s, 72°C for 1 min, followed by 72°C for 5 min. The PCR products were separated on 1.5% agarose gels by electrophoresis and visualized using Quantity One (BIORAD Laboratory Inc., USA). Relative band intensities of YHV and actin amplicons were monitored by the Scion Image software 4.0.2 (Scion Corporation, Maryland) and then analyzed using the GraphPad Prism Program version 5.03 (GraphPad Software Inc., CA).

Statistical analysis

Relative band intensities were compared using the nonparametric Student t-test. Results are displayed as scatter dot plots with the median indicated, with each spot representing single shrimp. Cumulative mortality was compared by Newman-Keuls multiple comparison tests. A P-value< 0.05 was considered to be statistically significant.

Results

Construction of recombinant PmYRP65 expression plasmid

To construct a recombinant PmYRP65 expression plasmid, the 1.5 kb of PmYRP65 coding sequence was amplified by RT-PCR and li-gated into the pColdI expression vector at *Xho*I and *Xba*I sites. The recombinant PmYRP65 plasmid was verified by DNA sequencing, which confirmed identity to the PmYRP65 sequence (GenBank Accession: AAZ22828). The recombinant PmYRP65 plasmid was transformed into *E. coli* Rosetta-gami for recombinant PmYRP65 protein expression.

Expression and purification of rPmYRP65 protein

The *E. coli* Rosetta-gami containing the recombinant PmYRP65 plasmid was cultured at 30 °C for 3 h with induction by 0.3 mM IPTG. To determine solubility induced cells were suspended in PCL buffer and lysed by sonication. The soluble and insoluble fractions were resolved by SDS-PAGE. The result showed that the expected protein band of 65 kDa was mainly located in the soluble fraction, and comparison with total lysate suggested that> 95% of the protein was in the soluble fraction (data not shown).

Therefore, the soluble fraction was passed through a 0.45 μM filter and the protein purified using a His-trap column. The results of the elution profile showed that the expected 65 kDa-protein could be observed to elute in the 300 mM imidazole fraction (Fig. 1A–B, lane P). This purified recombinant PmYRP65 protein was further confirmed by LC-MS/MS analysis and the MASCOT program (MASCOT value of 138).

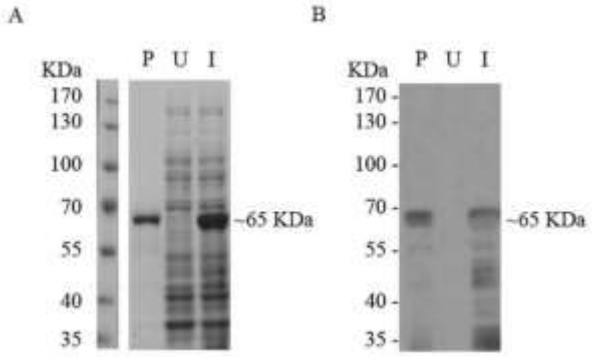

Fig. 1. SDS-PAGE profile and western-blot analysis of recombinant PmYRP65 production from *E. coli* Rosetta-gami using the pColdI system. The rPmYRP65 band was observed at approximately 65 kDa in both SDS-PAGE (A) and western-blot analysis using an anti-histidine monoclonal antibody (B). Lane P, purified rPmYRP65; Lane U, uninduced bacterial lysate; Lane I, induced bacterial lysate.

Specificity of Rab7 suppression via oral delivery of dsRab7

To investigate whether recombinant PmYRP65 protein could neutralize YHV, an in vitro neutralization assay was performed by co-injection of YHV with rPmYRP65 protein in the parallel injection of either YHV in PBS, PBS only or rPmYRP65 protein only. At 3 days post-injection, total RNA from gills was extracted from shrimp in the co-injection of YHV with PBS and YHV with rPmYRP65 protein groups and used as a template for semi-quantitative RT-PCR. The results showed that the YHV genome could be detected in six out of seven shrimp injected with co-injection of YHV with PBS, and five shrimp died on the third day (Fig. 2A, PBS co-injection). In contrast, the YHV genome was detected as low-intensity bands in only three out of eight shrimp injected with a co-injection of YHV with rPmYRP65, and only one shrimp died at the third day (Fig. 2A, YRP co-injection). Normalization of the YHV signal with actin showed that YHV genome signal was 4.39 fold less intense in the shrimp co-injected with rPmYRP65 and YHV as compared to the shrimp injected with PBS and YHV (Fig. 2B). Additionally, the remaining shrimp were continually observed for mortality for up to ten days. The results showed that co-injection of YHV with rPmYRP65 treatment could inhibit YHV as shrimp mortality was reduced approximately 30% when compared to the YHV infected only group (P-value < 0.001) (Fig. 2C). No mortality was seen in either the PBS or rPmYRP65 protein alone groups. To confirm the *in vitro* neutralizing property of rPmYRP65, the experiment was conducted by co-injection of YHV with either PBS or BSA or rPmYRP65. At 3 days post-injection, total RNA from gills was extracted from each shrimp and used as a template for semi-quantitative RT-PCR. The result showed that the YHV band could be detected in six out of ten shrimp on the third day in the PBS and BSA groups. In contrast, the YHV band could not be

observed in the rPmYRP65 group (Fig. 2D). According to semi-quantitative RT-PCR, the normalized band intensity ofrPmYRP65 group was less intense when compared with PBS and BSA groups (Fig. 2E). These results confirm that rPmYRP65 can significantly neutralize YHV infection (P-value < 0.05). The remaining shrimp were observed for mortality for ten days. The result showed that rPmYRP65 treatment strongly inhibited YHV as shrimp mortality was not observed as compared to the PBS group (*P*-value < 0.005) and BSA group (P-value < 0.001) (Fig. 2F).

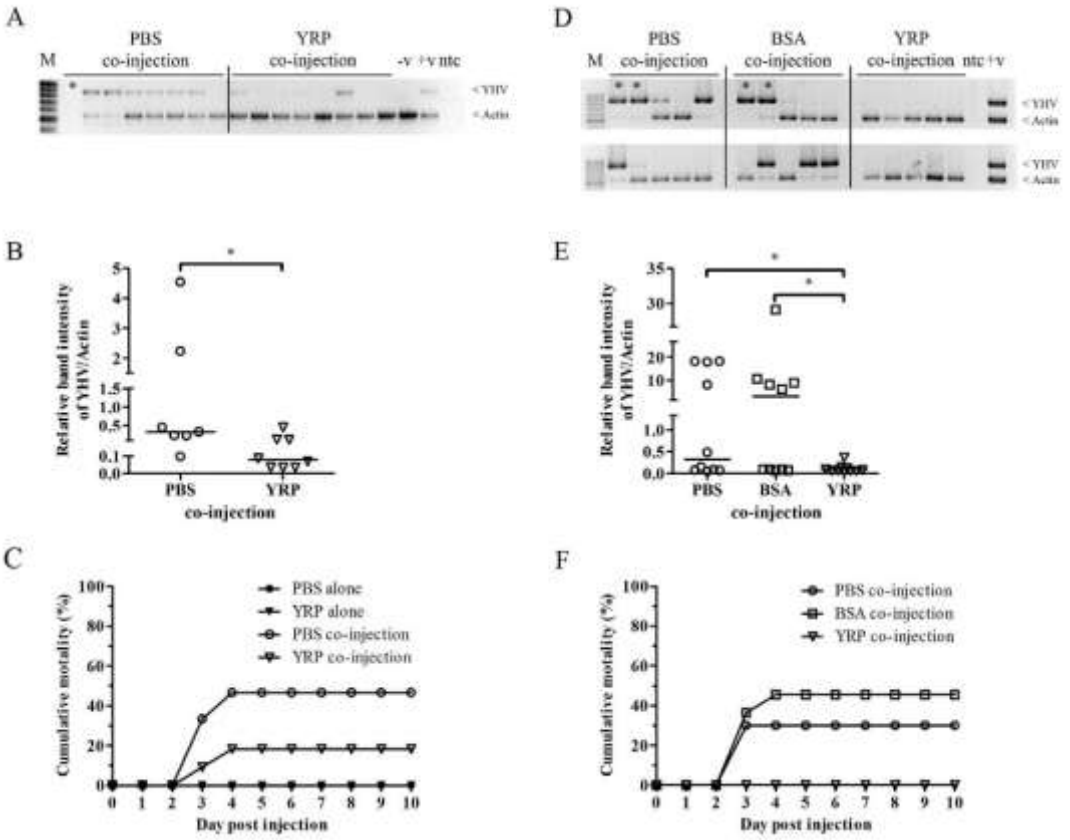

Fig. 2. Neutralization assay of YHV with rPmYRP65 protein. Shrimp were co-injected with a mixture of YHV (5×10^{-8} LD_{50}) and rPmYRP65 (1.5 μg) (YRP co-injection), BSA (1.5 μg) (BSA co-injection) or with YHV alone (PBS co-injection). Individual shrimp were collected to monitor the YHV genome by multiplex RT-PCR (A, D). The relative band intensity of YHV/ actin for individual shrimp together with the median is shown (B, E). The cumulative mortality of shrimp during YHV challenge was observed for 10 days (C, F). Lane M, 100 bp marker; PBS, control group; YRP, rPmYRP65 treatment group; -v, mock-infected shrimp; +v, YHV-infected shrimp; ntc, no temple PCR control; * degraded/dead sample.

To confirm the ability of rPmYRP65 to neutralize YHV infection in high dose, shrimp were injected with either a tenfold higher titer of YHV (5×10^{-7} LD_{90}) co-injected with the sixteen fold higher amount of rPmYRP65 (24 μg). After two days all shrimps were harvested and the level of the YHV genome assessed by semi-quantitative RT-PCR.

Interestingly, the result showed almost complete suppression ofYHV by rPmYRP65 treatment as no YHV band could be observed (Fig. 3A, Low panel). The relative band intensity of YHV/actin shows that rPmYRP65 treatment significantly lowered levels of YHV in tissues as compared to control YHV only injected shrimp (P-value < 0.001) (Fig. 3B).

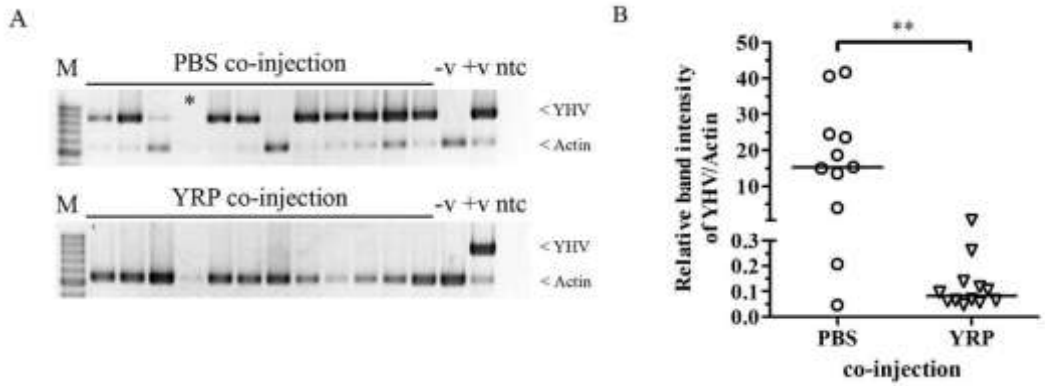

Fig. 3. Neutralization assay of YHV with rPmYRP65 protein. Shrimp were co-injected with a mixture of YHV (5 ×10−7 LD90) and rPmYRP65 (24μg) (YRP co-injection) or with YHV alone (PBS co-injection). Individual shrimp were collected on day 2 post challenge to monitor the YHV genome by multiplex RT-PCR (A). Relative band intensity of YHV/actin for individual shrimp together with the median is shown (B). Lane M, 100 bp marker; PBS, control group; YRP, rPmYRP65 treatment group; −v, mock-infected shrimp; +v, YHV-infected shrimp; ntc, no temple PCR control; * degraded sample was not included in the analysis.

Discussion

YHV is a pathogenic virus that causes a highly virulent and acute disease associated with high mortality in the black-tiger shrimp *Penaeus (Penaeus) monodon* (Boonyaratpalin et al., 1993). However, YHV can also cause high levels of mortality in farmed Pacific white-leg shrimp, *Penaeus (Litopenaeus) vannamei* (Senapin et al., 2010). Due to the widespread presence of this virus in Thailand and elsewhere, there is a need for novel anti-viral strategies to reduce economic losses caused by this virus.

Recombinant protein technology is a powerful approach to produce high amounts of protein. The *E. coli* expression system is the most commonly used cell factory for the production of therapeutic proteins as this system has the potential for high level expression, is fast growing and requires in expensive components and with the available technology this system is easy to manipulate (Rosano and Ceccarelli, 2014; Baeshen et al., 2015). A number of studies have used recombinant protein technology for the production of therapeutic proteins (Wurm, 2004) such as enzymes (Ni et al., 2016), cytokines (Jian et al., 2016) and anti-viral agents (Jiang et al., 2012; Nangola et al., 2012; Li et al., 2016; Yu et al., 2014).

A previous study identified PmYRP65 as a *P. monodon* receptor protein for YHV (Assavalapsakul et al., 2006). RNA interference induced knock-down of host expressed PmYRP65 using dsRNA successfully inhibited YHV infection in black-tiger shrimp primary Oka cells in vitro (Assavalapsakul et al., 2006) and in black-tiger

shrimp in vivo (Assavalapsakul et al., 2014). In this study, the coding sequences for PmYRP65 were cloned into the pCold™I *E. coli* expression system, and protein production was optimized and scaled-up to generate sufficient protein for an in vitro neutralization and mortality assay in a YHV challenge study. The results indicated that rPmYRP65 was able to inhibit YHV infection and reduce shrimp mortality through neutralizing the infectious YHV virion (Fig. 2A–F). This is in agreement with other studies that have shown that VBPs can inhibit viral infection in shrimp. For example, PmRab7 which directly binds to *VP*28 could neutralize WSSV infection through inhibition of viral endocytosis (Sritunyalucksana et al., 2006; Thagun et al., 2012). Similarly, PmLamr can bind to the YHV capsid protein resulting in reduced mortality from YHV challenge (Busayarat et al., 2011). This experimental in vitro study showed that rPmYRP65 could neutralize YHV prior to infection of shrimp resulting in reduced mortality as a consequence of YHV infection.

References

1. Assavalapsakul, W., Smith, D. R., Panyim, S., 2006. Identification and characterization of a *Penaeus monodon* lymphoid cell-expressed receptor for the yellow head virus. J. Virol. 80 (1), 262–269.
2. Assavalapsakul, W., Kiem, H.K., Smith, D.R., Panyim, S., 2014. Silencing of PmYRP65 receptor prevents yellow head virus infection in *Penaeus monodon*. Virus Res. 189, 133–135.
3. Baeshen, M.N., Al-Hejin, A.M., Bora, R.S., Ahmed, M.M., Ramadan, H.A., Saini, K.S., Baeshen, N.A., Redwan, E.M., 2015. Production of biopharmaceuticals in *E. coli*: current scenario and future perspectives. J. Microbiol. Biotechnol. 25 (7), 953–962.
4. Bearzotti, M., Delmas, B., Lamoureux, A., Loustau, A.M., Chilmonczyk, S., Bremont, M., 1999. Fish rhabdovirus cell entry is mediated by fibronectin. J. Virol. 73 (9), 7703–7709.
5. Boonyaratpalin, S., Supamattaya, K., Kasornchandra, J., Direkbusaracom, S., Aekpanithanpong, U., Chantanachooklin, C., 1993. Non-occluded Baculo-like virus, the causative agent of yellow head disease in the black tiger shrimp (*Penaeus monodon*). Gyohyo Kenkyu 2, 103–109.
6. Busayarat, N., Senapin, S., Tonganunt, M., Phiwsaiya, K., Meemetta, W., Unajak, S., Jitrapakdee, S., Lo, C.F., Phongdara, A., 2011. Shrimp laminin receptor binds with capsid proteins of two additional shrimp RNA viruses YHV and IMNV. Fish Shellfish Immunol. 31 (1), 66–72.
7. Chen, K.Y., Hsu, T.C., Huang, P.Y., Kang, S.T., Lo, C.F., Huang, W.P., Chen, L.L., 2009. *Penaeus monodon* chitin-binding protein (PmCBP) is involved in white spot syndrome virus (WSSV) infection. Fish Shellfish Immunol. 27 (3), 460–465.
8. Crane, M., Hyatt, A., 2011. Viruses of fish: an overview of significant pathogens. Viruses 3 (11), 2025–2046.
9. De la Rosa-Velez, J., Cedano-Thomas, Y., Cid-Becerra, J., Mendez-Payan, J.C., Vega-Perez, C., Zambrano-Garcia, J., Bonami, J.R., 2006. Presumptive detection of yellow head virus by reverse transcriptase-polymerase chain reaction and dot-blot hybridization in *Litopenaeus vannamei* and *L. stylirostris* cultured on the Northwest coast of Mexico. J. Fish Dis. 29, 717–726.

10. Flegel, T.W., Boonyaratpalin, S., Withyachumnarnkul, B., 1997. Progress in research on yellow-head virus and white-spot virus in Thailand. In: Flegel, T.W., MacRae, I.H. (Eds.), Diseases in Asian Aquaculture III. Asian Fisheries Society, Manila, Philippines, pp. 285–295.
11. Jian, Y., Chen, Y., Geng, C., Liu, N., Yang, G., Liu, J., Li, X., Deng, H., Chen, W., 2016. Target and resistance-related proteins of recombinant mutant human tumor necrosis factor-related apoptosis-inducing ligand on myeloma cell lines. Biomed. Rep. 4 (6), 723–727.
12. Jiang, Y., Yang, D., Li, W., Wang, B., Jiang, Z., Li, M., 2012. Antiviral activity of recombinant mouse beta-defensin 3 against influenza A virus in vitro and in vivo. Antivir. Chem. Chemother. 22 (6), 255–262.
13. Jitrapakdee, S., Unajak, S., Sittidilokratna, N., Hodgson, R.A., Cowley, J.A., Walker, P.J., Panyim, S., Boonsaeng, V., 2003. Identification and analysis of gp116 and gp64 structural glycoproteins of yellow head nidovirus of *Penaeus monodon* shrimp. J. Gen. Virol. 84 (Pt 4), 863–873.
14. Li, D.F., Zhang, M.C., Yang, H.J., Zhu, Y.B., Xu, X., 2007. Beta-integrin mediates WSSV infection. Virology 368 (1), 122–132.
15. Li, L., Zheng, Q., Zhang, Y., Li, P., Fu, Y., Hou, J., Xiao, X., 2016. Antiviral activity of recombinant porcine surfactant protein A against porcine reproductive and respiratory syndrome virus in vitro. Arch. Virol. 161 (7), 1883–1890.
16. Lightner, D.V., Hasson, K.W., White, B.L., Redman, R.M., 1998. Experimental infection of western hemisphere penaeid shrimp with Asian white spot syndrome virus and Asian yellow head virus. J. Aquat. Anim. Health 10, 271–281.
17. Liu, W.J., Li, Y.C., Kou, G.H., Lo, C.F., 2016. Laminin receptor in shrimp is a cellular attachment receptor for White Spot Syndrome Virus. PLoS One 11 (6), e0156375.
18. Lu, Y., Tapay, L.M., Brock, J.A., Loh, P.C., 1994. Infection of the yellow-head baculo- like vlrus in two species of penaeid shrimp, *Penaeus stylirostris* (Stimpson) and P. Vannamei (Boone). J. Fish Dis. 1, 649–656.
19. Nangola, S., Urvoas, A., Valerio-Lepiniec, M., Khamaikawin, W., Sakkhachornphop, S., Hong, S.S., Boulanger, P., Minard, P., Tayapiwatana, C., 2012. Antiviral activity of recombinant ankyrin targeted to the capsid domain of HIV-1 Gag polyprotein. Retrovirology 9, 17.
20. Ni, H., Guo, P.C., Jiang, W.L., Fan, X.M., Luo, X.Y., Li, H.H., 2016. Expression of nattokinase in Escherichia coli and renaturation of its inclusion body. J. Biotechnol. 231, 65–71.
21. Ongvarrasopone, C., Chomchay, E., Panyim, S., 2010. Antiviral effect of PmRab7 knockdown on inhibition of *Laem-Singh virus* replication in black tiger shrimp. Antivir. Res. 88 (1), 116–118.
22. Posiri, P., Panyim, P., Ongvarrasopone, C., 2016. Rab5, an early endosomal protein required for yellow head virus infection of *Penaeus monodon*. Aquaculture 459 (1), 43–53.
23. Rosano, G.L., Ceccarelli, E.A., 2014. Recombinant protein expression in Escherichia coli: advances and challenges. Front. Microbiol. 5, 172.
24. Senapin, S., Phongdara, A., 2006. Binding of shrimp cellular proteins to Taura syndrome viral capsid proteins VP1, VP2 and VP3. Virus Res. 122 (1–2), 69–77.

25. Senapin, S., Thaowbut, Y., Gangnonngiw, W., Chuchird, N., Sriurairatana, S., Flegel, T.W., 2010. Impact of yellow head virus outbreaks in the whiteleg shrimp, Penaeus vannamei (Boone), in Thailand. J. Fish Dis. 33 (5), 421–430.
26. Sittidilokratna, N., Hodgson, R.A., Cowley, J.A., Jitrapakdee, S., Boonsaeng, V., Panyim, S., Walker, P.J., 2002. Complete ORF1b-gene sequence indicates yellow head virus is an invertebrate nidovirus. Dis. Aquat. Org. 50 (2), 87–93.
27. Song, K.K., Li, D.F., Zhang, M.C., Yang, H.J., Ruan, L.W., Xu, X., 2010. Cloning and characterization of three novel WSSV recognizing lectins from shrimp *Marsupenaeus japonicus*. Fish Shellfish Immunol. 28 (4), 596–603.
28. Sritunyalucksana, K., Wannapapho, W., Lo, C.F., Flegel, T.W., 2006. PmRab7 is a VP28-binding protein involved in white spot syndrome virus infection in shrimp. J. Virol. 80 (21), 10734–10742.
29. Thagun, C., Srisala, J., Sritunyalucksana, K., Narangajavana, J., Sojikul, P., 2012. Arabidopsis-derived shrimp viral-binding protein, PmRab7 can protect white spot syndrome virus infection in shrimp. J. Biotechnol. 161 (1), 60–67.
30. Walker, P.J., Mohan, C.V., 2009. Viral disease emergence in shrimp aquaculture: origins, impact and the effectiveness of health management strategies. Rev. Aquac. 1, 125–154.
31. Wurm, F.M., 2004. Production of recombinant protein therapeutics in cultivated mammalian cells. Nat. Biotechnol. 22 (11), 1393–1398.
32. Yu, W., Yu, C., Wu, L., Fang, T., Qiu, R., Zhang, J., Yu, T., Fu, L., Chen, W., Hu, T., 2014. PEGylated recombinant human interferon-omega as a long-acting antiviral agent: structure, antiviral activity and pharmacokinetics. Antivir. Res. 108, 142–147.

Administration of co-expressed *Penaeus stylirostris* densovirus-like particles and dsRNA-YHV-Pro provide protection against yellow head virus in shrimp

The activation of the innate RNA interference pathway through double-stranded RNAs (dsRNAs) is one of the approaches to protecting shrimp from viruses. Previous studies have shown that injection of specific dsRNAs can successfully inhibit viral infection in shrimp. However, inhibition requires high levels of dsRNA and dsRNA stability in shrimp is limited. Virus-like particles (VLPs) have been applied to deliver nucleic acids into host cells because of the protection of dsRNAs from host endonucleases as well as the target specificity provided by VLPs. Therefore, this study aimed to develop *Penaeus stylirostris* densovirus (*Pst*DNV) VLPs for dsRNA deliver to shrimp. The *Pst*DNV capsid protein was expressed and can be self-assembled to form *Pst*DNV VLPs. Co-expression of dsRNA-YHV-Pro and *Pst*DNV capsid protein was achieved in the same bacterial cells, whose structure was displayed as the aggregation of VLPs by TEM. Tested for their inhibiting yellow head virus (YHV) from infecting shrimp, the dsRNA-YHV-Pro-PstDNV VLPs gave higher levels of YHV suppression and a greater reduction in shrimp mortality than the delivery of naked dsRNA-YHV-Pro. Therefore, *Pst*DNV-VLPs are a promising vehicle for dsRNA delivery that maintains the anti-virus activity of dsRNA in shrimp over a longer period of time as compared to native dsRNAs.

Introduction

To date, several shrimp viral diseases have been successfully inhibited by double-stranded RNAs via induction of the innate RNA interference (RNAi) system. In principle, long dsRNAs which target either viralgenes (Yodmuangetal., 2006; Attasartetal., 2010) or endogenous shrimp genes (Ongvarrasopone et al., 2011; Assavalapsakul et al., 2014) are cleaved by Dicer into short interfering RNAs (siRNAs). These siRNAs are incorporated into the RNA-induced silencing complex (RISC) and unwound into single-stranded siRNAs. Then, the antisense strand of the siRNA in the RISC is used as a guide to target the viral mRNA. The perfect base pairing of the mRNA with the siRNA promotes the subsequent degradation of the viral mRNA (Shekhar and Lu, 2009), leading to viral suppression and disease inhibition. Previous studies have shown that replication of yellow head virus (YHV) and the subsequent mortality of YHV-infected shrimp were strongly suppressed by injection of naked dsRNA corresponding to the YHV protease gene (dsRNA-YHV-Pro) (Yodmuang et al., 2006; Tirasophon et al., 2007; Assavalapsakul et al., 2009). However, the stability of the injected dsRNA in the shrimp, as well as efficiency of dsRNA uptake into shrimp cells, are limited. Several strategies such as chitosan-dsRNA based complexes (Threerawanitchpan et al., 2012; Kumar et al., 2016), lipiddsRNA based nanoparticles (Sanitt et al., 2016) and virus-like particles (VLPs) (Jariyapong et al., 2015b) have been investigated to solve these problems.

Amongst the strategies, VLP based approaches are the most promising as VLPs have structures and characteristics similar to native viruses but lack the viral genome in the particle (Buonaguro et al., 2011; Liew et al., 2012; Shao et al., 2012). Thus these VLPs are not infectious (Murawskietal., 2010) but can enterin to host cells with high efficiency and specificity. VLPs have been used as potential vehicles for delivery of therapeutic agents to target cells (Teunissen et al., 2013; Deng et al., 2015; Jariyapong,

2015a). In shrimp, the *Macrobrachium rosenbergii* nodavirus (*Mr*NV) capsid protein can be expressed in a prokaryote expression system with the formation of VLPs, which have been used as a vehicle to deliver double-stranded RNA for inhibition of white spot syndrome virus (Jariyapong et al., 2015b). However, the approach used required the disassembly and reassembly of the *Mr*NV capsid proteins to allow encapsulation of the dsRNA in vitro. In this study, therefore, we developed a single step strategy to form *Penaeus stylirostris* densovirus (*Pst*DNV) VLPs as well as to encapsulate dsRNAYHV-Pro in E. coli, through the co-expression of the shrimp *Pst*DNV capsid protein with dsRNA-YHV-Pro in the same E. coli cells. These dsRNA-YHV-Pro-*Pst*DNV VLPs were then purified and applied to the determination of anti-YHV property and stability in *Litopenaeus vannamei*.

Materials and methods

Cloning and expression of rPstDNV capsid protein

The full-length *Pst*DNV capsid protein coding sequence was amplified using specific primers. The PCR reaction consisted of 100ng *Pst*DNV genome as a template (kindly provided by Dr. Apinunt Udomkit, Institute of Molecular Bioscience, Mahidol University), 1x Thermopol Reaction Buffer, 0.2 mM dNTPs, 2 mM$MgSO_4$, 1 unit of Vent DNA Polymerase (New England BioLabs, Massachusetts, USA) and 0.2 μM (each) of cp PstDNV-F (5'-CAT ATG TGC GCC GAT TCA ACA AGA G-3') and cpPstDNV-R (5'-CTC GAG TTA TTA GTT AGT ATG CAT AAT ATA ACA TTT G-3') primers containing *Nde*I and *Xho*I restriction sites (underlined), respectively. The PCR amplification was carried out as follows: pre-heating at 94°C for 3min followed by 35 cycles of 94°C for 45s, 55°C for 30s, 72°C for 1.30min, then at 72°C for 10min. The PCR product was digested with *Nde*I and *Xho*I restriction enzymes and ligated into the pET28a expression vector pre-digested with the same restriction enzymes. As designed this vector would add an in-frame N-terminal histidine (His) tag to the expressed protein. The recombinant plasmids were transformed into *E. coli* DH5α and subsequently extracted using the QIAGEN Plasmid Extraction Kit (QIAGEN, Hilden, Germany). The recombinant plasmid was verified by PCR with specific *Pst*DNV capsid protein primers and DNA sequencing (1st Base DNA sequencing service, Malaysia). The selected recombinant plasmid (pET28a-cp *Pst*DNV) was then transformed into *E. coli* Rosetta-gami (pLysS) for r*Pst*DNV protein expression. The recombinant clone was grown in LB medium containing 50 μgml^{-1} kanamycin and 34 μgml^{-1} chloramphenicol at 30°C with shaking until $OD_{600}=0.4$. Protein expression was induced with isopropyl-β-D-thiogalactopyranoside (IPTG) at a final concentration of 0.4 mM and cells were further incubated at 30°C for 3h after which cells were harvested by centrifugation at 18890xg for 10min at 4°C. The recombinant PstDNV capsid (r*Pst*DNV cp) protein was analyzed by SDS-PAGE and western blotting analysis using an anti-his tag monoclonal antibody (R&D System Inc., Minneapolis, MN, USA).

Purification of rPstDNV cp protein

Induced *E. coli* cells expressing the r*Pst*DNV cp protein were lysed with lysis buffer (ENZhance Lysis Buffer, NSTDA) and soluble r*Pst*DNV cp proteins were collected by centrifugation. Briefly, the supernatant was increased to 5 ml with TS buffer (20 mM Tris-HCl, pH 8.0, 0.5M NaCl) and was then loaded onto a Ni-NTA affinity column (HisTrap HP; GE Healthcare, Sweden). The column was washed with Washing

Buffer (TS buffer containing 40 mM imidazole) and eluted with TS buffer containing 200 mM Imidazole. The remaining protein was eluted by washing the column with Stripping Buffer (TS buffer containing 50mM EDTA). Fractions were subsequently analyzed by SDS-PAGE and western blotting analysis. The selected fraction (200 mM imidazole) was replaced with TS Buffer using an Amicon® Ultra-4 (Merck Millipore ltd., Ireland) centrifugal filter, and the amount of protein was determined by the Bradford assay (BIO-RAD Laboratories Inc, CA) at 595 nm with a BSA standard.

Sample preparation for transmission electron microscopy (TEM)

The purified r*Pst*DNV cp protein or purified dsRNA-YHV-Pro*Pst*DNV VLPs were concentrated and dropped onto carbon-grids for 5min, then stained with 1% phosphotungstic acid (PTA) for 5min at room temperature. The grid was subsequently visualized with a JEOL JEM-1400 electron microscope operating at 120kV.

Co-expression of rPstDNV cp protein and dsRNA-YHV-Pro in rosetta gami

Are combinant plasmid, pET3a-dsRNA-YHV-Pro, encoding a double-stranded RNA directed to the protease gene of yellow head virus (dsRNA-YHV-Pro) was kindly provided by Dr. Witoon Tirasophon, Institute of Molecular Biosciences, Mahidol University. The details of the recombinant plasmid are as previously described in Yodmuangetal. (2006). Briefly, the stem region of the YHV-protease gene was amplified from the coding region of the YHV-protease gene with specific primers and then ligated into the pGEM-T easy vector in an inverted direction with GFP as a loop. Then, the stem-loop of dsRNA-YHV-Pro was digested with *Nde*I and subsequently cloned into the pET3a vector. The pET 3a-dsRNA-YHV-Pro was transformed into competent cells harboring the *Pst*DNV cp expression plasmid (pET28a-*Pst*DNV cp). Recombinant clones were selected by LB medium supplemented with 100 μgml^{-1} ampicillin, 50 μgml^{-1} kanamycin and 34μgml^{-1} chloramphenicol. To evaluate transformant containing both the two recombinant plasmids, colony PCR with multiplex primers for the two plasmids (*Pst*DNV cp primers; Forward 5'-CAT ATG TGC GCC GAT TCA ACA AGA G-3', Reverse 5'-CTC GAG TTA TTA GTT AGT ATG CAT AAT ATA ACATTTG-3' and dsRNA-YHV-Pro primers; YHV-Pro Antisense 5'ATG CCG ACG ATG TGA GCT CC-3', T7 Terminator 5'-GCT AGT TAT TGC TCA GCG G-3') was used. The multiplex PCR reaction was carried out as follows: pre-heating at 94°C for 5min followed by 30 cycles of 94°C for 30s, 54°C for 15s, 72°C for 30s, then at 72°C for 5 min. PCR products were analyzed by agarose gel electrophoresis.

Expression of both r*Pst*DNV cp protein and dsRNA-YHV-Pro was achieved by IPTG induction as already detailed (see methods 2.1). The r*Pst*DNV cp protein from the co-transformed cells was purified using a Ni-NTA affinity column (HisTrap HP; GE Healthcare, Sweden) exactly as described for the mono-transformed cells expressing the r*Pst*DNV cp protein alone. The purified r*Pst*DNV cp protein from the co-transfected cells was analyzed by SDS-PAGE and the VLPs visualized by transmission electron microscopy as previously described.

Extraction of dsRNA

For the extraction of double-stranded RNA two methods were employed. Firstly co-transformed recombinant cells after IPTG induction were resuspended in 0.1% SDS in 1X PBS buffer, boiled for 2 min and then incubated on ice for 30s. A total of 0.05 µg

of RNase A in 1X RNase A buffer (300 mM sodium acetate, 10 mM Tris-HCl, pH 7.5 and 5 mM EDTA) was added to the cell lysate which was then incubated at 37°C for 30 min, following which dsRNA was extracted using RiboZol™ RNA extraction reagent (AMRESCO, LCC., USA). To purify dsRNA from VLPs generated through co-transfection, VLPs purified as above were extracted directly with RiboZol™ RNA extraction reagent. Finally, dsRNA was dissolved in 150 mM NaCl and analyzed by nuclease digestion. Dissolved dsRNA was incubated with either 1 unit DNase I or with 0.05 μg RNase A, or with 0.5 unit RNase III at 37°C for 30min and then analyzed by gel electrophoresis.

To verify the association of dsRNA and *Pst*DNV VLPs, either *Pst*DNV VLPs or dsRNA-YHV-Pro-*Pst*DNV VLPs was digested with 0.5 unit RNase III at 37°C for 30 min before dsRNA extraction using RiboZol™ RNA extraction reagent (AMRESCO, LCC., USA) and analyzed by nuclease digestion (DNase I, RNase A and RNase III) followed by gel electrophoresis.

Inhibition effect and longevity of dsRNA-YHV-Pro-PstDNV VLPs in YHV infection

YHV suppression, semi-quantitative RT-PCR, and shrimp mortality

Shrimp (approimately 300 mg, 10–12 shrimp per group) were coinjected with either 150 mM NaCl, or 6 ng naked dsRNA-YHV-Pro, or 2 mg *Pst*DNV VLPs, or dsRNA-YHV-Pro-*Pst*DNV VLPs (6 ng dsRNA and 2 mg protein), together with a 5×10^{-7} dilution of stock YHV (titrated to cause 100% shrimp mortality within 4 days p.i.) after which they were maintained for 48h. At 48h post-YHV infection, the gills from individual shrimp were collected and total RNAs extracted using RiboZol™ RNA extraction reagent according to the manufacturer's protocol. The RNA pellet was resuspended in DEPC-treated water.

Two micrograms of total RNA was pre-heated with 10 μM random hexamers at 70°C for 5min after which the solution was immediately cooled for 2 min after which a RT-PCR reaction mix was added to give a final concentration of 1x reaction buffer, 25 mM $MgCl_2$, 10 mM dNTPs, and Improm-II™ reverse transcriptase (Promega). The reverse transcription was undertaken by incubating tubes at 25°C for 5min followed by 42°C for 60 min and finally 72°C for 15 min. One microliter of the cDNA reaction was used as a template for PCR comprising of 1x *Taq* DNA polymerase buffer, 0.2 mM dNTPs, 2 mM $MgCl_2$, 1 unit of *Taq* DNA Polymerase (Apsalagen, Thailand) and 0.2 μM (each) of YHVHelicase-F (5'-CAA GGA CCA CCT GGT ACC GGT AAG AC-3'), YHVHelicase-R (5'-GCG GAA ACG ACT GAC GGC TAC ATT CAC-3'), Actin-F (5'-ATG GCA TCT CGC AAG AAG ATT-3') and Actin-R (5'-TTA GCA AGA GCA TGC ATC CTG-3'). Reaction conditions were pre-heating at 94°C for 2 min followed by 20 cycles of 94°C for 45s, 55°C for 30s, 72°C for 1 min, then a final extension at 72°C for 10 min. The PCR products were separated on agarose gels by electrophoresis and visualized using Quantity One (BIORAD LaboratoryInc., USA). Relative band intensities of the YHV and actin amplicons were monitored using Scion Image software 4.0.2 (Scion Corporation, Maryland) and then analyzed using the GraphPad Prism Program version 5.03 (GraphPad Software Inc., CA). Relative band intensities were compared using 1-way ANOVA (Kruskal-Wallis test parameter). Results are displayed as scatter dot plots with the mean indicated, with each spot representing single shrimp.

To determine the effectiveness of YHV suppression, the experiment repeated but this time shrimp were maintained for up to 10 days, with mortality recorded daily.

Cumulative mortality was compared by the Student t-test. A *P*-value <0.05 was considered to be statistically significant.

Longevity of dsRNA-YHV-Pro- PstDNV VLP protection

To investigate the longevity of dsRNA-YHV-Pro-*Pst*DNV VLP protection, shrimp (approximately 300 mg, 10–12 shrimp per group) were injected with either 150 mM NaCl, or 6 ng naked dsRNA-YHV-Pro, or 2 mg *Pst*DNV VLPs, or dsRNA-YHV-Pro-*Pst*DNV VLPs (6 ng dsRNA and 2 mg protein) and the shrimp were maintained for 7 days before injection with YHV as above (a 5×10^{-7} dilution of stock YHV). After YHV infection, the shrimp were maintained with mortality recorded daily for 10 days. Cumulative mortality was compared by the Student t-test. A P-value < 0.05 was considered to be statistically significant.

Results

Expression and purification of rPstDNV cp protein

The full-length *Pst*DNV capsid (cp) coding sequence (~1000 bp) was cloned in pET28a. The r*Pst*DNV cp protein was successfully expressed in Rosetta-gami after induction with 0.4 mM IPTG at 30°C for 3 h. As the construct included a histidine (his)-tag at N-terminus of the r*Pst*DNV cp protein, an anti-histidine monoclonal antibody was used to detect the expressed r*Pst*DNV cp protein in a western blotting analysis. The correct size of the r*Pst*DNV cpprotein (plushis-tag) was observed at 37 kDa (Fig. 1). A Ni-NTA affinity column which specifically binds to the His-tag of the r*Pst*DNV cp protein was utilized to purify the r*Pst*DNV cp protein (Fig. 2), and approximately 90% recovery of the purified r*Pst*DNV cp protein was obtained. The yield of r*Pst*DNV cp protein was approximately 1.53 mgl^{-1}.

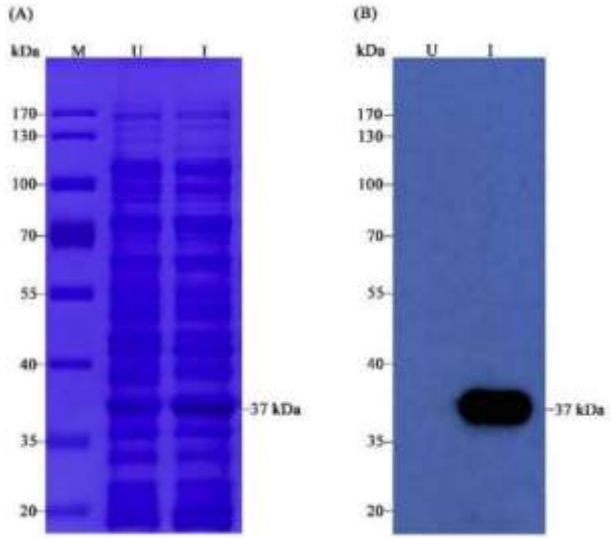

Fig. 1. Protein profile and western blot analysis of r*Pst*DNV cp protein in *E.coli* Rosetta-gami (pLysS). (A) SDS-PAGE analysis, (B) western blotting analysis with an anti-histidine monoclonal antibody. Lane M: prestained protein marker; Lane U: uninduced *E.coli* Rosetta-gami r*Pst*DNV cp protein; Lane I: induced *E.coli* Rosetta-gami r*Pst*DNV cp protein.

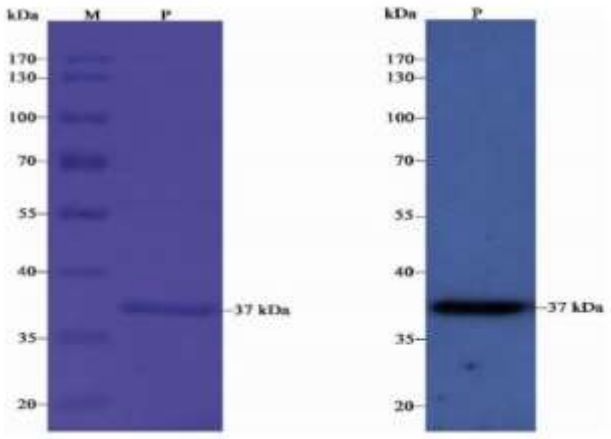

Fig. 2. SDS-PAGE and western blotting analysis of purified r*Pst*DNV cp protein after HisTrap column purification (A) SDS-PAGE and (B) western blotting analysis using anti-histidine monoclonal antibody. Lane M: prestained protein marker; Lane P: purified recombinant r*Pst*DNV cp protein.

Self-assembly of PstDNV VLPs

To determine whether the purified r*Pst*DNV cp protein self-assembled into VLPs, purified preparations were visualized under a transmission electron microscope (TEM). Results showed the presence of icosahedral shapes with an approximate size of 20 nm, similar to native *Pst*DNV virions (Hou et al., 2009; Lightner et al., 2012) (Fig. 3).

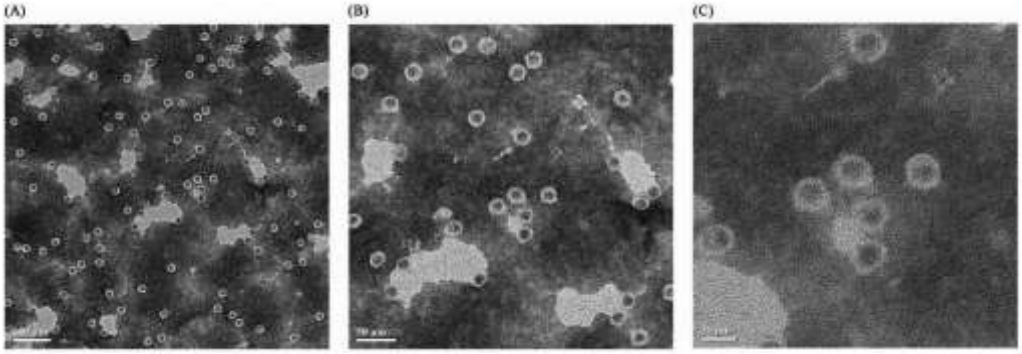

Fig. 3. Electron micrographs of PstDNV VLPs at different magnification. Scale bars show (A) 100 nm (B) 50 nm and (C) 20 nm.

Co-expression of rPstDNV cp protein and dsRNA-YHV-Pro in rosetta gami

Two plasmids expressing respectively r*Pst*DNV cp protein and dsRNA-YHV-Pro were maintained in the same *E. coli* cells by selection using two antibiotics (kanamycin and ampicillin) selection. Then, the coexistence of the two recombinant plasmids in each *E. coli* cell was verified by colony PCR with multiplex specific primers. The results (Fig. 4A) showed that the expected DNA fragments of the r*Pst*DNV cp gene and the dsRNA-YHV-Pro gene could be amplified with size 1000 and 500 bp, respectively, showing coexistent recombinant clones. While only either the 1000 bp or the 500 bp fragments were amplified from hosts containing only pET 28-*Pst*DNV cp or pET3a-dsRNA-YHV-Pro, respectively. Also, the expression host (*E. coli* Rosetta-gami)

showed no exprssion of either gene as expected. This result demonstrated that the two recombinant plasmids could be maintained in the same bacterial cell.

After IPTG induction, r*Pst*DNV cpprotein (37 kDa) and dsRNA-YHV-Pro (400 bp) synthesis were verified by SDS-PAGE and western blot analysis (Fig. 4B and C) and agarose gel electrophoresis (Fig. 4D), respectively. Nuclease (DNase I, RNase A and RNase III) digestion was used to verify the extracted dsRNA. The results showed the dsRNA-YHV-Pro was sensitive to only RNase III but not DNase I or RNase A indicating that this dsRNA-YHV-Pro was in the form of dsRNA (Fig.4D). Additionally, the protein yield of co-expressed dsRNA-YHV-Pro-*Pst*DNV-VLP was approximately 1.35mgl^{-1}. Then, the structure of the purified co-expressed dsRNA-YHV-Pro-*Pst*DNV-VLPs was again visualized under TEM. Large spherical shapes (approximately 500 nm) of dsRNA-YHV-Pro-*Pst*DNV-VLPs were observed (Fig. 5A). However, at high magnification, these large dsRNA-YHV-Pro-*Pst*DNV VLPs was clearly seen to be aggregates of single *Pst*DNV VLPs (~20 nm) (Fig. 5B and C).

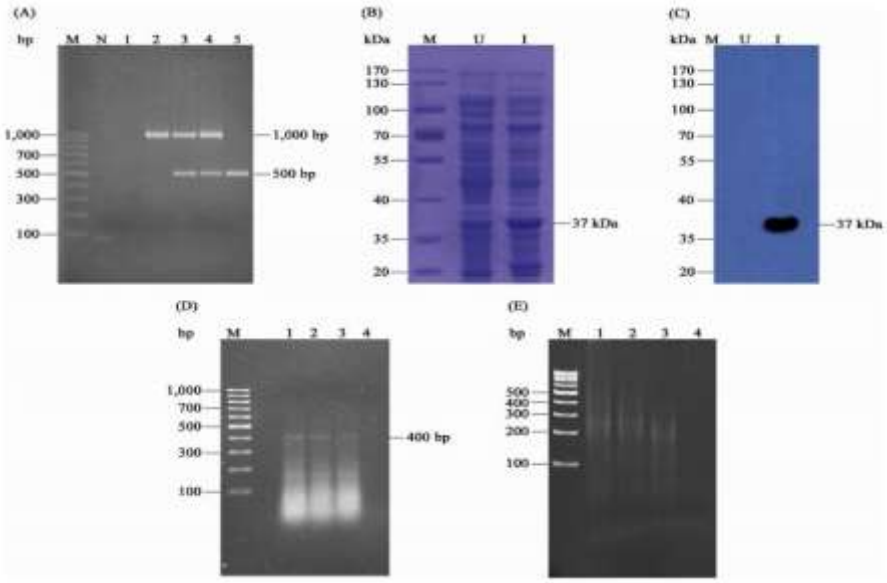

Fig. 4. Analysis of co-expressed r*Pst*DNV cp protein and dsRNA-YHV-Pro. (A) The existence of r*Pst*DNV cp protein and dsRNA-YHV-Pro plasmid analysis. Lane M: 100 bp DNA ladder marker; Lane N: No template control; Lane 1: *E.coli* Rosetta-gami host; Lane 2: *E.coli* Rosetta-gami contains only r*Pst*DNV cp protein expression plasmid; Lane 3–4: *E.coli* Rosetta-gami contains r*Pst*DNV cp protein and dsRNA-YHV-Pro expression plasmid; Lane 5: *E.coli* Rosetta-gami contains only dsRNA-YHV-Pro expression plasmid. (B) SDS-PAGE analysis, (C) western blotting analysis with an anti-histidine monoclonal antibody. Lane M: prestained protein marker; Lane U: uninduced *E.coli* Rosetta-gami r*Pst*DNV cp protein and dsRNA-YHV-Pro; Lane I: induced *E.coli* Rosetta-gami r*Pst*DNV cp protein and dsRNA-YHV-Pro. (D) dsRNA-YHV-Pro expression analysis; Lane M: 100 bp DNA ladder marker; Lane 1: untreated dsRNA-YHV-Pro; Lane 2–4: dsRNA-YHV-Pro treated with DNase I, RNase A and RNase III, respectively. (E) Extracted dsRNA-YHV-Pro from purified dsRNA-YHV-Pro-*Pst*DNV VLPs treated with DNase I, RNase A and RNase III, respectively. Lane M: 100 bp DNA ladder marker; Lane 1: untreated dsRNA-YHV-Pro; Lane 2–4: dsRNA-YHV-Pro treated with DNase I, RNase A and RNase III, respectively.

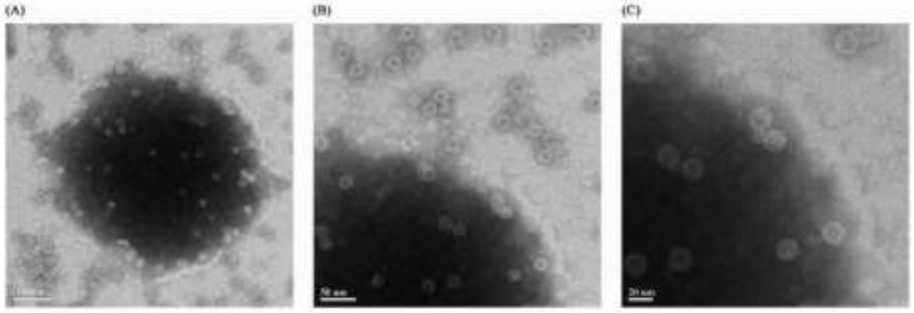

Fig. 5. Electron micrographs of dsRNA- YHV- Pro- *Pst*DNV VLPs at different magnification. Scale bars show (A) 100 nm (B) 50 nm and (C) 20 nm.

The dsRNA-YHV-Pro was packed into dsRNA-YHV-Pro-PstDNV VLPs

To determine whether the dsRNA- YHV- Pro- *Pst*DNV VLPs contains dsRNA-YHV- Pro, total RNA was extracted from this complex using Ribozol extraction and analyzed by polyacrylamide gel electrophoresis. The result showed that the extracted dsRNA-YHV-Pro had sizes ranging from 50 to 200 bp (Fig. 4E, Lane 1) and was sensitive only to RNase III (Fig. 4E, Lane 2–4). The amount of the extracted dsRNA-YHV-Pro was approximately 20 ng per 2 mg of purified co-expressed dsRNA-YHV-Pro-*Pst*DNV-VLPs. Then, dsRNA- YHV- Pro was extracted from either *Pst*DNV VLPs alone or from purified co-expressed dsRNA-YHV-Pro-*Pst*DNV-VLPs. The results showed that dsRNA-YHV-Pro could be extracted and observed from the purified co- expressed dsRNA- YHV- Pro-*Pst*DNV-VLPs (Fig. 6, Lane 2) and could be digested with RNase III (Fig. 6, Lane 3) while dsRNA- YHV- Pro could not be extracted or observed from purified *Pst*DNV VLPs alone (Fig. 6, Lane 1). This result indicates that dsRNA-YHV-Pro could associate with the *Pst*DNV VLPs either on the surface/outside or inside of the VLPs.

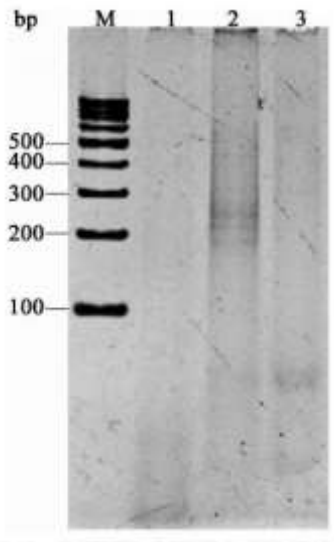

Fig. 6. Encapsulated dsRNA-YHV-Pro with *Pst*DNV VLPs; Lane M: 100 bp DNA ladder marker; Lane 1: Extracted dsRNA-YHV-Pro from purified *Pst*DNV VLPs.; Lane 2–3: Extracted dsRNA-YHV-Pro from purified dsRNA-YHV-Pro-*Pst*DNV VLPs untreated and treated with RNase III, respectively.

The anti-YHV property of dsRNA-YHV-Pro-PstDNV VLPs in shrimp

Suppression of YHV replication

To investigate the anti-YHV efficacy of the dsRNA-YHV-Proin dsRNA-YHV-Pro-*Pst*DNV VLPs, shrimp wereco-injected with naked dsRNA-pro or dsRNA-YHV-Pro-*Pst*DNV VLPs, or control injected (NaCl, BSA or *Pst*DNV VLPs) together with YHV. At 48 h postin jection, semi-quantitative RT-PCR of YHV in the gills normalized against actin was monitored. The result showed that the two groups of shrimp that received dsRNA-YHV-Pro, naked dsRNA-pro or dsRNA-YHV-Pro-*Pst*DNV VLPs, showed YHV suppression when compared with the controls shrimp with no dsRNA-YHVPro (NaCl, BSA, and *Pst*DNV VLPs) (Fig. 7). Amongst shrimp injected with dsRNA-YHV-Pro, shrimp with the dsRNA-YHV-Pro-*Pst*DNV VLPs had lower amounts of YHV than shrimp injected with the naked dsRNA-YHVPro, indicating that the dsRNA-YHV-Pro in the dsRNA-YHV-Pro-*Pst*DNV VLPs may enter into shrimp cells more efficiently.

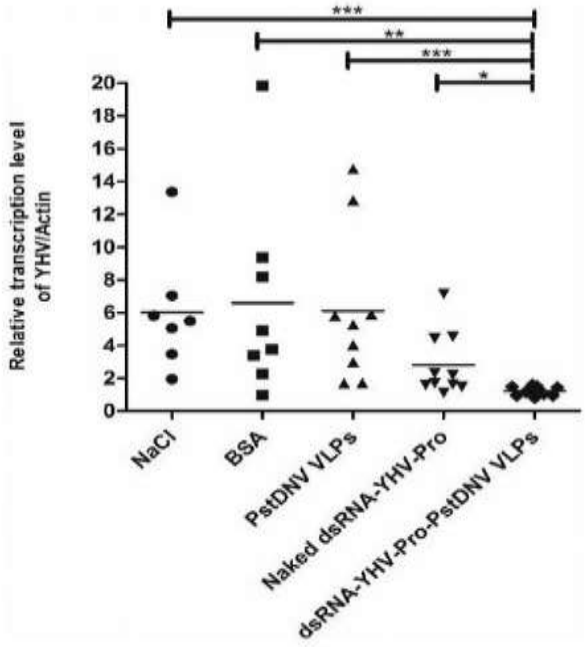

Fig. 7. Relative transcription levels of YHV/actin from YHV infected shrimp treated with NaCl, BSA, *Pst*DNV VLPs, naked dsRNA-YHV-Pro or dsRNA-YHV-Pro-*Pst*DNV VLPs as indicated.

Reduction of shrimp mortality

Shrimp were co-injected with NaCl, *Pst*DNV VLPs, naked dsRNA-YHV-Pro or dsRNA-YHV-Pro-*Pst*DNV VLPs and YHV and shrimp mortality were observed for 10 days. The result showed that all control shrimp with no dsRNA-YHV-Pro (NaCl and *Pst*DNV VLPs) died (100%) at day 3 post-injection while the mortality was reduced to 80% in dsRNA-YHV-Pro treatedshrimp (Fig. 8). However, the dsRNA-YHV-Pro-*Pst*DNV VLPs treated shrimp showed delayed mortality from day 5 to day 7 when compared with naked dsRNA-YHV-Pro treated shrimp.

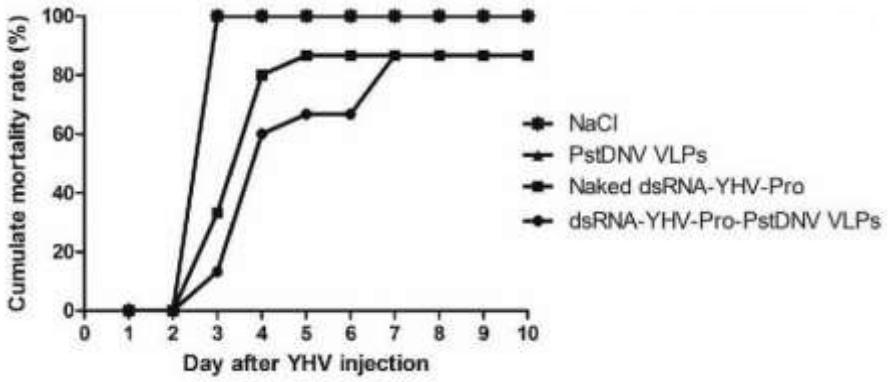

Fig. 8. Cumulative mortality of YHV infected shrimp treated with NaCl, *Pst*DNV VLPs, naked dsRNA-YHV-Pro or dsRNA-YHV-Pro-*Pst*DNV VLPs as indicated.

Longevity of dsRNA-YHV-Pro-PstDNV VLPs protection in shrimp for YHV inhibition

In order to evaluate the stability of the dsRNA-YHV-Pro in dsRNA-YHV-Pro-*Pst*DNV VLPs after injection into shrimp hemolymph, shrimp were injected with the dsRNA-YHV-Pro in either naked or complexed with VLPs 7 days prior to YHV infection. Shrimp mortality was then monitored for 10 days. The result showed that 100% cumulative mortality was observed in the control shrimp and shrimp with naked dsRNA-YHV-Pro. Interestingly, the mortality rate of the dsRNA-YHV-Pro-*Pst*DNV VLPs treated shrimp was reduced to 70% (Fig. 9), indicating that the dsRNA-pro in dsRNA-YHV-Pro-*Pst*DNV VLPs was more stable in shrimp hemolymph than the naked dsRNA-YHV-Pro and the anti-YHV effect was still retained to some degree.

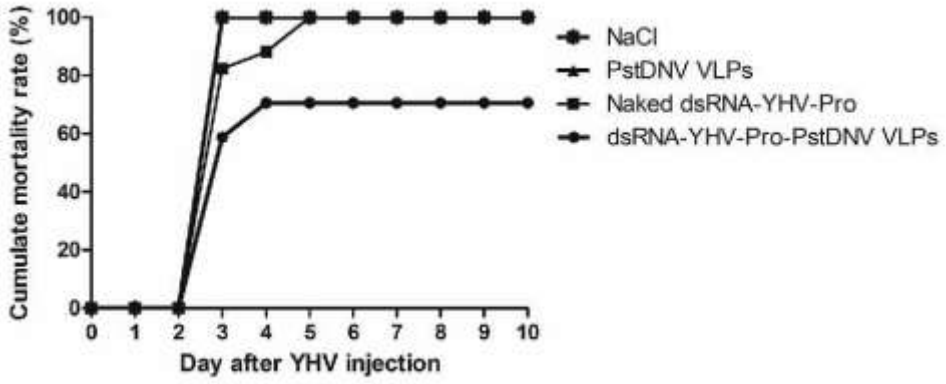

Fig. 9. Cumulative mortality of YHV infected shrimp treated with NaCl, *Pst*DNV VLPs, naked dsRNA-YHV-Pro and dsRNA-YHV-Pro-*Pst*DNV VLPs followed by challenge with YHV after 7days of maintenance.

Discussion

Studies have shown that some viral capsid proteins can undergo self-assembly forming virus like particles (VLPs), which have a structure similar to the particular native virus. However, VLPs lack encapsulation of the viral genome rendering the VLPs safe and not infectious, but still possessing the ability to encapsulate heterologous DNA or RNA (Voronkova et al., 2007; Hou et al., 2009; Zeltins, 2013). In this study the full-length *Pst*DNV cp protein coding sequences were cloned into the pET28a expression system, generating a protein with an in-framehexa-histidine tag attheN-terminus of the protein.To increase expression, the recombinant *Pst*DNV cp protein was expressed in Rosetta-gami, which has a rare codon tRNA for uncommon amino acid translation (Correa and Oppezzo, 2015). After IPTG induction, the *Pst*DNV cp protein was expressed and visualized by western blotting analysis. The molecular weight of the r*Pst*DNV cp protein as estimated by comparing with a standard protein marker was approximately 37 kDa, which correspond to the size of the r*Pst*DNV cp protein previous reported by Hou and his colleague (Hou et al., 2009), although the calculated molecular weight is 39 kDa. The purified r*Pst*DNV cp protein was able to self-assemble into VLPs similar to the natural *Pst*DNV virion despite the presence of the his-tag, indicating that the his-tag does not affect viral assembly. Previous studies have also shown that an Nterminal his-tag added as an aid to protein purification did not interfere with *Mr*NV VLPs assembly (Jariyapong et al., 2014).

In the past, strategies for loading nucleic acids into VLPs have generally required several steps, including the complete disassociation of the VLPs, encapsulation of the nucleic acid in vitro and re-association to reform the VLP, with specific conditions required for each step (O'Neil et al., 2011; Jariyapong et al., 2014; Jariyapong, 2015a; Jariyapong et al., 2015b). Therefore, in this study, we developed a onestep approach by co-expression of dsRNA-YHV-Pro and *Pst*DNV cp protein in the same *E. coli* cells. Colony PCR with multiplex primers indicated the coexistence of the pET3 and pET28a plasmids in the same bacterial cell. Plasmid persistence depends on the plasmid copy number, and the nature of any antibiotic resistance gene. Low copy number plasmids are more rapidly lost than high copy number plasmids under selective conditions, however, two plasmids can be maintained in the same bacterial cell for short generation periods (Velappan et al., 2007). Therefore, recombinant clones containing two plasmids should be freshly prepared from stock cultures to maintain the two plasmids in the same bacterial cell. Both dsRNA-YHV-Pro and *Pst*DNV cp protein were simultaneously expressed in Rosetta-gami although the dsRNA-YHV-Pro was somewhat degraded by the RNase III activity of Rosettagami. Under TEM visualization individual *Pst*DNV VLPs were seen to aggregate to form clusters of VLPs (~500nm) and the results also showed that dsRNA-YHV-Pro could be associated on the surface/outside and inside the VLPs. As shown in a previous report, plant virus-like particles can aggregate through linkage of the nucleic acid (CadenaNava et al., 2012). In this case, the dsRNA-YHV-Pro that is co-expressed with the *Pst*DNV cp protein may link *Pst*DNV VLPs together, and further experiments are needed to clarify this point.

To verify the dsRNA could be encapsulated inside the co-expressed dsRNA-YHV-Pro-*Pst*DNV-VLP, VLPs were treated with RNase III before dsRNA extraction, and the result showed that dsRNA-YHV-Pro was also observed after DNase I and RNase A digestion, however, the dsRNA-YHV-Pro could not be observed after RNase III digestion. This result indicates that the dsRNA-YHV-Pro could be encapsulated inside

the r*Pst*DNV VLPs during co-expression in the bacterial cell. The ability of r*Pst*DNV VLP to encapsulate nucleic acid has been previously shown (Hou et al., 2009). These results suggested that dsRNA-YHV-Pro could be associated with the surface (outside) or encapsulated (inside) in of r*Pst*DNV VLPs. Therefore, r*Pst*DNV VLPs could protect dsRNA-YHV-Pro or other nucleic acids from nuclease enzymatic digestion.

Nevertheless, when shrimp were co-injected with dsRNAs and YHV, the dsRNA-YHV-Pro in dsRNA-YHV-Pro-*Pst*DNV VLPs showed higher levels of YHV inhibition than the naked dsRNA-YHV-Pro and resulting shrimp mortality was delayed. The cellular uptake of VLPs, which will be similar to that of natural viruses, may help to deliver dsRNA-YHVPro into shrimp cells more efficiently than naked dsRNA is taken up (Voronkova et al., 2007; Chao et al., 2015; Jariyapong et al., 2015b). Several studies have shown that protection of shrimp through injection of dsRNA is hampered by the limited stability of the dsRNA in the hemolymph, possibly through degradation by shrimp endonucleases (Yodmuang et al., 2006; Teunissen et al., 2013). To test whether the VLPs can protect the dsRNA-YHV-Pro from endonuclease digestion, the dsRNA-YHV-Pro-*Pst*DNV VLPs or naked dsRNA-YHV-Pro were injected into shrimp 7 days prior to YHV infection. The results demonstrated that shrimp that received dsRNA-YHV-Pro in the dsRNA-YHV-Pro-*Pst*DNV VLPs had lower mortality than the control shrimp and naked dsRNA-YHV-Pro treated shrimp. This suggests that the VLPs may stabilize dsRNA-YHV-Pro and allow it to retain its anti-YHV effect within shrimp for at least 7 days after dsRNA injection.

In conclusion, a system in which dsRNA-YHV-Pro is associated with *Pst*DNV VLPs by co-expression in *E. coli* was developed, and its utility demonstrated for the first time. These dsRNA-YHV-Pro-*Pst*DNV VLPs can enhance cellular uptake of dsRNA as well as protect the dsRNA from enzymatic degradation in the shrimp hemolymph. Thus, these *Pst*DNV VLPs can possibly be used as a vehicle to deliver dsRNA and to maintain anti-viral inhibition of dsRNA in shrimp over a longer period of time.

References

1. Assavalapsakul, W., Chinnirunvong, W., Panyim, S., 2009. Application of YHV- protease dsRNA for protection and therapeutic treatment against yellow head virus infection in *Litopenaeus vannamei*. Dis. Aquat. Org. 84, 167–171.
2. Assavalapsakul, W., Tran Kiem, H.K., Smith, D.R., Panyim, S., 2014. Silencing of PmYPR65 receptor prevents yellow head virus infection in *Penaeus monodon*. Virus Res. 189, 133–135.
3. Attasart, P., Kaewkhaw, R., Chimwai, C., Kongphom, U., Namramoon, O., Panyim, S., 2010. Inhibition of *Penaeus monodon* densovirus replication in shrimp by double-stranded RNA. Arch. Virol. 155, 825–832.
4. Buonaguro, L., Tagliamonte, M., Tornesello, M.L., Buonaguro, F.B., 2011. Development in virus-like particle-based vaccines for infectious diseases and cancer. Vaccine 10, 1569–1583.
5. Cadena-Nava, R.D., Comas-Garcia, M., Garmann, R.F., Rao, A.L.N., Knobler, C.M., Gelbart, W.M., 2012. Self-assembly of viral capsid protein and RNA molecules of different sizes: requirement for a specific high protein/RNA mass ratio. J. Virol. 86, 3318–3326.
6. Chao, C.N., Huang, Y.L., Lin, M.C., Fang, C.Y., Shen, C.H., Chen, P.L., Wang, M., Chang, D., Tseng, C.E., 2015. Inhibition of human diffuse large B-cell

lymphoma growth by JC polyomavirus-like particles delivering a suicide gene. J. Transl. Med. 13, 1–9.
7. Correa, A., Oppezzo, P., 2015. Overcoming the solubility problem in *E. coli*: available approaches for recombinant protein production. Methods Mol. Biol. 1258, 27–44.
8. Deng, Y.N., Zeng, J.Y., Su, H., Qu, Q.M., 2015. Recombinant VLP-Z of JC polyomavirus: a novel vector for targeting gene delivery. Intervirology 58, 363–368.
9. Hou, L., Wu, H., Xu, L., Yang, F., 2009. Expression and self-assembly of virus-like particles of infectious hypodermal and hematopoietic necrosis virus in *Escherichia coli*. Arch. Virol. 154, 547–553.
10. Jariyapong, P., Chotwiwatthanakun, C., Somrit, M., Jitrapakdee, S., Xing, L., Cheng, H.R., Weerachatyanukul, W., 2014. Encapsulation and delivery of plasmid DNA by viruslike nanoparticles engineered from *Macrobrachium rosenbergii* nodavirus. Virus Res. 179, 140–146.
11. Jariyapong, P., Chotwiwatthanakun, C., Direkbusarakom, S., Hirono, I., Wuthisuthimethavee, S., Weerachatyanukul, W., 2015b. Delivery of double stranded RNA by Macrobrachium rosenbergii nodavirus-like particles to protect shrimp from white spot syndrome virus. Aquaculture 435, 86–91.
12. Jariyapong, P., 2015a. Nodavirus-based biological container for targeted delivery system. Artif. Cells. Nanomed. Biotechnol. 43, 355–360.
13. Kumar, D.R., Elumalai, R., Raichur, A.M., Sanjuktha, M., Rajan, J.J., Alavandi, S.V., Vijayan, K.K., Poornima, M., Santiago, T.C., 2016. Development of antiviral gene therapy for *Monodon baculovirus* using dsRNA loaded chitosan-dextran sulfate nanocapsule delivery system in *Penaeus monodon* post-larvae. Antiviral Res. 131, 124–130.
14. Liew, M.W.O., Chuan, Y.P., Middelberg, A.P.J., 2012. High yield and scalable cell-free assembly of virus-like particles by dilution. Biochem. Eng. J. 67, 88–96.
15. Lightner, D.V., Redman, R.M., Pantoja, C.R., Tang, K.F.J., Noble, B.L., Schofield, P., Mohney, L.L., Nunan, L.M., Navarro, S.A., 2012. Historic emergence, impact and current status of shrimp pathogens in the Americans. J. Invertebr. Pathol. 110, 174–183.
16. Murawski, M., McGinnes, L.W., Finberg, R.W., Kurt-Jones, E.A., Massare, M.J., Smith, G., Heaton, P.M., Fraire, A.E., Morrison, T.G., 2010. Newcastle disease virus-like particles containing respiratory syncytial virus G protein induced protection in BALB/c mice, with no evidence of immunopathology. J. Virol. 84, 1110–1123.
17. O'Neil, A., Reichhardt, C., Johnson, B., Prevelige, P.E., Douglas, T., 2011. Genetically programmed in vivo packaging of protein cargo and its controlled release from bacteriophage P22. Angew. Chem. Int. Ed. 50, 7425–7428.
18. Ongvarrasopone, C., Saejia, P., Chanasakulniyom, M., Panyim, S., 2011. Inhibition of Taura syndrome virus replication in *Litopenaeus vannamei* through silencing the LvRab7 gene using double-stranded RNA. Arch. Virol. 156, 1117–1123.
19. Sanitt, P., Apiratikul, N., Niyomtham, N., Yingyongnarongkul, B., Assavalapsakul, W., Panyim, S., Udomkit, A., 2016. Cholesterol-based cationic liposome increases dsRNA protection of yellow head virus infection in *Penaeus vannamei*. J. Biotechnol. 228, 95–102.

20. Shao, W., Paul, A., Abbasi, A., Chahal, P.S., Mena, J.A., Montes, J., Kamen, A., Prakash, S., 2012. A novel polyethyleneimine-coated adeno-associated virus-like particle formulation for efficient siRNA delivery in breast cancer therapy: preparation and in vitro analysis. Int. J. Nanomed. 7, 1575–1586.
21. Shekhar, M.S., Lu, Y., 2009. Application of nucleic-acid-based therapeutics for viral infections in shrimp aquaculture. Mar. Biotechnol. 11, 1–9.
22. Teunissen, E. A., de Raad, M., Mastrobattista, E., 2013. Production and biomedical applications of virus-like particles derived from polyomaviruses. J. Control. Release 172, 305–321.
23. Threerawanitchpan, G., Saengkrit, N., Sajomsang, W., Gonil, P., Ruktanonchai, U., Saesoo, S., Flegel, T.W., Saksmerprome, V., 2012. Chitosan and its quaternized derivative as effective long dsRNA carriers targeting shrimps virus in Spodoptera frugiperda 9 cells. J. Biotechnol. 160, 97–104.
24. Tirasophon, W., Yodmuang, S., Chinnirunvong, W., Plongthongkum, N., Panyim, S., 2007. Therapeutic inhibition of yellow head virus multiplication in infected shrimps by YHV-protease dsRNA. Antiviral Res. 74, 150–155.
25. Velappan, N., Sblattero, D., Chasteen, L., Pavlik, P., Bradbury, A.R., 2007. Plasmid incompatibility: more compatible than previously thought? Protein Eng. Des. Sel. 20, 309–313.
26. Voronkova, T., Kazaks, A., Ose, V., Ozel, M., Scherneck, S., Pumpens, P., Ulrich, R., 2007. Hamster polyomavirus-derived virus-like particles are able to transfer *in vitro* encapsidated plasmid DNA to mammalian cells. Virus Genes 34, 303–314.
27. Yodmuang, S., Tirasophon, W., Roshorm, Y., Chinnirunvong, W., Panyim, S., 2006. YHVprotease dsRNA inhibits YHV replication in *Penaeus monodon* and prevents mortality. Biochem. Biophys. Res. Commun. 341, 351–356.
28. Zeltins, A., 2013. Construction and characterization of virus-like particles: a Review. Mol. Biotechnol. 53, 92–107.

Identification and expression of white spot syndrome virus encoded microRNA in *Penaeus monodon*

White spot syndrome virus (WSSV) is the most devastating DNA virus that causes shrimp mortality worldwide. To understand WSSV and *Penaeus monodon* interaction, WSSV-encoded microRNAs (wsv-miRs) were identified by small RNA cloning and next generation sequencing. Ten wsv-miRs were identified and their expressions can be detected in only WSSV-infected tissues. These wsv-miRs and their flanking sequences can spontaneously form hairpin structure as predicted by Mfold. The expression profiles of 6 wsv-miRs increased dependent on time course of WSSV infection and slightly decreased after 48 hours post WSSV challenge. The highest expression was wsv-miR-9 followed by miR-13 and -15. Computational prediction of the candidate targets of wsv-miRs revealed possible functions of wsv-miRs in the controlling of apoptosis, transcription and signaling. This finding provided insights into WSSV-host interaction.

Introduction

White spot syndrome virus (WSSV) is a serious causative agent which originated white spot disease in shrimp and has highly impact to shrimp cultivation worldwide. Infection of WSSV leads to 100% shrimp mortality within a few days. In addition, this virus showed the highest percentage of infection in Thailand (Khawsak et al., 2008). This virus is classified in the *Whispovirus* of *Nimaviridae* family (Jehle et al., 2006). It has a double-stranded DNA genome approximately 300 kb, is packed with the nucleocapsid proteins and is surrounded by enveloped proteins such as VP28, VP26 and VP19. Currently, genome sequences of 4 WSSV isolates distinguished in the pandemic area and genome variation such as China (WSSV-Ch: AF332093), Taiwan (WSSV-Tw, AF440570), Thailand (WSSV-Th: AF369029) and Korea (WSSV-Kr: JX515788) (Chai et al., 2013). Several strategies were used to control WSSV such as environmental control, herbal treatment, recombinant vaccination and RNA interference (RNAi) approach (Sánchez-Paz, 2010). However, an effective strategy to prevent and cure WSSV infection remains limited due to the lack of understanding about WSSV pathogenesis and viral-host interaction. Insights studying in these areas will drive the advance therapeutic strategy.

Invertebrates lack of the adaptive immunity, nevertheless it is replaced by specific immunity as RNAi pathway. RNAi mechanism plays crucial roles in regulation of gene expression and antiviral defense by using the small interference RNA (siRNA) or micro RNA (miRNA). The miRNA is a non-coding single stranded RNA (ssRNA) about ~22 nucleotides (nt) in length, which function as regulatory small RNA in the RNA interference (RNAi) mechanism. It is believed to be involved in post-transcriptional gene regulation in many eukaryotic processes such as development, cell differentiation, apoptosis, and immune response (Dong et al., 2013). The miRNA is transcribed from genome into a non-perfect matched primary-miRNA (pri-miRNA) and is cleaved as a precursor-miRNA (pre-miRNA) by microprocessor, Drosha and its cofactor, Pasha (Denli et al., 2004; Gregory et al., 2004). The pre-miRNA is exported to the cytoplasm and is cleaved by Dicer and its partner, Loqs, to become a ~22 bp miRNA duplex (Saito et al., 2005; Park et al., 2011). The miRNA is preferentially selected based on the 5'

end thermostability to associate with an argonaute protein (AGO) in RNA-induced silencing complex (RISC) to become a mature miRNA (Khvorova et al., 2003; Schwarz et al., 2003). For siRNA processing, perfect matched dsRNA is a substrate which directly cleaved by Dicer into a siRNA duplex. The mature miRNA guides the RISC to target mRNA by using complementary base-pairing with the 3' untranslated region (UTR) of mRNA. An imperfect match with their target (Pasquinelli, 2012) resulted in translational inhibition, whereas perfectly matched caused mRNA degradation at post-transcriptional levels (Bartel, 2004; Kim, Han, and Siomi, 2009).

Recently, a number of miRNAs are found to be encoded by DNA viruses (Grundhoff and Sullivan, 2011). Presently, at least 530 viral-encoded miRNAs are deposited in the miRBase 22 (Kozomara and Griffiths-Jones, 2014) (www.mirbase.org). Virus that can encode miRNA usually has a DNA genome, invades into the nucleus of the host cell, has long term or persistent infection, and can switch between the lytic and latent stages of viral life cycle. Upon viral infection, host cells will encode miRNAs that function in the immune system to defend against the invading virus. On the other hand, virus can encode its own miRNAs by using host miRNA machineries and uses them to escape the host defense and also to remodel host gene expression to support the viral life cycle. For example, Epstein-Barr virus (EBV) encodes miR-BART5 which targeted to PUMA to prevent the infected cell undergoing apoptosis and also to promote latent infection (Choy et al., 2008). Simian virus 40 (SV40) encoded miR-S1 from the late transcripts, which cleaved an antisense transcript that encoded T-antigen and resulted in infected cells less susceptible to cytotoxic T cell mediated lysis (Sullivan et al., 2005). Meanwhile, some viruses encode miRNAs to control the viral gene itself. Herpes Simplex Virus 1 and 2 expressed miR-H2-3p from latency associated transcript (LAT) in its own antisense direction of an immediate early protein, ICP0. MiR-H2-3p is targeted to the viral coding gene and resulted in switching of virus to the latency stage (Jurak et al., 2010; Tang, Patel, and Krause, 2009; Umbach et al., 2008). An insect virus, *Heliothis virescens* ascovirus (HvAC), encodes miR-1 from the major capsid protein gene (MCP) which directly degrades its own DNA polymerase I transcript and thus, regulates its replication (Hussain, Taft, and Asgari, 2008).

To gain more insights into WSSV pathogenesis and viral-host interaction, this study aimed to identify the WSSV-encoded miRNAs from WSSV-Th during the late stage of viral infection in. The results identified 14 candidate WSSV-encoded miRNAs by using next generation Illumina Solexa sequencing. Six of the candidate miRNAs were specifically expressed in viral-infected cells and its expression were up-regulated dependent on time course of viral infection. *In silico* analysis identified potential cellular- and viral-gene targets of these candidate WSSV-miRNAs.

Materials and methods

Shrimp culture and WSSV stock

Healthy *P. monodon*, size about 10 g, was purchased from commercial shrimp farms in Nakhon Pathom, Thailand. Shrimps were reared in tanks containing 20 liter of continuously aerated saltwater at 10 ppt salinity and maintained at temperature 28°C. They were acclimatized a day before WSSV injection and fed with commercial feed every day.

WSSV-Th isolate stock was kindly provided by Dr. Sritunyalucksana, BIOTEC. The viral titer (10^6 virions μl^{-1}) was determined by real-time PCR (Sritunyalucksana et

al., 2006) and maintained at -80°C until used. For WSSV lysate, it was prepared according to the method of Natividad et al., (Natividad et al., 2007). Briefly, WSSV-infected gill tissue was homogenized in 10% w/v TNE buffer (50 mM Tris, 100 mM NaCl, 1 mM EDTA, pH 7.4) and the tissue debris was removed by centrifugation at 3000 ×g for 15 min at 4°C. The supernatant was filtered through a 0.45 μm membrane (Millipore) and stored at -80°C until use.

Sample preparation and RNA extraction

WSSV-infected or uninfected shrimp (control) were intramuscularly injected with 50 μl of the diluted purified-WSSV (~10^6 copies) or 150 mM NaCl (control) using tuberculin syringe needle, respectively. After 48 hours post challenge, gill tissues were collected and total RNAs were extracted by using TRIzol Reagent® (Molecular research center, Inc.) according to the manufacture's protocol. The quantity and integrity of the total RNAs were determined by Nanodrop spectrophotometer (Thermo Scientific, Wilmington, DE) and RNA agarose gel electrophoresis in Tris-EDTA-acetate (TAE) buffer, respectively.

Detection of WSSV infection

WSSV infection was confirmed by using reverse transcription PCR (RT-PCR) to amplify viral protein 28 gene (*vp28)*. Two micrograms of total RNAs were used as templates for complementary DNA (cDNA) synthesis by using reverse transcriptase (ImProm-II™ Reverse Transcriptase, Promega) and PRT primer (Supplementary Table 1). An actin was used as an internal control to standardize for loading. Condition of PCR was as followed: 94°C for 5 min followed by 25 cycles of 94°C for 30 s, 55°C for 30 s, 72°C for 30 s and continued with 72°C for 7 min to complete extension. The PCR products of WSSV-VP28 (447 bp) and actin (550 bp) were separated on 2% agarose gel electrophoresis.

Construction and sequencing of small RNA libraries

Total RNAs from WSSV-infected and WSSV-free tissues were submitted to Beijing Genome Institute (BGI), China, to construct the small RNAs libraries. Briefly, small RNAs ranged from 18-30 nt were purified by polyacrylamide gel electrophoresis before ligation with the 3' and 5' adaptors for Solexa sequencing. RT-PCR approach was used to convert the ligation products to DNA and amplified it. The amplicons were used as templates for cluster generation and directly sequenced by Illumina's Solexa sequencer.

Bioinformatics analysis of small RNAs

Raw small RNAs sequencing data were cleaned by eliminated fragments with size shorter than 18 nt, low quality reads, sequence with poly-A and adaptor contamination. Total clean reads were blasted against microRNA database or miRbase version 17 to identify the conserved miRNA that matched to mature RNAs in other species. The unannotated sequences were aligned using Rfam 10.1 and GenBank database to get rid of other small RNAs: rRNA, tRNA, snRNAs, and repeat associated RNAs. To identify novel candidate miRNAs derived from shrimp or WSSV, the remaining sequences were blasted against Express Sequence Tag (EST) database of *P. monodon* from Marine Genomics Project (www.marinegenomics.org) and WSSV genome Thai isolate from GenBank database (accession no. AF369029), respectively. Sequences that perfectly matched

viral genome, unmapable to shrimp's EST were considered for further analysis. To investigate the candidate miRNA ability to form hairpin structure, flanking sequence about ~100 nt from each side of the viral genome were collected and used in Mfold prediction with minimum free energy (MEF) less than -20 kcal/mol. The stem-loop structures were analyzed by MIREAP using the following criteria: mature miRNA length 20-24 nt, precursor miRNA has minimum 14 paired and minimum free energy <-18 kcal/mol, to predict the candidate WSSV-encoded miRNAs.

Stem loop RT-PCR for validation of candidate miRNAs

Total RNAs from WSSV-infected and uninfected gill tissues at 48 h were extracted and used in confirmation of WSSV infection by PCR before the miRNA validation. Stem-loop primers used to generate cDNA were designed according to Chen et al. (Chen et al., 2005). The primer contained an insertion of the universal sequence binding site of the reverse primer in the stem as described (Varkonyi-Gasic and Hellens, 2010). To set the RT reaction, 250 ng of the total RNA of each sample was mixed with 0.5 µl of 1 µM of stem-loop primers (SRT, SF and SR primers, Supplementary Table 1) before denaturation at 65°C for 5 min and quickly cooled on ice. Pre-denatured RNA was mixed with the reaction buffer containing 1X First-strand cDNA buffer, 250 nM of each dATP, dCTP, dGTP and dTTP, 10 mM DTT, 4 unit of RNaseOUT, 25 unit of SuperScript® III RT (Invitrogen) and adjusted the final volume with sterilized RNase-free water up to 10 µl. Reactions were incubated at 16°C for 30 min, followed by pulsed RT of 60 cycles at 30°C for 30 s, 42°C for 30 s and 50°C for 1 s and terminated by incubation at 85°C for 5 min. To perform the PCR reaction in a total volume 20 µl, the reaction contained 2 µl of cDNA, 1X *Taq* buffer with $[NH_4]_2SO_4$ (Fermentas), 2.5 mM $MgCl_2$, 0.5 mM dNTPs, 50 nM of specific forward primer (SF) and universal reverse primer (SR) and 1 unit of Taq DNA polymerase. The PCR condition was as followed: 95°C for 3 min followed by 35 cycles of 95°C for 10 s, 60°C for 20 s and cool downed at 20°C. The expected products have size approximately 62-65 bp were analyzed on 15% non-denaturing polyacrylamide gel electrophoresis.

Profiling of WSSV-encoded miRNAs expression

To prepare WSSV-infected tissues at various time points, 10 g of shrimp were challenged with the dose of WSSV lysate that resulted in shrimp death within 3 days. Gill tissues were collected at 0, 3, 6, 9, 18, 24, 36 and 48 h. Three shrimps were used for each time point. Then, total RNAs were extracted and WSSV detection was performed as described above. The expression of the candidate miRNAs were detected by stem loop RT-PCR. The relative expression levels of the wsv-miRs were determined by semi-quantitative RT-PCR. The intensity of the PCR products were measured by Scion Image 4.0 and normalized by the expression level of let-7 miRNA.

Target prediction of the WSSV-encoded miRNAs

To identify potential targets of the candidate miRNAs, miRanda 1.0 was employed (www.microrna.org). The miRanda scores that based on sequence complementarity between miRNA and their target was >90 and the free energy of miRNA: mRNA duplex was <-20 kcal/mol including a perfectly match in seed region at the 5' of miRNA. The dataset of identified miRNAs in this study and the EST of *P. monodon* or WSSV-Th genome were used as the input. The target genes that fit with above criteria were

identified by BLASTn against shrimp's EST and nucleotide database or translated into protein using BLASTp against protein database in NCBI. For viral target gene, WSSV genome sequence was used.

Results

Solexa sequencing data and Bioinformatics analysis of the small RNA libraries

In order to identify WSSV-encoded miRNAs, gill tissues from WSSV-infected and non-infected (control) shrimp were used in small RNAs library construction and were sequenced by NGS. The length distribution of raw sequence reads was similar between both small RNA libraries at 18-23 nt (Fig. 1), which are the ideal size of miRNA. A total of 16,257,357 and 16,513,781 raw sequence reads were obtained from control and WSSV-infected library, respectively. After removal of the low quality, adaptors and contaminated sequences, approximately 15 million clean reads were obtained from each library and 96% of the sequences were shared between the two libraries. Only a few unique sequences were found in the control (0.34%) and WSSV-infected (3.53%) libraries. The repeated sequences and other small RNAs: rRNA, tRNA, snRNA and snoRNA, were removed after analysis with Rfam10.1 and GenBank database. The remaining sequences were compared against miRBase17 to identify known and conserved miRNAs (Table 1). After alignment of the unannotated sequences with expressed sequence *tag* (EST) of *P. monodon* and genome of WSSV-Th isolate, the flanking regions of the matching sequences were collected and used for secondary structure prediction of precursor miRNAs by Mfold and analyzed by MIREAP. Finally, 17 miRNAs were obtained from WSSV-infected library; however, 3 of them matched with shrimp's EST, pmo-miR-1, -2 and -3. Therefore, 14 candidate miRNAs remained that were encoded from WSSV, wsv-miR-4 to -15. Notably, the candidate miRNAs, wsv-miR-4 and wsv-miR-7 were predicted to be derived from the 5' and 3' arms of pre-miRNAs (wsv-miR-4-5p, wsv-miR-4-3p, wsv-miR-7-5p and wsv-miR-7-3p) (Table 2).

Table 1 Summary of the Illumina Solexa sequencing data of WSSV-infected *P. monodon*

Small RNAs	Number of reads			
	Control		WSSV-infected	
	Unique[a]	Total reads	Unique	Total reads
Total clean reads	99,105	15,466,517	343,476	15,158,589
Conserved miRNAs	21,980	14,868,766	52,893	13,448,697
Other small RNA[b]	14,052	50,739	30,248	250,671
Unannotate[c]	63,073	547,012	260,335	1,459,221
Matched EST	588	2,314	1,842	27,880
Matched WSSV	122	882	39,195	369,354

[a]They are type of sequence
[b]Includes rRNA, tRNA, snRNA and snoRNA.
[c]Do not match with any-RNA

Table 2 Sequence and genomic position of the candidate miRNAs on WSSV genome.

miRNA	Location	strand	Sequence 5'→3'	Length (nt)
wsv-mir-4-5'	55069-55088	+	CAGGGAAGAAAUAGACCAUG	20
wsv-mir-4-3'	55123-55144		UGGAGCAUAUGUAUUCCCUGAA	22
wsv-mir-5	66621-66642	+	ACCCUUUUCGGUUGGCUGUGCU	22
wsv-mir-6	155594-155615	+	UUCGGUUCUUCAAAGAGGCUAA	22
wsv-mir-7-5'	188534-188555	+	CAGUAGUGUUGUUGCCUAUUCU	22
wsv-mir-7-3'	188578-188597		GAAAUAAUAAUAAUGCUGUC	20
wsv-mir-8	28262-28282	-	UGGACCGCUGGGUCGGGCCAA	21
wsv-mir-9	38575-38596	-	AGCCUAAAAAUCUCCCCUUCCU	22
wsv-mir-10	58933-58954	-	UCUUCUGGGUUUGGCUAAGAAA	22
wsv-mir-11	90678-90699	-	GACUUGGUGCGGCGGGGGCUGG	22
wsv-mir-12	186737-186758	-	UUUUUCCAACACAGAAGAUGCG	22
wsv-mir-13	209404-209425	-	CAGUCAUAUCCGUGAUCACAUU	22
wsv-mir-14	276164-276186	-	CCAAUGUCUUGAAGCUGUCGUGC	22
wsv-mir-15	288685-288707	-	AAUAUUGUCACCGAUGUUGGAGA	23

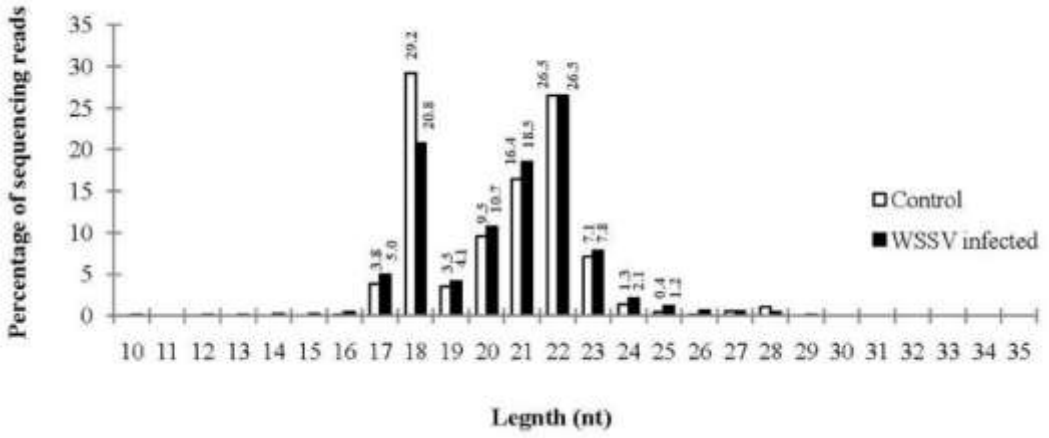

Fig. 1 Length distribution of small RNAs from control (□) and WSSV-infected libraries (■), with high frequency about 18-23 nt.

Characterization of candidate WSSV-encoded pre-miRNA

Secondary structure of WSSV pre-miRNAs were predicted using Mfold (Fig. 2). All the flanking sequences of each candidate WSSV-encoded miRNA could form stem-loop structure with the minimum energy fold (MEF) ranging from -18.3 to -27 kcal/mol. Hairpin structure of WSSV pre-miRNAs showed characteristics of internal mismatches with bulges in the stem and a terminal loop.

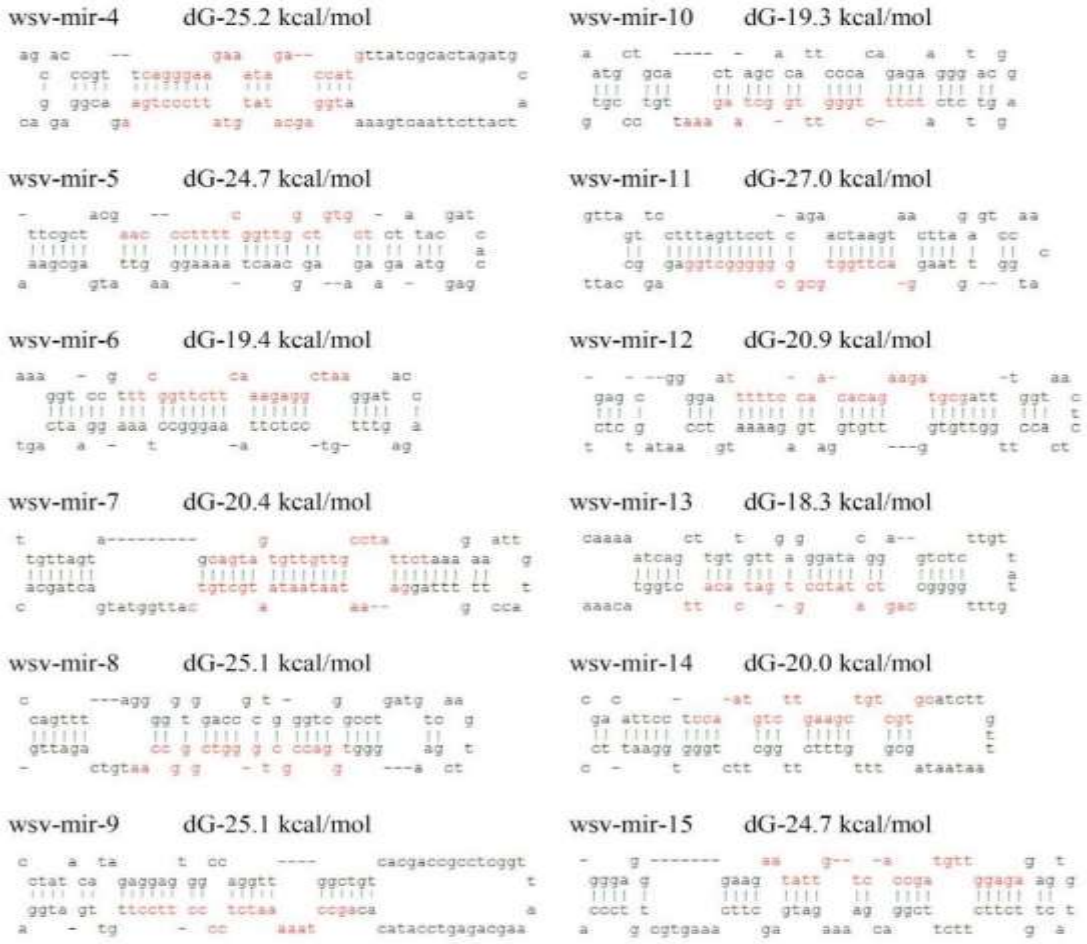

Fig. 2 Secondary structures of the 12 candidate WSSV-encoded pre-miRNAs. The minimum free energy (MFE) was predicted by Mfold program. Red nucleotides indicate mature sequences of miRNAs.

Mapping of WSSV-encoded miRNAs on WSSV genome

All 12 candidate WSSV-encoded pre-miRNAs were distributed along the WSSV genome. The nucleotides sequences and the genomic position of the candidate wsv-miRs are shown in a schematic diagram (Fig. 3). Candidate wsv-miRs were classified into 4 groups according to the transcriptional direction and location. In the first group, the candidate wsv-miRs (wsv-miR-4, -5, -6 and -7) were located on the sense strand and were encoded in the same direction as the open reading frame (ORFs) of WSSV. The second and third groups were embedded in the antisense strand of the viral genome and were either encoded in the opposite (wsv-miR-8, -9, -12, -13 and -14) or in the same transcriptional orientation with viral ORFs (wsv-miR-10 and -15). The last group which contained only a single candidate, wsv-miR-11, was located in the overlapping sequence between ORF63 and 64 in an antisense direction. Notably, wsv-mir-9 was found located in the antisense strand of the putative WSSV DNA polymerase (ORF27).

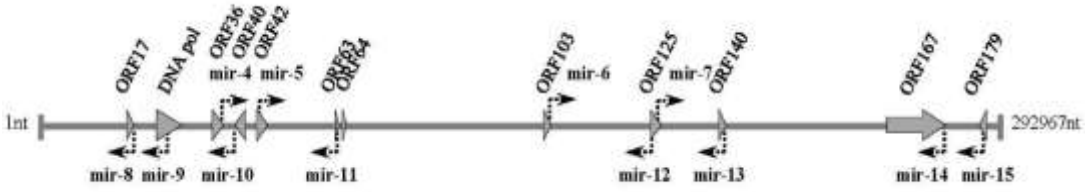

Fig. 3 A schematic diagram of the locations of the candidate WSSV-encoded miRNAs on WSSV genome (GenBank accession number: AF369029). ORFs of WSSV and candidate miRNAs are represented as big and small arrows with the transcriptional direction, respectively.

Validation of the candidate WSSV-encoded miRNAs expression

To verify whether the candidate miRNAs were specifically expressed in WSSV-infected tissue, stem loop RT-PCR technique was performed. Total RNA samples that were used to construct the small RNA libraries were employed as templates. The results showed that most of candidate wsv-miRs can be detected only from WSSV-infected tissue, except for wsv-miR-7-5p, -7-3p, -8 and -11. MicroRNA let-7 which was used as a positive control was found in all samples (Fig. 4).

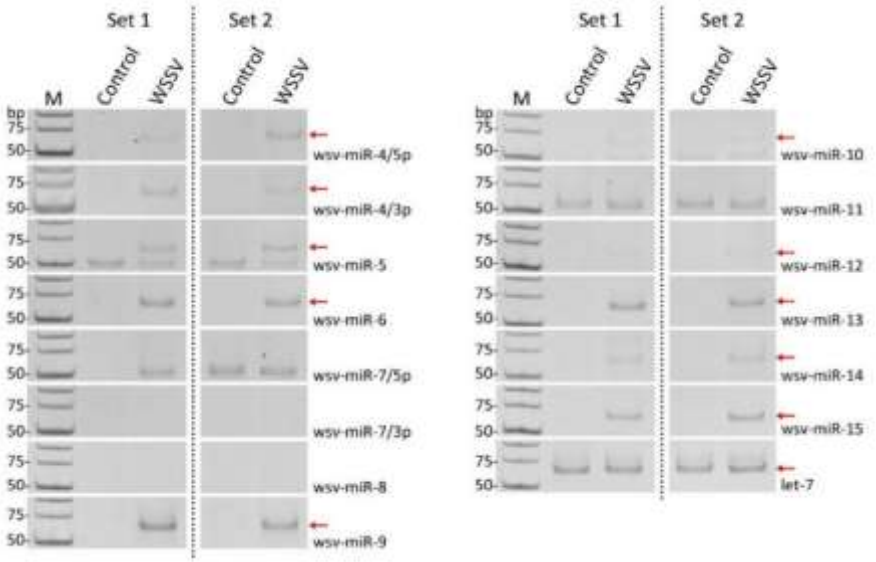

Fig. 4 Validation of the 14 candidate WSSV-encoded miRNAs by stem loop RT-PCR. The sample that was used to construct the small RNAs libraries (set 1) was compared to the other sample set (set 2). The expressed miRNAs was about 62 bp (red arrow). M is ultra low range DNA ladder.

Profiling of wsv-miRNA expressions depend on time course of WSSV infection

To investigate the expression profiles of wsv-miRs, the expression levels of wsv-miRs from control and WSSV-infected shrimp at several time points were determined by stem loop RT-PCR. Six wsv-miRs (wsv-miR-4-3p, -6, -9, -13, -14 and -15) were found to be expressed at different levels and were up-regulated depending on the time course of WSSV infection. Expressions of most wsv-miRs were increased after 9

or 18 hpi and were slightly decreased at 48 hpi. MicroRNA let-7 expression in all samples was relatively constant. Interestingly, expression of vp28 gene of WSSV can be detected at 6 hpi. A representative gel from three sets of experiments is shown in Fig. 5 with the expression level of vp28 (blue bars). After normalization the expression level of individual candidate miRNA with let-7, wsv-miR-9 showed the highest expression level among all candidate miRNAs, followed by wsv-miR-13 and -15.

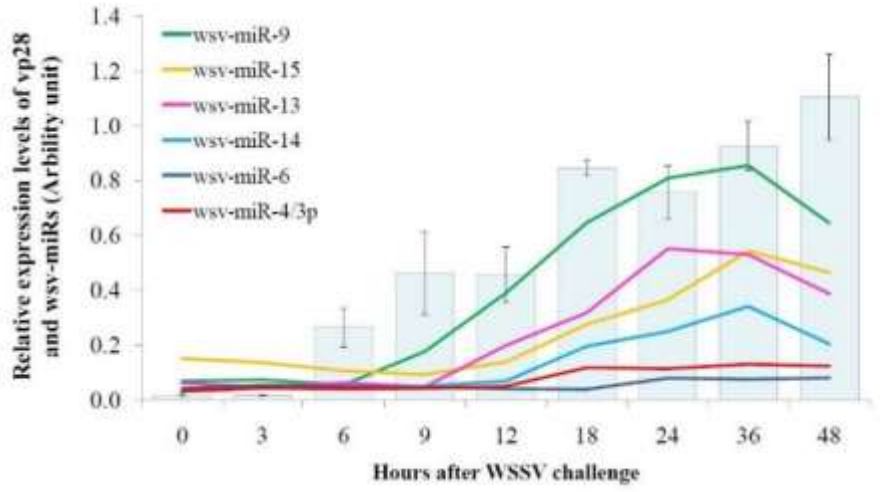

Fig. 5 Expression profiles of wsv-miRs at each time point of WSSV-infection. Viral-free shrimp is marked at 0 h. Semi-quantitative expression of 6 wsv-miRs (color lines) and vp28 (blue bats) that normalized with miRNA let-7 and actin, respectively. The result was shown as means from 3 shrimp at each time point.

Computational prediction of miRNA targets

Potential targets screening was performed using miRanda software. EST database of *P. monodon* was used for cellular target prediction. After blast search, cellular targets were identified and were classified into innate-immune related genes, transporter proteins, proteins involved in translation, and structural proteins (Table 3). The wsv-miR-10 and -13 were predicted to target to just one mRNA which was hemocyanin (HcVn) and *F. chinensis* double WAP domain-containing protein, respectively. Some wsv-miRNAs (miR-4-3p, -5, -6, -14 and -15) were predicted to recognize several mRNA targets for example; wsv-miR-6 predicted to recognize either anti-lipopolysaccharide factor or cyclophilin. Cellular genes such as anti-lipopolysaccharide factor and elongation factor-1 alpha of *P. monodon* may be recognized by multiple miRNAs. For example; elongation factor-1 alpha of *P. monodon* may be the candidate targets of wsv-miR-5, -14, and -15. For viral genes (Table 4), potential targets were distributed on the viral genome encoding either non-structural (helicase, ribonucleotide reductase large subunit (RR1)) or structural proteins (such asVP53a, VP664).

Table 3 The cellular targets of wsv-miRNAs as predicted by miRanda version 1.0 program with seed match.

Gene name	Candidate miRNAs
Innate-immune related	
P. monodon hemocyanin (HcVn) mRNA	4-3p, 5, 10
P. monodon anti-lipopolysaccharide factor	6, 15
P. monodon masquerade-like serine proteinase-like protein 3	5
F. chinensis double WAP domain-containing protein	4-3p, 13, 14
Transporter proteins	
P. monodon putative ligand-gated ion channel-like protein	15
P. monodon NADH dehydrogenase subunit F-like protein	15
Protein translation	
P. monodon elongation factor-1 alpha	5, 14, 15
L. vannamei ribosomal protein L8	5
Structural and other proteins	
P. monodon cathepsin D	15
F. paulensis cyclophilin	6

Table 4 The viral target of wsv-miRNAs as predicted by miRanda version 1.0 program with seed match.

wsv-miRs	Potential viral target genes
wsv-miR-4-5p	ORF105, ORF110, ORF154 VP53a, VP15, VP57, VP664, VP544, VP136b ICP11
wsv-miR-4-3p	ORF89, ORF135, ORF142 (Mj. homolog), ORF169, ORF14, ORF38 VP53a, VP300, VP664 TK-TMK, Helicase
wsv-miR-5	ORF18, ORF19, ORF42, ORF43, ORF56, ORF89, ORF96, ORF121, ORF122, ORF125, ORF12, ORF14, ORF25, ORF38, ORF53, ORF82, ORF83, ORF104, ORF108 VP357, VP507, VP387, VP53c P-collagen, CBP, STF[a], class1 cytokine receptor, Helicase, dUTPase, RR1 repeat4
wsv-miR-6	ORF5, ORF73, ORF89, ORF97, ORF47 VP53a, VP320, VP544 STK
wsv-miR-9	ORF121
wsv-miR-10	ORF4, ORF43, ORF63, ORF65, ORF97, ORF122, ORF123, ORF138, ORF67, ORF82, ORF154 VP53B, VP664 P-collagen, E3[b], AAP-1, STK repeat4, repeat8, repeat7
wsv-miR-12	ORF37, ORF90

wsv-miRs	Potential viral target genes
wsv-miR-4-5p	ORF105, ORF110, ORF154 VP53a, VP15, VP57, VP664, VP544, VP136b ICP11
wsv-miR-4-3p	ORF89, ORF135, ORF142 (Mj. homolog), ORF169, ORF14, ORF38 VP53a, VP300, VP664 TK-TMK, Helicase
wsv-miR-5	ORF18, ORF19, ORF42, ORF43, ORF56, ORF89, ORF96, ORF121, ORF122, ORF125, ORF12, ORF14, ORF25, ORF38, ORF53, ORF82, ORF83, ORF104, ORF108 VP357, VP507, VP387, VP53c P-collagen, CBP, STF[a], class1 cytokine receptor, Helicase, dUTPase, RR1 repeat4
wsv-miR-6	ORF5, ORF73, ORF89, ORF97, ORF47 VP53a, VP320, VP544 STK
wsv-miR-9	ORF121
wsv-miR-10	ORF4, ORF43, ORF63, ORF65, ORF97, ORF122, ORF123, ORF138, ORF67, ORF82, ORF154 VP53B, VP664 P-collagen, E3[b], AAP-1, STK repeat4, repeat8, repeat7
wsv-miR-12	ORF37, ORF90 VP664
wsv-miR-13	ORF55, ORF3, ORF33, ORF116, ORF159, ORF166 VP38a, VP136b TK-TMK, RR1
wsv-miR-14	ORF4, ORF17, ORF19, ORF49, ORF175, ORF33, ORF111, ORF179 VP53a, VP51a, VP664, VP26 class1 cytokine receptor, RR1
wsv-miR-15	ORF26, ORF136, ORF85, ORF154 VP216, VP136b PK1

TK-TMK: Chimeric Thymidine/Thymidylate kinase, CBP: CREB-binding protein, STF: SOX-transcription factor, RR1: Ribonucleotide reductase I, STK: Putative Serine/ Threonine protein kinase, E3: E3 ubiquitin ligase, AAP-1: Anti-poptosis protein 1, PK1: Protein kinase 1

[a](Li et al., 2007), [b](He et al., 2006)

See footnote in (Marks, 2005)

Discussion

Several miRNAs were identified from various organisms and they were conserved in metazoans, including in aquatic invertebrates such as *M. japonicus* (Huang, Xu, and Zhang, 2012; Ruan et al., 2011), *P. monodon* (Kaewkascholkul et al., 2016), *L. vannamei* (Sun et al., 2016) and *F. chinensis* (Li et al., 2017). After viral-encoded miRNAs were first found in the Epstein-Barr virus (EBV) (Pfeffer et al., 2004), a number of viral-encoded miRNAs were usually identified from other DNA and some RNA viruses (Klase, Sampey, and Kashanchi, 2013). Here, NGS and small RNAs cloning were used to identify WSSV-encoded miRNAs in *P. monodon*. Fourteen candidate viral-encoded miRNAs were predicted to derive from 12 precursors which spontaneously form hairpin structure (MEF <-20 kcal/mol) (Fu et al., 2011). Using stem loop RT-PCR approach, 10 candidate wsv-miRs were validated. However, some of them could not be detected by non-radioactive northern blotting (data not shown). This might be due to the very low expression level of some wsv-miRs which might be *below* the *detection limit* of this method. This was not unexpected as other studies also failed to detect viral encoded miRNAs such as HSV-1-5p and MuHV-M1-1, by northern blot (Diebel et al., 2010; Tang et al., 2008)

Different from the eukaryote, the viral-derived miRNAs are less conserved in sequence except the closely related viruses such as HSV-1 and HSV-2 that showed high similarity of miRNAs (Umbach and Cullen, 2009). Novel candidate miRNAs in this study do not appear to share high sequence homology against viral miRNAs in miRNA database. In addition, the number and sequence of our wsv-miRNAs were different from the 101 previously identified WSSV-miRNAs from WSSV-Cn (Huang, Cui, and Zhang, 2014; Liu et al., 2016). This may be because of distinction of viral isolate, stage of WSSV infection, shrimp tissues and methods to identify miRNAs. However, the stem loops of pre-miRNAs in this study were conserved among of the four WSSV isolates. WSSV-Th genome sequence differs from that of WSSV-Cn isolate. WSSV-Th has a big deletion of 12 kb (Marks et al., 2004). Two WSSV-Cn miRNAs from the study of He and Zhang, WSSV-miR197 or -miR 201 located in the deleted region of WSSV-Th therefore these miRNAs could not be identified in this study. This result suggested that either WSSV-miR197 or -miR201 are not necessary for WSSV-Th. Moreover, one of our wsv-miRs, wsv-miR-5 showed sequence overlaps with WSSV-miR12 of the previous study (He and Zhang, 2012). The location of WSSV-miR12 embedded in the precursor of wsv-miR-5, suggesting that they might conserve in the genomic location similar to the miR-1 of some members in polyomavirus family; SV-40, JCV and BKV (Lagatie, Tritsmans, and Stuyver, 2013). This study identified wsv-miRs from the gill tissue in the late stage of WSSV infection at 48 h whereas most of the previously identified WSSV-encoded miRNAs from other study appeared to detect in the early stage of WSSV infection (He and Zhang, 2012). Furthermore, the tissue distribution of wsv-miRs expression was different (Liu et al., 2016).

WSSV miRNA expression profile showed that 6 wsv-miRs increased upon viral infection at 9-18 h after vp28, a viral late gene, expression, suggesting that these wsv-miRs might function at late stage of viral infection. The viral-encoded miRNA that controls late stage or lytic life cycle of virus is usually up-regulated after late protein expression (Tang, Patel, and Krause, 2009). For example, HvAv encoded miR-1 form a major capsid protein (MCP) gene whose expression was increased during the late stage of HvAv infection and targeted to its own DNA polymerase I mRNA, resulting

in the inhibition of viral replication (Hussain, Taft, and Asgari, 2008). Among wsv-miRs, the expression level of wsv-miR-9 was highest, followed by wsv-miR-13 and -15, when compared to other wsv-miRs at the identical time. MicroRNA-mediated translational inhibition requires an imperfect binding between miRNA and their target at the ratio of at least 1:1 (tenOever, 2013). Therefore, high expression levels of wsv-miRs refered to the abundance of the mRNA target or virus attempted to quickly depress the mRNA target. The decreased wsv-miRs expression at 48 h might be caused by WSSV infection. WSSV can induce apoptosis which can be observed by TUNEL techniques after 24 hpi in haematopoietic and gill tissue (Wongprasert et al., 2003).

The potential cellular and viral gene targets were screened by computational prediction. As the complete genome sequence shrimp is not available, this study picked up potential cellular targets from EST of *P. monodon*. Some potential target genes, such as NADH dehydrogenase and elongation factor 1 have been shown to be down-regulated during WSSV-challenged (Wongpanya et al., 2007; Wu et al., 2007). This study used the WSSV genome sequence instead of the WSSV 3'UTR (Huang, Xu, and Zhang, 2012) for viral target prediction because some viral mRNAs have an initial ribosome entry site (IRES) and share a poly-A tail (Han and Zhang, 2006; Kang et al., 2009; Kang et al., 2013); and more importantly most of the 3'UTRs are shorter than 10 nt. Wsv-miRs could target many non-structural genes such as DNA polymerase, anti-apoptosis protein 1 and dUTPase, suggesting that WSSV might use wsv-miRs to control its expression through various mechanisms such as transcription, apoptosis and signaling pathway. Some targets may be recognized by multiple miRNAs, such as the elongation factor-1 alpha and hemocyanin of *P.monodon* or the DNA polymerase and VP664 gene of WSSV. This event was demonstrated by Kaposi sarcoma-associated herpesvirus (KSHV)-encoded multiple miRNAs targeting to THBS1 or MAF mRNA (Hansen et al., 2010; Samols et al., 2007). In contrast, the result showed some candidate targets such as wsv-miR-4-3p that recognized *P. monodon* hemocyanin and VP35a. Similarly, WSSV-miR-66, miR-68 (He, Yang, and Zhang, 2014) and miR-32 (He, Ma, and Zhang, 2017) each of which bound to two WSSV mRNAs. In addition, this was also demonstrated in *M. japonicus* that encoded *Mj*-miR-12 (Shu and Zhang, 2017) and miR-965 (Shu, Li, and Zhang, 2016) to control both shrimp and WSSV gene for down regulation of the virus. Furthermore, wsv-miRs were targeted to WSSV-related sequences such as helicase and putative serine/threonine protein kinase (Huang et al., 2011), suggesting that this wsv-miRs might be switch to target either virus or host gene.

Accumulation of wsv-miRNAs in this study and other study resulted that WSSV is a virus containing the highest miRNA number when compared to other viruses in the miRBase database. The results showed wsv-miRNAs that expressed in the late stage of WSSV infection could crosstalk control between host and viral itself. Identification of wsv-miRs and their targets combines with the shrimp's miRNAs that have been reported will reveal the complexity of miRNA-mediated WSSV-host interaction. This knowledge will provide insights into the understanding of WSSV-host interaction and pathogenesis and possibly could be applied to find the effective approaches to control the WSSV infection in shrimp.

References

1. Bartel, D. P. (2004). MicroRNAs: Genomics, Biogenesis, Mechanism, and Function. Cell 116(2), 281-297.

2. Chai, C. Y., Yoon, J., Lee, Y. S., Kim, Y. B., and Choi, T.-J. (2013). Analysis of the complete nucleotide sequence of a white spot syndrome virus isolated from pacific white shrimp. Journal of Microbiology 51(5), 695-699.
3. Chen, C., Ridzon, D. A., Broomer, A. J., Zhou, Z., Lee, D. H., Nguyen, J. T., Barbisin, M., Xu, N. L., Mahuvakar, V. R., Andersen, M. R., Lao, K. Q., Livak, K. J., and Guegler, K. J. (2005). Real-time quantification of microRNAs by stem–loop RT–PCR. Nucleic Acids Research 33(20), e179.
4. Choy, E. Y.-W., Siu, K.-L., Kok, K.-H., Lung, R. W.-M., Tsang, C. M., To, K.-F., Kwong, D. L.-W., Tsao, S. W., and Jin, D.-Y. (2008). An Epstein-Barr virus–encoded microRNA targets PUMA to promote host cell survival. The Journal of Experimental Medicine 205(11), 2551-2560.
5. Denli, A. M., B. B. J. Tops, et al. (2004). "Processing of primary microRNAs by the Microprocessor complex." Nature 432(7014): 231-235.
6. Dong, H., J. Lei, et al. (2013). "MicroRNA: Function, Detection, and Bioanalysis." Chemical Reviews 113(8): 6207-6233.
7. Gregory, R. I., K.-p. Yan, et al. (2004). "The Microprocessor complex mediates the genesis of microRNAs." Nature 432(7014): 235-240.
8. Fu, Y., Shi, Z., Wu, M., Zhang, J., Jia, L., and Chen, X. (2011). Identification and Differential Expression of MicroRNAs during Metamorphosis of the Japanese Flounder (*Paralichthys olivaceus*). PLoS ONE 6(7), e22957.
9. Grundhoff, A., and Sullivan, C. S. (2011). Virus-encoded microRNAs. Virology 411(2), 325-343.
10. Han, F., and Zhang, X. (2006). Internal initiation of mRNA translation in insect cell mediated by an internal ribosome entry site (IRES) from shrimp white spot syndrome virus (WSSV). Biochemical and Biophysical Research Communications 344(3), 893-899.
11. Hansen, A., Henderson, S., Lagos, D., Nikitenko, L., Coulter, E., Roberts, S., Gratrix, F., Plaisance, K., Renne, R., Bower, M., Kellam, P., and Boshoff, C. (2010). KSHV-encoded miRNAs target MAF to induce endothelial cell reprogramming. Genes Dev 24(2), 195-205.
12. He, Y., Ma, T., and Zhang, X. (2017). The Mechanism of Synchronous Precise Regulation of Two Shrimp White Spot Syndrome Virus Targets by a Viral MicroRNA. Frontiers in Immunology 8(1546).
13. He, Y., Yang, K., and Zhang, X. (2014). Viral microRNAs targeting virus genes promote virus infection in shrimp *in vivo*. J Virol 88(2), 1104-12.
14. He, Y., and Zhang, X. (2012). Comprehensive characterization of viral miRNAs involved in white spot syndrome virus (WSSV) infection. RNA Biol 9(7), 1019-1029.
15. Huang, S.-W., Lin, Y.-Y., You, E.-M., Liu, T.-T., Shu, H.-Y., Wu, K.-M., Tsai, S.-F., Lo, C.-F., Kou, G.-H., Ma, G.-C., Chen, M., Wu, D., Aoki, T., Hirono, I., and Yu, H.-T. (2011). Fosmid library end sequencing reveals a rarely known genome structure of marine shrimp *Penaeus monodon*. BMC Genomics 12(1), 242.
16. Huang, T., Cui, Y., and Zhang, X. (2014). Involvement of viral microRNA in the regulation of antiviral apoptosis in shrimp. J Virol 88(5), 2544-54.
17. Huang, T., Xu, D., and Zhang, X. (2012). Characterization of host microRNAs that respond to DNA virus infection in a crustacean. BMC Genomics 13(1), 159.
18. Hussain, M., Taft, R. J., and Asgari, S. (2008). An insect virus-encoded microRNA regulates viral replication. Journal of Virology 82(18), 9164-9170.

19. Jehle, J. A., Blissard, G. W., Bonning, B. C., Cory, J. S., Herniou, E. A., Rohrmann, G. F., Theilmann, D. A., Thiem, S. M., and Vlak, J. M. (2006). On the classification and nomenclature of baculoviruses: A proposal for revision. Archives of Virology 151(7), 1257-1266.
20. Jurak, I., Kramer, M. F., Mellor, J. C., van Lint, A. L., Roth, F. P., Knipe, D. M., and Coen, D. M. (2010). Numerous conserved and divergent microRNAs expressed by Herpes simplex viruses 1 and 2. Journal of Virology 84(9), 4659-4672.
21. Kaewkascholkul, N., Somboonviwat, K., Asakawa, S., Hirono, I., Tassanakajon, A., and Somboonwiwat, K. (2016). Shrimp miRNAs regulate innate immune response against white spot syndrome virus infection. Developmental & Comparative Immunology 60, 191-201.
22. Kang, S.-T., Leu, J.-H., Wang, H.-C., Chen, L.-L., Kou, G.-H., and Lo, C.-F. (2009). Polycistronic mRNAs and internal ribosome entry site elements (IRES) are widely used by White spot syndrome virus (WSSV) structural protein genes. Virology 387(2), 353-363.
23. Kang, S.-T., Wang, H.-C., Yang, Y.-T., Kou, G.-H., and Lo, C.-F. (2013). The DNA virus WSSV uses an internal ribosome entry site (IRES) for translation of the highly expressed non-structural protein ICP35. Journal of Virology.
24. Khawsak, P., Deesukon, W., Chaivisuthangkura, P., and Sukhumsirichart, W. (2008). Multiplex RT-PCR assay for simultaneous detection of six viruses of penaeid shrimp. Molecular and Cellular Probes 22(3), 177-183.
25. Khvorova, A., A. Reynolds, et al. (2003). "Functional siRNAs and miRNAs exhibit strand bias." Cell 115(2): 209 - 216.
26. Kim, V. N., Han, J., and Siomi, M. C. (2009). Biogenesis of small RNAs in animals. Nat Rev Mol Cell Biol 10(2), 126-139.
27. Kozomara, A. and S. Griffiths-Jones (2014). "miRBase: annotating high confidence microRNAs using deep sequencing data." Nucleic Acids Research 42(D1): D68-D73.
28. Klase, Z. A., Sampey, G. C., and Kashanchi, F. (2013). Retrovirus infected cells contain viral microRNAs. Retrovirology 10(1), 15.
29. Kozomara, A., and Griffiths-Jones, S. (2014). miRBase: annotating high confidence microRNAs using deep sequencing data. Nucleic Acids Research 42(D1), D68-D73.
30. Lagatie, O., Tritsmans, L., and Stuyver, L. J. (2013). The miRNA world of polyomaviruses. Virology Journal 10(1), 268.
31. Li, X., Meng, X., Luo, K., Luan, S., Shi, X., Cao, B., and Kong, J. (2017). The identification of microRNAs involved in the response of Chinese shrimp *Fenneropenaeus chinensis* to white spot syndrome virus infection. Fish & Shellfish Immunology 68, 220-231.
32. Liu, C., Li, F., Sun, Y., Zhang, X., Yuan, J., Yang, H., and Xiang, J. (2016). Virus-derived small RNAs in the penaeid shrimp *Fenneropenaeus chinensis* during acute infection of the DNA virus WSSV. Scientific Reports 6, 28678.
33. Marks, H., Goldbach, R. W., Vlak, J. M., and van Hulten, M. C. W. (2004). Genetic variation among isolates of white spot syndrome virus. Archives of Virology 149(4), 673-697.
34. Natividad, K. D. T., Hagio, M., Tanaka, M., Nomura, N., and Matsumura, M. (2007). White spot syndrome virus (WSSV) inactivation in *Penaeus japonicus*

using purified monoclonal antibody targeting viral envelope protein. Aquaculture 269(1–4), 54-62.
35. Park, J.-E., I. Heo, et al. (2011). "Dicer recognizes the 5' end of RNA for efficient and accurate processing." Nature 475(7355): 201-205.
36. Pasquinelli, A. E. (2012). MicroRNAs and their targets: recognition, regulation and an emerging reciprocal relationship. Nat Rev Genet 13(4), 271-282.
37. Pfeffer, S., Zavolan, M., Grässer, F. A., Chien, M., Russo, J. J., Ju, J., John, B., Enright, A. J., Marks, D., Sander, C., and Tuschl, T. (2004). Identification of virus-encoded microRNAs. Science 304(5671), 734-736.
38. Ruan, L., Bian, X., Ji, Y., Li, M., Li, F., and Yan, X. (2011). Isolation and identification of novel microRNAs from *Marsupenaeus japonicus*. *Fish &* Shellfish Immunology 31(2), 334-340.
39. Saito, K., A. Ishizuka, et al. (2005). "Processing of pre-microRNAs by the Dicer-1–Loquacious complex in *Drosophila* cells." PLoS Biol 3(7): e235.
40. Samols, M. A., Skalsky, R. L., Maldonado, A. M., Riva, A., Lopez, M. C., Baker, H. V., and Renne, R. (2007). Identification of cellular genes targeted by KSHV-encoded microRNAs. PLoS Pathog 3(5), e65.
41. Sánchez-Paz, A. (2010). White spot syndrome virus: an overview on an emergent concern. Veterinary Research 41(6), 43.
42. Shu, L., Li, C., and Zhang, X. (2016). The role of shrimp miR-965 in virus infection. Fish & Shellfish Immunology 54, 427-434.
43. Shu, L., and Zhang, X. (2017). Shrimp miR-12 Suppresses White Spot Syndrome Virus Infection by Synchronously Triggering Antiviral Phagocytosis and Apoptosis Pathways. Frontiers in Immunology 8, 855.
44. Sritunyalucksana, K., Srisala, J., McColl, K., Nielsen, L., and Flegel, T. W. (2006). Comparison of PCR testing methods for white spot syndrome virus (WSSV) infections in penaeid shrimp. Aquaculture 255(1–4), 95-104.
45. Sullivan, C. S., Grundhoff, A. T., Tevethia, S., Pipas, J. M., and Ganem, D. (2005). SV40-encoded microRNAs regulate viral gene expression and reduce susceptibility to cytotoxic T cells. Nature 435(7042), 682-686.
46. Sun, X., Liu, Q.-h., Yang, B., and Huang, J. (2016). Differential expression of microRNAs of *Litopenaeus vannamei* in response to different virulence WSSV infection. Fish & Shellfish Immunology 58, 18-23.
47. Tang, S., Patel, A., and Krause, P. R. (2009). Novel less-abundant viral microRNAs encoded by Herpes Simplex Virus 2 latency-associated transcript and their roles in regulating ICP34.5 and ICP0 mRNAs. Journal of Virology 83(3), 1433-1442.
48. tenOever, B. R. (2013). RNA viruses and the host microRNA machinery. Nat Rev Micro 11(3), 169-180.
49. Umbach, J. L., and Cullen, B. R. (2009). The role of RNAi and microRNAs in animal virus replication and antiviral immunity. Genes & Development 23(10), 1151-1164.
50. Umbach, J. L., Kramer, M. F., Jurak, I., Karnowski, H. W., Coen, D. M., and Cullen, B. R. (2008). MicroRNAs expressed by herpes simplex virus 1 during latent infection regulate viral mRNAs. Nature 454(7205), 780-783.

51. Varkonyi-Gasic, E., and Hellens, R. (2010). qRT-PCR of Small RNAs. *In* "Plant Epigenetics: Methods in Molecular Biology", Vol. 631, pp. 109-122. Humana Press.
52. Wongpanya, R., Aoki, T., Hirono, I., Yasuike, M., and Tassanakajon, A. (2007). Analysis of gene expression in haemocytes of shrimp *Penaeus monodon* challenged with white spot syndrome virus by cDNA microarray. *ScienceAsia* 33, 161-164.
53. Wongprasert, K., Khanobdee, K., Glunukarn, S. S., Meeratana, P., and Withyachumnarnkul, B. (2003). Time-course and levels of apoptosis in various tissues of black tiger shrimp *Penaeus monodon* infected with white-spot syndrome virus. Diseases of Aquatic Organisms 55(1), 3-10.
54. Wu, J., Lin, Q., Lim, T. K., Liu, T., and Hew, C.-L. (2007). White spot syndrome virus proteins and differentially expressed host proteins identified in shrimp epithelium by shotgun proteomics and cleavable isotope-coded affinity tag. Journal of Virology 81(21), 11681-11689.

Suppression of Argonautes compromises viral infection in *Penaeus monodon*

Argonaute (Ago) proteins, the catalytic component of an RNA-induced silencing complex (RISC) in RNA interference pathway, contain diverse functions and play potent roles in antiviral defense and transposon regulation. So far, cDNAs encoding at least four members of Argonaute were found in *Penaeus monodon* (*PmAgo1-4*). Two isoforms of PmAgo protein, PmAgo1 and PmAgo3 shared high percentage of amino acid identity to Ago1 and Ago2, respectively in other Penaeid shrimps. Therefore, the possible roles of *PmAgo1* and *PmAgo3* in shrimp antiviral immunity were characterized in this study. The level of *PmAgo1* mRNA expression in shrimp hemolymph was stimulated upon YHV challenge, but not with dsRNA administration. Interestingly, silencing of either PmAgo1 or *PmAgo3* using sequence-specific dsRNAs impaired the efficiency of *PmRab7*-dsRNA to knockdown shrimp endogenous *PmRab7* expression. Inhibition of yellow head virus (YHV) replication and delayed mortality rate were also observed in both *PmAgo1*- and *PmAgo3*-knockdown shrimp. In addition, silencing of *PmAgo3* transcript, but not *PmAgo1*, revealed partial inhibition of white spot syndrome virus (WSSV) infection and delayed mortality rate. Therefore, our study provides insights of PmAgo1and *PmAgo3* functions that are involved in a dsRNA-mediated gene silencing pathway and play roles in YHV and WSSV replication in the shrimp.

Introduction

Multiple innate defenses including cellular and humoral immune reactions and RNA interference (RNAi) of invertebrates were wildly known as host defense mechanisms against microbial infection. In shrimp, discoveries of several molecules related to both cellular (encapsulation, coagulation, and melanization) and humoral (Toll, Immune deficiency (IMD) and JAK/STAT pathway) immune reactions reveal the existence of innate immune activities to fight against invading pathogens (1,2). In addition, RNAi is also known as one of the potent antiviral immunities in many organisms such as mammals, plants, insects and shrimp (3,4,5). The RNAi pathway is triggered by different classes of small regulatory RNAs originating from either endogenous transcripts or exogenous dsRNAs such as small interfering RNA (siRNA), microRNA (miRNA) and piwi-interacting RNA (piRNA). These small RNAs serve as guide sequences to direct the formation of an RNA-induced silencing complex (RISC), which contains an Argonaute (Ago) family protein as the catalytic core, to regulate viral replication by specific cleavage of the corresponding viral mRNA or translation inhibition (6).

Regarding structural features, four domains are identified in a bilobate architecture of Ago proteins; one lobe with N and PAZ domains and the other lobe with MID and PIWI domains. Based on crystal structure analysis, the N domain takes part in unwinding of small RNA duplex (7), and a specific binding pocket on the PAZ domain binds to the 3' end of small RNA duplex (8,9). The 5' phosphate of small RNAs is held onto the Ago protein by the MID domain (10,11), while a catalytic motif Asp-Asp-His (DDH) in the PIWI domain is responsible for the endonucleolytic activity (12,13).

Multiple members of the Argonaute proteins family exist in a wide range of organisms and are highly conserved among species. Ago proteins can be separated according to phylogenetic analysis into Ago and Piwi subfamilies (14-18). Members of

the Ago subfamily mediate post-transcriptional gene regulation by associating with either miRNA or siRNA. Piwi subfamily proteins are germ cell specific Argonautes associating with piRNAs, which behave as a small RNA-based immune system to safeguard genome integrity against transposon movement in germ cells and/or to control spermatogenesis and germ cell differentiation (19,20). In addition, another class of Argonaute proteins, a worm-specific Argonaute (WAGO), was exclusively found in the nematodes where they play a role in RNAi pathway to mediate a variety of cellular processes (18). Numbers of Argonaute genes are different among organisms, ranging from a single member in *Schizosaccharomyces pombe* to twenty-seven members in *Caenorhabditis elegans* (21). So far, Ago2 of Drosophila and human were demonstrated to possess slicer activity (22,23) and mediate antiviral defense via RNAi cleavage mechanism (24,25).

To date, at least two Ago subfamily members were identified and characterized in Penaeid shrimps. In *Litopenaues vannamei*, two Argonaute genes, *LvAgo1* and *LvAgo2* were identified; only *LvAgo2* was involved in siRNA mediated post-transcriptional gene silencing (26,27). Likewise, *MjAgo1* and *MjAgo2* were found in *Masupenaeus japonicus*. *MjAgo1* play important role in antiviral response in shrimp (28), while *MjAgo2* acts as a key protein in viral siRNA biogenesis and function (29). These studies suggest that Argonaute 2 proteins were essential for the functional siRNA-associated RISC and play a role in antiviral defense via siRNA-mediated viral mRNA degradation in the shrimp.

Interestingly, cDNAs encoding four types of the Ago subfamily proteins were reported in the black tiger shrimp, *Penaeus monodon* (*PmAgo1-4*). From phylogenetic analysis, PmAgo1 is clustered in the same group with *LvAgo1* and *MjAgo1*, and was demonstrated for its important function in effective RNAi pathway in the primary culture of lymphoid cells (30). *PmAgo3* was classified into the same group of Argonaute 2 proteins in penaeid shrimp i.e. *LvAgo2* and *MjAgo2*, and was shown to be involved in the pathway of dsRNA-mediated gene silencing (31). In addition, *PmAgo2* and *PmAgo4* were classified in the same cluster but located on a separate branch from *PmAgo3*. The expression of *PmAgo2* was responsive to both viral and bacterial infections, and was also activated upon dsRNA and ssRNA administration (32). All the members of *PmAgos*, except *PmAgo4* are expressed ubiquitously in all shrimp tissues. Interestingly, PmAgo4 displays a gonad-specific expression similar to that of the Piwi subfamily. The gonad-specific *PmAgo4* was suggested to be involved in the protection of shrimp genome integrity against transposons invasion (14). Although accumulating evidences have demonstrated that *PmAgos* could exhibit diversefunctions, no report has thus far indicated the actual function of Argonaute proteins for innate immunity in shrimp compared to model organisms such as *Drosophila*. In this study, we reported the possible involvement of *PmAgo1* and *PmAgo3*, homologs of DdmAgo1 and DmAgo2, respectively in the mechanism of dsRNA-mediated gene silencing. Moreover, the involvement of *PmAgo1* and *PmAgo3* in shrimp antiviral immunity was also characterized. Functional analysis of *PmAgo1* and *PmAgo3* in the RNAi mechanism for shrimp antiviral defense will provide a basis for further development of effective strategies to control viral diseases in the economically important Penaeid shrimp.

Materials and methods

Animals

Live adolescent black tiger shrimp (approximately 10-15 g body weight) were purchased from shrimp farms around the central area of Thailand. They were first screened for yellow head virus (YHV) and white spot syndrome virus (WSSV) infection by RT-PCR as previously described (33,34). The virus-free shrimps were used in all experiments. Shrimp were gradually acclimatized to the laboratory condition in 10 ppt (parts per thousand) sea water with aeration for 2 days. They were also fed with commercial shrimp feed (CP, Thailand) twice a day for a few days before setting the experiment.

Viral stock preparation

To obtain fresh viral stock of YHV and WSSV, crude viruses were injected into the healthy virus-free shrimps. After 48 h, haemolymph was drawn from moribund shrimp, and the viruses were then purified and determined for viral titer as described by Assavalapsakul et al. 2003 (35). Appropriate dilutions of the viral stock (100-fold and 10-fold for YHV and WSSV, respectively) that gave complete mortality within 3 days post infection (dpi) were freshly prepared before use.

Detection of gene transcripts by reverse transcription-polymerase chain reaction (RT-PCR)

Gills were dissected from individual shrimp and homogenized in TRI REAGENT® (Molecular Research Center), while hemolymph was collected and subsequently mixed with TRI- REAGENT®. Total RNA was isolated according to the manufacturer's protocol. The concentration and purity of the extracted total RNA was examined by Nanodrop® ND-1000 spectrophotometer (Nanodrop Technologies). First strand cDNA was reverse transcribed from 1-2 µg of total RNA priming with PRT-oligo-dT12 primer by Impromp-II™ reverse transcriptase (Promega) using the following condition: 25°C for 5 min, 42°C for 60 min, and 70°C for 15 min. The oligonucleotide sequence of PRT-oligo dT12 primer is shown in table 1.

One microliter of the first strand cDNA was used as a template to examine mRNA expression. Multiplex-PCR with two primer pairs was applied to determine the expression of the mRNA of interest and β-actin mRNA (internal control) simultaneously. The reaction contains the standard components according to *Tag* DNA polymerase's protocol (Thermo scientific). *PmAgo1* transcript was amplified with Ago- amp and 5'Ago-R1 primers using the following condition: 94°C for 5 min, 2 cycles of 94°C for 1 min, 60°C for 1 min, 72°C for 1 min and additional 30 cycles of 94°C for 1 min, 55°C for 1 min, 72°C for 1 min. The final extension was performed at 72°C for 7 min. Amplification of *PmAgo3*, *PmRab7*, YHV- helicase (YHV- Hel) and WSSV vp28 mRNAs were carried out with specific primer pairs and specific conditions as previously described (31, 36, 33, 34). In the experiment, two *β-actin* PCR products of either 550 bp or 350 bp were amplified with the same forward primers (Actin- F) and different reverse primers, Actin- R or Actin- R2, respectively. The oligonucleotide sequences of all primers are shown in table1.

Double-stranded RNA (dsRNA) production

The hair- pin dsRNA precursor was produced by in vivo bacterial expression system as described by Ongvarrasopone et al., 2007 (37). The recombinant plasmids

pET17b-st *PmAgo1* (previously construct in our laboratory), pET17b-st-*PmAgo3* (31) and pET17b-st PmRab7 (36) and pET3a-st-*GFP* (kindly provided by Asst. Prof. Witoon Tirasophon) harboring the cassette for producing hair-pin dsRNA of corresponding genes were used to transform ribonuclease III-deficient *Escherichia coli* strain HT115 (DE3). The expression of hair-pin dsRNAs were induced by 0.4 mM IPTG for 4 h with shaking. The hair-pin dsRNAs were extracted by ethanol extraction method (38) before dissolving in 150 mM NaCl. The concentration and purity of hair-pin dsRNAs were monitored by agarose gel electrophoresis and Nanodrop® ND-1000 spectrophotometer. The hair-pin dsRNAs were verified by RNase digestion assay as described previously (38).

Analysis of PmAgo1 expression in response to dsRNA or virus injection

Alteration in PmAgo1 transcripts level in shrimp hemolymph was investigated upon either dsRNA or viral injections. Shrimp, approximately 10 g body weight (b.w.) were injected with GFP-dsRNA at 2.5 μg.g^{-1} b.w. or challenged with 50 μl of the 10-2 dilution of YHV stock. After that, the haemolymph was collected from ten individual shrimp from each group at 0, 3, 6, 9, 12, 24, 36, 48 and 72 hour post injection (hpi) for determination of *PmAgo1* mRNA expression by RT-PCR. Multiplex amplification of *PmAgo1* and the internal control, *β-actin* transcripts was carried out by specific primers for each gene as described in 2.3, and the PCR products were subsequently analyzed by agarose gel electrophoresis. The Scion image analysis program was applied to quantify the band intensity of PmAgo1 PCR product normalized with that of β-actin, and presented as mean ± standard error of mean (SEM) as relative expression levels of *PmAgo1* (n=10). The significant difference of relative PmAgo1 expression level ($p < 0.05$) between each time point was analyzed by sample T-Test.

Investigation of the effect of PmAgo1 and PmAgo3 knockdown on the efficiency of RNAi.

P. monodon (approximately 10 g b.w.) were injected with *PmAgo1*- or *PmAgo3* dsRNA at 2.5 μg g-1 b.w. Either 150 mM NaCl or GFP-dsRNA was injected into shrimp as control groups. At 2 days-post injection, the haemolymph sample from shrimp in each group (n = 5) was collected to determine the expression levels of *PmAgo1* and *PmAgo3*. Subsequently, *PmRab7*-dsRNA was injected into *PmAgo* knocked-down shrimp at 0.63 μg g-1 b.w. to suppress *PmRab7* mRNA expression. Expression of *PmRab7* was determined by multiplex RT-PCR analysis as described in 2.3 at 0, 24, 48 and 72 h post *PmRab7*-dsRNA injection.

Biological assay for antiviral function of PmAgo1 and PmAgo3

Shrimps (approximately 10 g b.w.) were injected with 25 μg of *PmAgo1*-, *PmAgo3*- or GFP-dsRNA (5–10 shrimp per group). The haemolymph was collected at 48 h post dsRNA injection to determine the transcript levels of *PmAgo1* and *PmAgo3* as described in 2.3. The shrimp were subsequently injected with 50 μl of either the 100 fold diluted YHV or 10 fold diluted WSSV stock. Shrimps injected with 150 mM NaCl alone or NaCl following with viruses were used as negative and positive control groups, respectively. Multiplex RT PCR analysis of helicase gene of YHV (hel) or *Vp28* gene of WSSV was performed to determine viral mRNA expression relative to that of actin in the shrimp at 0, 36, and 48 h post viral injection. PCR detection of WSSV genome

was also performed to determine the level of WSSV genome. In addition, mortality of individual shrimp in each group was also recorded.

Results

Expression of Ago1 in P. monodon upon YHV and GFP-dsRNA administration

Because the two isoforms of *Ago1* in *P. monodon*, *PemAgo1* (30) and *PmAgo1* (39) contain the same coding sequences and cannot be differentiated by the RT-PCR detection, they were collectively referred to as *PmAgo1* in this study. In order to determine whether *PmAgo1* expression is correlated to its possible role in antiviral immunity and dsRNA mediated gene silencing as reported earlier, the expression of PmAgo1 in response to YHV injection or GFP-dsRNA in the hemolymph of shrimp at various time points was determined by multiplex RT-PCR. Successful YHV infection was confirmed at 72 hpi by the detection of YHV helicase gene expression in the hemolymph of individual shrimp. The result in Figure 1A revealed that the expression levels of PmAgo1 in YHV injected shrimp gradually increased from 0 hpi to the highest level of approximately 2-fold with significant difference ($p < 0.05$) at 9 hpi before continuously decreasing until 72 hpi. On the other hand, *PmAgo1* expression in shrimp hemolymph at every time point post GFP-dsRNA injection was rather constant throughout the course of the experiment (Figure 1B). These data demonstrated that *PmAgo1* expression was activated by YHV, but not by dsRNA administration.

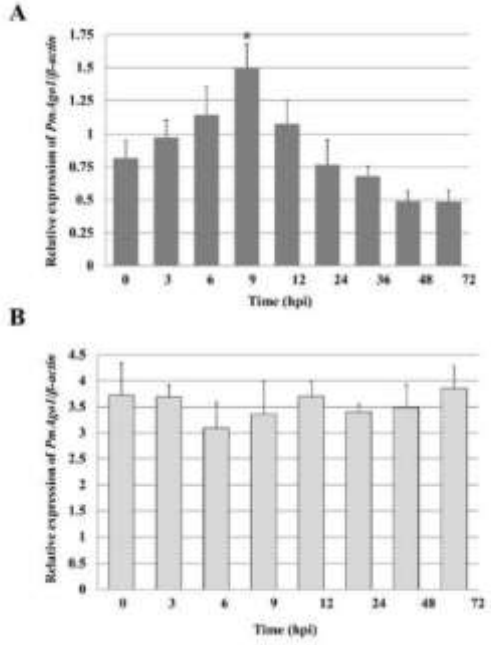

Fig. 1. *PmAgo1* expression in response to yellow head virus (YHV) and *GFP*-dsRNA administration

Multiplex RT-PCR was used to determine the expression of *PmAgo1* in the hemolymph of *P. monodon* at different time points after injected with either 50 µl of 100-fold dilution of purify YHV lysate (A; n=10) or *GFP*-dsRNA at 2.5 µg g-1 shrimp (B; n=5). The bar-graphs represent expression level of PmAgo1 normalized with that of *β-actin*. Each bar represents mean ± SEM. Asterisk indicates significant difference from 0 hpi ($p<0.05$).

Silencing of PmAgo1 and PmAgo3 by specific dsRNAs

To study the function of *PmAgo1* and *PmAgo3*, their expression was first suppressed by dsRNA-mediated gene silencing approach. The injection of *PmAgo1*-dsRNA significantly suppressed *PmAgo1* transcript level ($p < 0.05$) approximately 60% and 50% on day 2 and day 4 post-injection, respectively. More than 95% suppression of *PmAgo3* transcript was found in the hemolymph after one day post *PmAgo3*-dsRNA injection, and this level of suppression lasted for at least 3 days (Figure S1). Moreover, *PmAgo1*-dsRNA did not have effect on *PmAgo3* expression and vice versa (Figure 2A and 2B). Therefore, these dsRNAs were able to efficiently and specifically suppress *PmAgo1* and *PmAgo3* expression, and thus could be used for further functional analysis of both *PmAgos*.

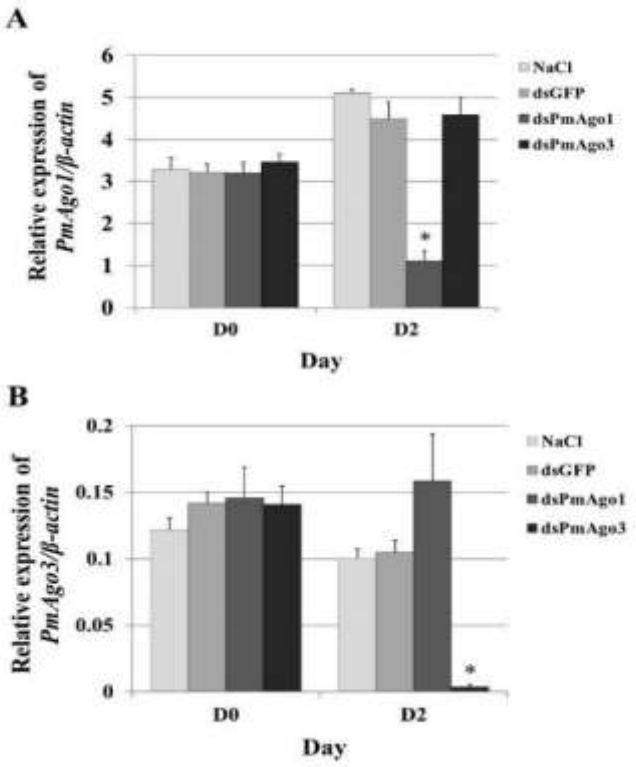

Fig. 2. Suppression of *PmAgo1* and *PmAgo3* transcript by dsRNA

P. monodon were injected with 2.5 µg g-1 shrimp b.w. of either *PmAgo1*-dsRNA or *PmAgo3*-dsRNA. The expression of *PmAgos* in the haemolymph was determined by multiplex RT-PCR at 2 days post-injection comparing with that in shrimp injected with NaCl and GFP-dsRNA as control groups. The levels of *PmAgo1*, *PmAgo3* transcript in the hemolymph of shrimp in each group were analyzed by agarose gel electrophoresis together with the internal control *β-actin* transcript. Numbers represent individual shrimp in each group. The histogram showing the relative expression of *PmAgo1* (A) and *PmAgo3* (B) normalized with that of *β-actin* as measured by Scion image analysis program. Each bar represents mean ± SEM (n=7). Asterisks (*) indicate the significant difference ($p<0.05$) between *PmAgo1*-dsRNA or PmAgo3-dsRNA injection groups and the control groups at each time point.

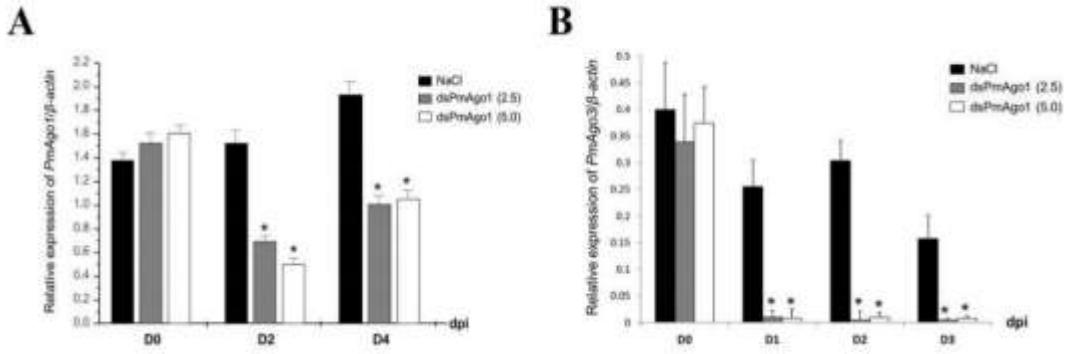

Fig. S1 Suppression of *PmAgo1* and *PmAgo3* transcript by dsRNA in the hemolymph of *P. monodon*

Shrimp were injected with 2.5 µg g-1 shrimp and 5 µg g-1 shrimp of *PmAgo1*-dsRNA (n=7) or *PmAgo3*-dsRNA (n=5). Shrimp injected with NaCl were used as a control group. The expression of *PmAgo1* in the hemolymph was determined by multiplex RT-PCR at 0, 2 and 4 days post injection, whereas *PmAgo3* expression was determined at 0, 1, 2 and 3 days post injection. The histogram showed the relative expression of *PmAgo1* and *PmAgo3* normalized with that of *β-actin* as measured by Scion image analysis program. Each bar represents mean ± SEM. Asterisks (*) indicate the significant difference ($p<0.05$) between PmAgo1-dsRNA or *PmAgo3*-dsRNA injected groups and the control group at each time point.

Efficiency of PmRab7 repression by PmRab7-dsRNA in PmAgo-knockdown shrimp

To investigate possible involvement of *PmAgo1* and *PmAgo3* in dsRNA-mediated RNAi pathway, the efficiency of *PmRab7*-dsRNA to repress shrimp endogenous *PmRab7* mRNA expression was studied in *PmAgo*-knockdown shrimp. The silencing of *PmAgo1* and *PmAgo3* expression in shrimp hemolymph was confirmed on day 2 after injected with corresponding dsRNAs compared with that in the control shrimp injected with NaCl or an unrelated *GFP*-dsRNA (Figure S2), whereas the expression of *PmRab7* among each group was not dramatically different (Figure 3; T0). Shrimp in each group were then injected with *PmRab7*-dsRNA, and *PmRab7* expression was determined at 24 h interval after *PmRab7* dsRNA injection. The result in Figure 3 showed the complete suppression of *PmRab7* mRNA expression in both control groups (NaCl or GFP-dsRNA injection followed by *PmRab7*-dsRNA) at 24, 48 and 72 h post *PmRab7*-dsRNA injection. Interestingly, the expression of *PmRab7* could be detected in *PmAgo1*- and *PmAgo3*-knockdown shrimp to a certain extent, but significantly different ($p < 0.05$) from the control shrimp, at all time-points from 24 to 72 h after injected with *PmRab7*-dsRNA indicating that dsRNA-mediated *PmRab7* suppression in *PmAgo*-knockdown shrimp was not as efficient as that in the control shrimp.

Effect of PmAgo1 and PmAgo3 knockdown on viral infection in shrimp

To investigate the function of *PmAgo1* and *PmAgo3* on virus infection, viral replication and shrimp mortality after YHV or WSSV challenge in *PmAgo*-knockdown shrimp were determined compared with that in the control groups (NaCl or GFP-dsRNA injcetion). The expression of *PmAgo1* and *PmAgo3* was knocked down by the injection of specific dsRNA two days before YHV challenge. The YHV-hel transcript could be

detected in the hemolymph of both control groups at 48 hours post-YHV injection (hpi), but not in the hemolymph of PmAgo1-knockdown shrimp (Figure 4A). In addition, the control shrimp that had been injected with NaCl or *GFP*- dsRNA prior to YHV challenge started to die after 84 hpi, and the cumulative mortality reached 100% at 108 hpi, whereas the mortality of *PmAgo1*- knockdown shrimp was observed after 120 h after YHV challenge and reached 100 % at 138 hpi (Figure 4B). Similarly, barely detectable level of YHV-hel and delayed cumulative mortality rate upon YHV challenge was also observed in *PmAgo3* knockdown shrimp when compared with the control groups (Figure 5A and 5B). The detection of YHV hel gene in gill tissue from all dead shrimp confirming that the shrimp were infected with the virus (Figure 4C and 5C).

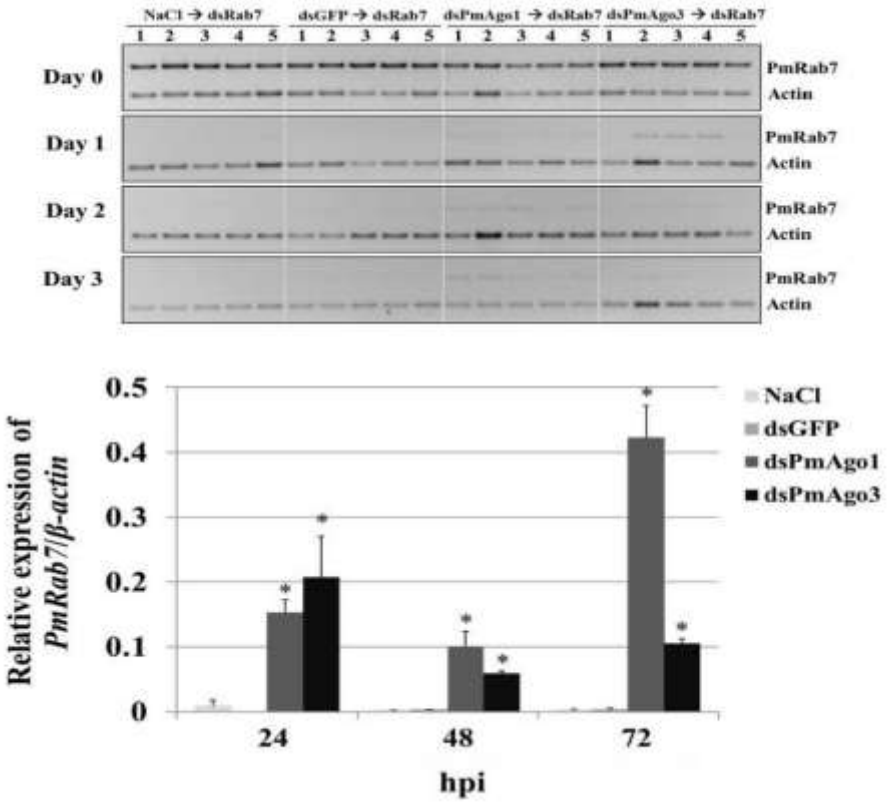

Fig. 3. Impairment of *PmRab7* silencing by *Rab7*-dsRNA in *PmAgo1* and *PmAgo3* knockdown shrimp

The *PmAgo1* and *PmAgo3* expression was suppressed by the injection of *PmAgo1*- or *PmAgo3*-dsRNA at 2.5 µg g-1 b.w., whereas NaCl and *GFP*-dsRNA injection were used as the control groups. Two days following the dsRNA injection, shrimp in each group were subsequently injected with *PmRab7*-dsRNA (0.6 µg g-1 shrimp b.w.), and the expression of *PmRab7* in the hemolymph was determined at 0, 24, 48 and 72 h post *PmRab7*-dsRNA injection (upper panel). *β-actin* was detected as an internal control. Numbers represent individual shrimp. The histogram showing the relative expression of *PmRab7* normalized with that of *β-actin* as measured by Scion image analysis program. Each bar represents mean ± SEM (n=5). Asterisks (*) indicate the significant difference ($p<0.05$) between PmAgo1 dsRNA or *PmAgo3*-dsRNA injection groups and the control groups at each time point.

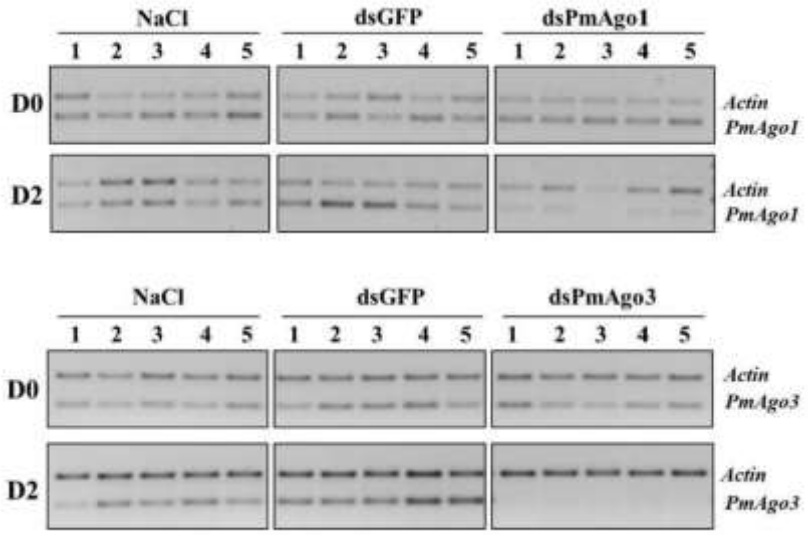

Fig. S2 Verification of *PmAgo1* and *PmAgo3* knockdown by dsRNA prior to *PmRab7* dsRNA injection

The expression of *PmAgo1* (upper panel) and *PmAgo3* (lower panel) in the hemolymph of *P. monodon* at 0 and 2 days after injected with *PmAgo1*- or *PmAgo3*-dsRNA at 2.5 µg g-1 was detected by multiplex RT-PCR compared with that in the control groups injected with either NaCl or *GFP*- dsRNA. The shrimp were subsequently injected with *PmRab7*-dsRNA (0.6 µg g-1 shrimp) to determine the effect of *PmAgo1* and *PmAgo3* knockdown on *PmRab7* suppression by *PmRab7*-dsRNA

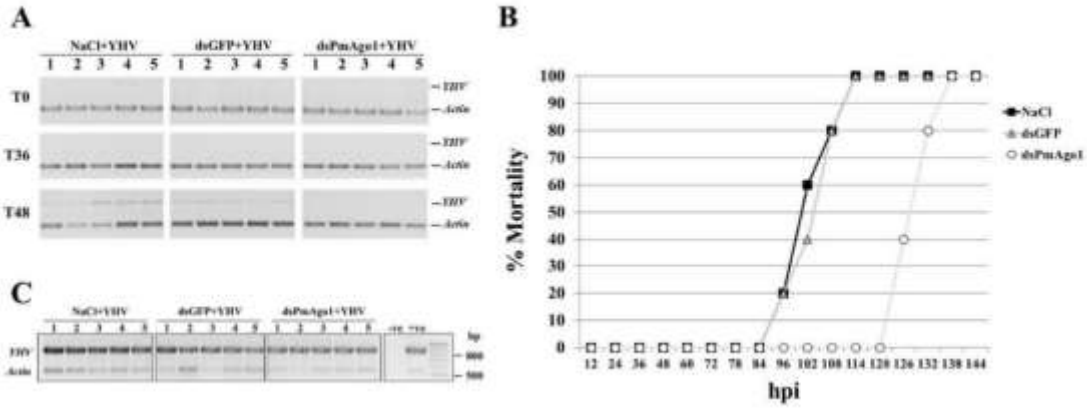

Fig. 4. Effect of *PmAgo1* knockdown on YHV replication and cumulative mortality in shrimp upon YHV infection

Suppression of *PmAgo1* expression was carried out by *PmAgo1*-dsRNA injection with NaCl and *GFP*-dsRNA injection as controls. On day 2 after injected with dsRNA, shrimp were subsequently challenged with YHV, and the expression of YHV helicase gene (YHV hel) in the hemolymph of *PmAgo1*-knockdown shrimp (ds*PmAgo1*+YHV) and the control shrimp (NaCl+YHV, ds*GFP*+YHV) was detected by multiplex RT-PCR compared with that of *β-actin* at 0, 36 and 48 hours post YHV infection (n=5 at each time point) (A). Mortality of individual shrimp in each group was also recorded, and presented as cumulative percent mortality (B). Virus infection in the shrimp was verified by detection of YHV-hel mRNA in gill tissue from dead shrimp in all groups (C).

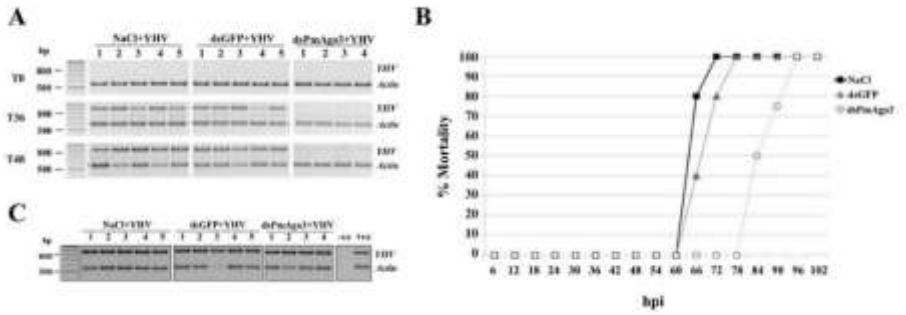

Figure 5. Effect of *PmAgo3* knockdown on YHV replication and cumulative mortality in shrimp upon YHV infection

Suppression of *PmAgo3* expression was carried out by *PmAgo1*-dsRNA injection with NaCl and *GFP*-dsRNA injection as controls. The *PmAgo3*-knockdown shrimp were infected with YHV (ds*PmAgo3*+YHV), and the expression of YHV-hel gene in the hemolymph was detected by multiplex RT-PCR compared with that of control shrimp (NaCl+YHV, ds*GFP*+YHV) at 0, 36 and 48 hours post YHV infection (n=5 at each time point) (A). *β-actin* transcript was determined as internal control. Mortality of individual shrimp in each group was also recorded, and presented as cumulative percent mortality (B). Expression of YHV hel mRNA in gill tissue from dead shrimp was examined to confirm virus infection in the shrimp (C).

Since WSSV is one of major viruses that cause high mortality in the shrimp, the role of *PmAgo1* and *PmAgo3* in WSSV infection was also investigated. The result showed that the levels of WSSV *vp28* transcript as well as WSSV genomic DNA in *PmAgo1*-knockdown shrimp infected with WSSV was comparable to that in both control groups that were injected with either NaCl or *GFP*-dsRNA prior to viral challenge (Figure 6A and 6B). In addition, the cumulative mortality rate of the shrimp in all groups was not different; shrimp started to die after 36 h, and all were dead by 48 h (Figure 6C). By contrast, lower levels of WSSV *vp28* transcript, notably with undetectable level in two out of five shrimp, and lower amounts of viral DNA genome in the pleopod were detected in *PmAgo3*-knockdown shrimp at 36 h post WSSV infection compared with that in both control groups (Figure 6A and 6B). Moreover, the delay in the cumulative mortality rate in *PmAgo3*-knockdown shrimp was observed upon WSSV challenge when compared to the control groups (Figure 6C). The WSSV *vp28* transcript could be detected in gill tissue from dead shrimp in all groups confirming that the shrimp died of WSSV infection (Figure 6D).

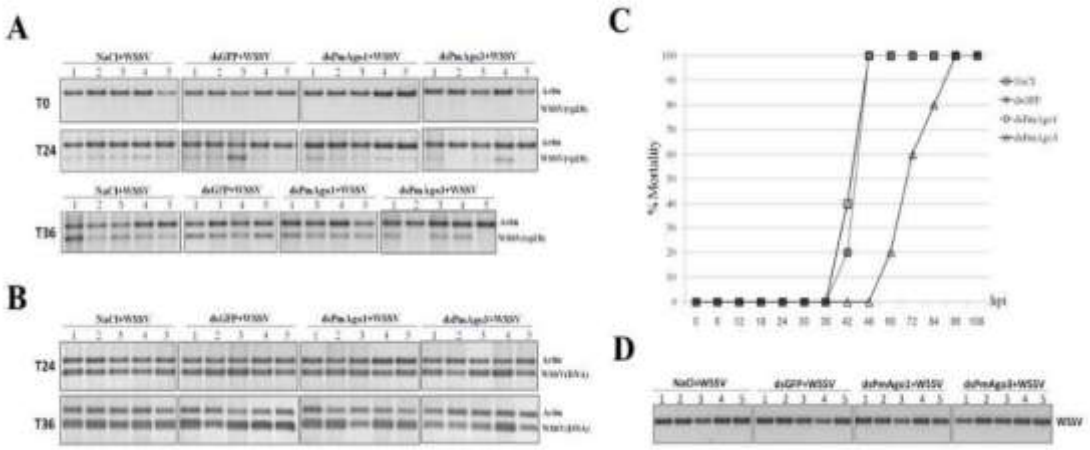

Fig. 6. WSSV replication and shrimp mortality upon WSSV infection in *PmAgo1* knockdown *P. Monodon*.

P. monodon were injected with either 2.5 µg g-1 shrimp of *PmAgo1*-dsRNA, *PmAgo3* dsRNA *GFP*-dsRNA or 150 mM NaCl (n=5 in each group) 2 days prior to WSSV challenge. WSSV replication in *PmAgo1*-knockdown shrimp (ds*PmAgo1*+WSSV), *PmAgo3* knockdown shrimp (ds*PmAgo3*+WSSV) comparing with control shrimp (NaCl+WSSV and ds*GFP*+WSSV) was determined by both RT-PCR detection of WSSV *Vp28* mRNA (A) and PCR amplification of WSSV genomic DNA (B) at 0, 24 and 36 hours post WSSV infection. *β-actin* transcript was determined as an internal control. Mortality of individual shrimp in each group was also recorded, and presented as cumulative percent mortality (C). WSSV infection in all dead shrimp was confirmed by RT-PCR of WSSV-*vp28* mRNA in gill tissue (D).

Discussion

Four types of Argonaute protein were previously identified in *P. monodon*. They are all classified as the Ago subfamily. Nevertheless, the mechanism underlying the Ago-related antiviral immunity in shrimp remains largely unknown. In this study, functional significance of *PmAgo1* and *PmAgo3* on YHV and WSSV replication and their role in dsRNA-mediated post-transcriptional gene silencing were characterized.

Expression of key proteins in the effective innate antiviral RNAi mechanism was usually stimulated by exogenous RNAs (31,32,40,41). Injection of dsRNA could induce expression of *dicer*-2 and *argonaute*-2 in tobacco hornworm (40). In *Neurospora crassa*, the induction of *dicer* (DCL-2) and *argonaute* (QDE-2) expression by dsRNA resulted in an increase in the efficiency of dsRNA-mediated RNAi pathway (41). These evidences suggested that *dicer*-2 and a*rgonaute*-2 are involved in dsRNA-mediated gene silencing pathway. Up-regulation of the expression of genes encoding core RNAi proteins e.g. *Dcr2*, *Ago2* and *Ago3* and associated components such as TRBP, TSN and Mov-10 upon dsRNA challenge were also demonstrated in penaeid shrimps (42,32,31,43-45). In addition, suppression of *HsAgo2* by *HsAgo2*-siRNA in Human Embryonic Kidney 293 cells (HEK 293) impeded the efficiency of RNAi mechanism to knock-down histone deacetylase 2 (HDAC2) by specific HDAC2-siRNA (46). Similarly, silencing of *PmAgo1* and *PmAgo3* expression by specific dsRNAs in this study reduced the efficiency of P*mRab7* mRNA suppression by *PmRab7*-dsRNA, indicating the involvement of *PmAgo1*

and *PmAgo3* in dsRNA-mediated gene silencing process. These results strongly supported the study of Dechklar et al., 2008 where repression of Ago1 reduced the competency of 5'HT-dsRNA in suppressing 5'HT gene in *P. monodon*'s Oka cells (30). In addition, knockdown of PmTSN or MjTRBP expression by specific dsRNA in shrimp also impaired the efficiency of dsRNA/siRNA mediated gene silencing (44,47). Previous reports on the Argonaute interacting protiens in shrimp revealed that argonaute-2 of L. vannamei and M. japonicus bound to dicer-2 and TRBP1, respectively. These *Ago2* complexes played a role in dsRNA/siRNA-mediated sequence-specific RNAi process while argonaute-1 primarily functioned in an miRNA pathway (48,29). However, the interacting proteins and small RNAs associated with either *PmAgo1* or *PmAgo3* need to be identified to confirm the precise mechanism of each *PmAgo* in the RNAi pathway.

Previous studies in other species demonstrated that the responsive expression of Ago transcripts upon virus infection enhanced the effective RNAi antiviral defense (49,50). For instance, the increased expression of *Nb*Ago1 mRNA in Cymbidun ringspot virus (CymRSV) infected Nicotiana benthamiana and the accumulation of argonaute-1 protein enhanced the RNAi antiviral activity by reducing the levels of CymRSV accumulation in the plant (50). In addition, high levels of *MjAgo1*A and *MjAgo1*B transcript were accumulated upon WSSV infection in *M. japonicus* (28). Similarly, our result showed that the increased levels of *PmAgo1* expression was noticed in the haemolymph of YHV-infected shrimp. This phenomenon was also observed in YHV-infected lymphoid organ (39) indicating a possible involvement of *PmAgo1* in antiviral mechanism. Up-regulation of argonaute 2 (GrAgo2) transcripts were exhibited in grass carp reovirus-infected rare minnow *Gobiocypris rarus* (51). Likewise, infection of tomato yellow leaf curl virus in tomato, *Solanum lycopersicum* induced the expression of dicers and Agos (52). In P. monodon, Yang et al. 2014 demonstrated that *PmAgo2* mRNA expression was escalated by WSSV challenge (32) while the expression of *PmAgo3* and *PmAgo4* was not altered in YHV infected shrimp (31,14). Virus infection in Penaeid shrimps could also evoke other RNAi components such as LvDicer-1, LvDrosha and FcTRBP (53,54,55). Nonetheless, the responsive expression of *PmAgos* upon viral challenge may not necessarily specify *PmAgos*' function in antiviral defense. Whether or not *PmAgos* take part in RNAi antiviral defense in shrimp was therefore further characterized in this study.

The function of Argonaute proteins in RNAi-mediated antiviral defense in invertebrates was generally demonstrated by an increase in susceptibility to viruses in *Ago*-knockdown animals (28). For instance, the hypersensitivity to *Drosophila C* virus infection and high viral RNA accumulation were presented in DmAgo2 mutant drosophila comparing to wild type and DmAgo1 mutant flies (24). A significant increase of viral loads was also observed in the shrimp, in which the expression of RNAi machinery e.g. *Ago1*, *dicer-1*, *TRBP* and *Mov10* had been knocked down (28,56,47,45). Therefore, the functional significant of P*mAgo1* and *PmAgo3* in RNAi antiviral mechanism were investigated by determination the level of viral transcript and cumulative mortality in *PmAgos* suppressed shrimp comparing to the control groups.

In general, once the hosts are infected by RNA viruses, the dsRNA replicative intermediates of the viruses are recognized by Dicer and cleaved into viral-derived siRNAs (viRNAs). The complex between viRNAs and Ago proteins in the RISC subsequently trigger the activity of RNA silencing-mediated antiviral immunity (57-60). However, some viruses could express viRNAs that interfered with host gene expression

and promoted viral infection (61,62). For example, the expression of two callose synthase genes in tomato plant was down-regulated by an siRNA derived from potato spindle tuber viroid leading to the accumulation of viroids and the severity of disease (62). Likewise, siRNAs derived from Cucumber mosaic virus (CMV) Y satellite RNA (Y-sat) could decrease the expression chlI gene in the chlorophyll synthesis pathway, and enhanced the yellowing symptom in tobacco plants (63). Our results revealed that inhibition of YHV replication and delay mortality were noticeably observed in *PmAgo1*- and *PmAgo3*- knockdown shrimp when compared with that in both control groups (injection with either NaCl or GFP-dsRNA prior to viral challenge). These evidences suggest that the positive single-stranded YHV might produce viRNAs that were subsequently loaded into either *PmAgo1* or *PmAgo3* RISC to regulate cellular gene expression of shrimp, and accounted for promoting viral replication and disease severity. However, the gene required for YHV replication, whose expression was affected by YHV derived small RNA in the shrimp needed to be further identified.

In addition to RNA viruses, a number of DNA viruses could also produce viral-derived small RNAs. For example, viRNAs derived from shrimp DNA virus, WSSV were reported in Penaeid shrimps (29), and they required shrimp Ago2 protein for the effective function in response to WSSV infection (32). Our results also showed that the replication of WSSV in *P. monodon* was suppressed in *PmAgo3*- knockdown shrimp, but not in *PmAgo1* knockdown shrimp suggesting that *PmAgo3* might play an important role in both DNA and RNA virus replication in the shrimp. The preference for each Ago protein in response to RNA and DNA viruses is not surprising as it has been demonstrated that Arabidopsis Ago1 and Ago2 played a major role in the anti-RNA viral response (64-67), while Ago4 functions in an antiviral activity against several RNA (68,69) and DNA viruses (70,71)

In conclusion, the function in antiviral immunity of *PmAgo1* and *PmAgo3* of *P. monodon* was reported in this study. *PmAgo1* expression in the hemolymph was elevated upon YHV challenge suggesting its association with shrimp antiviral response. Suppression of *PmAgos* by specific dsRNA indicated that *PmAgo1* was preferentially required for YHV replication, whereas *PmAgo3* has more extensive effect on the replication of both YHV and WSSV. Our findings expand an understanding in Argonaute-associated RNA silencing mechanism and antiviral defense in the Penaeid shrimp.

References

1. Hoffmann JA, Kafatos FC, Janeway CA, Ezekowitz RA. Phylogenetic perspectives in innate immunity. Science. 1999; 284: 1313-8.
2. Borregaard N, Elsbach P, Ganz T, Garred P, Svejgaard A. Innate immunity: from plants to humans. Immunol Today. 2000; 21: 68-70.
3. Wang XH, Aliyari R, Li WX, Li HW, Kim K, Carthew R, et al. RNA interference directs innate immunity against viruses in adult *Drosophila*. Science. 2006; 312: 452-4.
4. Zambon RA, Vakharia VN, Wu LP. RNAi is an antiviral immune response against a dsRNA virus in D*rosophila* melanogaster. Cell Microbiol. 2006; 8: 880-9.
5. Robalino J, Browdy CL, Prior S, Metz A, Parnell P, Gross P, et al. Induction of antiviral immunity by double-stranded RNA in a marine invertebrate. J Virol. 2004; 78: 10442-8.

6. Aliyari. R., Wu, Q., Li, H.W., Wang, X.H., Li, F., Green, L.D., Han, C.S., Li, W.X., Ding, S.W. . Mechanism of induction and suppression of antiviral immunity directed by virus-derived small RNAs in *Drosophila*. Cell Host. Microbe. 2008; 4: 387–397.
7. Kwak PB, Tomari Y. The N domain of Argonaute drives duplex unwinding during RISC assembly. Nat Struct Mol Biol. 2012; 19: 145-51.
8. Lingel A, Simon B, Izaurralde E, Sattler M. Structure and nucleic-acid binding of the Drosophila Argonaute 2 PAZ domain. Nature. 2003; 426: 465-9.
9. Ma JB, Ye K, Patel DJ. Structural basis for overhang-specific small interfering RNA recognition by the PAZ domain. Nature. 2004; 429: 318-22.
10. Till S, Lejeune E, Thermann R, Bortfeld M, Hothorn M, Enderle D, Heinrich C, Hentze MW, Ladurner AG. A conserved motif in Argonaute-interacting proteins mediates functional interactions through the Argonaute PIWI domain. Nat Struct Mol Biol. 2007; 14: 897–903.
11. Kiriakidou M, Tan GS, Lamprinaki S, De Planell-Saguer M, Nelson PT, Mourelatos Z. An mRNA m(7)G cap binding-like motif within human Ago2 represses translation. Cell. 2007; 129: 1141–1151.
12. Song JJ, Smith SK, Hannon GJ, Joshua-Tor L. Crystal structure of Argonaute and its implications for RISC slicer activity. Science. 2004; 305: 1434-7.
13. Wang Y, Sheng G, Juranek S, Tuschl T, Patel DJ. Structure of the guide-strand containing argonaute silencing complex. Nature. 2008; 456: 209-13.
14. Leebonoi W, Sukthaworn S, Panyim S, Udomkit A. A novel gonad-specific Argonaute 4 serves as a defense against transposons in the black tiger shrimp *Penaeus monodon*. Fish Shell fish Immunol. 2014; 42: 280-288.
15. Chen PY, Meister G. MicroRNA-guided posttranscriptional gene regulation. Biol Chem. 2005; 386: 1205-18.
16. Janowski BA, Huffman KE, Schwartz JC, Ram R, Nordsell R, Shames DS, et al. Involvement of AGO1 and AGO2 in mammalian transcriptional silencing. Nat Struct Mol Biol. 2006; 13: 787-92.
17. Hammond SM, Bernstein E, Beach D, Hannon GJ. An RNA-directed nuclease mediates post-transcriptional gene silencing in *Drosophila* cells. Nature. 2000; 404: 293-6.
18. Yigit E, Batista PJ, Bei Y, Pang KM, Chen CC, Tolia NH, et al. Analysis of the C. elegans Argonaute family reveals that distinct Argonautes act sequentially during RNAi. Cell. 2006; 127: 747-57.
19. Kalmykova AI, Klenov MS, Gvozdev VA. Argonaute protein PIWI controls mobilization of retrotransposons in the *Drosophila* male germline. Nucleic Acids Res. 2005; 33: 2052-9.
20. Kuramochi-Miyagawa S, Kimura T, Ijiri TW, Isobe T, Asada N, Fujita Y, et al. Mili, a mammalian member of piwi family gene, is essential for spermatogenesis. Development. 2004; 131: 839-49.
21. H €ock J, Meister G. The Argonaute protein family. Genome Biol 2008; 9: 210. 1-210.8.
22. Miyoshi K, Tsukumo H, Nagami T, Siomi H, Siomi MC. Slicer function of *Drosophila* Argonautes and its involvement in RISC formation. Genes & development. 2005; 19(23): 2837–48.

23. Meister G, et al. Human Argonaute2 mediates RNA cleavage targeted by miRNAs and siRNAs. Mol. Cell. 2004; 15: 185–197.
24. Van Rij, R. P., M. C. Saleh, B. Berry, C. Foo, A. Houk, C. Antoniewski, R. Andino. The RNA silencing endonuclease Argonaute 2 mediates specific antiviral immunity in Drosophila melanogaster. Genes Dev. 2006; 20: 2985–2995.
25. Chen S, Chahar HS, Abraham S, Wu H, Pierson TC, Wang XA, Manjunath N. Ago-2 mediated slicer activity is essential for anti-flaviviral efficacy of RNAi. PLoS One. 2011; 6: e27551.
26. Labreuche Y, Veloso A, de la Vega E, Gross PS, Chapman RW, Browdy CL, et al. Non-specific activation of antiviral immunity and induction of RNA interference may engage the same pathway in the Pacific white leg shrimp Litopenaeus vannamei. Dev Comp Immunol. 2010; 34: 1209-18.
27. Chen YH, Jia XT, Zhao L, Li CZ, Zhang S, Chen YG, et al. Identification and functional characterization of Dicer2 and five single VWC domain proteins of Litopenaeus vannamei. Dev Comp Immunol. 2011; 35: 661-71.
28. Huang T, Zhang X. Contribution of the argonaute-1 isoforms to invertebrate antiviral defense. PLoS One. 2012; 7: e50581.
29. Huang T, Zhang X. Host defense against DNA virus infection in shrimp is mediated by the siRNA pathway. Eur J Immunol. 2013; 43: 137-46.
30. Dechklar M, Udomkit A, Panyim S. Characterization of Argonaute cDNA from *Penaeus monodon* and implication of its role in RNA interference. Biochem Biophys Res Commun. 2008; 367: 768-74.
31. Phetrungnapha A, Ho T, Udomkit A, Pamyim S, Ongvarrasopone C. Molecular cloning and functional characterization of Argonaute-3 gene from *Penaeus monodon*. Fish Shell fish Immunol. 2013; 35: 874-882.
32. Yang L, Li X, Jiang S, Qiu L, Zhou F, Liu W, et al. Characterization of Argonaute2 gene from black tiger shrimp (*Penaeus monodon*) and its responses to immune challenges. Fish Shell fish Immunol. 2014; 36: 261-9.
33. Yodmuang S, Tirasophon W, Roshorm Y, Chinnirunvong W, Panyim S. YHV-protease dsRNA inhibits YHV replication in *Penaeus monodon* and prevents mortality. Biochem. Biophys. Res. Commun. 2006; 341: 351-356.
34. Attasart P, Kaewkhaw R, Chimwai C, Kongphom U, Namramoon O, Panyim S. Inhibition of white spot syndrome virus replication in *Penaeus monodon* by combined silencing of viral rr2 and shrimp PmRab7. Virus Res. 2009; 145: 127-133.
35. Assavalapsakul W, Smith DR, Panyim S. Propagation of infectious yellow head virus particles prior to cytopathic effect in primary lymphoid cell cultures of *Penaeus monodon*. Dis Aquat Org. 2003; 55: 253-8.
36. Ongvarrasopone, C., Chanasakulniyom, M., Sritunyalucksana, K. and Panyim, S. Suppression of PmRab7 by dsRNA inhibits WSSV or YHV infection in shrimp. Mar Biotechnol (NY). 2008; 10: 374-81.
37. Ongvarrasopone C, Roshorm Y, Panyim S. A simple and cost effective method to generate dsRNA for RNAi studies in invertebrates. Science Asia. 2007; 33: 35-9.
38. Posiri P, Ongvarrasopone C, Panyim S. A simple one-step method for producing dsRNA from *E. coli* to inhibit shrimp virus replication. J Virol Methods. 2013; 188: 64-9.

39. Unajak S, Boonsaeng V, Jitrapakdee S. Isolation and characterization of cDNA encoding Argonaute, a component of RNA silencing in shrimp (*Penaeus monodon*). Comp Biochem Physiol B Biochem Mol Biol. 2006; 145: 179-87.
40. Garbutt J.S., Reynolds S.E. Induction of RNA interference genes by double-stranded RNA; implications for susceptibility to RNA interference. Insect Biochem. Mol. Biol. 2012; 42: 621–628.
41. Choudhary S, Lee HC, Maiti M, He Q, Cheng P, Liu Q, Liu Y. A double-strandedRNA response program important for RNA interference efficiency. Mol Cell Biol. 2007; 27: 3995–4005.
42. Li X, Yang L, Liang S, Fu M, Huang J, Jiang S. Identification and expression analysis of Dicer2 in black tiger shrimp (*Penaeus monodon*) responses to immune challenges. Fish Shellfish Immunol. 2013; 35: 1-8.
43. Yang L, Li X, Huang J, Zhou F, Su T, Jiang S. Isolation and characterization of homologous TRBP cDNA for RNA interference in *Penaeus monodon*. Fish Shellfish Immunol. 2013; 34: 704-711.
44. Phetrungnapha A, Panyim S, Ongvarrasopone C. A Tudor staphylococcal nuclease from *Penaeus monodon*: cDNA cloning and its involvement in RNA interference. Fish Shellfish Immunol. 2012; 31: 373-380.
45. Phetrungnapha A, Kondo H, Hirono I, Panyim S, Ongvarrasopone C. Molecular cloning and characterization of Mj-MOV10, a putative RNA helicase involved in RNAi of Kuruma shrimp. Fish Shellfish Immunol. 2015; 44: 241-247.
46. Naoghare PK, Tak YK, Kim MJ, Han E, Song JM. Knock-Down of Argonaute 2 (AGO2) Induces Apoptosis in Myeloid Leukaemia Cells and Inhibits siRNA-Mediated Silencing of Transfected Oncogenes in HEK-293 Cells. Basic Clin Pharmacol Toxicol. 2011; 109: 274–282.
47. Wang S, Chen A-J, Shi L-J, Zhao X-F, Wang J-X. TRBP and eIF6 homologue in *Marsupenaeus japonicus* play crucial roles in antiviral response. PLoS ONE. 2012; 7(1): e30057.
48. Chen YH, Jia XT, Zhao L, Li CZ, Zhang S, Chen YG, et al. Identification and functional characterization of Dicer2 and five single VWC domain proteins of *Litopenaeus vannamei*. Dev Comp Immunol. 2011; 35: 661-71.
49. Sun Q, Choi GH, Nuss DL. A single Argonaute gene is required for induction of RNA silencing antiviral defense and promotes viral RNA recombination. Proc Natl Acad Sci U S A. 2009; 106: 17927–17932.
50. Várallyay É, Válóczi A, Ágyi Á, Burgyán J, Havelda Z. Plant virus-mediated induction of miR168 is associated with repression of argonaute1 accumulation. EMBO J. 2010; 29: 3507–3519.
51. Su J, Zhu Z, Wang Y, Jang S. Isolation and characterization of Argonaute2: A key gene of the RNA interference pathway in the rare minnow, Gobiocypris rarus. Fish Shell fish Immunol. 2009; 29: 164-170.
52. Bai M, Yang G-S, Chen W-T, Mao Z-C, Kang H-X, Chen G-H, Yang Y-H, Xie Y-B. Genome-wide identification of Dicer-like, Argonaute and RNA-dependent RNA polymerase gene families and their expression analyses in response to viral infection and abiotic stresses in Solanum lycopersicum. Gene. 2012; 501: 52-62.
53. Yao X, Wang L, Song L, Zhang H, Dong C, Zhang Y, Qiu L, Shi Y, Zhao J, Bi Y. A Dicer-1 gene from white shrimp *Litopenaeus vannamei*: expression pattern

in the processes of immune response and larval development. Fish Shellfish Immunol. 2010; 29: 565-70
54. Huang T, Xu D, Zhang X. Characterization of shrimp Drosha in virus infection. Fish Shellfish Immunol. 2012; 33: 575-81
55. Wang S, Liu N, Chen Aj, Zhao XF, Wang JX. TRBP homolog interacts with eukaryotic initiation factor 6 (eIF6) in *Fenneropenaeus chinensis*. J Immunol. 2009; 182: 5250-8.
56. Su J, Oanh DT, Lyons RE, Leeton L, Van Hulten MC, Tan SH, Song L, Rajendran KV, Walker PJ. A key gene of the RNA interference pathway in the black tiger shrimp, *Penaeus monodon*: identification and functional characterization of Dicer-1. Fish Shellfish Immunol. 2008; 24(2): 223-33.
57. Molnar A, Csorba T, Lakatos L, Varallyay E, Lacomme C, Burgyan J. Plant virusderived small interfering RNAs originate predominantly from highly structured single stranded viral RNAs. J Virol. 2005; 79: 7812–7818.
58. Pantaleo V, Szittya G, Burgyán J. Molecular bases of viral RNA targeting by viral small interfering RNA-programmed RISC. J Virol. 2007; 81: 3797–3806.
59. Parameswaran P, Sklan E, Wilkins C, Burgon T, Samuel MA, Lu R, Ansel KM, Heissmeyer V, Einav S, Jackson W, Doukas T, Paranjape S, Polacek C, dos Santos FB, Jalili R, Babrzadeh F, Gharizadeh B, Grimm D, Kay M, Koike S, Sarnow P, Ronaghi M, Ding SW, Harris E, Chow M, Diamond MS, Kirkegaard K, Glenn JS, Fire AZ. Six RNA viruses and forty-one hosts: viral small RNAs and modulation of small RNA repertoires in vertebrate and invertebrate systems. PLoS Pathog. 2010; 6: e1000764.
60. Weng KF, Hsieh PT, Huang HI, Shih SR. Mammalian RNA virus-derived small RNA: biogenesis and functional activity. Microbes and infection/Institut Pasteur. 2015; 17: 557–563.
61. Wang J, Tang Y, Yang Y, Ma N, Ling X, Kan J, et al. Cotton Leaf Curl Multan VirusDerived Viral Small RNAs Can Target Cotton Genes to Promote Viral Infection. Front Plant Sci. 2016; 7: 1162.
62. Adkar-purushothama CR, Brosseau C, Giguère T, Sano T, Moffett P, Perreault JP. Small RNA derived from the virulence modulation region of the Potato spindle tuber viroid silences callose synthase genes of tomato plants. The Plant Cell. 2015; 27: 2178-2194.
63. Smith NA, Eamens AL, Wang MB. Viral small interfering RNAs target host genes to mediate disease symptoms in plants. PLoS Pathog. 2011; 7: e1002022
64. Wang XB, Jovel J, Udomporn P, Wang Y, Wu Q, Li WX, Gasciolli V, Vaucheret H, Ding SW. The 21-nucleotide, but not 22-nucleotide, viral secondary small interfering RNAs direct potent antiviral defense by two cooperative Argonautes in Arabidopsis thaliana. Plant Cell. 2011; 23: 1625–1638.
65. Dzianott A, Sztuba-Solinska J, Bujarski JJ. Mutations in the antiviral RNAi defense pathway modify Brome mosaic virus RNA recombinant profiles. Mol Plant Microbe Interact. 2012; 25: 97–106.
66. Garcia-Ruiz H, Carbonell A, Hoyer JS, Fahlgren N, Gilbert KB, Takeda A, Giampetruzzi A, Garcia Ruiz MT, McGinn MG, Lowery N, et al. Roles and Programming of Arabidopsis ARGONAUTE Proteins during Turnip Mosaic Virus Infection. PLoS Pathog. 2015; 11: e1004755

67. Jaubert MJ, Bhattacharjee S, Mello AF, Perry KL, Moffett P. AGO2 mediates RNA silencing anti-viral defenses against Potato virus X in Arabidopsis. Plant Physiol. 2011; 156: 1556–1564.
68. Hamera S, Song X, Su L, Chen X, Fang R. Cucumber mosaic virus suppressor 2b binds to AGO4-related small RNAs and impairs AGO4 activities. Plant J. 2012; 69: 104–115.
69. Bhattacharjee S, Zamora A, Azhar MT, Sacco MA, Lambert LH, Moffett P. Virus resistance induced by NB-LRR proteins involves Argonaute4-dependent translational control. Plant J. 2009; 58: 940–951.
70. Raja P, Sanville BC, Buchmann RC, Bisaro DM. Viral genome methylation as an epigenetic defense against geminiviruses. J Virol. 2008; 82: 8997–9007.
71. Raja P, Jackel JN, Li S, Heard IM, Bisaro DM. Arabidopsis double-stranded RNA binding protein DRB3 participates in methylation-mediated defense against geminiviruses. J Virol. 2014; 88: 2611–2622.

Endocytosis participates in cellular uptake of injected dsRNA into hepatopancreas but not gill of *Litopenaeus vannamei*

RNA interference (RNAi) technology is widely applied in shrimp research areas for functional genomics with potential anti-viral applications. The SID-1 of *Litopenaeus vannamei*, which has been reported to be participated in injected dsRNA uptake into shrimp cells may not be only one mechanism required for this process. Therefore, possible role of the endocytosis pathway on delivery of the injected dsRNA into shrimp hepatopancreatic and gill cells was evaluated in this study. Shrimp were initially inhibited their clathrin-mediated endocytosis pathway by injection of pharmacological inhibitors (chlorpromazine and bafilomycin-A1) before dsSTAT administration. Levels of STAT suppression in the treated shrimp as compared to the control shrimp reflect the capability of cells to take up the dsSTAT. Inhibition of clathrinmediated endocytosis pathway showed reduction of STAT suppression in shrimp hepatopancreas. In contrast, neither chlorpromazine nor bafilomycin-A1 can effectively block RNAi of STAT in gill tissue. These results support our conclusion that clathrin-mediated endocytosis is required in cellular uptake of injected dsRNA into shrimp hepatopancreas but is not participated in the process in gills. This article reports for the first time on the involvement of different pathways in cellular dsRNA uptake into different tissues of shrimp.

Introduction

RNA interference (RNAi) technology is widely applied in shrimp research areas for functional genomics (Phetrungnapha et al., 2015; Sagi et al., 2013) with potential anti-viral applications (Assavalapsakul et al., 2014; Escobedo-Bonilla, 2011; Sagi et al., 2013; Shekhar and Lu, 2009). Injection of dsRNA into haemocoel or muscle is routinely used for delivering dsRNA into shrimp (Labreuche et al., 2010; Sutthangkul et al., 2015). While systemic circulation within shrimp body cavity, the dsRNA may be taken up by cells in different tissues. In invertebrates, at least two pathways for exogenous dsRNA uptake have been described so far, namely the systemic RNA interference defective (SID) transmembrane channel protein-mediated and the endocytosis-mediated mechanisms (Huvenne and Smagghe, 2010). Participation of the SID-1 in dsRNA uptake has been demonstrated in *Caenorhabditis elegans* (*C. elegans*) (Winston et al., 2002), *Diabrotica virgifera* (Miyata et al., 2014), *Leptinotarsa decemlineata* (Cappelle et al., 2016), *Nilaparvata lugens* (Xu et al., 2013) and *Apis mellifera* (Aronstein et al., 2006). Even though the *Tribolium castaneum* has three SID-1 homologues but they do not participate in dsRNA uptake. Instead, the clathrin-mediated endocytosis is proven to be involved (Tomoyasu et al., 2008; Xu and Han, 2008). The endocytosis is a major pathway for cellular dsRNA uptake in some insects. Blocking of endocytic pathway by specific inhibitors of clathrin-coated pith formation and vacuolar H+ ATPase (V-ATPase) effectively inhibits the internalization of dsRNA in *Drosophila* S2 cells (*Drosophila melanogaster*) (Ulvila et al., 2006; Winston et al., 2002), red flour beetle (*Tribolium castaneum*) (Xiao et al., 2015) and desert locust (*Schistoceca gregaria*) (Luo et al., 2012). Moreover, colorado potato beetle (*Leptinotarsa decemlineata*) requires both the SID-1 and endocytosis pathways for dsRNA uptake into midgut cells (Cappelle et al., 2016). Therefore, the SID-1 of *Litopenaeus vannamei* (*Lv*SID-1), which has been reported to be participated in injected dsRNA uptake into shrimp cells

(Maruekawong et al., 2018), may not be only one mechanism required for this process. Possible role of the endocytosis pathway on delivery of the injected dsRNA into shrimp cells in hepatopancreas and gill tissues was evaluated in this study. Shrimp were initially inhibited their clathrin-mediated endocytosis pathway using chlorpromazine (Cpz) or bafilomycin-A1 (BafA) to block two important steps, clathrin-coated pits formation (Wang et al., 1993; Yao et al., 2002) or vacuolar acidification by V-ATPase (Yamamoto et al., 1998), respectively. The treated shrimp were then injected with a dsRNA specific to shrimp signal transduction and transcription protein (STAT) mRNA (dsSTAT). Levels of STAT suppression in the treated shrimp as compared to the control shrimp reflect the capability of cells to take up the dsSTAT.

Materials and methods

Shrimp specimens

Post larval (Pl15-Pl20) white leg shrimp (*L. vannamei*) were purchased from Chuchai farm in Chonburi province and maintained in 10 ppt of seawater with aeration in a 500 L tank. Commercial diet (CP) was used to feed shrimp until they reached a juvenile stage of roughly 200-300 mg of body weight. During experiments, shrimp were kept in individual cages in the same tank to avoid cannibalism.

Production of dsRNA

The plasmid containing expression cassette of dsRNA targeting the shrimp STAT mRNA (dsSTAT) was transformed into *E. coli* HT115 (a RNase III defective strain). Expression of dsRNA was followed the previous protocol (Ongvarrasopone et al., 2007). A single colony was inoculated in LB medium containing 100 μg/ml ampicillin and 12.5 μg/ml tetracycline and grown overnight at 37ºC. This overnight starter culture (0.5 OD) was inoculated in 15 ml of new medium and grown until OD600 reached 0.4. Expression of dsRNA was induced with 0.4 mM of isopropyl-β-d thiogalactopyranoside (IPTG) for 4 hours. According to the protocol of Posiri *et al*. (Posiri et al., 2013), one OD of bacterial cells was collected by centrifugation at 8,000x g at 4ºC for 5 min and resuspended in 100 μl 75% ethanol in phosphate buffer saline (PBS) and incubated at room temperature for 5 min. The treated cells were collected by centrifugation at 8000 × g for 5 min at 4ºC before resuspending in 100 μl of 150 mM NaCl and incubated at room temperature for 1 hour. The cell suspension was centrifuged at 12000 × g at 4ºC for 5 min to generate a cell-free supernatant. The dsRNA in the supernatant was diluted before loading into agarose gels to estimate the concentration by comparing with a standard marker.

Evaluation of endocytosis inhibitors' effect on RNAi

Due to suppression of clathrin heavy chain (Chc) by dsRNA is lethal to shrimp, therefore, the clathrin-mediated endocytosis pathway was blocked by injection with specific drug inhibitors (chlorpromazine (Sigma-Aldrich) (inhibitor of clathrin-coated pits formation) and bafilomycin-A1 (Abcam) (inhibitor of v-ATPase)). To ensure the shrimp endocytosis was inhibited, different amount of drugs (1.8 and 9.0 μg of Cpz and 1.8 and 3.0 μg of BafA per shrimp body weight (g)) were injected into shrimp. Twelve hours later, dsSTAT was administered. The STAT mRNA suppression in shrimp tissues (hepatopancreas and gill) were determined at 10-12 hpi (hours post dsSTAT injection).

Injection of dsRNA into shrimp

The dsSTAT solution was diluted in 150 mM NaCl to make 15 ng/μl before injection. Twenty microliters of dsRNA solut ion (approximately 200-300 ng) was injected into shrimp haemocoel using a 0.5 ml syringe with 29G needle.

Shrimp RNA extraction and cDNA synthesis

Hepatopancreas and gill tissues (approximately 10 mg each) were dissected from *L. Vannamei* using scissors and forceps. Total RNA was extracted using RiboZol™ (Amresco) following the manufacturer's instruction. The extracted RNA (1-2 μg) was heated at 70ºC for 5 min in a reaction tube containing 2μM of random primers and RNase-free sterile distilled water and quickly cooling on ice. The primers were then allowed to anneal with RNA at 25ºC for 5 min. The following components, 1X ImProm-II™ reaction buffer, 0.5 mM dNTPs, 30 mM $MaCl_2$, 1μl of ImProm-II™ reverse transcriptase and RNase-free sterile distilled water were added into the reaction. The cDNA was synthesized at 42ºC for 60 min before termination at 70ºC for 15 min.

Semi-quantitative RT-PCR

The 25 μl PCR reaction composed of 2 μl of cDNA template, 1x PCR buffer (75 mM Tris-HCl (pH 8.8 at 25ºC), 20 mM $(NH_4)_2SO_4$ and 0.01% Tween 20), 0.2 mM dNTPs, 0.2 μM of each primer, 2 mM of $MgCl_2$, 200 μM of dNTPs mix, 1.25 unit (0.25 μl) of *Taq* DNA polymerase (homemade or Aspalagen) and sterile distilled water. For optimal condition, which did not give saturated amplified products, ratio of actin gene primers (5' GACTCGTACGTCGGGCGACGAGG 3' and 5' AGCAGCGGTGGTCATCTCCTGCTC 3') and STAT gene primers (5' ATGTCGTTGTGGAACAGAGC 3' and 5' GTTTGTTGCATGTGAAACACCTCC 3') were 1:4. The PCR conditions were held at 94ºC for 2 min and repeated 25 cycles of denaturation at 94ºC for 10 sec, annealing at 55ºC for 30 sec, and extension at 72ºC for 1 min. Lastly, the amplification was held at 72ºC for 5 min. The PCR products were analyzed by agarose gel electrophoresis. Levels of PCR products were then relatively quantified using the Scion Image program.

Statistical analysis

Graphs are presented as mean ± standard error of mean (SEM) by using GraphPad Prism 5 program. The *p*-value below 0.05 ($p < 0.05$) of nonparametric test (Mann-Whitney test) or paired t test comparing between treatment group and its control was considered as statistically significant.

Results

Level of STAT mRNA suppression was used as a marker to determine whether endocytosis pathway involved in cellular uptake of injected dsSTAT into shrimp gill and hepatopancreatic cells. Shrimp were pre-injected with drug inhibitors (Cpz and BafA) to block clathrin endocytosis pathway before injection of dsSTAT. Thereafter, suppression of STAT mRNA in hepatopancreas and gill tissues of the treated shrimp were monitored and compared with the suppression level of the control shrimp (without drug treatment).

Effect of two endocytosis inhibitors on RNAi in shrimp hepatopancreas

In the first experiment, two doses of drugs (1.8 and 9.0 μg of Cpz and 1.8 and 3.0 μg of BafA per one gram of shrimp body weight) were used to block the shrimp

clathrin-mediated endocytosis. The relative transcript of STAT in hepatopancreas of the unblocked shrimp was significantly suppressed by approximately 40% from the control levels (STAT mRNA level of shrimp injected with drug-dissolved solvents (NaCl for Cpz or EtOH for BafA, respectively) (Figure 1a and 1b). However, suppression level of shrimp pre-treated with two doses of Cpz or BafA were significantly reduced to approximately 10% from the control levels (STAT mRNA level of shrimp injected with Cpz or BafA without dsSTAT). Another experiment, the dose 9 μg/g of Cpz and 3.0 μg/g of BafA were used, shrimp were first injected with NaCl or drugs before injection with NaCl or dsSTAT. Compared to the suppression control (Na-Na/Na-St and Et-Na/Et-St) in which the RNAi reponse was not affected, the STAT mRNA suppression of shrimp after blocking with Cpz (Cpz-Na/ Cpz-St) and with BafA (Baf-Na/Baf-St) were recovered approximately 18% and 29%, respectively (Figure 1c and 1d). However, the change of RNAi efficiency of STAT after treatment with Cpz was not statistically different. Taken the results together, it indicated that inhibition of clathrin-mediated endocytosis affected the dsSTAT uptake in shrimp hepatopancreas resulting in reduction of RNAi-mediated STAT suppression.

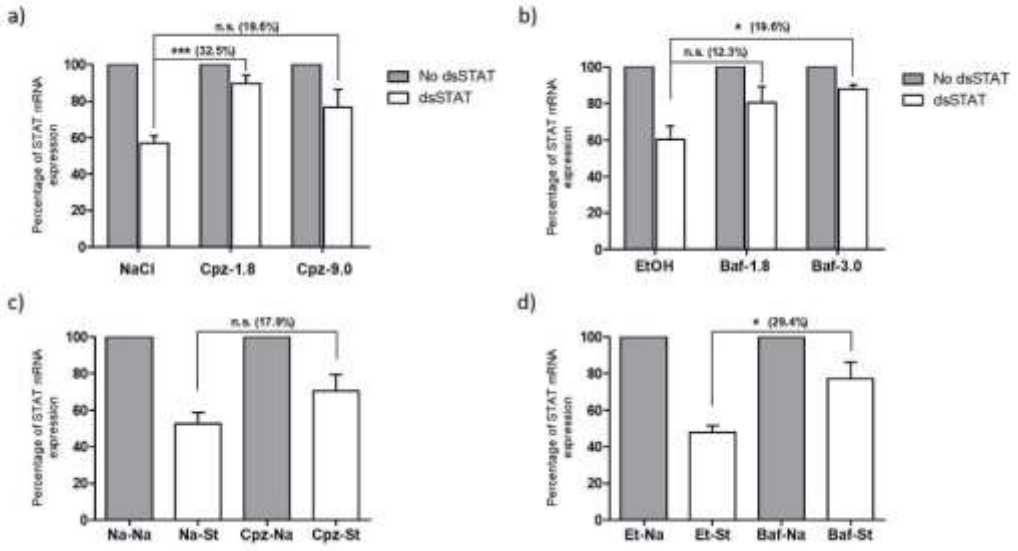

Fig. 1. Effect of inhibitors (chlorpromazine (Cpz) and bafilomycin A1 (Baf)) on endocytic uptake of injected dsRNA into shrimp hepatopancreatic cells. Shrimp (n=3-9/group) were preinjected with the solvents [NaCl (Na) or EtOH (Et)] and drug inhibitors [(a) Cpz (at 1.8 or 9 μg/g of shrimp) or (b) Baf (at 1.8 or 3 μg/g of shrimp)] before injection of NaCl (no dsSTAT) or dsSTAT (St). Twelve hours later, relative expression of STAT mRNA in hepatopancreas of shrimp in each group was monitored by RT-PCR and plotted as mean +/- SEM. Different percentage of STAT mRNA expression of the shrimp treated and untreated with drug are presented. The statistical analysis was performed by Mann-Whitney test at p-value less than 0.05 (*) and less than 0.001 (***). Another set of experiment was performed (n=5-10/group) (c and d). Different percentage of STAT mRNA expression of the shrimp treated (Cpz-St and Baf-St) and untreated with drug (Na-St and Et-St) are presented. The statistical analysis was performed by paired t test at p-value less than 0.05 (*).

Effect of two endocytosis inhibitors on RNAi in shrimp gills

In the experiments mentioned in 3.1, effect of two endocytosis inhibitors on STAT suppression was also determined in gill tissue of the same shrimp. In contrast to hepatopancreas, the results showed levels of STAT suppression after blocking with two drugs (Cpz and BafA) were not significantly reduced (Figure 2a-d). It indicated that inhibition of clathrin-mediated endocytosis did not affect the dsSTAT uptake in shrimp gill tissue.

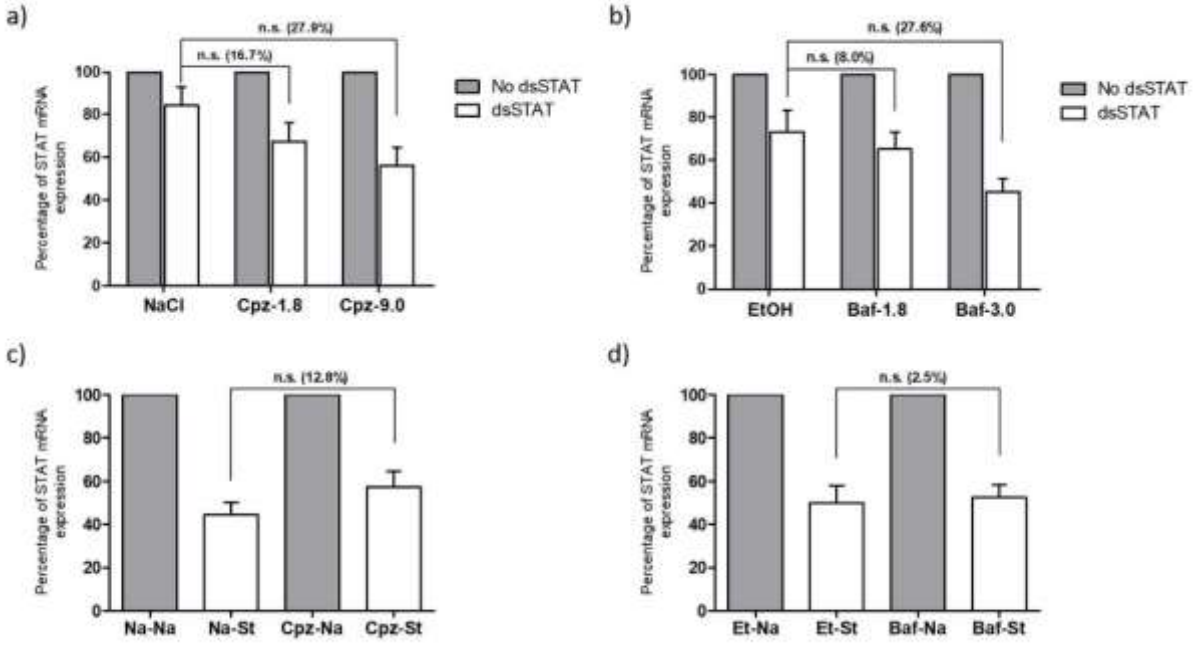

Fig. 2. Effect of inhibitors (chlorpromazine (Cpz) and bafilomycin A1 (Baf)) on endocytic uptake of injected dsRNA into shrimp gill cells. Shrimp (n=3-9/group) were pre-injected with the solvents [NaCl (Na) or EtOH (Et)] and drug inhibitors [(a) Cpz (at 1.8 or 9 μg/g of shrimp) or (b) Baf (at 1.8 or 3 μg/g of shrimp)] before injection of NaCl (no dsSTAT) or dsSTAT (St). Twelve hours later, relative expression of STAT mRNA in hepatopancreas of shrimp in each group was monitored by RT-PCR and plotted as mean +/- SEM. Different percentage of STAT mRNA expression of the shrimp treated and untreated with drug are presented. The statistical analysis was performed by Mann-Whitney test. Another set of experiment was performed (n=5-10/group) (c and d). Different percentage of STAT mRNA expression of the shrimp treated (Cpz-St and Baf-St) and untreated with drug (Na-St and Et-St) are presented. The statistical analysis was performed by paired t test.

Discussion

In the last few years, the role of endocytic pathway in cellular uptake of dsRNA has been studied in several insects either using drug inhibitors (Cappelle et al., 2016; Saleh et al., 2006; Ulvila et al., 2006; Xiao et al., 2015) or RNAi dependent silencing of the key genes in the pathway (Cappelle et al., 2016; Ulvila et al., 2006; Xiao et al., 2015). In most insect species, either SID-1 like transmembrane protein (Aronstein et

al., 2006; Miyata et al., 2014) or endocytosis (Ulvila et al., 2006; Winston et al., 2002; Xiao et al., 2015) or both (Cappelle et al., 2016) is required for cellular importation of dsRNA. There is no consensus about which pathway is involved in dsRNA uptake for several insects.

In shrimp, our previous study (Maruekawong et al., 2018) showed that the *Lv*SID-1 is involved in cellular uptake of injected dsRNA into shrimp gills and hemocytes. Whether an endocytic pathway was participated in this process was investigated in this study. By using pharmacological inhibitors (Cpz and BafA) in conjunction of RNAi of STAT as a marker gene, STAT suppression was diminished by both drugs in shrimp hepatopancreas. In contrast, these Cpz and BafA did not show any significant effect on STAT silencing in gill tissue. It indicated that the injected dsRNA taken up into shrimp hepatopancreas requires the clathrin-mediated endocytosis pathway. However, this pathway does not seem to play an important role in delivering that dsRNA into shrimp gill. In conclusion, when dsRNA being circulated in shrimp body cavity, the SID-1 mediated pathway is a major mechanism in cellular uptake of dsRNA into shrimp gill and hemocyte cells (Maruekawong et al., 2018) while clathrin mediated endocytosis is required in dsRNA uptake of shrimp hepatopancreatic cells. Nevertheless, because dsRNA does not affect the *Lv*SID-1 mRNA expression in hepatopancreas, the *Lv*SID-1 requirement in dsRNA uptake via over expression strategy couldn't be performed (Maruekawong et al., 2018). Therefore, the possible involvement of the *Lv*SID-1 (together with clathrin endocytosis) in dsRNA delivery into shrimp hepatopancreatic cells is still not excluded.

From these knowledge, factors such as species of organism and examined tissues have to be taken into account when elucidating dsRNA uptake mechanism. For instance, two closely related species of coleopteran, *Tribolium castaneum* (Tomoyasu et al., 2008) and *Diabrotica virgifera* (Miyata et al., 2014) require different mechanisms for dsRNA uptake. The latter needs the SID-1 for this process whereas the former does not and requires endocytosis. Uptake of injected dsRNA into shrimp hepatopancreatic cells required endocytic pathway, however this pathway did not play important role in dsRNA delivery into gill tissue (this study). Moreover, the introduced dsRNA from different route may utilized different mechanism for cellular dsRNA uptake. This work, the dsRNA was introduced into shrimp by injection. Mechanism identified in this study and our previous study (Maruekawong et al., 2018) was used to take up the dsRNA that being circulated in the shrimp body cavity into the hemolymph contacted cells in gill and hepatopancreas tissues. Other routes of dsRNA administration such as feeding and soaking may require different pathway, which is needed to be investigated.

References

1. Aronstein, K., Pankiw, T., Saldivar, E., 2006. SID-I is implicated in systemic gene silencing in the honey bee. Journal of apicultural research 45, 20-24.
2. Assavalapsakul, W., Kiem, H.K.T., Smith, D.R., Panyim, S., 2014. Silencing of PmYPR65 receptor prevents yellow head virus infection in *Penaeus monodon*. Virus Research 189, 133-135.
3. Cappelle, K., de Oliveira, C.F., Van Eynde, B., Christiaens, O., Smagghe, G., 2016. The involvement of clathrin-mediated endocytosis and two Sid-1-like transmembrane proteins in double-stranded RNA uptake in the Colorado potato beetle midgut. Insect molecular biology.

4. Escobedo-Bonilla, C.M., 2011. Application of RNA Interference (RNAi) against Viral Infections in Shrimp: A Review. J Antivir Antiretrovir S9.
5. Huvenne, H., Smagghe, G., 2010. Mechanisms of dsRNA uptake in insects and potential of RNAi for pest control: a review. Journal of insect physiology 56, 227-235.
6. Labreuche, Y., Veloso, A., de la Vega, E., Gross, P.S., Chapman, R.W., Browdy, C.L., Warr, G.W., 2010. Non-specific activation of antiviral immunity and induction of RNA interference may engage the same pathway in the Pacific white leg shrimp *Litopenaeus vannamei*. Developmental and comparative immunology 34, 1209-1218.
7. Luo, Y., Wang, X., Yu, D., Kang, L., 2012. The SID-1 double-stranded RNA transporter is not required for systemic RNAi in the migratory locust. RNA Biol 9, 663-671.
8. Maruekawong, K., Tirasophon, W., Panyim, S., Attasart, P., 2018. Involvement of LvSID-1 in dsRNA uptake in *Litopenaeus vannamei*. Aquaculture 482, 65-72.
9. Miyata, K., Ramaseshadri, P., Zhang, Y., Segers, G., Bolognesi, R., Tomoyasu, Y., 2014. Establishing an In Vivo Assay System to Identify Components Involved in Environmental RNA Interference in the Western Corn Rootworm. PLoS ONE 9, e101661.
10. Ongvarrasopone, C., Roshorm, Y., Panyim, S., 2007. A simple and cost effective method to generate dsRNA for RNAi studies in invertebrates. ScienceAsia 33, 35-39.
11. Phetrungnapha, A., Kondo, H., Hirono, I., Panyim, S., Ongvarrasopone, C., 2015. Molecular cloning and characterization of Mj-mov-10, a putative RNA helicase involved in RNAi of kuruma shrimp. Fish & Shellfish Immunology 44, 241-247.
12. Posiri, P., Ongvarrasopone, C., Panyim, S., 2013. A simple one-step method for producing dsRNA from *E. coli* to inhibit shrimp virus replication. J Virol Methods 188, 64-69.
13. Sagi, A., Manor, R., Ventura, T., 2013. Gene Silencing in Crustaceans: From Basic Research to Biotechnologies. Genes 4, 620-645.
14. Saleh, M.C., van Rij, R.P., Hekele, A., Gillis, A., Foley, E., O'Farrell, P.H., Andino, R., 2006. The endocytic pathway mediates cell entry of dsRNA to induce RNAi silencing. Nat Cell Biol 8, 793-802.
15. Shekhar, M.S., Lu, Y., 2009. Application of Nucleic-acid-based Therapeutics for Viral Infections in Shrimp Aquaculture. Marine Biotechnology 11, 1-9.
16. Sutthangkul, J., Amparyup, P., Charoensapsri, W., Senapin, S., Phiwsaiya, K., Tassanakajon, A., 2015. Suppression of shrimp melanization during white spot syndrome virus infection. The Journal of biological chemistry 290, 6470-6481.
17. Tomoyasu, Y., Miller, S.C., Tomita, S., Schoppmeier, M., Grossmann, D., Bucher, G., 2008. Exploring systemic RNA interference in insects: a genome-wide survey for RNAi genes in Tribolium. Genome Biol 9, R10.
18. Ulvila, J., Parikka, M., Kleino, A., Sormunen, R., Ezekowitz, R.A., Kocks, C., Ramet, M., 2006. Double-stranded RNA is internalized by scavenger receptor-mediated endocytosis in *Drosophila* S2 cells. The Journal of biological chemistry 281, 14370-14375.

19. Wang, L.H., Rothberg, K.G., Anderson, R.G., 1993. Mis-assembly of clathrin lattices on endosomes reveals a regulatory switch for coated pit formation. J Cell Biol 123, 1107-1117.
20. Winston, W.M., Molodowitch, C., Hunter, C.P., 2002. Systemic RNAi in C. elegans requires the putative transmembrane protein SID-1. Science 295, 2456-2459.
21. Xiao, D., Gao, X., Xu, J., Liang, X., Li, Q., Yao, J., Zhu, K.Y., 2015. Clathrin-dependent endocytosis plays a predominant role in cellular uptake of double-stranded RNA in the red flour beetle. Insect Biochem Mol Biol 60, 68-77.
22. Xu, H.J., Chen, T., Ma, X.F., Xue, J., Pan, P.L., Zhang, X.C., Cheng, J.A., Zhang, C.X., 2013. Genome-wide screening for components of small interfering RNA (siRNA) and micro-RNA (miRNA) pathways in the brown planthopper, Nilaparvata lugens (*Hemiptera: Delphacidae*). Insect molecular biology 22, 635-647.
23. Xu, W., Han, Z., 2008. Cloning and Phylogenetic Analysis of Sid-1-Like Genes from Aphids. Journal of Insect Science 8, 30.
24. Yamamoto, A., Tagawa, Y., Yoshimori, T., Moriyama, Y., Masaki, R., Tashiro, Y., 1998. Bafilomycin A₁ Prevents Maturation of Autophagic Vacuoles by Inhibiting Fusion between Autophagosomes and Lysosomes in Rat Hepatoma Cell Line, H-4-II-E Cells. Cell Structure and Function 23, 33-42.
25. Yao, D., Ehrlich, M., Henis, Y.I., Leof, E.B., 2002. Transforming Growth Factor-β Receptors Interact with AP2 by Direct Binding to β2 Subunit. Molecular Biology of the Cell 13, 4001-4012.

PmEEA1, the early endosomal protein is employed by YHV for a successful infection in *Penaeus monodon*

Yellow head disease (YHD) is an infectious disease of *Penaeus monodon* which caused by yellow head virus (YHV). YHV infection leads to 100% shrimp mortality within 3-5 days. Currently, an effective method to prevent or cure shrimp from YHV infection has been elucidated. Therefore, the molecular mechanism underlying YHV infection should be examined. In this study, early endosome antigen 1 (EEA1) protein that involved in the tethering step of the vesicle and early endosome fusion was investigated during YHV infection. The open reading frame of *P. monodon* EEA1 (PmEEA1) was cloned and sequenced as 3,000 bp encoding a putative protein of 999 amino acids. It consists of Zinc finger C_2H_2 domain signature at the N-terminus and FYVE domain at the C-terminus. Suppression of PmEEA1 by specific dsRNA in shrimp showed an inhibition of YHV replication at both of 24 and 48 hours post YHV injection (hpi). On the other hand, shrimp received only NaCl without any dsRNA showed high YHV levels at approximately one hundred thousand times over a 24 hpi to 48 hpi. Moreover, silencing of PmEEA1 by specific dsRNA followed by YHV challenge demonstrated a delay in shrimp mortality from 60 hpi to 168 hpi when compared to the control. These results indicated that YHV required PmEEA1 to invade into the shrimp cells. In addition, PmEEA1 is a potential target protein that can be used to improve the method for prevention of YHV infection in *P. monodon*.

Introduction

YHD outbreak has been reported since 1990 as an epizootic in the eastern, central and southern parts of Thailand, and caused shrimp production loss worldwide. A causative agent of this disease is Yellow head virus (YHV) (1). YHV is a positive-sense single stranded RNA virus that is classified into genus *Okavirus*, family *Roniviridae*, in the order *Nidovirales* (2, 3) and closely related to gill-associated virus (GAV) from Australia particularly in terms of the nucleotide and amino acid sequences, clinical, histological, and morphological observations (4, 5). YHV has a particle size approximately 50-60 × 190-200 nm with enveloped bacilliform surrounded by prominent peplomers or spikes (6). The genome of the virus contains approximately 27 kb in length and consists of ORF1a, ORF1b, ORF2 and ORF3. In addition, an enveloped glycoprotein, gp116 involving in an entry process of YHV is encoded from ORF3 (7).

Currently, the major route of YHV entry into the shrimp cell has been characterized as clathrin-mediated endocytosis. The clathrin heavy chain and AP17 protein that involved in this step were identified in *Penaeus monodon* (8, 9). After YHV internalization via clathrin dependent pathway, it is packed into the clathrin coated vesicle and moved to the next station. The vesicle containing YHV requires a small GTPase Rab5 protein to regulate the transportation from plasma membrane where the vesicle budding toward to the sorting station early endosome. *P. monodon* Rab5 was identified and showed colocalization with YHV particles (10, 11). For the tethering step at the early endosomal compartment, Rab5 protein binds with Rab5 effector that is early endosome antigen 1 (EEA1) to promote the vesicle membrane and early endosome fusion resulting a cargo protein including the virus transported toward inside early endosome (12).

Rab5 effector EEA1 functions with SNAREs complexes to promote the transported vesicle-endosome membrane tethering and fusion (12). EEA1 location is associated with

the early endosome and showed the colocalization with Rab5 protein (13). The EEA1 structure is a long parallel coiled coil homodimer that contains C_2H_2 zinc finger (ZF) domain at the N-terminus and FYVE domain at the C-terminus (14). Tightly interacting between the N-terminal ZF domain of EEA1 with Rab5 protein and recruit SNARE complexes facilitate docking and fusion process. Furthermore, the fusion step of the vesicle and early endosome requires phosphatidylinositol-3-OH kinase (PI(3)K) activity, which the C-terminal FYVE domain of EEA1 can bind directly to the product of PI(3)K phosphatidylinositol-3-phosphate (PtdIns3P). Taken together, the specific binding with Rab5-GTP bound form and coordinates with PI(3)K activity involves in the vesicle-early endosome membrane fusion (15-18). Furthermore, EEA1 has been shown to colocalization with semliki forest virus (SFV) (19) and hepatitis C virus (HCV) (20). In addition, the EEA1 protein also demonstrated the colocalization with YHV (data not shown) suggesting that the protein may involve in YHV infection process. From our previous study found that YHV utilized clathrin heavy chain, Rab5 and Rab7 protein for invading into the shrimp host cell (9, 11, 21). It was possible that YHV required Rab5 effector early endosome antigen 1 (EEA1) protein to help the virus infection. Therefore, a role of EEA1 for the YHV infection and shrimp mortality in *P. monodon* was investigated.

Materials and methods

The black tiger shrimp

Penaeus monodon or the black tiger shrimp were obtained from Choochai farm in Chonburi province and shrimp genetic improvement center in Surat Thani province, Thailand. Shrimp were acclimatized for at least 2 days and maintained in large containers with oxygenated sea water at 10-30 ppt salinity before use in the experiments. They were fed with commercial feed every day. The water was changed every 2 days.

Cloning of the full-length open reading frame of PmEEA1

Coding region of EEA1 from *Marsupenaeus japonicus* kindly provided by Dr. Hidehiro Kondo was used to design a specific primers amplifying the region of PmEEA1. Firstly, total RNA from ovary was extracted by Tri Reagent® (Molecular Research Center) and cDNA was synthesized by Improm-II™ reverse transcriptase (Promega) according to the manufacturer protocol. The full-length open reading frame of EEA1 was amplified by Q5 DNA polymerase (New England Biolabs) using cdEEA1-F and cdEEA1-R primers (Table 1) with an expected size approximately 3,000 bp. The PCR condition was amplified following condition: denaturation at 98°C for 30 sec, 35 cycles of 98°C for 10 sec, 55°C for 20 sec, 72°C for 3 min. The PCR product was purified and cloned into pGEMT-easy vector and subjected for sequencing using T7, SP6, EEA1-Fseq, EEA1-Rseq and asEEA1-R2 (Table 1) by First Base Co, Ltd. (Malaysia).

Nucleotide and protein of PmEEA1 sequence analysis

The nucleotide sequences of PmEEA1 was confirmed and analyzed by BLASTN programs search nucleotide databases (https://blast.ncbi.nlm.nih.gov). Prediction of molecular weight and isoelectric point (PI) of the protein were performed by Expert Protein Analysis System (www.expasy.org). Conserved motifs of the deduced amino acid were scanned by Scan Prosite tool (http://prosite.expasy.org/scanprosite). Amino acid sequences of EEA1 protein from several organisms were supported from GenBank database. Phylogenetic analysis was performed by using Phylogeny.fr with "A la Carte"

mode (http://www.phylogeny.fr) based on neighbor-joining method and 1000 replicates of bootstrap with distance methods (22, 23).

Construction of two dsRNAs targeting PmEEA1 mRNA

Recombinant plasmid containing stem-loop of dsRNA of PmEEA1 was constructed in pET-17b (Novagen) vectors. Two plasmids containing dsRNA-Cter and dsRNA-Nter which targeting near stop codon and start codon of *PmEEA1* gene, respectively were constructed. Sense-loop regions of the dsRNAs located on near stop and start codon were amplified from the first-stranded cDNA by specific primers, sEEA1-F1 and lEEA1-R1 for dsRNA-Cter and nSLEEA1-F1 and nSLEEA1-R1 for dsRNA-Nter (Table 1). In addition, antisense regions were amplified by asEEA1-F2 and asEEA1-R2 for dsRNA-Cter and nASEEA1-F2 and nASEEA1-R2 for dsRNA-Nter (Table 1). All of PCR fragments were gel-purified and subjected to restriction enzyme digestion. The purified fragments of the sense-loop and antisense of the Cter region were digested with *Eco*RI and ligated together by T4 DNA ligase (NEB). Then, the sense fragment was digested by *Xba*I whereas the antisense fragment was cut by *Xho*I. The ligated fragment of the sense and antisense of PmEEA1 was cloned into pET-17b to obtain pET-17b-dsRNA-Cter. In addition, the PCR fragment of sense-loop of the Nter region was cloned into pGEM-3Zf+ at *Xba*I and *Kpn*I site and then the antisense fragment of the Nter region was subsequently cloned into *Kpn*I and *Eco*RI site of this recombinant plasmid. Then, the sense-loop and antisense fragments of the Nter region in pGEM-3Zf+ was cut and subcloned into pET-17b vector to construct recombinant plasmid named pET-17b-dsRNA-Nter. Both the recombinant plasmids were used for dsRNA production by *in vivo* bacterial expression.

Production of dsRNAs by in vivo bacterial expression

The recombinant plasmid pET-17b-dsRNA-Cter and Nter were transformed into a RNase III mutant HT115 *E.coli* strain. DsRNAs expression were induced by 0.1 mM IPTG. Then, they were extracted by using ethanol method (24, 25). The quality of the dsRNAs were characterized by ribonuclease digestion assay using RNase A and RNase III digestions. Concentration of dsRNA was estimated by agarose gel electrophoresis comparing with the intensity of 100 bp DNA marker.

Yellow head virus (YHV) preparation

YHV stock was prepared by hemolymph of YHV infected moribund the black tiger shrimp. The hemolymph was drawn with AC-1 solution (27 mM Sodium citrate, 34.33 mM NaCl, 104.5 mM Glucose, 198.17 mM EDTA, pH 7.0), at ratio 1:1 and centrifuged at 20,000 ×g for 20 minute at 4 °C to remove hemocyte debris. Only supernatant was collected and separated the virus from hemolymph by ultracentrifugation at 100,000 ×g for 1 h. YHV pellet was dissolved with 150 mM NaCl and stored at -80°C until used. The viral titer that caused 100% mortality within 3-4 days was used in this study.

Shrimp injection by dsRNAs

The efficiency of dsRNA-Cter and N-ter were examined by injection of dsRNAs into shrimp hemocoel. Shrimp were injected with 2.5 µg. g^{-1} shrimp of dsRNA-Cter, -Nter, C+Nter and unrelated dsRNA-GFP dissolved in 150 mM NaCl. Injection of 150 mM NaCl was used as control. After 24 h post dsRNA injection, gill of the individual shrimp

was collected for total RNA extraction. Suppression effect of dsRNAs were analyzed by reverse-transcription PCR (RT-PCR) to determine PmEEA1 mRNA level.

Study of the knock down effect by dsRNAs upon YHV infection and shrimp mortality assay

In order to investigate the silencing effect of PmEEA1 upon YHV infection, shrimp were injected with 2.5 µg. g^{-1} shrimp of the combination of dsRNA-C+Nter (1.25 µg. g^{-1} shrimp each) or unrelated dsRNA-GFP following YHV challenged after 24 h post dsRNA injection. Five shrimp per group were performed. Twenty four and forty eight hours post YHV injection (hpi), gill of individual shrimp was collected to analyze the PmEEA1 and YHV levels. Moreover, the shrimp mortality of this experiment was recorded every 12 h post YHV injection (hpi) for 144 hpi. Three replicates of the experiments were investigated.

Total RNA extraction and RT-PCR analysis

Total RNA from gill tissue was isolated by Tri Reagent® (Molecular Research Center) following the manufacturer's protocol. Two microgram of the total RNA was used to produce generated to be the first-stranded cDNA by Improm-II™ reverse transcriptase (Promega) using PRT primer (Table 1). PCR products were amplified by using Taq DNA polymerase (New England Biolabs). Multiplex PCR of PmEEA1 (by PmEEA1-F and PmEEA1-R1 primer (Table 1) and PmActin (by PmActin-F and PmActin-R1 (Table 1) transcript levels were amplified under a condition; 95°C for 5 min, 30 cycles of 95°C for 30 s, 61°C for 30 s, and 68°C for 45 s, followed by 68°C for 7 min. The PCR products were analyzed on 1.5% agarose gel. The intensity of each band was quantitated by using Scion Image program. Relative mRNA transcript levels of PmEEA1 was normalized with PmActin level and recorded as an arbitrary unit.

Detection of YHV mRNA levels by quantitative real time PCR (qPCR)

For qPCR analysis, cDNA template was diluted at 1:4 and mixed with qPCR reaction using KAPA™ SYBR® Fast qPCR master mix (2X) ABI Prism™ (KAPABiosystems) following manufacturer's protocol. The qPCR was analyzed by using MasterCycler RealPlex4 from eppendorf. qYHV-F and qYHV-R specific primers (Table X) were used to amplify YHV mRNA. In addition, EF1-α that amplified by EF1α-F and EF1α-R primers (Table X) was used as an internal control. The qPCR condition was followed according to this condition: 95°C for 3 min; 40 cycles of 95°C for 5 s, 60°C for 30 s. The cycle threshold (Ct) value of YHV and EF1-α was compared and calculated by $2^{-\Delta\Delta C_T}$ method (26).

Statistical analysis

The relative transcription levels of PmEEA1 or YHV that normalized with PmActin or EF1α was presented as mean ± SD. In addition, cumulative percent shrimp mortality was plotted as mean ± SD. A significant difference of the experiment groups was examined by analysis of variance (ANOVA). A probability *(P)* value less than 0.05 was accepted to define a significant difference.

Table 1 Primer sequences used in this study

Name	Sequence (5'--> 3')	Purposes
cdEEA1-F	ATGTCAGAGAGAGGAATG	Amplification of full-length cDNA coding region of PmEEA1
cdEEA1-R	TCACATTTTTGAAGTGAG	
T7	TAATACGACTCACTATAGGG	Sequencing of PmEEA1 nucleotides
SP6	ATTTAGGTGACACTATAG	
EEA1-Fseq	GCAGGGTTGAAGGAAGAGATG	
EEA1-Rseq	CCCTTAGCAGCTTCTCTCTCC	
PRT	CCGGAATTCAAGCTTCTAGAGGATCCTT TTTTTTTTTTTTTT	The first strand cDNA synthesis
sEEA1-F1	*Xba*I GCTCTAGAACAAAATGAAGCCAAGCAGC	Construction of the recombinant plasmid expressing dsRNA-Cter targeting PmEEA1 mRNA
lEEA1-R1	*Eco*RI GGAATTCTAGCAACCTCAGCCTCCAG	
asEEA1-F2	*Xho*I CCGCTCGAGACAAAATGAAGCCAAGCAGC	
asEEA1-R2	*Eco*RI GGAATTCGGCATCAATTTCAAGCTGG	
nSLEEA1-F1	*Xba*I GCTCTAGAGGGCTTCTTGTGTCCAAC	Construction of the recombinant plasmid expressing dsRNA-Nter targeting PmEEA1 mRNA
nSLEEA1-R1	*Kpn*I GGGGTACCACCTTTTCAGCTTGTAGGG	
nASEEA1-F2	*Eco*RI GGAATTCGGGCTTCTTGTGTCCAAC	
nASEEA1-R2	*Kpn*I GGGGTACCCGCAAGGAACTGTTCAAC	
PmEEA1-F	AGCTTGAAATTGATGCCCAGAAG	Detection of PmEEA1 mRNA level
PmEEA1-R	TTGTTGCAGCTGTGGCAATTTAG	
PmActin-F	GACTCGTACGTGGGCGACGAGG	Detection of PmActin mRNA level
PmActin-R1	AGCAGCGGTGGTCATCTCCTGCTC	
qYHV-F	ATCATCAGCTCACAGGCAAGTTCC	Detection of YHV mRNA level by realtime PCR
qYHV-R	GGGTCTAAATGGAGCTGGAAGACC	
EF-1α-F	GAACTGCTGACCAAGATCGACAGG	Detection of EF-1α mRNA level by realtime PCR
EF-1α-R	GAGCATACTGTTGGAAGGTCTCCA	

Results

Cloning and sequence analysis of PmEEA1 coding region

The sequence of early endosome antigen 1 from *Marsupenaeus japonicus* (MjEEA1) (kindly provided by Dr. Hidehiro Kondo) was used to design primers to amplify the coding region of PmEEA1 from ovary of *Penaeus monodon*. Full-length open reading frame sequences of PmEEA1 is 3,000 bp including stop codon (TGA) which encoded a putative protein for 999 amino acids (Supplementary Fig. 1). The coding region sequence of PmEEA1 was submitted into the GenBank database under the accession number..... An estimated molecular weight and a pI of PmEEA1 protein are 112.6 kDa and 5.04, respectively. The protein contains a signature domain of EEA1 protein which are two Zinc finger C_2H_2 type domain signature at the amino acid 43-64

and 73-94 and the FYVE domain at the amino acid 938-996. The signature domains are conserved in both invertebrates and vertebrates including CeEEA1, DrEEA1, HsEEA1, LaEEA1, LpEEA1, and RnEEA1 (Fig. 1 and Table 2). Phylogenetic tree analysis revealed that PmEEA1 was closely related to the invertebrate group and obviously separated from the vertebrate group (Fig. 2).

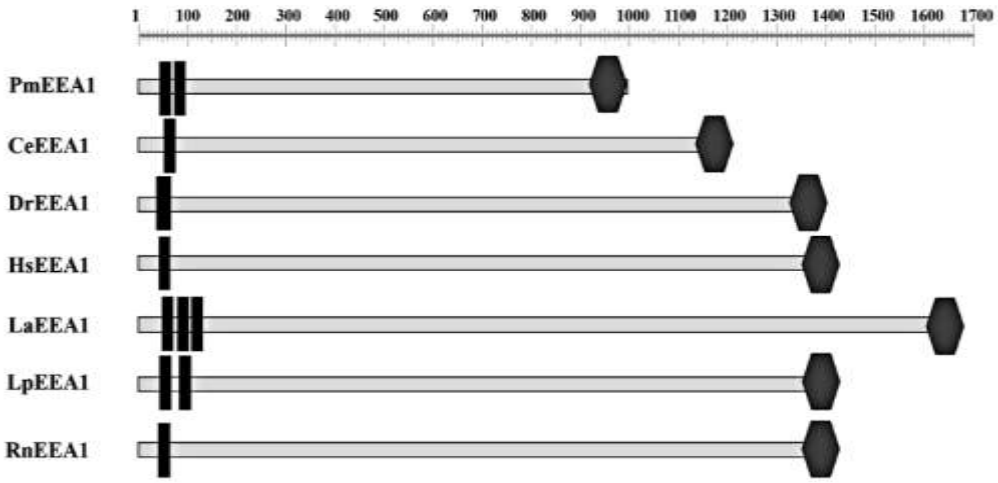

Fig. 1. The schematic of the predicted protein domain of early endosome antigen 1 (EEA1) as well as a number of homologues among several species. The amino acid number of EEA1 protein presented on each organism is different but containing signature motifs of the protein including Zinc finger C_2H_2 type domain (▌) at N-terminus and FYVE domain (⬮) at C-terminus. *Penaeus monodon* EEA1 (PmEEA1) possess 999 amino acids which compose of two domains of Zinc finger C_2H_2 signature motifs at the position aa 43-64 and aa 73-94 and one FYVE domain at aa 938-996. EEA1 protein from several species including *Penaeus monodon* (PmEEA1), *Caenorhabditis elegans* (CeEEA1), *Danio rerio* (DrEEA1), *Homo sapiens* (HsEEA1), *Lingula anatine* (LaEEA1), *Limulus Polyphemus* (LpEEA1), *and Rattus norvegicus* (RnEEA1) were used for domain analysis. Genbank accession number of each organism was demonstrated in Table 2.

Production of two dsRNAs which are dsRNA-Cter and dsRNA-Nter targeting their PmEEA1 mRNA region

In order to investigate the function of PmEEA1, RNAi technology was performed. Two dsRNAs which are dsRNA-Cter and dsRNA-Nter of PmEEA1 mRNA were constructed and produced by *in vivo* bacterial expression. In addition, dsRNA-GFP was produced and used as an unrelated dsRNA control. Then, the hairpin dsRNAs were extracted by ethanol method and verified by RNase digestion assay. All of dsRNAs which are dsRNA-Cter, -Nter, and -GFP could be cleaved by RNase III but not by RNase A suggesting that they were a good quality of dsRNA. An expected size of these dsRNAs were approximately 400 bp (Supplementary Fig.2).

Table 2 Early endosome antigen 1 (EEA1) proteins used for multiple sequence alignment and phylogenetic analysis

Abbreviations	Species	Accession number
AcEEA1	*Aplysia californica*	XP_005095892.2
BaEEA1	*Balaenoptera acutorostrata scammoni*	XP_007166165.1
BgEEA1	*Biomphalaria glabrata*	XP_013093515.1
CeEEA1	*Caenorhabditis elegans*	NP_001024127.1
DrEEA1	*Danio rerio*	XP_003200485.1
FhEEA1	*Fundulus heteroclitus*	XP_012731526.1
HsEEA1	*Homo sapiens*	NP_003557.2
LaEEA1	*Lingula anatina*	XP_013419201.1
LpEEA1	*Limulus polyphemus*	XP_013777228.1
NgEEA1	*Nannospalax galili*	XP_008822059.1
ObEEA1	*Octopus bimaculoides*	XP_014782058.1
PmEEA1	*Penaeus monodon*	
TcEEA1	*Tupaia chinensis*	ELW61492.1
TrEEA1	*Takifugu rubripes*	XP_003967354.1
RnEEA1	*Rattus norvegicus*	NP_001101556.1
XtEEA1	*Xenopus tropicalis*	XP_002935361.1

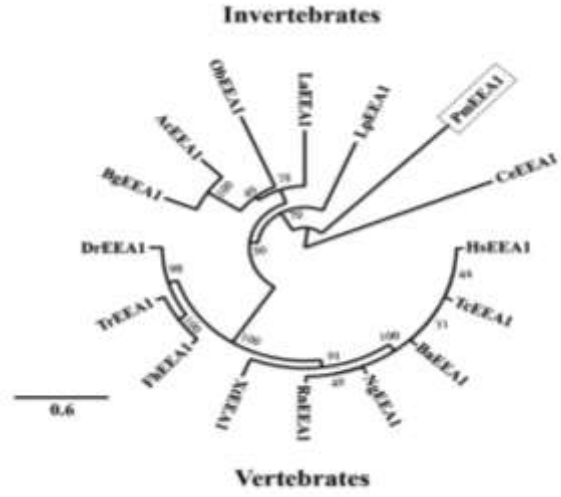

Fig. 2. Phylogenetic analysis of EEA1 protein. The phylogenetic tree was constructed using the Neighbor-joining method based on the full amino acid sequences of EEA1 with bootstrap value of 1,000. Organisms that used for the tree construction were *Aplysia californica* (AcEEA1), *Balaenoptera acutorostrata scammoni* (BaEEA1), *Biomphalaria glabrata* (BgEEA1), *Caenorhabditis elegans* (CeEEA1), *Danio rerio* (DrEEA1), *Fundulus heteroclitus* (FhEEA1), *Homo sapiens* (HsEEA1), *Lingula anatine* (LaEEA1), *Limulus Polyphemus* (LpEEA1), *Nannospalax galili* (NgEEA1), *Octopus bimaculoides* (ObEEA1),

Penaeus monodon (PmEEA1), *Tupaia chinensis* (TcEEA1), *Takifugu rubripes* (TrEEA1), *Rattus norvegicus* (RnEEA1), *and Xenopus tropicalis* (XtEEA1). Genbank accession number of each species was shown in Table 2.

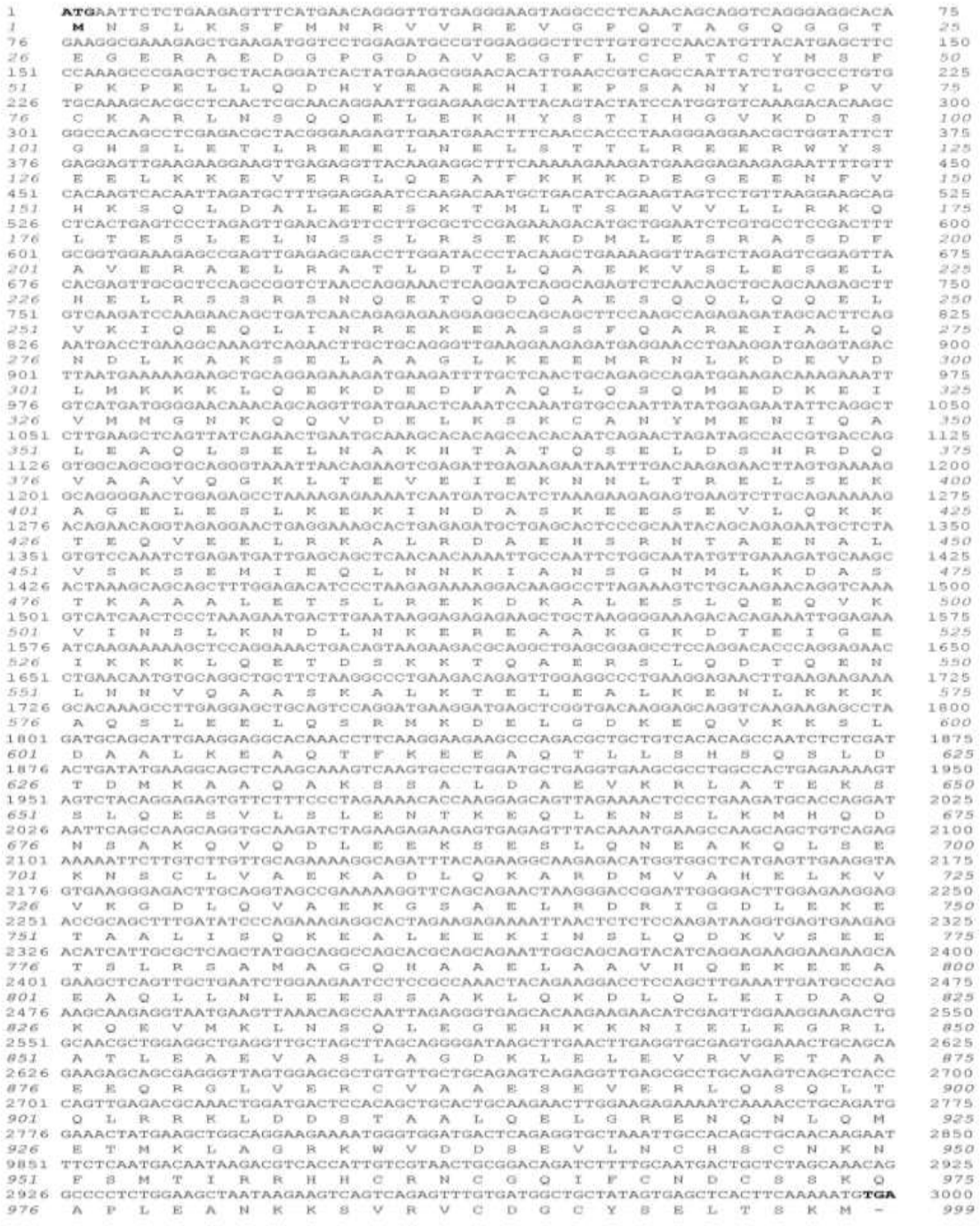

Supplementary Fig. 1. The nucleotide and deduced amino acid sequences of *Penaeus monodon* Early endosome antigen 1 (PmEEA1). The coding region of PmEEA1 is 3,000 bp encoding the protein of 999 amino acid. Start or stop codons are in bold letters; the dash represents the stop codon. The nucleotide sequences was published in the GenBank database under the accession number……..

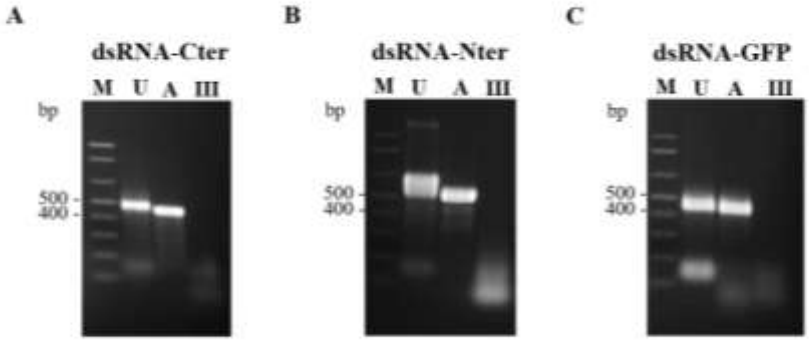

Supplementary Fig. 2. Quality of targeting PmEEA1 including dsRNA-Cter, dsRNA-Nter and dsRNA-GFP which produced by *in vivo* bacterial expression. The dsRNAs were produced by *in vivo* bacterial expression and then extracted by ethanol method. The dsRNAs were verified by RNase digestion assay. Lane M, U, A, and III represent 1 kb+ DNA ladder, undigested dsRNAs, dsRNA treated with RNase A and dsRNA treated with RNase III, respectively.

Silencing of PmEEA1 mRNA levels by two dsRNAs

The effectiveness of dsRNA-Cter and dsRNA-Nter on silencing of PmEEA1 mRNA were observed. Shrimp were injected with dsRNAs targeting PmEEA1 or unrelated dsRNA-GFP for 24 hours. NaCl injection was employed as an experimental control. The result found that shrimp received dsRNA-Cter and dsRNA-Nter showed a significant reduction of PmEEEA1 mRNA levels at 81% and 76%, respectively. Surprisingly, shrimp injected with a combination between dsRNA-Cter and dsRNA-Nter that called dsRNA-C+Nter hardly detected the levels of the pmEEA1 mRNA. Suppression results of the combination group was approximately 91% when compared to NaCl control group. Interestingly, PmEEA1 mRNA level could be silenced at about 33% in dsRNA-GFP injected shrimp (Fig. 3). This result indicating that PmEEA1 mRNA level could be suppressed by the combination dsRNA-C+Nter.

Knockdown effect of PmEEA1 reduced YHV replication levels

A role of PmEEA1 on YHV life cycle was investigated during YHV replication. The combination dsRNA-C+Nter was used to silence PmEEA1 mRNA target. Therefore, shrimp received the dsRNA at 24 h was challenged with YHV. After 24 and 48 hours post YHV injection (hpi), gill of the individual shrimp and five shrimp per group were used to determine the PmEEA1 and YHV mRNA levels. Injected shrimp with dsRNA-C+Nter following YHV challenge showed the significant reduction of PmEEA1 at 24 and 48 hpi about 82% and 78% when compared to NaCl→YHV control group, respectively. Moreover, shrimp injected with unrelated dsRNA-GFP → YHV showed no significant difference of the PmEEA1 mRNA levels both of 24 and 48 hpi when compared to the control (Fig. 4A).

Level of YHV mRNAs were determined by real time PCR. The YHV levels of NaCl → YHV control group showed fold change as mean ± SD of the levels about 1.37 ± 1.06 and 99,336 ± 117,209, while non-specific dsRNA-GFP → YHV expressed the rate of YHV replication at 1.36 ± 0.47 and 26,530 ± 39,773 at 24 and 48 hpi,

respectively. The time course from 24 to 48 hpi demonstrated high YHV propagation rate of the control groups which were about 100,000 and more than 25,000 times for NaCl → YHV and dsRNA-GFP → YHV groups, respectively. Interestingly, the decreasing levels of the PmEEA1 in the dsRNA-C+Nter → YHV group showed no significant difference of YHV propagation rate between 24 and 48 hpi. The YHV levels of dsRNA-C+Nter → YHV group showed about 1.16 ± 0.53 and 1.28 ± 1.31 at 24 and 48 hpi, respectively (Fig. 4B). The fold change of YHV mRNA levels were compared to NaCl → YHV group at 24 hpi. These results indicated that PmEEA1 was essential for YHV replication.

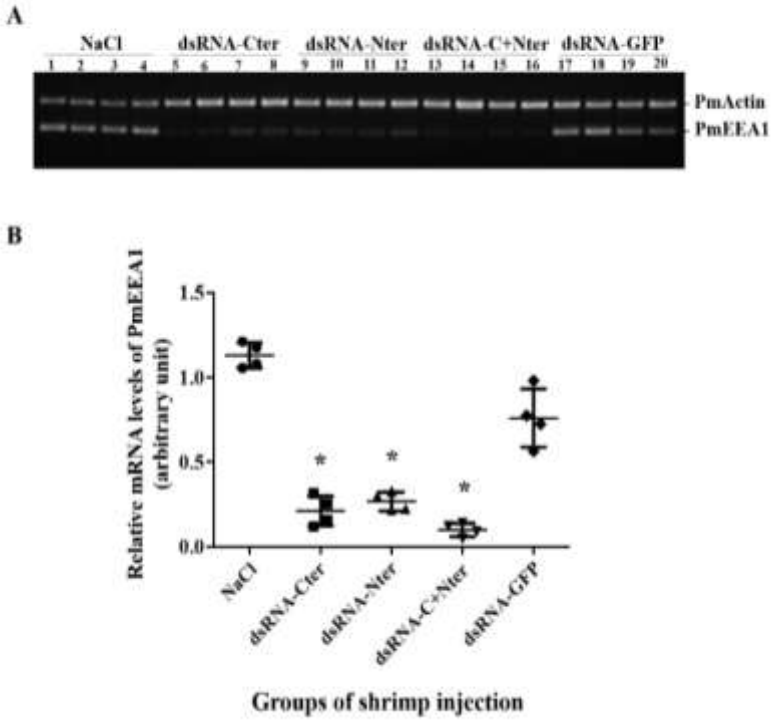

Fig. 3. Effectiveness of two type of dsRNAs targeting PmEEA1 mRNA. A representative gel of RT-PCR products was presented as an expression levels of PmEEA1 and PmActin of shrimp injected with NaCl control (lane 1-4), each dsRNA targeting PmEEA1 which are dsRNA-Cter (lane 5-8) and dsRNA-Nter (lane 9-12), the combination between dsRNA-Cter and -Nter (dsRNA-C+Nter) (lane 13-16) and unrelated dsRNA-GFP (lane 17-20) at 2.5 $\mu g.g^{-1}$ shrimp at 24 h post dsRNA injection (n=4) (A). The relative mRNA expression levels of PmEEA1 normalized with PmActin are shown as mean ± SD (n= 4) (B). (*) Statistically significant difference between dsRNA injected shrimp compared to NaCl injected group ($P < 0.05$).

Silencing effect of PmEEA1in YHV-infected shrimp decreased shrimp mortality

The shrimp mortality was further observed to investigate the involvement of PmEEA1 on YHV infection. There were 10-15 shrimp per group and the experiments were performed for three replicates. Shrimp received dsRNA-C+Nter targeting PmEEA1 mRNA followed by YHV challenge showed a significant delay in shrimp mortality since 60 hpi to 168 hpi when compared to NaCl → YHV and unrelated dsRNA-GFP →

YHV groups (*P* value = 0.05). At 60 hpi, no shrimp in dsRNA-C+Nter → YHV group died whereas shrimp in the control groups of NaCl → YHV and unrelated dsRNA-GFP → YHV had 80% and 50% shrimp mortality, respectively. In addition, at 84 hpi, shrimp in both control groups showed 100% cumulative shrimp mortality. Interestingly, knock down of PmEEA1 in the dsRNA-C+Nter → YHV group demonstrated only 40% of the mortality (Fig. 5). Therefore, this result suggested that YHV required PmEEA1 for a successful infection.

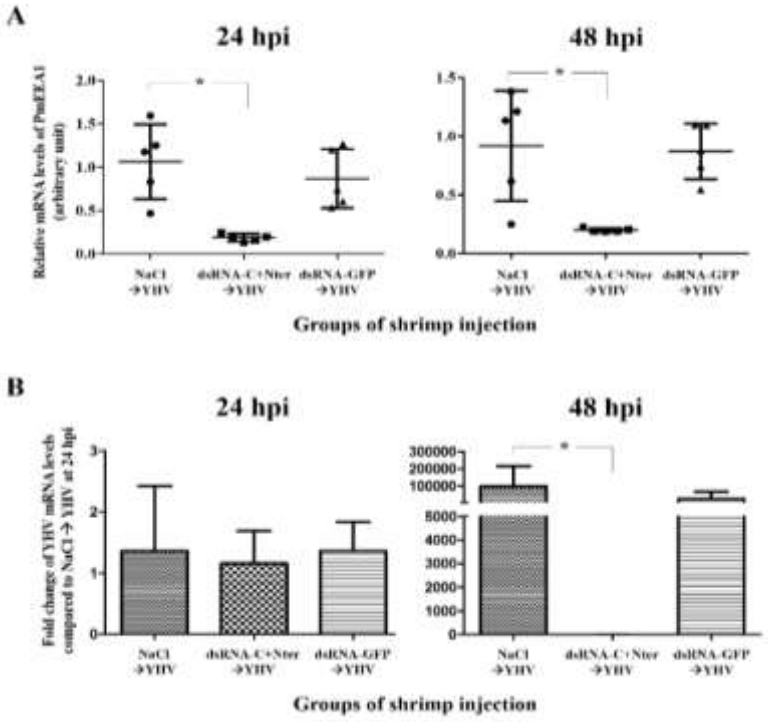

Fig. 4. Effect of PmEEA1 depletion during YHV infection. Shrimp were injected with NaCl alone, dsRNA-C+Nter, and dsRNA-GFP at 2.5 $\mu g.g^{-1}$ shrimp for 24 h followed by YHV challenge and detected at 24 and 48 hpi from gill tissues (n=5). The relative mRNA levels of PmEEA1 normalized with PmActin are present as dot graphs of arbitrary unit of mean ± SD (A). Bar graphs represent the quantitative RT-PCR of fold change of YHV mRNA levels compared to NaCl → YHV at 24 hpi. The result was demonstrated as mean ± SD (B). Asterisks indicate significant differences between experimental group and the control group ($P < 0.05$).

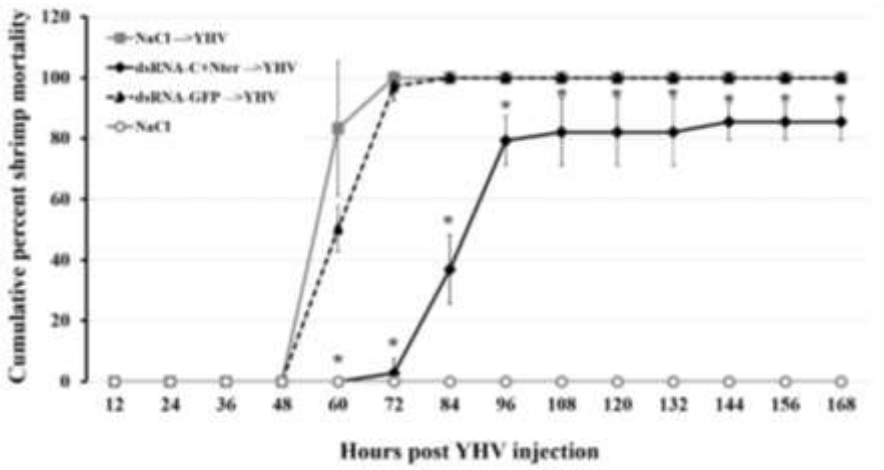

Fig. 5. Silencing effect of PmEEA1 by the combination dsRNA-C+Nter on YHV infection delayed cumulative shrimp mortality. The cumulative percent mortality of shrimp injected with NaCl, dsRNA targeting PmEEA1 (dsRNA-C+Nter), unrelated dsRNA-GFP at 2.5 $\mu g.g^{-1}$ shrimp followed by YHV injection were observed. Dead shrimp were recorded every 12 hpi. The graph was plotted as mean ± SD from three replications per group (n=12-15 shrimp per group). Asterisks represents a statistically significant difference between NaCl → YHV and dsRNA-C+Nter → YHV group ($P < 0.05$).

Discussion

Internalization pathway of yellow head virus (YHV) has been recently characterized. Clathrin-mediated endocytosis is a major route of the virus penetration inside the shrimp host cell (8, 9). After invasion, YHV requires a small GTPase Rab5 protein to regulate the transportation from plasma membrane to early endosome via vesicle transportation. Colocalization between YHV and *Penaeus monodon* Rab5 (PmRab5) was observed in the hemocytes from 10 min to 3 h post YHV infection (11). The Rab5 on vesicle membrane is tethered with Rab5 effector early endosome antigen 1 (EEA1) that appeared on the surface of the early endosome to promote the two membrane fusion (12, 17, 18). For YHV, the vesicle containing YHV that regulated by PmRab5 may precisely move from plasma membrane to early endosome, and PmRab5 may bind with *Penaeus monodon* EEA1 (PmEEA1) to fuse the membrane together. Previous study found that YHV particles inside early endosome of shrimp cell were observed under transmission electron microscopy (27). Therefore, the role of PmEEA1 on YHV infection was studied. The PmEEA1 protein contains 999 amino acids, while other species including CeEEA1, DrEEA1, HsEEA1, LaEEA1, LpEEA1, and RnEEA1 have more than 1,200 amino acids demonstrated that the proteins were different among the organisms (Fig. 1). Although the size of the protein from different species presented a wide range of sizes, but the protein of each species showed signature characteristics of EEA1 that had two Zinc finger C_2H_2 Zn^{2+} finger and FYVE domain of N- and C-terminal sites of EEA1 protein (14). Moreover, the function of EEA1 during YHV infection in *P. Monodon* was examined. Two dsRNAs targeting N- and C-terminusof PmEEA1 were produced and used for

silencing of PmEEA1 transcripts. A combination of two dsRNAs had been ever used to improve the inhibition of YHV infection in shrimp resulting in increasing an efficacy of RNAi technology to prevent and cure shrimp from the virus (28). Therefore, the combination of the two dsRNAs was used to study the function of PmEEA1. Since, dsRNA targeting C-terminus of PmEEA1 region (the first construction) was located near 3' end of the open reading frame (dsRNA-Cter). This dsRNA was first injection into shrimp resulting in inhibition of PmEEA1 mRNA levels only 50-80% compared to the control (data not shown). Local protein factors involving in termination of protein synthesis may cause the positional effect that interrupts the accessibility of RISC-siRNA complex to the local target (29). After obtaining the full-length coding region of PmEEA1, another dsRNA targeting PmEEA1 mRNA was constructed. This dsRNA was located on the middle that near 5' end of the open reading frame (dsRNA-Nter). In this study, the combination between dsRNA-Cter and -Nter of PmEEA1 was used to inject into hemocoel of shrimp and compared to the single dsRNA injection. The result demonstrated that injection of the combined two types of dsRNA targeting PmEEA1 could silence the mRNA levels more than using only one type of the dsRNA (Fig. 3). This is probably due to a variety of siRNA population generated from the combined two dsRNAs. It could increase the efficiency of siRNA to bind to the mRNA target. The siRNA could bind with the secondary structure of mRNA as stem and loop structure better than the hairpin structure (30, 31).

After testing the effectiveness of the dsRNA, the role of PmEEA1 during YHV infection was further investigated. Group of shrimp that injected with NaCl → YHV at 48 hpi showed the increasing of YHV replication about 100,000 times when compared to 24 hpi. On the other hand, injected shrimp with dsRNA targeting PmEEA1 (using the combination between dsRNA-Cter and –Nter (dsRNA-C+Nter)) followed by YHV challeng demonstrated no significant difference of YHV levels at 24 and 48 hpi (Fig. 4B). In addition, dsRNA-C+Nter → YHV group showed a delay of shrimp mortality when compared to the control NaCl → YHV group (Fig.5). All of shrimp die are possibly resulted from YHV infection. Injection of dsRNA targeting PmEEA1 alone has no effect on shrimp mortality (Supplementary Fig. 3). Unlikely, shrimp received dsRNA-PmCHC (9) and dsRNA-PmRab5 (11) that demonstrated the effect of lethal gene. These results indicated that PmEEA1 involved in YHV infection process. The death of the shrimp after receiving dsRNA-C+Nter followed by YHV challenge started at 84 to 96 hpi (about 108 to 120 h post dsRNA injection) is probably caused by the loss of the effectiveness of its dsRNA and the increasing number of virus progenies. Longevity of dsRNA inside the shrimp cells is about five days (120 h) after dsRNA injection and YHV challenge (32). Therefore, to improve the effectiveness of dsRNA-C+Nter targeting PmEEA1 during YHV infection, shrimp may be injected with the dsRNA more than one times every 72 h post dsRNA injection. This strategy may be used to improve shrimp mortality from YHV infection. Based on this study, silencing of PmEEA1 which is not lethal is possibly used as an alternative approach to prevent YHV replication. Taken together, this study demonstrated the crucial role of PmEEA1 during YHV transportation inside the cells.

References

1. Boonyaratpalin S, Supamattaya K, Kasornchandra J, Direkbusaracom S, Aekpanithanpong U, Chantanachooklin C. Non-occluded baculo-like virus, the

causative agent of yellow head disease in the black tiger shrimp (*Penaeus monodon*). Fish Pathol. 1993; 28(3): 103-9.
2. Mayo MA. A summary of taxonomic changes recently approved by ICTV. Arch Virol. 2002; 147: 1655-6.
3. Walker PJ, Bonami JR, Boonsaeng V, Chang PS, Cowley JA, Enjuanes L, Flegel TW, Lightner DV, Loh PC, Snijder EJ, Tang K. Virus taxonomy: classification and nomenclature of viruses: eighth report of the international committee on the taxonomy of viruses. Elsevier. 2005: 975-9.
4. Cowley JA, Dimmock CM, Wongteerasupaya C, Boonsaeng V, Panyim S, Walker PJ. Yellow head virus from Thailand and gill-associated virus from Australia are closely related but distinct prawn viruses. Dis Aquat Org. 1999; 36(2): 153-7.
5. Spann KM, Donaldson RA, Cowley JA, Walker PJ. Differences in the susceptibility of some penaeid prawn species to gill-associated virus (GAV) infection. Dis Aquat Org. 2000; 42: 221-5.
6. Nadala ECB, Tapay LM, Cao S, Loh PC. Yellow-head virus: a rhabdovirus-like pathogen of penaeid shrimp. Dis Aquat Org. 1997; 31: 141-6.
7. Sittidilokratna N, Dangtip S, Cowley JA, Walker PJ. RNA transcription analysis and completion of the genome sequence of yellow head nidovirus. Virus Res. 2008; 136(1-2): 157-65.
8. Jatuyosporn T, Supungul P, Tassanakajon A, Krusong K. The essential role of clathrin-mediated endocytosis in yellow head virus propagation in the black tiger shrimp *Penaeus monodon*. Dev Comp Immunol. 2014; 44: 100–10.
9. Posiri P, Kondo H, Hirono I, Panyim S, Ongvarrasopone C. Successful yellow head virus infection of *Penaeus monodon* requires clathrin heavy chain. Aquaculture. 2015; 435: 480–7.
10. Chavrier P, Parton RG, Hauri HP, Simons K, Zerial M. Localization of low molecular weight GTP binding proteins to exocytic and endocytic compartments. Cell. 1990; 62: 317-29.
11. Posiri P, Panyim S, Ongvarrasopone C. Rab5, an early endosomal protein required for yellow head virus infection of *Penaeus monodon*. Aquaculture 2016;459:43-53.
12. Christoforidis S, McBride HM, Burgoyne RD, Zerial M. The Rab5 effector EEA1 is a core component of endosome docking. Nature. 1999; 397(6720): 621-5.
13. Mu FT, Callaghan JM, Steele-Mortimer O, Stenmark H, Parton RG, Campbell PL, McCluskey J, Yeo JP, Tock EP, Toh BH. EEA1, an early endosome-associated protein. EEA1 is a conserved alpha-helical peripheral membrane protein flanked by cysteine "fingers" and contains a calmodulin-binding IQ motif. J Biol Chem. 1995; 270(22): 13503-11.
14. Callaghan JSA, Gaullier JM, Toh BH, Stenmark H. The endosome fusion regulator early-endosomal autoantigen 1 (EEA1) is a dimer. Biochem J. 1999; 338: 539-43.
15. Simonsen A, Lippé R, Christoforidis S, Gaullier JM, Brech A, Callaghan J, Toh BH, Murphy C, Zerial M, Stenmark H. EEA1 links PI(3)K function to Rab5 regulation of endosome fusion. Nature. 1998; 394(6692): 494-8.
16. Callaghan J, Nixon S, Bucci C, Toh BH, Stenmark H. Direct interaction of EEA1 with Rab5b. Eur J Biochem. 1999; 265(1): 361-6.

17. Lawe DC, Patki V, Heller-Harrison R, Lambright D, Corvera S. The FYVE domain of early endosome antigen 1 is required for both phosphatidylinositol 3-phosphate and Rab5 binding. J Biol Chem. 2000; 275(5): 3699–705.
18. Merithew E, Stone C, Eathiraj S, Lambright DG. Determinants of Rab5 interaction with the N terminus of early endosome antigen 1. J Biol Chem. 2003; 278(10): 8494-500.
19. Vonderheit A, Helenius A. Rab7 associates with early endosomes to mediate sorting and transport of semliki forest virus to late endosomes. PLoS Biol. 2005; 3(7): 1225-38.
20. Lai CK, Jeng KS, Machida K, Lai MM. Hepatitis C virus egress and release depend on endosomal trafficking of core protein. J Virol. 2010; 84(21): 11590-8.
21. Ongvarrasopone C, Chanasakulniyom M, Sritunyalucksana K, Panyim S. Suppression of PmRab7 by dsRNA inhibits WSSV or YHV infection in shrimp. Mar Biotechnol. 2008; 10(4): 374-81.
22. Dereeper A, Guignon V, Blanc G, Audic S, Buffet S, Chevenet F, Dufayard JF, Guindon S, Lefort V, Lescot M, Claverie JM, Gascuel O. Phylogeny.fr: robust phylogenetic analysis for the non-specialist. Nucleic Acids Res 2008; 36: 465-9.
23. Dereeper A, Audic S, Claverie J-M, Blanc G. BLAST-EXPLORER helps you building datasets for phylogenetic analysis. BMC Evol Biol. 2010; 12: 10:8.
24. Ongvarrasopone C. Roshorm Y, Panyim S. A simple and cost effective method to generate dsRNA for RNAi studies in invertebrates. ScienceAsia. 2007; 33: 35-9.
25. Posiri P, Ongvarrasopone C, Panyim S. A simple one-step method for producing dsRNA from *E. coli* to inhibit shrimp virus replication. J Virol Methods. 2013; 188: 64-9.
26. Livak KJ, Schmittgen TD. Analysis of relative gene expression data using real-time quantitative PCR and the $2^{-\Delta\Delta C_T}$ method. Methods. 2001; 25: 402–8
27. Duangsuwan P, Tinikul Y, Withyachumnarnkul B, Chotwiwatthanakun C, Sobhon P. Cellular targets and pathways of yellow head virus infection in lymphoid organ of *Penaeus monodon* as studied by transmission electron microscopy. Songklanakarin J Sci Technol. 2011; 33(2): 121-7.
28. Posiri P, Ongvarrasopone C, Panyim S. Improved preventive and curative effects of YHV infection in *Penaeus monodon* by a combination of two double stranded RNAs. Aquaculture 2011; 314: 34-8.
29. Holen T, Amarzguioui M, Wiiger MT, Babaie E, Prydz H. Positional effects of short interfering RNAs targeting the human coagulation trigger tissue factor. Nucleic Acids Res. 2002; 30(8): 1757-66.
30. Luo KQ, Chang DC. The gene-silencing efficiency of siRNA is strongly dependent on the local structure of mRNA at the targeted region. Biochem Biophys Res Commun. 2004; 318(1): 303-10.
31. Pascut D, Bedogni G, Tiribelli C. Silencing efficacy prediction: a retrospective study on target mRNA features. Biosci Rep. 2015; 35(2) e00185.
32. Yodmuang S, Tirasophon W, Roshorm Y, Chinnirunvong W, Panyim S. YHV-protease dsRNA inhibits YHV replication in *Penaeus monodon* and prevents mortality. Biochem Biophys Res Commun 2006; 341(2): 351-6..

Research Outputs
(ทุนวิจัยพื้นฐานเชิงยุทธศาสตร์)

Research Outputs (ทุนวิจัยพื้นฐานเชิงยุทธศาสตร์)

ผลงานตีพิมพ์ในวารสารวิชาการนานาชาติ

1. *In vitro* assembly of *Penaeus monodon* densovirus (PmDNV)-like particles produced in a prokaryote expression system. Sinnuengnong R, Attasart P, Smith D R, Panyim S, Assavalapsakul W. Aquaculture Research (2017) 48, 4975-4981. Doi:10.11.11/are13315.
2. Suppression of PmRab11 inhibits YHV infection in *Penaeus monodon*. Kongprajug A, Panyim S, Ongvarrasopone C. Fish & Shellfish Immunology (2017) 66, 433-444.
3. In vitro study of a putative role of gonad-inhibiting hormone in oocyte growth stimulation in *Penaeus monodon*. Sathapondecha P, Panyim S, Udomkit A. Aquaculture Research (2017) 1-9, Doi:10.11.11/are13407.
4. An essential role of Rieske domain oxygenase Neverland in the molting cycle of black tiger shrimp, *Penaeus monodon*. Sathapondecha P, Panyim S, Udomkit A. Comparative biochemistry and physiology, Part A (2017) 213, 11-19.
5. Involvement of LvSID-1 in dsRNA uptake in *Litopenaeus vannamei*. Maruekawong K, Tirasophon W, Panyim S, Attasart P. Aquaculture (2018) 482, 65-72.
6. In vitro neutralization of yellow head virus infection in shrimp using recombinant PmYRP65 protein. Kanokudom S, Prateeprat T, Attasart P, Roytrakul S, Panyim S, Smith D R, Assavalapsakul W. Aquaculture (2018) 486, 266-270.
7. Administration of co-expressed *Penaeus stylirostris* densovirus-like particles and dsRNA-YHV-Pro provide protection against yellow head virus in shrimp. Sinnuengnong R, Attasart P, Smith D R, Panyim S, Assavalapsakul W. Journal of Biotechnology. (2018) 267, 63-70.

ผลงานเตรียมตีพิมพ์ในวารสารวิชาการนานาชาติ

1. PmEEA1, the early endosomal protein is employed by YHV for a successful infection in *Penaeus monodon*.
2. *Piwi* controls transposon expression and spermatogenesis in *Penaeus monodon*.
3. Endocytosis participates in cellular uptake of injected dsRNA into hepatopancreas but not gill of *Litopenaeus vannamei*.

4. Suppression of argonautes compromises viral infection in *Penaeus monodon*.
5. Identification and expression of white spot syndrome virus encoded microRNA in *Penaeus monodon*.

มีนักศึกษาปริญญาโท 2 คน

1. นางสาวสุภัทรา แก้วมณี (Miss Suphattha Kaewmani) หัวข้อวิทยานิพนธ์ Molecular cloning and functional characterization of the Rab11-family interaction proteins of *Penaeus monodon* during yellow head virus infection.
2. นางสาวญาณิศา เกตุงามขำ (Miss Yanisa Ketngamkum) หัวข้อวิทยานิพนธ์ Characterization and functional study of a gonad-specific Argonaute cDNA of *Litopenaeus vannamei*.

มีนักศึกษาปริญญาเอก 5 คน

1. นายธีระพงษ์ โห (Mr. Teerapong Ho) หัวข้อวิทยานิพนธ์ Functional characterization of proteins in the Argonaute subfamily from black tiger shrimp.
2. นางสาวธนียา นันทาพจน์ (Miss Thaneeya Nantapojd) หัวข้อวิทยานิพนธ์ Indentification and characterization of white spot syndrome virus-encoded miRNA.
3. นางสาวสุจิตราภรณ์ สุขถาวร (Miss Suchitraporn Sukthaworn) หัวข้อวิทยานิพนธ์ Molecular cloning and functional characterization of proteins in the PIWI subfamily from black tiger shrimp.
4. นายภูรวินทร์ สนิท (Mr. Poorawind Sanitt) หัวข้อวิทยานิพนธ์ Mechanism of extracellular dsRNA internalization and subcellular localization in shrimp cells.
5. นายจักรพงษ์ เคลือบแสงเนียน (Mr. Jakkapong Kluebsoongnaen) หัวข้อวิทยานิพนธ์ Regulation of shrimp vitellogenesis by gonad inhibiting hormone.